TAMPEREEN TEKNILLINEN YLIOPISTO
TAMPERE UNIVERSITY OF TECHNOLOGY

Tobias Hidalgo Stitz

Filter Bank Techniques for the Physical Layer in Wireless Communications

Julkaisu 919 • Publication 919

Tampere 2010

Tampereen teknillinen yliopisto. Julkaisu 919
Tampere University of Technology. Publication 919

Tobias Hidalgo Stitz

Filter Bank Techniques for the Physical Layer in Wireless Communications

Thesis for the degree of Doctor of Science in Technology to be presented with due permission for public examination and criticism in Tietotalo Building, Auditorium TB109, at Tampere University of Technology, on the 29th of October 2010, at 12 noon.

Tampereen teknillinen yliopisto - Tampere University of Technology
Tampere 2010

Supervisor
Markku Renfors, Dr.Tech., Professor
Department of Communications Engineering
Tampere University of Technology
Tampere, Finland

Pre-examiners
Behrouz Farhang-Boroujeny, Ph.D., Professor
Department of Electrical and Computer Engineering
University of Utah
Salt Lake City, Utah, USA

Risto Wichman, D.Sc., Professor
Department of Signal Processing and Acoustics
Aalto University School of Science and Technology
Helsinki, Finland

Opponents
Eleftherios Kofidis, Ph.D., Assistant Professor
Department of Statistics and Insurance Science
University of Piraeus
Piraeus, Greece

Risto Wichman, D.Sc., Professor
Department of Signal Processing and Acoustics
Aalto University School of Science and Technology
Helsinki, Finland

ISBN 978-952-15-2451-6 (printed)
ISBN 978-952-15-2496-7 (PDF)
ISSN 1459-2045

Abstract

Filter bank based multicarrier is an evolution with many advantages over the widespread OFDM multicarrier scheme. The author of the thesis stands behind this statement and proposes various solutions for practical physical layer problems based on filter bank processing of wireless communications signals. Filter banks are an evolved form of subband processing, harnessing the key advantages of original efficient subband processing based on the fast Fourier transforms and addressing some of its shortcomings, at the price of a somewhat increased implementation complexity. The main asset of the filter banks is the possibility to design very frequency selective subband filters to compartmentalize the overall spectrum into well isolated subbands, while still making very efficient use of the assigned bandwidth.

This thesis first exploits this main feature of the filter banks in the subband system configuration, in which the analysis filter bank divides the original signal into its subbands and the subsequent synthesis filters reconstruct the original signal in a properly processed form. Here the application is narrowband interference cancellation in a direct sequence spread spectrum system. Using complex modulated filter banks, complex valued data is efficiently processed and the interference notched out without its effect leaking to adjacent subbands. Means for detecting and estimating the location and power of the interferer are presented here, and a novel recursive excision algorithm leads to enhanced interference mitigation performance.

In multicarrier communications, the filter banks are switched into the transmultiplexer configuration, with a synthesis filter bank in the transmitter and an analysis filter bank in the receiver. The high selectivity of the subchannel filters allows them to separate data streams as clusters of contiguous subbands without the need of additional filtering. This raises the question: How much processing can be moved to the low rate subband streams, after the analysis filter bank? Subcarrier-wise processing enables independent processing of data streams allocated to different frequency blocks and sepa-

rated by the filter bank selectivity. These blocks could correspond to different users in an uplink, with different timing and frequency offsets that are difficult to resolve from the compound high rate signal. Our research objective was to perform subcarrier-wise channel estimation and synchronization, including equalization, as well as narrowband interference cancellation when needed.

At the start of the studies of our research group, subchannel equalization was not well understood. Its analysis resulted in efficient equalization methods and later in techniques to estimate the channel impairments to perform the equalization. In this sense, this thesis presents alternative approaches for estimating channel parameters, such as timing, frequency offset and channel frequency response. One estimation technique is pilot based, suitable for systems in which the channel frequency response is almost flat within the subchannels. The other relies on training sequences, an alternative that fits well in implementations with moderate number of subchannels and mildly frequency selective fading channel within the subcarriers. Both approaches are known for the forerunner in multicarrier communications, OFDM, but here the particular difficulties of the filter bank multicarrier signal are tackled.

The presented techniques result in a well performing and quite complete multicarrier communications solution. Its application in a WiMAX-like setup proved to provide throughput gains of up to 20% compared to the original, OFDM based reference system. Based on the extended research and on the results published in the publications that are compiled as part of this thesis, the author strongly believes that the filter bank approach is the right direction to follow in multicarrier communications.

Preface

The roots of the research work leading to this thesis can be traced back to 1999, when I was accepted at the Telecommunications Laboratory of the Tampere University of Technology (TUT). Since then I have worked at the Institute of Communications Engineering and the Department of Communications Engineering (DCE), being the three of them the same unit. The research was funded by the department and also through following projects: "Digital and Analog Techniques in Flexible Receivers," by the National Technology Agency of Finland (Tekes) and with the cooperation of Insta Group (formerly Instrumentointi); "Advanced Multicarrier Techniques for Wireless Communications," by the Academy of Finland; close cooperation with Nokia; the European Commission Project PHYDYAS. The Tampere Graduate School in Information Science and Engineering (TISE) partly supported travel to conferences. I gratefully acknowledge the support of all the mentioned sponsors.

First and foremost I would like to express my deepest gratitude to my supervisor, Prof. Markku Renfors for accepting me back then, allowing me to prey on his genius and for a perfect guidance. He was always there when I had any request and patiently clarified all my doubts. Actually, I have never seen him stress in a hurry in 11 years! My gratitude extends to the reviewers of this thesis Prof. Behrouz Farhang-Boroujeny and Prof. Risto Wichman for their feedback and constructive comments that greatly improved this text. I also thank Prof. Wichman and Assistant Prof. Eleftherios Kofidis for agreeing to act as opponents at my dissertation.

This research could not have been accomplished without the fruitful discussions and interaction with my research partners. From outside of DCE, I would like to acknowledge the cooperation of Dr. Mika Rinne and the colleagues of the PHYDYAS project, especially Dr. Frank Schaich.

After such a long time at DCE and because of the great work environment there, the line between work colleagues and friends has blurred. It has been an honor and a pleasure working shoulder to shoulder with Dr. Ari Viholainen

and Tero Ihalainen. Without them I would not be here right now. It is possible that Tero is thinking of the preface of his thesis at this moment, and I hope to attend his dissertation very soon. My current office mates Ahmet and Ali, the former ones, and all the other personnel at the department have made room TG113 a second home and the streets and bars of Tampere a second office for me. Thank you Abdelmonaem, Adina, Ari Asp, Juha, Jukka, Juuso, Lauri, Meng, Mikko, Nick, Simona, Tero Isotalo, Toni, Turbomies, Vesa, Yaning, Yuan, and all the other people that I have had the pleasure to meet in the corridors or numerous events organized by DCE.

Regarding organizational matters, a special mention goes to our secretaries and managers in different units at TUT: Tarja Erälaukko, Sari Kinnari, Elina Orava, Ulla Siltaloppi and also Jani Tuomisto and his predecessors from the computer and network maintenance staff. Their work may not be always visible but without their support, efficient research would be unimaginable at DCE.

If I wanted to list all my friends that have provided encouragement and support in harder times and refreshing alternatives to work, I would have to write another book. Here in Tampere or spread around the world, Spanish, German, Finnish, Russian, from everywhere, you know who you are, you are the best. Thank you for providing nourishment and exercise for body and mind.

Last and definitely not least I wish to thank the ones closest to me. My parents Edith and José Luis for everything, especially pushing me to discover the wild wide world and then not complaining too much that I have not returned yet. My brother Patrick for enduring all my teasing and still being the coolest brother. Rhimo for being there from almost since I can remember. And Kirsi, for her support, love, and understanding, especially when I take my laptop to bed because I have another section to write. Turning my head while typing and watching you calmly asleep next to me puts the important things of life back into the correct perspective.

Tampere, October 2010

Tobias Hidalgo Stitz

Contents

Abstract i

Preface iii

Table of Contents v

List of Abbreviations vii

List of Principal Symbols ix

List of Figures xi

1 Introduction 1
- 1.1 Background and Motivation . . . 2
- 1.2 Scope and Objectives of Research . . . 5
- 1.3 Outline and Main Results of the Thesis . . . 7
- 1.4 List of Publications . . . 9

2 Basics on Filter Banks 11
- 2.1 Multirate Filter Banks . . . 12
  - 2.1.1 Basic Multirate Operations . . . 13
  - 2.1.2 Transfer Relations and Reconstruction Conditions . . . 17
- 2.2 Modulated Filter Banks . . . 19
- 2.3 Filter Bank Implementation . . . 22
  - 2.3.1 Prototype Design . . . 22
  - 2.3.2 Efficient Implementation and Complexity . . . 23

3 Filter Banks for Narrowband Interference Mitigation 27
- 3.1 Narrowband Interference Mitigation in Time Domain . . . 31
- 3.2 Narrowband Interference Mitigation in Frequency Domain . . . 32

3.2.1 NBI Detection 35
3.2.2 Post-NBI-Mitigation Transient Mitigation 37
3.2.3 Recent Developments in NBI Mitigation 37
3.3 Further Applications of Analysis-Synthesis Systems 38

4 Channel Synchronization in FBMC **41**
4.1 Channel Equalization 42
4.1.1 Conditions for ISI and ICI Cancellation 45
4.1.2 Low Complexity Subcarrier Equalization 49
4.2 Narrowband Interference Suppression 51
4.3 Channel Estimation and Synchronization 54
4.3.1 Data Aided Channel Estimation 57
4.3.2 Timing Synchronization 62
4.3.3 Frequency Synchronization 67
4.3.4 Applied Synchronization and Estimation Schemes . . . 70

5 Conclusions **77**
5.1 Summary of the Main Differences between OFDM and FBMC . 78
5.2 Suggestions for Future Research 80

6 Summary of Publications **83**
6.1 Overview of the Publication Results 83
6.2 Author's Contribution to the Publications 86

Bibliography **89**

Publications **105**

List of Abbreviations

This is a list of the most important and recurrently appearing abbreviations in this thesis.

AFB	Analysis filter bank
AP-SCE	Amplitude and phase subchannel equalizer
AWGN	Additive white Gaussian noise
BER	Bit error ratio
CDMA	Code division multiple access
CFO	Carrier frequency offset
CMFB	Cosine modulated filter bank
CP	Cyclic prefix
CR	Cognitive radio
DFT	Discrete Fourier transform
DSSS	Direct sequence spread spectrum
ELT	Extended lapped transform
EMFB	Exponentially modulated filter bank
FBMC	Filter bank based multicarrier
FB	Filter bank
FFT	Fast Fourier transform
FIR	Finite impulse response
FTD	Fractional time delay
ICI	Intercarrier interference
IFFT	Inverse fast Fourier transform
IIR	Infinite impulse response
ISI	Intersymbol interference
LMS	Least mean squares
LT	Lapped transform
LTE	Long term evolution

MC	Multicarrier
MDFT	Modified discrete Fourier transform
MIMO	Multiple input multiple output
MMSE	Minimum mean squared error
MSE	Mean squared error
NBI	Narrowband interference
NPR	Nearly perfect reconstruction
OFDMA	Orthogonal frequency division multiple access
OFDM	Orthogonal frequency division multiplexing
OQAM	Offset quadrature amplitude modulation
PAPR	Peak to average power ratio
PHYDYAS	Physical layer for dynamic spectrum access and cognitive radio
PN	Pseudo noise
PR	Perfect reconstruction
QAM	Quadrature amplitude modulation
QPSK	Quadrature phase shift keying
SC-FDE	Single carrier frequency domain equalization
SC-FDMA	Single carrier frequency division multiple access
SFB	Synthesis filter bank
SMFB	Sine modulated filter bank
SNR	Signal to noise ratio
SS	Spread spectrum
TMUX	Transmultiplexer
WiMAX	Worldwide interoperability for microwave access
ZF	Zero forcing

List of Principal Symbols

This is a list of the principal symbols and notations used throughout the thesis.

$\mathrm{Re}[\cdot]$	Real part of the argument $\cdot$
$\mathrm{Im}[\cdot]$	Imaginary part of the argument $\cdot$
$\mathfrak{F}[\cdot]$	Fourier transform of the argument $\cdot$
$*$	Complex conjugation operation
$\star$	Convolution operation
M	Filter bank size, total number of subchannels
k	Subcarrier index, $k = 0, 1, ...M-1$
K	Overlapping factor
Δf	Subcarrier separation
f_s	Sampling rate, at SFB output and AFB input
T_s	Sampling interval at SFB output and AFB input, $T_s = 1/f_s$
m	Time index at high sampling rate f_s, at SFB output and AFB input
n	Time index at low sampling rate, at AFB output and SFB input
$h_p[m]$	Prototype filter
$H_p(e^{j\omega})$	Frequency response of the prototype filter, $\mathfrak{F}[h_p[m]]$
$f_k[m]$	Analysis filter for subchannel k
$g_k[m]$	Synthesis filter for subchannel k
$h(t,\tau), h[n,m]$	Time-varying channel impulse response

List of Figures

1.1 Spectral representation of the subcarriers in a multicarrier system. 3
1.2 OFDM symbols with cyclic prefix in time. 4
1.3 Spectra of OFDM and FBMC subchannels. 5

2.1 Most general filter bank. 11
2.2 Subband system and transmultiplexer configurations. 12
2.3 Downsampling by $N = 2$. a) Time domain representation. b) Frequency domain presentation showing the aliasing effect produced because the highest frequency of the input signal is larger than $\pi/2$. 14
2.4 Decimation of a bandpass signal with complex filters. a) Spectrum of the input signal. b) Spectrum after bandpass anti-alias filtering. c) Resulting spectrum after downsampling by $N = 8$. 15
2.5 Upsampling by $N = 2$. a) Insertion of the zero valued samples in the time domain. b) Frequency domain representation with imaging when $\omega > \pi/2$. 16
2.6 Interpolation. a) Spectrum of the input signal. b) Spectrum of the upsampled signal, highlighting the band of interest. c) Spectrum of the output signal, after complex anti-imaging bandpass filter. 17
2.7 Identities in multirate signal processing. 17
2.8 Modulated filter banks with even and odd stacking. 20
2.9 Efficient implementation of the EMFB based on cosine and sine modulated filter banks. 25
2.10 Efficient implementation of the FBMC/OQAM filter banks. . . 26

3.1 Constellation and spectrum of a QPSK signal affected by NBI. 28
3.2 Robustness against NBI in a spread spectrum signal. 29

3.3 Constellation of a QPSK signal affected by NBI and after excision of the NBI. 30
3.4 NBI excision on the frequencies at which the interference is detected. 33
3.5 Threshold detection principle. 35
3.6 Transient occurrence after NBI mitigation. (a) Interfered signal and processed signal. (b) Processed signal only, for better appreciation. 37

4.1 Efficient multicarrier transmission principle. 42
4.2 Mildly frequency selective channel response in the subchannels. 43
4.3 TMUX with oversampled analysis bank and per-subcarrier equalizers in (a) EMFB implementation and (b) FBMC/OQAM implementation. 44
4.4 Potential ICI spectrum affecting subchannel $k = 0$ in the odd stacked EMFB implementation. 46
4.5 ISI from the folded spectrum of the overall transfer function $\tilde{z}_k[m]$. 48
4.6 Complex FIR subcarrier equalizer for equalization at 3 frequency points. 50
4.7 Amplitude and phase subcarrier equalizer for equalization at 3 frequency points. 50
4.8 Three point equalization working principle. 51
4.9 NBI mitigation in the adjacent subchannel. 52
4.10 Locating NBI affecting two subbands. 54
4.11 Complex TMUX receiver with oversampled analysis bank and per-subcarrier equalizers. 56
4.12 Subchannel frequency response distortion due to CFO for normalized frequency offsets $\varepsilon = 0.01$, 0.05, 0.1, and 0.2. 68
4.13 Subchannel receiver signal model in the presence of CFO, with CFO compensation and subchannel equalization. (a) Basic model. (b) Equivalent form. 70
4.14 Training sequence behavior in the frequency domain. 72
4.15 Extending the non-ambiguity ranges. 74

Chapter 1

Introduction

There are two trends in modern telecommunications that can be recognized as persistent. First, the continuous increase in data rates in digital communications. From the first Morse symbols per second in telegraph communications [22] in the mid of the 19th century, continuing with the first landline modems at hundreds of bauds (symbols per second) hundred years later [60], and the 9.6 kbps in early 2G [125] cellular communications, up to the over 300 Mbps already considered in the long term evolution (LTE) [126] standards of next generation mobile communications, the transmission speed has been rising at a steady pace. Research in this field and development of applications that benefit from the enhanced data rates or require even more throughput continue to fuel each other. The means for increasing data rates are widening the transmission bandwidth and improving spectral efficiency, i.e, the data rate that can be sent per unit bandwidth (bps/Hz).

The second trend is the growing ability to access and send any kind of information independently of location or time. It was not so long ago when two persons that wanted to communicate had to decide a fixed location and a time to do so. Also, watching one's favorite movie or program required that the watcher be on a certain location such as home or the theaters. Mobile telephony started to free us from these constraints in the 80ies and nowadays high speed data communications independent from our location and in vehicles moving at high speeds are becoming commonplace. The tool for enabling this are wireless communications. Although most of the customers may take it for granted, efficiently transmitting wirelessly over wide bandwidths and at changing locations is a challenging task because of the difficult channel conditions the signal encounters. Wideband signals are affected by frequency

selective fading due to multipath propagation and can suffer from narrowband interference within the desired signal bandwidth. Relative mobility between transmitter and receiver and also the changing conditions of the propagation channel produce time fading.

There are several physical layer choices to overcome the challenges of efficient wideband wireless communications. Among them we encounter spread spectrum techniques [99], multicarrier (MC) communications, combinations of both [11, 35], and even updated single carrier communication with frequency domain receiver processing [30], which share the multirate signal processing from the multicarrier systems. The main focus of this thesis is on communications that apply multirate signal processing.

1.1 Background and Motivation

In MC communications the data is transmitted over many frequencies instead of a single carrier, dividing the wideband frequency selective communication channel into several subbands with mildly selective fading. This leads to advantages in channel estimation and equalization, when performed at subcarrier level. The composite MC symbol has much longer duration than the symbol of a single carrier system transmitting within the same bandwidth, leading to easier timing synchronization. Furthermore, limited narrowband interference can be mitigated by shutting down the subchannels that are interfered. In general, the option provided by MC systems to easily and conveniently schedule data transmission over different subchannels at one's will enables scalable and flexible communications [133].

The main advantage from the efficiency point of view is that the carriers can be selected to be orthogonal, in such a way that their spectra overlap but without causing interference to the other carriers [23]. In digital communications, the inverse fast Fourier transform (IFFT) generates such a waveform with little computational complexity [81]. The result is an orthogonal frequency division multiplexed (OFDM) signal [133], which has been the most prominent MC signal so far. In OFDM, frequency selective channels can be elegantly equalized with a single complex coefficient at subcarrier level if a cyclic prefix (CP) is appended to the OFDM symbol. This holds as long as the CP covers the maximum delay spread of the channel. The interesting properties of MC communications and the simplicity of OFDM have led this scheme to be a fundamental part in a number of wireless communication systems, including emerging cellular standards such as WiMAX (Worldwide

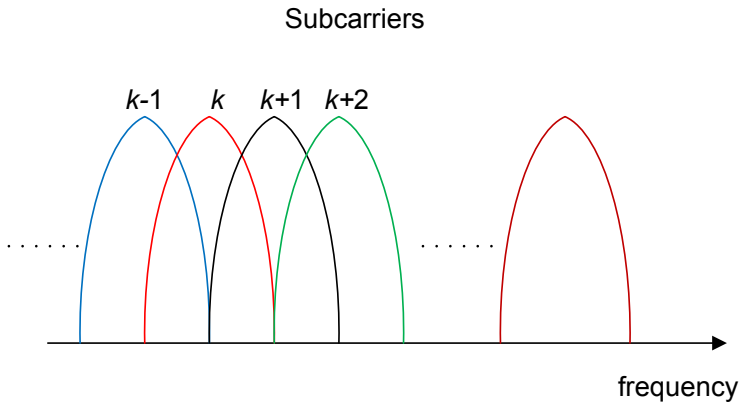

Figure 1.1: Spectral representation of the subcarriers in a multicarrier system.

Interoperability for Microwave Access) [154] (based on the IEEE 802.16e [2] standard) and E-UTRA LTE (Evolved UMTS Terrestrial Radio Access Long Term Evolution) [126].

WiMAX and LTE are the remaining competing standards for evolving third generation (3G) mobile networks towards 4G data rate, spectral efficiency and flexibility requirements, after other (also OFDM-based) candidates such as flash-OFDM [70] and Ultra-Mobile Broadband have lost momentum or been discontinued, respectively. At the moment it seems that LTE is gathering more industry support, although WiMAX has a small time advantage because the first commercial networks have already been deployed. In their origins, WiMAX evolves from fixed data communications and LTE has its roots in mobile cellular networks. Nevertheless, both aim at improved power and spectral efficiency and high data rates in the order of hundreds of Mbps at high mobilities with the help of the OFDM air interface, multiple input multiple output (MIMO) techniques and smart scheduling. The spectrum allocation in both systems is scalable from around 1 MHz to 20 MHz, and the subcarrier separation is in the order of 10 kHz. Further, WiMAX and LTE are based on an all-IP network architecture. Returning to the MC aspect, the two systems exploit the flexibility of OFDM to also provide multiple access in time and frequency through orthogonal frequency division multiple access (OFDMA). However, the LTE uplink builds on DFT-spread-OFDM for providing single carrier frequency division multiple access (SC-FDMA) [89] because it has a lower peak to average power ratio (PAPR) and thus uses the mobile terminal power more efficiently.

Unfortunately, OFDM has some shortcomings. The cyclic prefix is a copy of part of the transmitted OFDM symbol that is then appended at the beginning of the OFDM symbol. This redundancy reduces the effective throughput of the transmission as can be seen in Figure 1.2. Additionally to worsening the spectral efficiency, transmit power is wasted on the CP. Furthermore, the spectral localization of the OFDM subcarriers is weak, giving rise to spectral leakage and interference problems with unsynchronized signals. These shortcomings have motivated researchers to develop alternative solutions overcoming these problems, bringing filter bank (FB) processing into the spotlight as an interesting alternative.

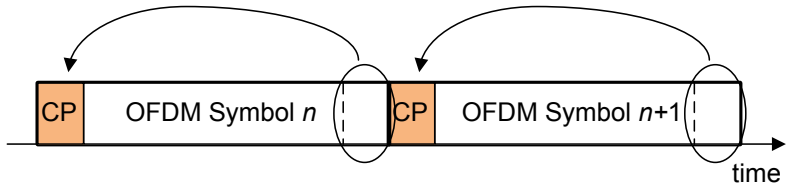

Figure 1.2: OFDM symbols with cyclic prefix in time.

During the research that resulted in this thesis, the scientific community witnessed the rise of a new paradigm in telecommunications: Cognitive Radio (CR) [41, 88]. CR is a response to the problem of suboptimal use of spectral resources in licensed bands. The available communication channels are not being occupied at all locations and all possible times. A cognitive radio is a device that possesses the intelligence to sense the spectrum (SSA, spectrum sensing and awareness) and recognize the transmission opportunities, also called spectral white spaces, to dynamically utilize them (DSA, dynamic spectrum access) for information transmission. CR can be expected to bring a wide reaching revolution in wireless communications. From the physical layer point of view, multicarrier waveforms are an excellent match to perform spectral sensing and to dynamically access free bands because of their intrinsic property of dividing the spectrum into small portions. Especially filter banks, with their efficient and isolated compartmentalization of the subbands, appear as strong candidates for cognitive radio signal processing. This observation gave a timely motivational push to continue with the research on the capabilities of filter banks for the wireless communications physical layer.

1.2 Scope and Objectives of Research

Filter bank based multicarrier (FBMC) modulation can be considered an evolved OFDM due to the advantages it presents over it. Furthermore, one way of implementing the filter banks is by building on the core blocks of OFDM, i.e., the IFFT/FFT pair [118]. The filter banks address the main drawbacks of OFDM mentioned in the previous section: Firstly, their subchannels can be optimally designed in the frequency domain to have desired spectral containment [81]. Secondly, FBMC systems do not make use of the redundant CP, enabling a more efficient use of channel resources. The subchannel filters are designed with the Nyquist pulse shaping principle [99], which means that the consecutive symbol waveforms are overlapping in time.

The excellent spectral containment achieved in FBs is crucial for avoiding distortion from asynchronous signals in adjacent bands. This contrasts with the mere 13 dB by which the adjacent subbands are attenuated in OFDM. In this sense, further spectral efficiency advantages appear at the edges of the transmission band, where one subchannel suffices as guard band to the next transmission band. An OFDM system with slowly decaying sidelobes needs many more subbands acting as guard band or unrealistically sharp additional filtering to provide similar attenuation at frequencies adjacent to the transmission band. The different power spectral densities of OFDM and FBMC with pulses that overlap over 4 symbols are presented in Figure 1.3. The lower level of subchannel sidelobes, resulting in smaller potential intercarrier interference (ICI) between non-adjacent subchannels is evident from the figure.

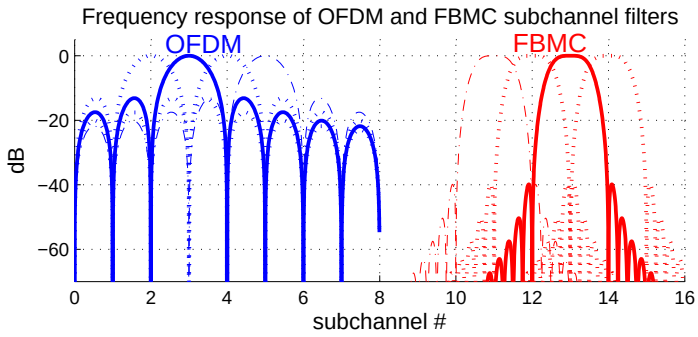

Figure 1.3: Spectra of OFDM and FBMC subchannels.

With high enough out of band attenuation of the subband filters, the filter bank itself can provide sufficient frequency isolation to efficiently implement

the needed reception band selectivity. This enables moving all signal processing functions after the filter bank, to the low sampling rate. Further, the channelization can be done in a dynamically adjustable manner, efficiently suppressing immediately adjacent and even narrowband interference components falling within the transmission bandwidth. OFDM cannot offer this advantage due to the low containment of its subchannel filters.

In the context of CR, where a secondary user scans the spectrum assigned to primary users for a transmission opportunity, the high spectral definition of FBMC is especially valuable. The performance of Haykin's method of choice for radio scene analysis [42], the multitaper method [123], can be well approximated using FBs with greatly reduced complexity [33, 34].

The main research objective of our small team within the Digital Transmission Group at the Tampere University of Technology has been to prove that filter banks are a viable alternative for an evolved and efficient physical layer in wireless communications. Under the lead of Prof. Markku Renfors, Dr. Ari Viholainen, M.Sc. Tero Ihalainen and myself have researched over the last decade the broad aspects and problems present in a complete communication system with filter banks. The general plan included the design of efficient filter banks for processing complex valued signals. The filter banks were then used in different applications for wireless communications, in single carrier and in multicarrier environments, with research branching into several areas such as synchronization and equalization, multiantenna communications, cognitive radio capabilities and more. Original research on filter bank design led to the dissertation of Dr. Viholainen [143], while more recent results on communication aspects are the main constituents of M.Sc. Ihalainen's doctoral thesis and of this document. Even nowadays, filter banks in wireless communications are a rather open research topic with challenges to be tackled, such as efficient space-time coding, among others.

In this context, this thesis addresses two research questions: Firstly, how well and with what implications can an analysis-synthesis filter bank pair efficiently mitigate narrowband interference at a receiver in a single carrier system? Intentional jamming of military communications and also the possibility of better spectral usage with overlaid signal spectra led to long lasting research in interference mitigation in spread spectrum signals. Here the research objective was to exploit the better spectral containment of the filter banks for performing accurate excision of a narrowband interferer within the signal bandwidth without power leakage to adjacent bands, as is the case in FFT-based excision.

The second research problem faced the synchronization, channel estimation and channel equalization in FBMC communication systems, in which the synthesis-analysis configuration is used. The objective was the study of the channel impairments and the solutions to combat them at the receiver in order to build them into a multicarrier communication alternative capable of competing with the omnipresent OFDM. These crucial stages for the transmission chain can substantially differ depending on the applied FBMC approaches. Our research objectives included two implementations. One focused on a multicarrier system working with a moderate number of subchannels, only a fraction of the number used in OFDM. In this case, flat channel fading cannot be assumed anymore at subchannel level. The second approach was developed envisioning an FBMC system to substitute a currently existing OFDM scheme, maintaining the global transmission parameters.

1.3 Outline and Main Results of the Thesis

The main objective when writing this thesis was to provide a fluent summary of the ideas, analysis and results included in the appended publications [P1]-[P5]. The background and results regarding narrowband interference mitigation and channel synchronization, estimation and equalization are the subject matter of Chapters 3 and 4. The next paragraphs give a brief outline of the contents of this thesis.

In this introductory chapter the motivation for the research leading to this dissertation is presented. The research problems posing the objectives of this work are introduced to define the scope of the thesis. Its contents are outlined, indicating the main results of the research, where applicable. This thesis is presented as a compilation of publications. At the end of this chapter we list the relevant publications that are appended in the second part of the thesis. Additionally, a list with some supplementary publications in which the author was involved is presented. Their results are not directly under the scope of this dissertation, but are closely related.

Chapter 2 introduces the concept of multirate filter banks and refreshes the basic multirate operations. The two configurations of the filter bank pairs, namely subband system (analysis-synthesis) and transmultiplexer (synthesis-analysis) are described. The special case of modulated filter banks is reviewed, since these are the types of filter banks relevant to this thesis. Finally, implementation issues such as prototype filter design and efficient implementation structures are briefly revisited.

In Chapter 3 the application of filter banks to mitigate the problem of narrowband interference in direct sequence spread spectrum signals is discussed. State of the art methods at the time of the research that led to [P1] are introduced. At that time, the methods for combating the interference were mainly subdivided into time-domain and frequency-domain methods. This division is maintained to localize the filter bank based method as belonging to the latter group. The main problems arising in the filter bank based narrowband interference detection and mitigation are introduced, shortly indicating also the devised solutions: The adaptive detection threshold and the shortened despreading for efficient transient mitigation. Also in Chapter 3, a more modern classification of the mitigation methods is cited, and several research results that have surfaced after publication of [P1] are presented. At the end of the chapter, some other applications of the filter banks in the subband system configuration are listed.

Chapter 4 describes how FBs have been applied in this thesis in the TMUX configuration for FBMC and how the channel effect has been countered. For equalization, subcarrier equalizers (SCE) of few taps are able to equalize each subchannel better than the multiplication by a single complex coefficient, if the channel frequency response is not flat within the subchannel. As a result, the use of higher order SCEs enables to increase the relative subchannel bandwidth, because the subchannel responses are allowed to take mildly frequency selective shapes. Another interpretation is that the number of subchannels to cover a given signal bandwidth by FBMC can be reduced. In general, higher order SCE structures offer a trade-off between the number of required subchannels and complexity of the subcarrier equalizers, providing flexibility and scalability to the system design. Also in this chapter, a narrowband interference mitigation technique that makes use of the low complexity equalizers, is presented. After the equalization problem is solved, the channel parameter estimation that feeds the equalizers is discussed. Similar estimation methods as in OFDM can be applied, taking into account the particularities of the FBMC signal, i.e., the inherent complex interference introduced by the filter bank. In this chapter, analysis for channel estimation and synchronization is presented and two practical estimation approaches are proposed: One for wider subchannels is based on training sequences. The other, in which the channel fading within the subchannels can be considered flat, uses scattered pilots. The research introduced in this chapter is a crucial component of the simulation testbed for the complete FBMC system that resulted from the joint efforts of our research team.

Chapter 5 draws final conclusions of the thesis, briefly summarizes the main differences between OFDM and FBMC, and offers possible future research directions. A short summary of the results published in [P1]-[P5] is given in Chapter 6, where also the author's contributions to these publications are clarified.

The compilation of the publications included in this thesis can be found after the Bibliography.

1.4 List of Publications

This thesis consists of the following publications, which in the text are referred to as Publications [P1]-[P5]. The first three publications are journal publications, while [P4,P5] were papers presented at conferences. The author of this thesis is the main contributor to [P1], [P3]-[P5], and has decisively contributed to [P2].

[P1] T. Hidalgo Stitz, and M. Renfors, "Filter-bank-based narrowband interference detection and suppression in spread spectrum systems" in *EURASIP Journal on Applied Signal Processing*, 2004 (Jan. 2004), pp. 1163-1176.
DOI= http://dx.doi.org/10.1155/S1110865704312102.

[P2] T. Ihalainen, T. Hidalgo Stitz, M. Rinne, and M. Renfors, "Channel equalization in filter bank based multicarrier modulation for wireless communications" in *EURASIP Journal on Advances in Signal Processing*, vol. 2007, Article ID 49389, 18 pages, 2007.
DOI= http://dx.doi.org/10.1155/2007/49389.

[P3] T. Hidalgo Stitz, T. Ihalainen, A. Viholainen, and M. Renfors, "Pilot-based synchronization and equalization in filter bank multicarrier communications" in *EURASIP Journal on Advances in Signal Processing*, vol. 2010, Article ID 741429, 18 pages, 2010.
DOI= http://dx.doi.org/10.1155/2010/741429.

[P4] T. Hidalgo Stitz, T. Ihalainen, and M. Renfors, "Mitigation of narrowband interference in filter bank based multicarrier systems," in *Proc. IEEE Int. Conf. Communications.* 2006, vol.7, pp. 3241-3246, Istanbul, Turkey, June 2006.
DOI= http://dx.doi.org/10.1109/ICC.2006.255306.

[P5] T. Hidalgo Stitz, T. Ihalainen, and M. Renfors, "Practical issues in frequency domain synchronization for filter bank based multicarrier transmission" in *Proc. IEEE Int. Symp. Communications, Control and Signal Processing.*, pp. 411-416, March 2008.
DOI= http://dx.doi.org/10.1109/ISCCSP.2008.4537260.

List of Supplementary Publications

The following list enumerates the publications that are not included in this thesis, but are closely related and have been co-authored by the author of this thesis with significant contribution.

[S1] A. Viholainen, T. Hidalgo Stitz, J. Alhava, T. Ihalainen and M. Renfors, "Complex modulated critically sampled filter banks based on cosine and sine modulation" in *Proc. IEEE Int. Symp. Circuits and Systems*, Scottsdale, USA, May 2002, pp. 833-836.
DOI= http://dx.doi.org/10.1109/ISCAS.2002.1009970.

[S2] Y. Yang, T. Hidalgo Stitz, and M. Renfors, "Implementation of a filter bank based narrowband interference suppression algorithm on a DSP processor" in *Proc. Int. Conf. Telecommunications*, Beijing, China, June 2002, pp. 608-611.

[S3] Y. Yang, T. Hidalgo Stitz, M. Rinne, and M. Renfors, "Mitigation of narrowband interference in SC transmission with filter bank equalization" in *Proc. IEEE Asia Pacific Conf. Circuits and Systems*, Singapore, December 2006, pp. 748-751.
DOI= http://dx.doi.org/10.1109/APCCAS.2006.342116.

[S4] U. Rahim, T. Hidalgo Stitz, and M. Renfors, "Analysis of Clipping-Based PAPR-Reduction in Multicarrier Systems" in *Proc. IEEE Vehicular Technology Conf.*, Barcelona, Spain, Apr. 2009, pp. 1-5.
DOI= http://dx.doi.org/10.1109/VETECS.2009.5073391

Chapter 2

Basics on Filter Banks

In the most general sense, a filter bank is an array of M filters that processes its M input signals to produce M outputs.

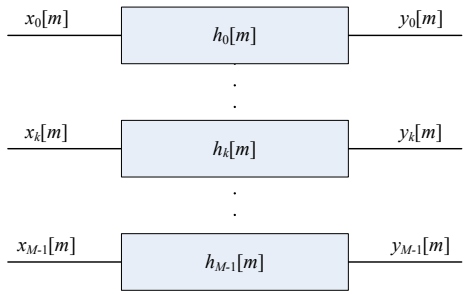

Figure 2.1: Most general filter bank.

If all the inputs in Figure 2.1 are connected together, then the same signal is sent through the filter bank, i.e., $x_i[m] = x[m], k = 0, 1, ..., M-1$. In this case the bank can be considered to be analyzing the input signal $x[m]$ according to the characteristics of each filter. Hence this filter bank is called analysis filter bank (AFB). Although any imaginable filtering may be applied, a logical way to analyze the input signal of the AFB is to look at its characteristics at different frequency subbands.

Conversely, if individual signals are filtered and the outputs connected together, adding up all the outputs, a new, composed signal $y[m] = \sum_{k=0}^{M-1} y_i[m]$ is synthesized. Therefore, the name of this configuration is called synthesis filter bank (SFB).

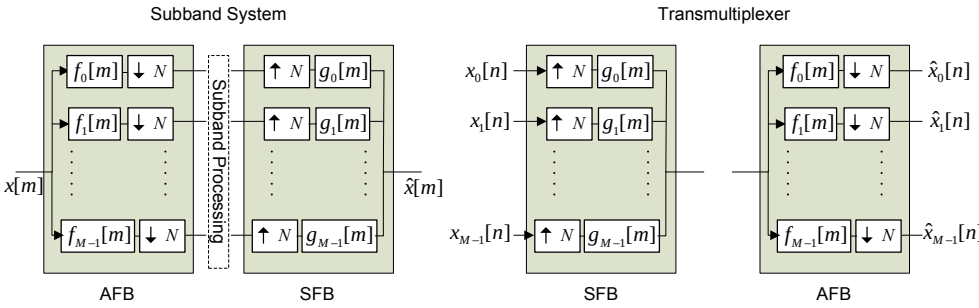

Figure 2.2: Subband system and transmultiplexer configurations.

2.1 Multirate Filter Banks

In subband processing, the outputs of the analysis filters retain desired portions of the spectrum of the input signal for further processing. The resulting signal occupies only a fraction of the original spectrum and the sampling rate can be reduced to lower the number of operations without losing the original signal information, as long as the Nyquist-Shannon sampling theorem [93, 117] is fulfilled. In an analogous manner, the input signal of the SFB can be upsampled and filtered to occupy a desired spectral region. By adding signals that occupy different portions of the spectrum, a broader bandwidth signal can be synthesized. Filter banks that work at different sampling rates are called multirate filter banks and are key elements in multirate signal processing [24, 27, 36, 81, 129].

The real power of the filter banks is harnessed when they are used in pairs, combining them as subband systems (analysis-synthesis configuration) or transmultiplexers (synthesis-analysis configuration), as indicated in Figure 2.2. In the figure, it is assumed that rate conversions by N are the same in all subbands. An example application using a subband system is an equalizer, in which the subbands of a signal are amplified as required. On the other hand, the transmultiplexer configuration is applied in multicarrier communications [129].

Figure 2.2 also shows the input signals $x[m]$ and $x_k[m]$ to the subband system and the transmultiplexer subbands, respectively. Furthermore, the outputs are labeled $\hat{x}[m]$ and $\hat{x}_k[m]$, hinting to their relation with the corresponding inputs. As a matter of fact, it is desirable that the input and the output are as similar as possible, if no further processing apart from the filter banks takes place. If the filter banks are designed so that the inputs and the

outputs of the filter bank pairs are exactly the same, except for the processing delay, the filter banks are called perfect reconstruction (PR) filter banks. Another design possibility is to permit a limited distortion, in which case a nearly perfect reconstruction (NPR) is obtained [129, 130].

The design conditions necessary for obtaining these filter bank types can be deduced from the transfer functions that relate the input and the output of the banks with the help of the multirate operations presented next.

2.1.1 Basic Multirate Operations

The described operations of rate reduction or increase, preceded or followed by filtering, respectively, are the basic multirate operations. They are respectively known as decimation and interpolation, and are briefly described in the following subsections [25, 129].

Decimation

Decimation takes place in the AFB and consists of the filtering of the input signal (anti-aliasing filtering) and the subsequent downsampling, as can be seen in the branches of the analysis filter banks of Figure 2.2. Downsampling reduces the sampling rate by only selecting every Nth sample of the filtered signal

$$v_k[m] = x[m] \star f_k[m] = \sum_{r=0}^{L-1} x[m-r] f_k[r], \tag{2.1}$$

where $\star$ denotes the convolution sum and L is the length of the analysis filter $f_k[m]$, assumed to be a finite impulse response (FIR) filter here. Downsampling can be expressed mathematically in the time domain and the z-transform domain as follows:

$$y_k[n] = v_k[Nn], \tag{2.2}$$

$$Y_k(z) = \frac{1}{N} \sum_{l=0}^{N-1} V_k\left(z^{1/N} e^{-j2\pi l/N}\right). \tag{2.3}$$

In the transmultiplexer configuration of Figure 2.2, $y_k[n] \equiv \hat{x}_k[n]$, and in the subband system, $y_k[n]$ are the inputs to the subband processing block.

In the frequency domain, the output spectrum is formed by a repetition of N shifted replicas of the input spectrum expanded by the factor N. The size of the shift in frequency is 2π, as can be deducted from equation (2.3). Figure 2.3 graphically presents the effect of equations (2.2) and (2.3). The figure also

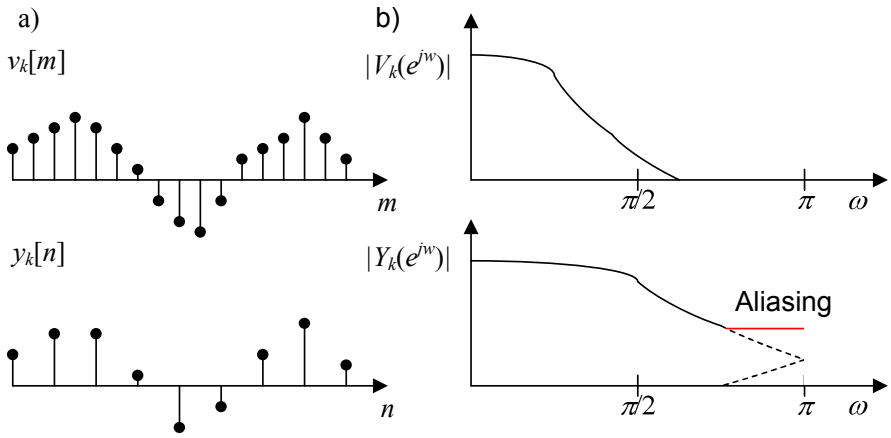

Figure 2.3: Downsampling by $N = 2$. a) Time domain representation. b) Frequency domain presentation showing the aliasing effect produced because the highest frequency of the input signal is larger than $\pi/2$.

presents the aliasing problem, which appears when the filtering prior to the downsampling is not sharp enough.

The previous equations can be extended to include the anti-aliasing filter $f_k[m]$:

$$y_k[n] = v_k[Nn] = \sum_{r=0}^{L-1} x[Nn - r] f_k[r]. \tag{2.4}$$

In the z-domain,

$$V_k(z) = F_k(z)X(z), \tag{2.5}$$

$$\begin{aligned} Y_k(z) &= \frac{1}{N} \sum_{l=0}^{N-1} V_k \left(z^{1/N} e^{-j2\pi l/N} \right) \\ &= \frac{1}{N} \sum_{l=0}^{N-1} F_k \left(z^{1/N} e^{-j2\pi l/N} \right) X \left(z^{1/N} e^{-j2\pi l/N} \right). \end{aligned} \tag{2.6}$$

Figure 2.4 details the frequency domain representation of the signals at different stages of the decimation, for $N = 8$.

Interpolation

The interpolation is the dual operation to the decimation, and takes place in the SFB. It consists of an upsampler and an interpolation filter $g_k[m]$, as

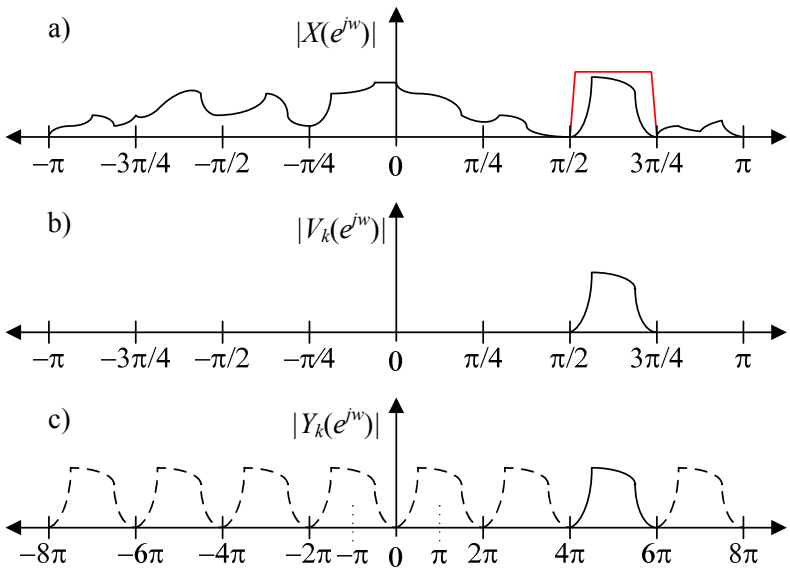

Figure 2.4: Decimation of a bandpass signal with complex filters. a) Spectrum of the input signal. b) Spectrum after bandpass anti-alias filtering. c) Resulting spectrum after downsampling by $N = 8$.

depicted in the SFB branches of Figure 2.2. The upsampler raises the sampling frequency by N and introduces $N-1$ zero samples between the low sampling rate symbols. This can be described in time- and z-domains by equations (2.7) and (2.8), respectively.

$$w_k[m] = \begin{cases} x_k[m/N] & \text{if } m/N \in \mathbb{Z} \\ 0 & \text{otherwise.} \end{cases} \tag{2.7}$$

$$W_k(z) = X_k\left(z^N\right), \tag{2.8}$$

where $w_k[m]$ and $W_k(z)$ represent the signal after the upsampler in time- and z-domains, respectively. The effect in time and frequency domains is sketched in Figure 2.5. It can be seen that the signal spectrum is compressed and that the images that were beyond half the sampling frequency appear now inside the sampling range, at a frequency shift of $2\pi/N$. The interpolation filter interpolates between the actual upsampled symbols and eliminates the images that have appeared inside the sampling range. Therefore, the interpolation filter is also called anti-imaging filter.

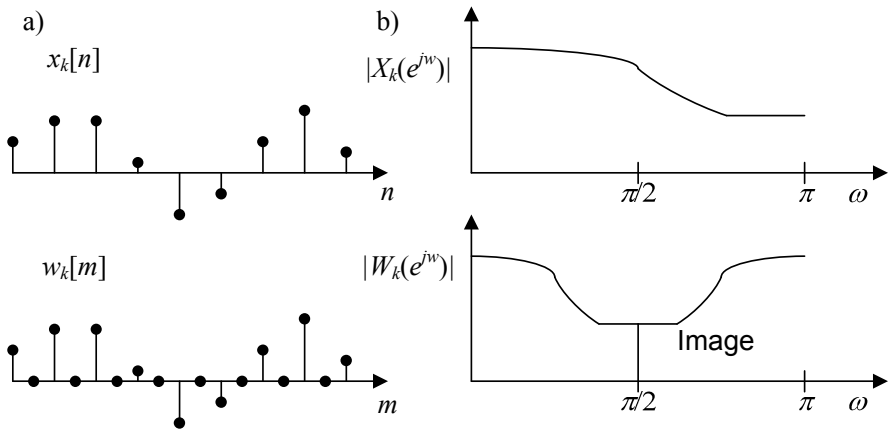

Figure 2.5: Upsampling by $N = 2$. a) Insertion of the zero valued samples in the time domain. b) Frequency domain representation with imaging when $\omega > \pi/2$.

To include the filter effect in a similar manner as in the decimation definition above, the equations including the filtering by the anti-imaging filter $g_k[m]$ are given next:

$$\tilde{x}_k[m] = w_k[m] \star g_k[m] = \sum_{r=0}^{r=L-1} g_k[r] w_k[m-r] = \sum_{r=0}^{r=L-1} g_k[r] x_k[(m-r)/N], \tag{2.9}$$

and

$$\tilde{X}_k(z) = G_k(z) W_k(z) = G_k(z) X_k\left(z^N\right). \tag{2.10}$$

Therefore, $\tilde{x}_k[m]$ is the high rate version of $x_k[m]$. In the subband system of Figure 2.2, $\hat{x}[m] = \sum_{k=0}^{M-1} \tilde{x}_k[m]$.

Figure 2.6 details the frequency domain representation of the signals at the different stages of the interpolation. Here, $N = 8$, and the interpolation filter is bandpass, therefore locating the resulting high-rate signal around a desired frequency.

Multirate Identities

To finalize this section, it is practical to recall the identities in multirate signal processing in Figure 2.7. These multirate identities permit switching the order of the up/downsampling operation with the corresponding filters. Now

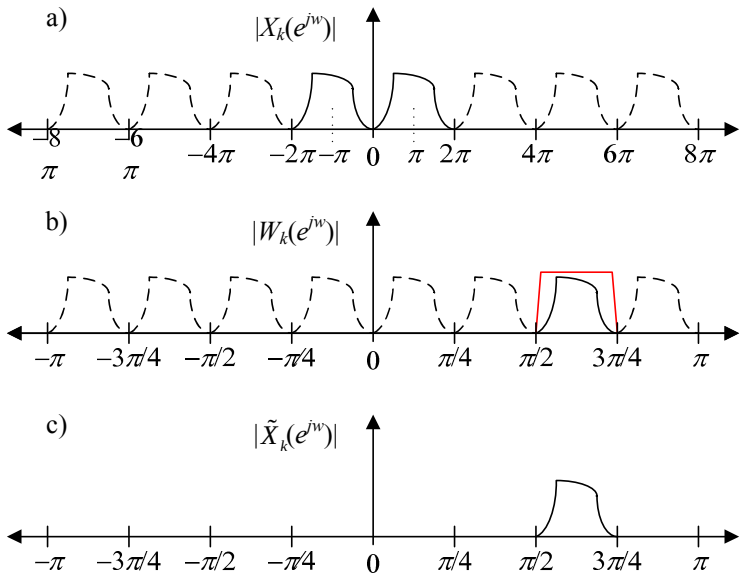

Figure 2.6: Interpolation. a) Spectrum of the input signal. b) Spectrum of the upsampled signal, highlighting the band of interest. c) Spectrum of the output signal, after complex anti-imaging bandpass filter.

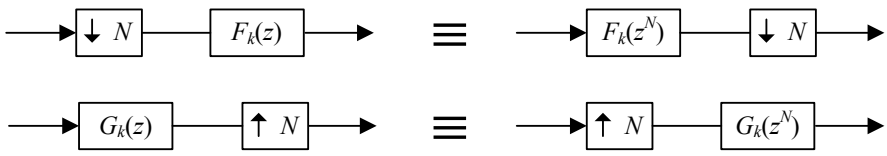

Figure 2.7: Identities in multirate signal processing.

the filtering takes place at the lower rate, and with decimated filters, which allows for more efficient and less complex processing. The identities are exploited when aiming for implementing the filter bank in an efficient manner, as described in Section 2.3.

2.1.2 Transfer Relations and Reconstruction Conditions

Using the introduced multirate processing equations, the input-output relations for the subband system of Figure 2.2 can be written in the z-domain as

$$\hat{X}(z) = \frac{1}{N} \sum_{k=0}^{M-1} F_k(z) \sum_{l=0}^{N-1} G_k\left(ze^{-j2\pi l/N}\right) X\left(ze^{-j2\pi l/N}\right). \tag{2.11}$$

The elements of the summations can be redistributed and grouped to yield

$$\hat{X}(z) = T_0(z)X(z) + \sum_{l=1}^{N-1} T_l(z)X\left(ze^{-j2\pi l/N}\right), \tag{2.12}$$

where

$$T_0(z) = \frac{1}{N} \sum_{k=0}^{M-1} F_k(z)G_k(z) \tag{2.13}$$

and

$$T_l(z) = \frac{1}{N} \sum_{k=0}^{M-1} F_k(z)G_k\left(ze^{-j2\pi l/N}\right). \tag{2.14}$$

The distortion transfer function $T_0(z)$ measures the distortion between the original signal and the reconstructed one coming from the convolution of the analysis and synthesis subband filters. Additionally the aliasing transfer function $T_i(z)$ quantifies the effect of the aliasing spectra of the replicas that appear in the downsampling operation at the analysis bank.

Similarly, in the transmultiplexer configuration of Figure 2.2, we obtain

$$\hat{X}_i(z) = \frac{1}{N} \sum_{l=0}^{N-1} G_i\left(z^{1/N}e^{-j2\pi l/N}\right) \sum_{k=0}^{M-1} F_k\left(z^{1/N}e^{-j2\pi l/N}\right) X_k(z). \tag{2.15}$$

This equation can be reordered into

$$\hat{X}_i(z) = T_{ii}(z)X_i(z) + \sum_{\substack{k=0 \\ k\neq i}}^{M-1} T_{ik}(z)X_k(z), \tag{2.16}$$

where

$$T_{ii}(z) = \frac{1}{N} \sum_{l=0}^{N-1} G_i\left(z^{1/N}e^{-j2\pi l/N}\right) F_i\left(z^{1/N}e^{-j2\pi l/N}\right), \tag{2.17}$$

is the transfer function that links the subband input and output signals of subband i. Moreover,

$$T_{ik}(z) = \frac{1}{N} \sum_{l=0}^{N-1} G_i\left(z^{1/N}e^{-j2\pi l/N}\right) F_k\left(z^{1/N}e^{-j2\pi l/N}\right), \; k \neq i \tag{2.18}$$

describes how much of the signal of subband k leaks into subband i.

Therefore, to accomplish perfect reconstruction in the subband system, $T_l(z) = 0$, for $l = 1, 2, ..., N-1$ and $T_0(z) = z^{-N_d}$, i.e., a pure delay of N_d samples. Analogously, $T_{ii}(z)$ and $T_{ik}(z)$ have to be a pure delay and 0, respectively, to obtain a PR transmultiplexer. If these conditions are only approximately fulfilled, then a NPR system is obtained. If the systems are critically sampled, i.e., if $M = N$, the problem of designing a PR analysis-synthesis system and a PR transmultiplexer are equivalent, since the systems are dual if the transfer functions are a function of z^{-M} [140]. This does not impose a great limitation in the design, since the system can be devised with arbitrary delay due to the filters and the required additional delay to fulfill the indicated condition for the transfer functions can be artificially added to one of the banks [129]. Filter banks in which $N < M$ are oversampled filter banks.

2.2 Modulated Filter Banks

Uniform filter banks divide the spectrum into subbands of the same size and in which the subchannels have similar sampling rate conversion [129]. Other choices of dividing the spectrum are also possible, for example octave filter banks or wavelet filter banks [36]. Historically, uniform filter banks started out in the mid-seventies as the quadrature mirror filter (QMF), a two-channel system [26]. In the next decade, the QMF bank idea was generalized to the case of M-channel filter banks. The first approach was to use the QMF as a repeating base element in a nested tree structure, in which each subchannel is divided recursively into smaller subbands by using the two-channel bank. The same properties as for the building block are conserved for the overall structure [119, 120, 144]. The next step was the introduction of a parallel M-channel structure, instead of the tree configuration [90, 139]. One important finding was that perfect reconstruction without aliasing is possible even with subchannel overlapping, if the filters are designed to cancel the aliasing [138].

In the nineties, a special class of M-channel PR filter banks was developed: the modulated filter banks. This class is founded on the idea of a prototype filter that gets modulated, for example with a cosine modulation, to yield the channel filters of the filter bank [82, 112]. This simplifies the design process of the filter bank to the optimization of the prototype filter. Although there are modulated filter banks that use infinite impulse response (IIR) filters as the prototype [92], we only focus on finite impulse response (FIR) filters here. The modulation can be obtained by multiplication by a cosine, a sine or a complex

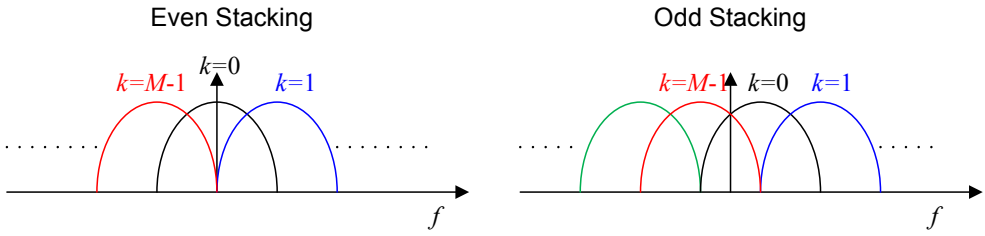

Figure 2.8: Modulated filter banks with even and odd stacking.

exponential. In the last case, a most general way to write the impulse response of the subchannel filters $h_k[m]$ is

$$h_k[m] = h_p[m]e^{-j\Delta f(k+k_0)(m+m_0)}, \tag{2.19}$$

where Δf is the subband frequency separation. Usually, in an M-channel filter bank, $\Delta f = 2\pi/M$. This expression coincides with the definition of the generalized DFT (GDFT) [17] filter banks, where m_0 and k_0 permit setting the time and frequency origins as desired. For example, depending on the frequency origin, the filter banks can be even or odd stacked. In an even stacked filter bank, $h_0[m]$ is centered around DC, whereas in the odd stacked case the first and last modulated filters $h_0[m]$ and $h_{M-1}[m]$ are symmetrically placed next to DC. These stacking options are depicted in Figure 2.8. The exponentially modulated filter bank (EMFB) [7, 8, 143] utilized in the narrowband interference cancellation scheme of Chapter 3 is odd stacked. An example for even stacking is the FBMC/offset QAM (FBMC/OQAM, also called OFDM/OQAM) [118] filter bank used in most of the multicarrier research of Chapter 4.

First, orthogonal cosine modulated filter banks appeared [129], where the same prototype is used to obtain the subband filters in the analysis and in the synthesis bank. The orthogonality term comes from grouping equations (2.11)-(2.14) into matrices that relate the input signal and its aliased versions with the output and its aliased versions. The transfer functions of the subchannel filters and their aliased versions stack up to matrices and perfect reconstruction can be obtained if the matrices of the analysis filters and the synthesis filters are orthogonal to each other, i.e., one is the conjugate transpose of the other. This leads to the property that the analysis filters $f_k[m]$ and the synthesis filters $g_k[m]$ are just the complex conjugated and time reversed version of each other, i.e.,

$$g_k[m] = f_k^*[L_p - 1 - m], \tag{2.20}$$

where $*$ is the complex conjugation operator. If the filters are real valued and have linear phase, then the analysis and synthesis subband filters are the same. It was shown in [8], that a PR prototype filter designed for an M-channel cosine modulated filter bank also yields perfect reconstruction for a similarly sized sine modulated filter bank. Moreover, the same prototype filter can provide PR in a complex modulated filter of $2M$ channels [66]. There is a small possibility for confusion here, since in real modulated filter banks the number of subbands is referred to half of the spectrum and in complex filter banks it is referred to the whole spectrum. In an M-channel cosine modulated filter bank, each subchannel filter is separated from the next by π/M, and the negative part of the spectrum is not considered because the signals and the filter bank are real. In complex modulated filter banks, the M subchannels are separated by $2\pi/M$ from their neighbors. Since this thesis basically builds on complex filter banks, M is from now on associated with the whole spectrum from $-\pi$ to π. With this notation in mind, the analysis filters of length L_p in the EMFB and in the FBMC/OQAM implementations can respectively be expressed as [56]

$$f_k^{\text{FBMC/OQAM}}[m] = h_p[m] e^{j\frac{2\pi k}{M}\left(m-\frac{L_p-1}{2}\right)} \tag{2.21}$$

$$f_k^{\text{EMFB}}[m] = h_p[m] e^{j\frac{2\pi}{M}\left(k+\frac{1}{2}\right)\left(m+\frac{M/2+1}{2}\right)}, \tag{2.22}$$

and the corresponding synthesis filters are obtained applying equation (2.20).

Here it is important to mention that critical sampling cannot directly be obtained in linear-phase PR M-channel complex filter banks by changing the sampling rate by M at once. Instead, real and/or purely imaginary subband signals have to be used, together with up and downsampling of $M/2$ [143]. In the even stacked modified DFT (MDFT) filter banks [66], this is implemented by two-stage down- and upsampling. In the analysis bank subband filters, first downsampling by $M/2$, duplication of the signal and delay of one sample for one copy of it takes place, before the final downsampling by 2 and taking the real or imaginary part, depending on the branch. The inverse processing takes place at the synthesis bank. In the exponentially modulated filter banks of [143], critical sampling is achieved when taking the real part of the subband signals after analysis, downsampling by $M/2$ and possible processing at oversampled rate. This does not signify a disadvantage, for example when comparing the transmission rates of EMFB with OFDM in multicarrier communications. Transmitting two real valued symbols at subcarrier rate $f_s/\frac{M}{2}$ is equivalent to transmitting one complex symbol at subcarrier rate f_s/M.

2.3 Filter Bank Implementation

There are some important aspects that have to be considered when implementing a modulated filter bank. The prototype filter has to be designed and optimized to fulfill the criteria established by the application for which the bank is going to be used. Then, the implementation of the modulated bank with the designed prototype offers some alternatives with effect on computational complexity. These aspects interact with each other and are briefly introduced in the following subsections. For detailed analysis and further interesting implementation issues, such as the effect of quantizing the subband filter coefficients with a limited number of bits, the interested reader is referred to [143].

2.3.1 Prototype Design

Orthogonal modulated filter banks are often designed by modulating a linear-phase lowpass FIR prototype filter with good spectral localization. Since bands of $2\pi/M$ bandwidth are desired, the cut-off frequency of the prototype filter is $\omega_c = \pi/M$ and the stopband edge ω_s depends on the excess bandwidth or roll-off factor ρ as

$$\omega_s = \frac{(1+\rho)\pi}{M}. \tag{2.23}$$

The roll-off factor $\rho > 0$ determines how much adjacent filters overlap. For example, if $\rho = 1$ the stopband edge is located at the center of the adjacent subchannels, i.e. only adjacent subbands overlap. Assuming that the filter has been designed with good selectivity, the effect of frequencies further away from the stoppand edge is negligible. The subchannel filter examples in Figures 1.2 and 2.8 have $\rho = 1$ and the cut-off frequency of the subband filters is the point where the frequency responses of adjacent filters cross each other.

Prototype filters of order $KM-1$, where K is an integer, have been proven to result in highly frequency selective PR filter banks [82]. The overlapping factor K indicates how much time overlap there is in consecutive filtered blocks of $M/2$ samples at high rate. The term "overlapping" comes from the interpretation of the PR filter banks as orthogonal transforms in which the basis functions (subchannel filters) overlap in time, such as the extended lapped transform (ELT). For $K = 1$ and $K = 2$ there are closed form analytical expressions for the prototype filter that provides PR in a cosine modulated filter bank [81], and therefore also in the complex modulated filter bank.

For higher overlapping factor values, the prototype filter has to be designed by optimizing its coefficients to fulfill the desired conditions. They are usually stopband attenuation level, cut-off frequency, passband transition width and PR constraints. If NPR is desired, then the PR constraints are relaxed and acceptable distortion and aliasing levels are defined to be met by the system. Generally, when using NPR prototype filters, the same attenuation as in PR can be achieved with shorter filter lengths, or, conversely, filters of the same length as PR prototype filters can achieve higher stopband attenuation. Different criteria to optimize the prototype filter are described in [18, 142, 143]:

Least squares: This criterion aims to minimize the energy of the stopband of the prototype filter. It presents low stopband attenuation at the stopband edge, but the attenuation quickly increases when moving further away from the passband.

Minimax: The objective here is to minimize the maximum ripple value of the frequency response in the stopband. The stopband attenuation at the edge is high, but the stopband level has an almost constant value over the whole stopband, with increased total energy.

Peak constraint least squares: Intermediate solution that minimizes the stopband energy subject to a maximum ripple value.

Total interference: In NPR designs, this criterion, which complements the desired spectral mask constraints, has as a goal to minimize the total interference originating from the filter bank, i.e., intersymbol and intercarrier interferences (ISI & ICI).

2.3.2 Efficient Implementation and Complexity

The modulated filter banks can be implemented directly by obtaining the modulated versions of the prototype filter optimized above and then filtering and downsampling in the analysis bank or upsampling and filtering in the synthesis part. However, this implies filtering at the high rate and then, in the analysis case, discarding $N-1$ samples after downsampling by N. This is clearly not efficient and leads to a high number of operations. Instead, the multirate identities in Figure 2.7 can be used to perform the filtering at low rate, along with exploiting other characteristics of the prototype filter and the modulation part.

Cosine and sine modulated filter banks can efficiently be implemented with the help of the discrete cosine or sine transforms (DCT/DST) and preceding logic [81, 143]. One solution is based on the fast ELT. The DCT-IV (DST-IV for sine modulated filter banks) performs the modulation and the prototype filter is obtained from cascaded and orthogonal structures defined by butterfly matrices in which only the diagonal and anti-diagonal are non-zeros. In the analysis bank, the filter is first implemented by the butterflies after downsampling and then the block transform is applied. These operations are performed in the inverse order in the synthesis bank.

Another efficient implementation structure is based on the polyphase decomposition of the filter bank. In the analysis bank, a polyphase filter structure follows the downsampling. Then a cosine or sine modulation block that can be built using DCT-IV or DST-IV, respectively, is applied. These blocks are configured in inverse order at the synthesis bank. The polyphase structure can be divided into polyphase component pairs sharing a common delay line. In the case of PR banks, the polyphase component pairs can be represented by two-channel lossless rotation lattices [129].

Applying the mentioned structures, the number of multiplications and additions needed in the filter banks can be reduced from a quadratic order of the number of subbands M to a log-linear order ($O(M^2) \rightarrow O(M \log(M))$).

The filter banks utilized during the research leading to this thesis are complex filter banks for efficient processing of complex signals. Therefore, it is interesting to build them based on efficient implementation structures, too. In the case of the odd stacked EMFBs, the efficient structures mentioned above for the sine and cosine modulated filter banks can be combined to yield an efficient EMFB implementation. The way to connect them to yield the desired subbands in the analysis-synthesis configuration is presented in Figure 2.9 [143], [S1]. For the 2x oversampled transmultiplexer configuration that is useful in multicarrier signal processing, an implementation based on DFT and polyphase filters has also been proposed in [141].

More recently, we have been using the even stacked FBMC/OQAM filter banks. The FBMC/OQAM model is equivalent to the MDFT model [66, 118], and has efficient implementation structures based on the inverse and forward fast Fourier transforms, (IFFT/FFT), at the synthesis and analysis bank, respectively. The fast Fourier transforms are accompanied by polyphase filtering [13], to implement the subchannel selectivity. Efficient implementation structures for the analysis and synthesis banks are sketched in Figure 2.10 [56]. Here it is necessary to say that, although the implementations of EMFB and

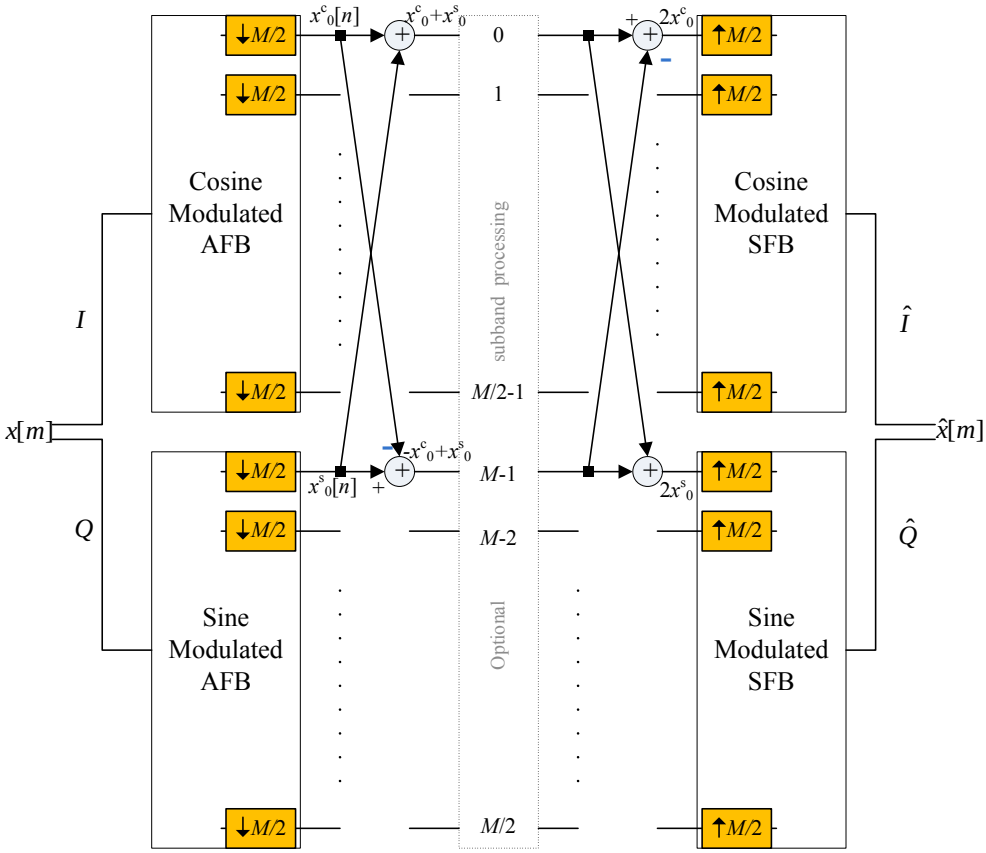

Figure 2.9: Efficient implementation of the EMFB based on cosine and sine modulated filter banks.

FBMC/OQAM depicted in Figures 2.9 and 2.10 may seem very different, both approaches are very closely related to each other. In [143] the relation between an EMFB bank with subbands carrying real valued Q-level modulated signals and an MDFT (FBMC/OQAM) with subbands carrying complex valued Q^2-level modulated signals is detailed with the help of the GDFT. Therefore, signal processing solutions based on one implementation can easily be adjusted with minimal modifications to work with the other implementation.

These efficient implementation structures for the complex filter banks drastically reduce the amount of operations compared to the direct implementation. Nevertheless, it is necessary to point out that the computational complexity (number of multiplications) is still considerably higher than when comparing with the basic FFT-based OFDM [56].

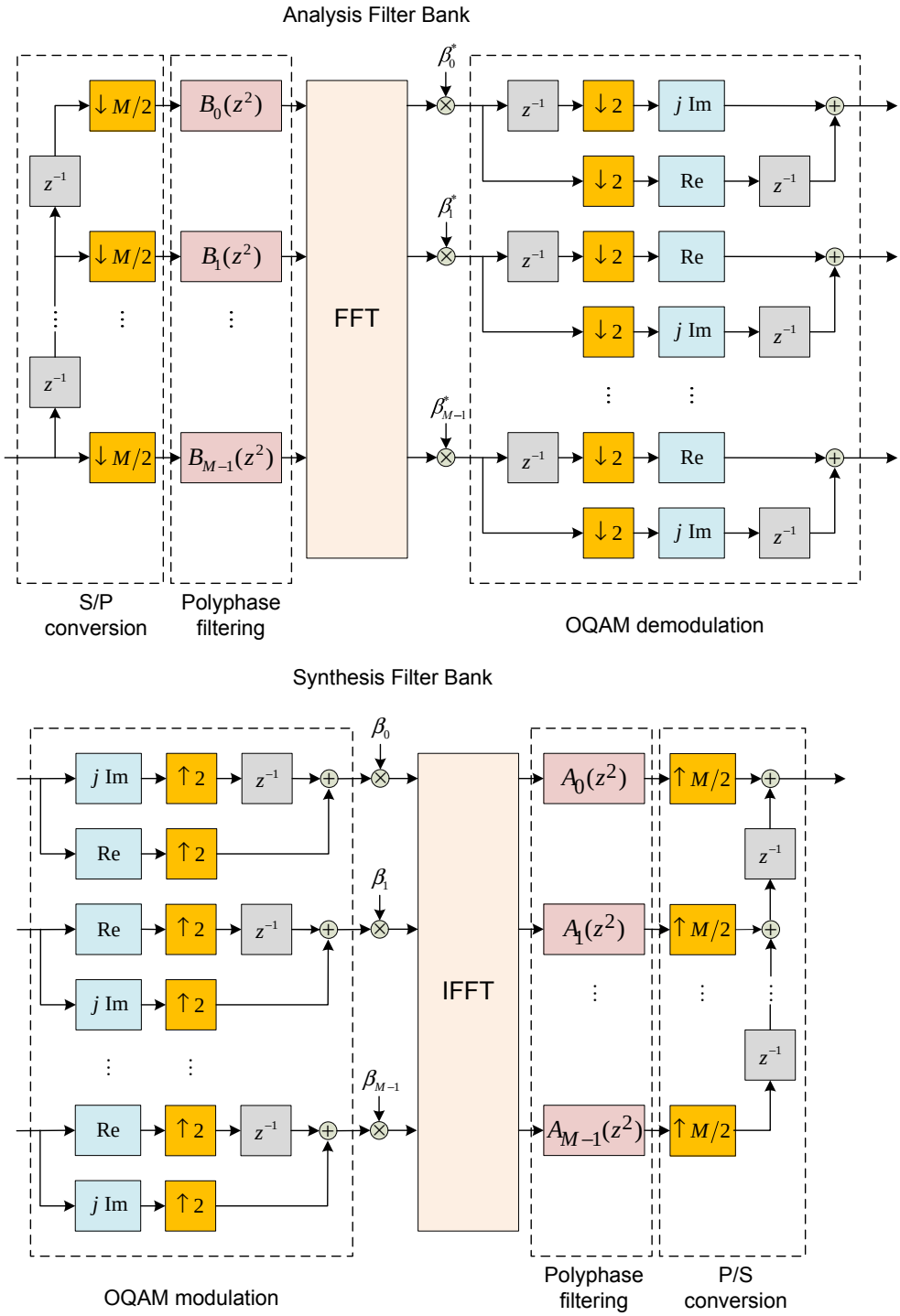

Figure 2.10: Efficient implementation of the FBMC/OQAM filter banks.

Chapter 3

Filter Banks for Narrowband Interference Mitigation

A narrowband interference or interferer (NBI) is an additive signal that distorts a desired signal by occupying only a small fraction of its bandwidth. In a simple AWGN channel model, one can write the received signal $r(t)$ as

$$r(t) = s(t) + i(t) + \eta(t), \tag{3.1}$$

where $s(t)$ is the desired signal, $i(t)$ is the NBI and $\eta(t)$ is the AWG noise. The interferer can be generated on purpose to interfere with the given signal as for example in intentional jamming in military electronic warfare. It can also be a signal that appears inside the bandwidth of the signal of interest, for example in overlaid transmission, or a spurious spectral component produced by RF imperfections in a transmitter. Figure 3.1 shows how a QPSK signal and its constellation are distorted by a continuous wave interference with the same power.

Spread spectrum (SS) communication techniques are a form of transmission that count inherent robustness against NBI among their advantages [99]. In spread spectrum communications, the transmitted signal occupies (much) more bandwidth than theoretically necessary to transmit the desired information. Its exciting history [98, 116] originates at the beginning of the 20th century, but it is during World War II that the use of SS communications lifts off in military applications, finally finding its way to commercial applications since the 1980ies. A curious anecdote is that Hollywood actress Hedy Lamarr was granted a patent [84] on one type of spread spectrum implementation, namely frequency hopping spread spectrum. In frequency hopping or

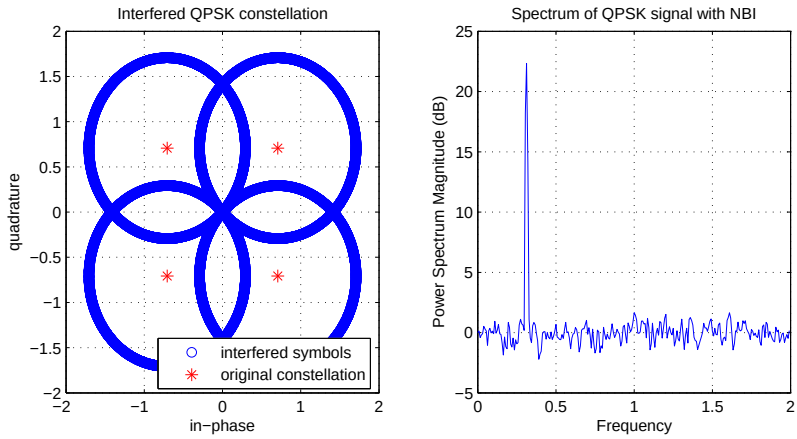

Figure 3.1: Constellation and spectrum of a QPSK signal affected by NBI.

time hopping SS, the signal hops among pseudorandomly changing frequency or time allocations, respectively. Other implementations are direct sequence (DS) SS, and chirp SS, in which chirp modulation [15] is used to generate the spectrally spread signal. DSSS is used in code division multiple access systems (CDMA) like IS-95 [10] and the third generation CDMA based standards such as wideband CDMA (WCDMA) and CDMA2000 [1, 62]. Chirp SS is found in the low rate wireless personal area network (WPAN) standard IEEE 802.15.4a [4].

The loss in spectral efficiency because of using a higher bandwidth than needed is compensated by the following advantages of SS communications [99]:

- *Good performance in environments with interference* compared with conventional narrowband modulation techniques.

- *Low power spectral density,* which permits communications with a low probability of detection and intercept, and is especially interesting for military applications.

- *Resistance to multi-path fading,* because of the signal's similarity to white noise. The autocorrelation function of the spread signal is like an impulse function and different multi-paths can be independently detected and coherently combined to effectively raise the signal to noise ratio (SNR). The RAKE Receiver takes advantage of this property.

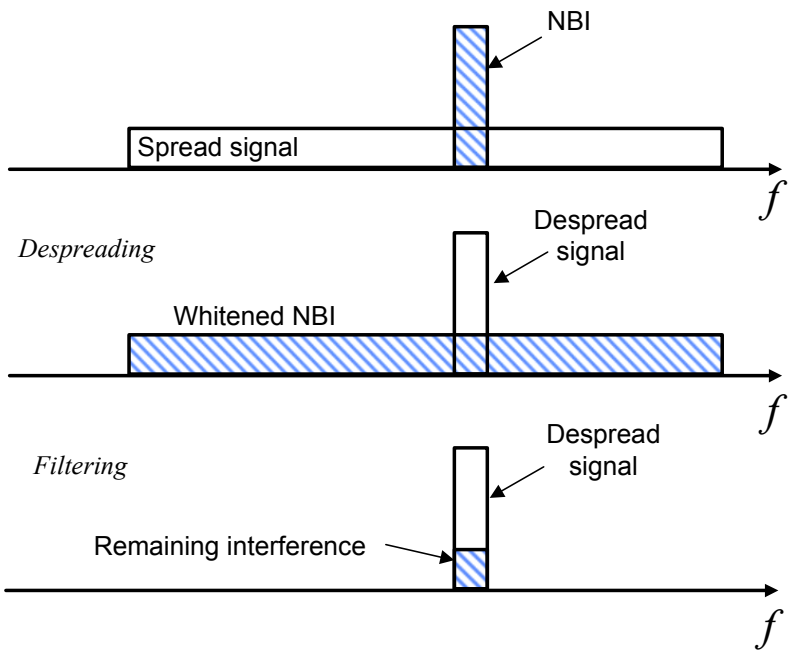

Figure 3.2: Robustness against NBI in a spread spectrum signal.

- *Privacy and selective addressing capability for multiple access communications.* The signal of each user is spread by a unique spreading signal, in principle only known to the communicating parts, and, also after despreading, it looks like noise to other users with other spreading signals.

The research relevant to this chapter was performed with DSSS signals, in which every original data bit is multiplied by a pseudorandom (or pseudonoise (PN)) sequence of 'chips' (0s and 1s). This increases the bandwidth by the length of the sequence, also referred to as spreading gain. At the other end, the received signal is despread: the received chips are correlated with the same sequence. Despreading yields the originally transmitted low bandwidth bits. By carefully designing the PN-sequences with the adequate autocorrelation and cross-correlation properties, only the desired signal is recovered into the low bandwidth. Other wideband signals, e.g., other code division multiplexes or noise, remain additive white Gaussian noise (AWGN) -like. Narrowband signals falling inside the spread spectrum are whitened at the despreading stage, as sketched in Figure 3.2. Only some residual, AWGN-like distortion remains. Nevertheless, the depicted robustness to the NBI is limited, and

when the interferer is much stronger than the desired signal, the whitened interference remainder might well be strong enough to render the resulting signal useless. This is not such an unlikely case, since very often SS signals are transmitted at very low powers, as explained above. In this case, NBI mitigation techniques have to be applied to enhance the quality of the received signal [99].

The narrowband interferer's property of spectral localization makes it easier to mitigate its effect, compared to other more common distortion types, such as additive white Gaussian noise (AWGN) or multipath channel propagation. Ideal mitigation means removing the interfering signal without affecting the desired signal. Not affecting the signal is almost impossible, and the common approach is to excise the interferer, by filtering it out of the signal bandwidth. Even though part of the signal is also removed, the BER performance is improved [87], as exemplified in Figure 3.3.

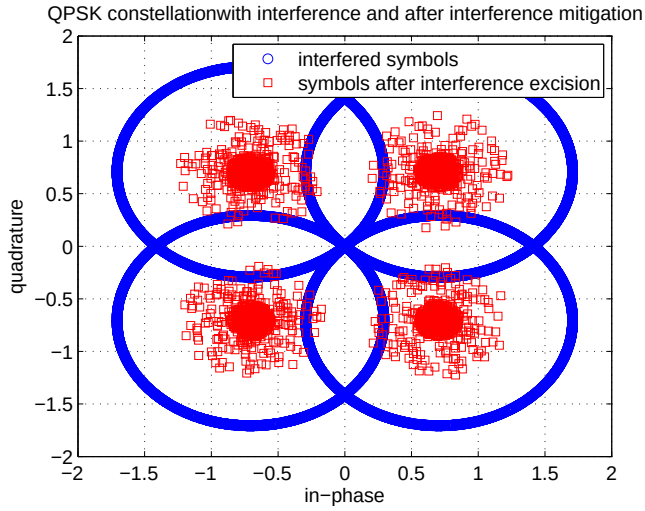

Figure 3.3: Constellation of a QPSK signal affected by NBI and after excision of the NBI.

If the receiver has multiple antennas, spatial filtering (beamforming) [134] can be applied to steer a null antenna gain towards the direction of interference and thus silencing it to the receiver. However, this is a technique that can be applied to all kinds of interference coming from a known direction, not only NBI, and is not further pursued here. The focus of the research in this part was the mitigation of NBI affecting a single DS-SS signal. Milstein's milestone

review of early methods to achieve that objective can be found in [87], with further developments being reviewed in [95] and [71] A more recent review, focusing on NBI mitigation in the multiuser application of DS-SS as multiple access method, namely CDMA, has been published by Buzzi et al. [20].

The NBI interference mitigation methods can be classified into time and frequency domain methods, as for example in [87]. With the advent of more advanced, non-linear mitigation techniques, the classification was reformulated into linear and non-linear methods, including the frequency domain techniques in the former group [71, 95]. Here we stick to the first interpretation, briefly introducing the time domain methods. Then the focus is directed to the frequency domain methods, since our filter bank based approach belongs to this group of techniques.

3.1 Narrowband Interference Mitigation in Time Domain

Time domain NBI mitigation is mainly based on filters that estimate the narrowband interferer to then subtract it from the received signal, hoping that an interference-less signal remains. Exploiting the narrowband properties of the interference, the result is notch filtering or whitening of the received signal. To estimate the NBI, linear predictor filters, such as the Wiener filter, or interpolation filters can be used. Both make use of the fact that the narrowband interference samples are correlated. For example, it can be modeled as an autoregressive process [99]. Hence, the current value of the interference can be predicted from the previous samples (predictor) or from the previous and future samples (interpolator). The prediction or interpolation filter can be implemented with a one sided or two sided tapped delay line, respectively [87]. The result is equivalent to whitening the input signal.

Some improvement can be obtained, if instead of whitening the input signal, only the noise and interference is whitened. This can be achieved by using a estimate of the NBI-free signal after mitigation and feeding it back to the interference rejection filter. By subtracting that estimate from the input, ideally the noise and the NBI is sent through the estimation filter and a better elimination of the NBI is obtained. Direct feedback is susceptible to error propagation, but in [121] it is shown, that this effect is negligible.

Other approaches reviewed in [71, 87], not directly related to digital signal processing, include adaptive analog-to-digital conversion and estimation of the

NBI with help of a phase locked loop (PLL). If the interference is narrow and strong enough, the PLL can lock its phase to the NBI and this estimate can be used to remove it from the signal of interest.

Usually, the underlying statistics of the AR process modeling the NBI are not known or the interferer is non-stationary, changing in time. In these cases, adaptive algorithms [43], such as for example least mean squares (LMS) have to be applied to update the filter coefficients. The reviewing papers cited in this section describe several variations and evolutions of adaptive algorithms for NBI rejection, trying to improve the trade-off between the NBI estimation accuracy and the convergence speed of the adaptive methods. Some authors [74, 113] propose the adaptive lattice filter structure for faster convergence and because the convergence of each lattice is independent of each other.

The previously presented methods to estimate the NBI assume that the signal in which it is embedded is Gaussian. In that case, the linear prediction/interpolation is optimal in the minimum mean squared error (MMSE) sense. In the 1990ies the research shifted towards non-linear prediction/interpolation filters based on the knowledge that the DSSS signal is not Gaussian and the linear approaches cannot yield optimal solutions[95, 99]. Poor and Rush [95] model the CDMA signal as having a binomial density function. The same authors assume that the interferer can be a digitally modulated signal, for example an overlaid communication with CDMA, and introduce the use of multiuser detection techniques. The NBI is then modeled as a virtual user of the CDMA signal and the multiuser detection techniques are applied to separate it from the useful signal. In [20], different adaptive multiuser detection algorithms are reviewed and compared. More recent research (after the publication of [P1]) focuses on locally optimum detection [106, 107].

3.2 Narrowband Interference Mitigation in Frequency Domain

The rationale for mitigating NBI in the frequency domain seems quite obvious. A strong interferer with small bandwidth compared to the spectrally relatively flat signal of interest will stand out in the form of a peak if looking at the spectrum of the composite signal. The spectral representation is obtained by means of its transform to the frequency domain. Here, the frequencies containing NBI can be processed independently to mitigate the interference. The affected frequencies can be nulled, notching out the jammer, as shown in

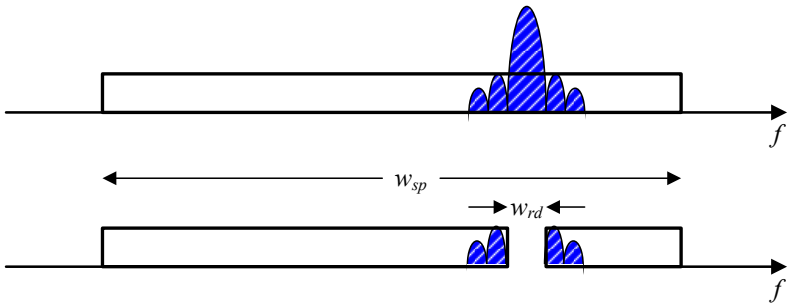

Figure 3.4: NBI excision on the frequencies at which the interference is detected.

Figure 3.4. This is often called interference excision. The performance of the excision method can be bounded by calculating the degradation of the SNR due to 'biting off' a chunk of the DSSS signal. Approximating that the excised spectral region is the rectangular band w_{rd} and the overall bandwidth of the spread spectrum signal is w_{rd}, the SNR degradation compared to the NBI-less case in AWGN is [96]

$$\Delta\frac{S}{N} = 10\log_{10}\left(1 - \frac{w_{rd}}{w_{sp}}\right). \tag{3.2}$$

Other choices are scaling the frequency components such as to whiten the spectrum [65, 97] or substituting the interfered frequencies with other values exploiting some knowledge of the desired signal [28]. After processing, the inverse transform is applied to obtain the interference-less signal. The subband system from Figure 2.2 is a valid means for performing these operations.

The resolution of the processed band depends on the transformation, therefore it is usually not possible to exactly match the interference when removing its band. On the other hand, no further assumptions about the NBI are made, so it can have any statistics as long as it has narrow bandwidth with respect to the signal of interest. The main advantage of using transform domain mitigation is that it can adapt faster to changing interference environments, compared to adaptive filtering in time domain approaches [5, 96].

First approaches in the frequency domain used real-time Fourier transforms on the continuous-time received signal to obtain its frequency distribution [86, 87]. As processing moved from the analog to the digital side of the receivers, the discrete version of the Fourier transform (DFT) and its fast implementation, the FFT, was applied to yield the necessary frequency repre-

sentation of the received signal. However, the FFT has the problem of slowly decaying sidelobes. The first ones reach only 13 dB of attenuation, as described in Section 1.2 and depicted in Figure 1.3. A strong interference will not only appear in its corresponding frequency bins, but it will also be present, attenuated only by the limited attenuation provided by the FFT, in neighboring frequency bins. The stronger the interference, the wider its energy will leak around its frequency location. One way to improve the sidelobe performance in the FFT is to apply prior windowing [69], although this degrades the desired signal when the NBI power is low [39, 148]. Another line of research, at the change of the millennium, focused on applying other types of transforms, moving from block transforms to lapped transforms (LTs) [5, 44], such as the modulated lapped transform (MLT) and ELTs and the closely related filter banks. In the LTs, the spectral containment is a design parameter, so the spectral leakage can be avoided very effectively.

Our Publication [P1] follows this line of research successfully applying the exponentially modulated filter bank in Figure 2.9 to excise the interferer. By using a complex filter bank, which can be implemented for example with the ELT, complex signals can be processed. This is useful for efficient processing of the interfered DSSS signal at baseband. Our research attempted to expand the results by applying the methods presented in [28]: The fact that the desired signal was real, suggested to clone the symmetric frequencies with respect to DC (the frequency origin), after taking the complex conjugate, to fill the gap left after excision. Unfortunately, the performance did not improve in our results.

As already mentioned in Chapter 2, the computational complexity of the EMFB is higher than the FFT. Nevertheless, with the technology of 2002 [S2] it was already viable to implement the whole excision system with overlapping factor $K = 5$ on a single TMS320C6414 digital signal processor (DSP) with sampling rate in the order of 6 to 9 MHz, depending on the size of the filter bank.

Here it is also worth mentioning that when the spectral containment is increased, the basis functions of the transforms (length of the subchannel filters in the filter bank interpretation) become increasingly long. The abruptness in frequency comes at the cost of expansion in time domain, which in turn is not favorable when the interference is quickly changing its frequency position. This could happen for example if the interference or the reference system includes frequency hopping features. Therefore, some research has concentrated on analyzing the narrowband interference as accurately as possible in

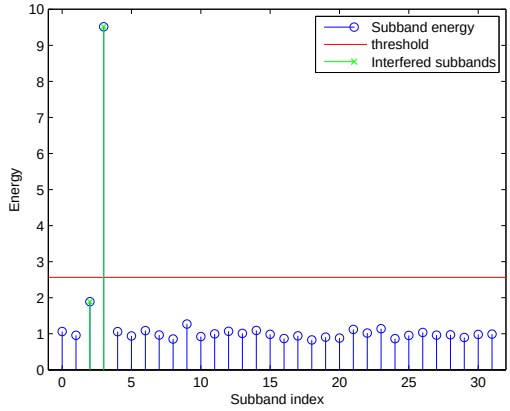

Figure 3.5: Threshold detection principle.

the time-frequency plane to optimize the trade-off between the spectral and time containments. For example, in [5] an adaptive time-frequency excision scheme decides in which domain it is more convenient to perform NBI mitigation. The authors in [85] use the wavelet transform, in which the trade-off between the time and frequency resolution can be tuned.

3.2.1 NBI Detection

Detecting presence of an NBI is a binary hypothesis testing problem. Recently, fueled by the research in the cognitive radio field of spectral sensing, this area has gained momentum and efforts are focused toward detecting a low energy signal (primary user) embedded in noise [122]. Fortunately, the NBI affecting a DSSS signal has to be quite powerful to affect the performance due to the processing gain of the spreading code and the interference can be easily detected using thresholds. This is sketched in Figure 3.5.

The threshold could be fixed, but it is more logical to have a threshold that adapts to the signal conditions. In any case, it is important to carefully set it, since too high a threshold might lower the probability of detection of the NBI and too low a threshold might return false positives. In [96] different approaches to set the threshold in an AWGN channel are explored. The general idea is to obtain an estimate of the energy in the subbands after the transformation into frequency domain for calculating an estimation of what subband power should be expected. A certain safety margin t_f is then added

and all the subbands that exceed the computed threshold θ_{th} apply mitigation processing as described above: excision, scaling, etc. The authors in [96] conclude that using the arithmetic mean to calculate the subband energy averages yields best performance. Therefore, this was the approach utilized in [P1]. For example, in the excision case, assuming zero mean subband signals,

$$\hat{x}_k[n] = \begin{cases} x_k[n] & \text{if } x_k[n] < \theta_{th} \\ 0 & \text{if } x_k[n] \geq \theta_{th}, \end{cases} \tag{3.3}$$

where

$$\theta_{th} = \frac{t_f}{M} \sum_{k=0}^{M-1} E\left[|x_k[n]|^2\right]. \tag{3.4}$$

Here, $x_k[n]$ and $\hat{x}_k[n]$ are the subband signals before and after the excision processing, respectively.

Figure 3.5 also reflects a possible shortcoming of the presented way for calculating the threshold. A very narrow interferer mainly affects one subband (number 3 in the Figure). However, because neighboring subbands overlap as described in Chapter 2, the NBI is also present in the neighboring subband. With a strong interferer, it might be that the average power calculated for setting the threshold θ_{th} is so high that the interfered subband (2) is not detected as such and excision does not take place there. In [P1] we present a recursively adaptive threshold that iterates the calculation of θ_{th} after eliminating the interfered subbands. The computation is iterated until no more subbands are left that exceed θ_{th}. The iteratively adaptive threshold can be described by

$$\theta_{th}^{(i)} = \frac{t_f}{M^{(i)}} \sum_{\substack{k=0 \\ k \notin R^{(i)}}}^{M-1} E\left[|x_k[n]|^2\right], \tag{3.5}$$

where $R^{(i)}$ is the set of indices of subbands in which a NBI has been detected before iteration i and $M^{(i)}$ is the difference between M and the number of elements in $R^{(i)}$. This iteratively adaptive approach increases the excision performance and has been independently studied by Henttu and Saarnisaari, who were granted several patents on it [45, 46, 47].

Further fine tuning could be obtained by adapting t_f in equations (3.4) and (3.5). Furthermore, if transmission occurs through a frequency selective channel and channel knowledge is available, the threshold can be shaped according to the frequency response of the channel.

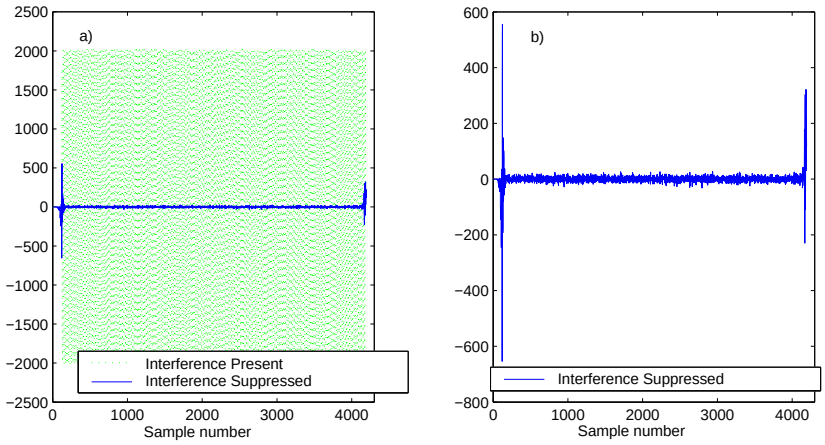

Figure 3.6: Transient occurrence after NBI mitigation. (a) Interfered signal and processed signal. (b) Processed signal only, for better appreciation.

3.2.2 Post-NBI-Mitigation Transient Mitigation

When the interference frequency changes or appears or disappears instantaneously, it is natural to use relatively short processing blocks of an integer multiple of the symbol interval. In such an environment, excising strong NBI with the filter bank leads to transients similar to the edge effects in transform domain image processing. The effect is visualized in Figure 3.6. Plot (a) shows the samples of the signal without interference suppression and the same signal with the interference removed. Plot (b) shows only the signal in which the interference has been removed, and now the transients are clearly visible at the beginning and the end of the sample sequence. These transients are an important source of bit errors after despreading, if no further correction takes place. In [P1], a shortened despreading approach is proposed to reduce the number of errors without having to give up the leading and/or trailing bit.

3.2.3 Recent Developments in NBI Mitigation

The research that culminated with publication [P1] was performed during the first years of the century. After the publication in 2004, the author's focus moved to filter bank based multicarrier development as described in Chapter 4. Nevertheless, the research in NBI mitigation has continued to produce a vast amount of results since then. The advances are in many areas, like perfecting

the performance in different interference scenarios, various spectrum spreading techniques, statistical signal processing methods and so on. For example, [108] proposes applying jammer knowledge to optimize the performance in frequency hopping minimum frequency shift keying satellite SS communications. A recent overview of the research up to 2005 can be found in [109]. One line of research follows the path of [20] already mentioned above, in which multiuser detection techniques are applied to improve detection performance and synchronization in the presence of one or several narrowband interferers [19, 152] and using statistical knowledge of the interference to improve performance [147]. More closely related to the presented filter bank approach, [148, 149] use the modified DFT to achieve NBI mitigation. Another interesting approach is to adaptively apply the most convenient transform before removing the interferer [79, 136] or to adaptively select the most convenient suppression algorithm after the frequency domain transformation [21]. The authors in [75] propose estimating the tone interferer in the frequency domain to generate an error signal to subtract from the interfered signal, avoiding thus the inverse transform. The generalization of multiple antenna receivers and the increasing computational power of the hardware permit complex statistical methods like independent component analysis for blindly estimating the interference and its direction of arrival for subsequent cancellation [101].

As a final remark to this section, it is delightful to notice that a lot of the results in this field originate from Finland, especially, but not only, from CWC at the University of Oulu. References [44, 45, 46, 47, 69, 96, 97, 101, 109, 136] above were published by Finnish authors, and the research leading to [S2] was done in Finland, although the main author is not Finnish. The interested reader can find much more literature regarding NBI mitigation from these authors than the references briefly introduced here.

3.3 Further Applications of Analysis-Synthesis Systems

In the spirit of advocating for the use of filter banks, the author would like to mention several other applications of the filter banks in the analysis-synthesis configuration, although not directly related to the problem of narrowband interference mitigation. Subband systems can be used for subband coding, for example for compression of video and audio signals. Other applications include error correction coding, where the filter banks are used with different

sampling rate conversion factors, and signal enhancement. Subband systems are also used for audio and image enhancement. Using an analysis-synthesis filter bank pair at both transmitter and receiver, low probability of intercept transmissions can be generated. Descriptions of these and other applications can be found in [5, 81]. Different types of transforms or filter banks are derived depending on the requirements of each application.

Closer related to the type of filter banks used in our research group, an interesting communications application is the frequency domain equalization in single carrier systems (SC-FDE) [30]. The transmitted signal is modulated onto a single carrier, avoiding problems such as the effect of high peak to average power ratio of multicarrier signals. At the receiver, the subband system permits frequency domain equalization [157] and also the use of the equalizer for reducing the effect of NBI [S3]. In [53], a filter bank based approach for SC-FDMA (also known as DFT-spread-OFDMA) [89] is presented under the name of FB-spread-FBMC. Here, the analysis-synthesis bank with different down- and upsampling factors is used in the transmitter to spread a user's data and allocate it to the desired spectral bands. At the receiver, a subband system performing the inverse operation recovers the originally transmitted data.

Chapter 4

Channel Synchronization in FBMC

The principle of efficient multicarrier transmission is conceptually quite simple. Data is modulated onto different carriers, called subcarriers and multiplexed in frequency. Using orthogonal transforms, the spectra of the subcarriers can be overlapping, leading to better usage of the spectral resources. The idea, using a synthesis filter bank at the transmitter, is sketched in Figure 4.1. The figure also shows the simplicity in spectrally shaping the transmitted signal. At the receiver, the analysis filter bank implementing the inverse transform recovers the data, ideally free of system induced distortion. The simplest way to implement this technique is by means of the FFT. The sidelobe limitations already mentioned in the previous chapter have motivated research in modulated filter banks with pulse shapes that can provide better spectral containment.

Pulse shaping in multicarrier transmission dates back to the early work of Chang [23] and Saltzberg [110] in the 60'ies. Since then, various multicarrier concepts based on the Nyquist pulse shaping idea with symbols that overlap in time and bandlimited subcarrier signals have been developed by Hirosaki [49], Le Floch et al. [72], Sandberg and Tzannes [111], Vahlin and Holte [128], Wiegand and Fliege [153], Nedic [91], Vandendorpe et al. [135], Van Acker et al. [131], Siohan et al.[118], Wyglinski et al. [155], Farhang-Boroujeny [31, 32], Phoong et al.[94], and others. One central ingredient in the later developments is the theory of efficiently implementable, modulation-based uniform filter banks, developed by Vetterli [137], Malvar [81], Vaidyanathan [129], Karp and Fliege[66] and Viholainen [143], among others. The implementations used in our research are based on the EMFB concept with ELTs in [143] and

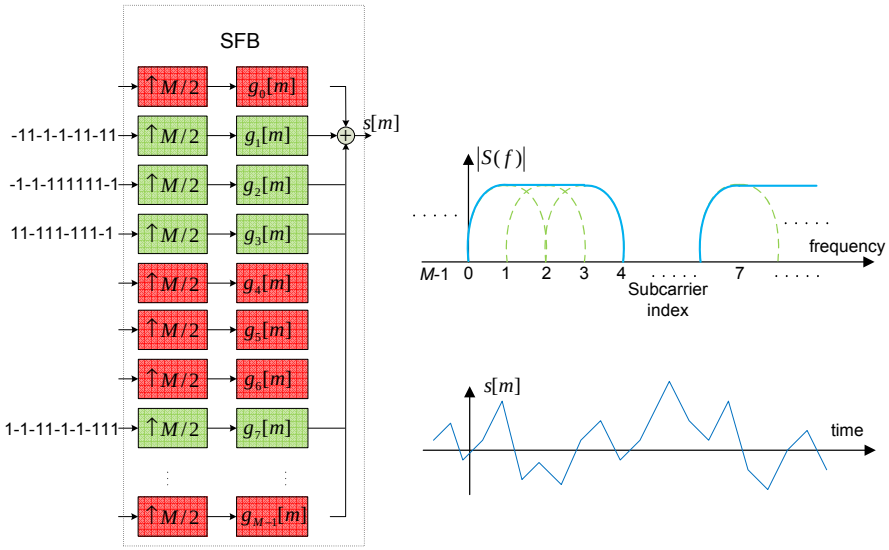

Figure 4.1: Efficient multicarrier transmission principle.

the FBMC/OQAM [118], efficiently implemented with DFT and polyphase filtering as in Bellanger and Daguet [13].

In Chapter 1 we introduced the advantages of MC modulation, counting among them the easier channel equalization. In OFDM, a cyclic prefix longer than the channel delay spread converted the propagation channel into flat fading at subcarrier level. FBMC lacks the CP but the frequency flatness of subchannel responses is approximately valid if the ratio between subcarrier spacing and the coherence bandwidth of the channel is small enough, i.e., for high M. Otherwise, the channel becomes frequency selective at subcarrier level, usually mildly, as exemplified in Figure 4.2. This fact is the starting point of this chapter, which builds on the analysis of the subchannel response of the propagation channel to propose a low complexity subchannel equalizer. The derived equalizer is tuned for NBI notching in Section 4.2. Then we study the means of estimating channel parameters to feed the equalizer for tuning its coefficients and for synchronizing the communications.

4.1 Channel Equalization

At the time of our research leading to [P2], the problem of equalizing the fading frequency-selective channel in the FBMC context was not so well understood

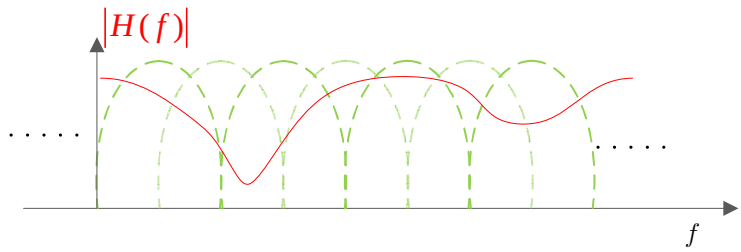

Figure 4.2: Mildly frequency selective channel response in the subchannels.

as in the DFT based systems. Three main approaches to solve this problem can be found in the literature. The first uses well localized FBMC waveforms i.e., the pulse energy both in time and frequency domains is well contained to limit the effect on consecutive symbols and neighboring subchannels [72, 118, 128]. In this context, a basic subcarrier equalizer structure of a single complex coefficient per subcarrier is usually considered. Another approach uses FIR filters as subcarrier equalizers with cross-connections between the adjacent subchannels to cancel the intercarrier interference (ICI) [111, 135]. A third line of studies applies a receiver filter bank structure providing oversampled subcarrier signals to avoid the cross connections between subchannels, and performs per-subcarrier equalization using FIR filters [49, 91, 131, 153, 155]. More recently, Waldhauser et al. have presented MMSE and decision feedback subcarrier equalizers explicitly designed for FBMC/OQAM [12, 145, 146]. The main idea here is that equalization of the oversampled subcarrier signals restores the orthogonality of the subcarrier waveforms and there is no need for cross-connections between the subcarriers. Our research contributed to this line of studies by developing low-complexity linear per-subcarrier channel equalizers for FBMC. Implementation examples as block diagrams for the EMFB and FBMC/OQAM types of transmultiplexers can be seen in Figure 4.3 a) and b), respectively. In the figure, the receiver with oversampled processing can be distinguished. The earlier contributions either lack connection to the theory of efficient multirate filter banks, use just a complex multiplier as subcarrier equalizer or, in case of non-trivial subcarrier equalizers, lack the analysis of needed equalizer length in practical wireless communication applications (many of such studies have focused purely on wireline transmission). Also various practical issues like peak-to-average power ratio and effects of timing and frequency offsets had not properly been addressed in this context before publication of [P2].

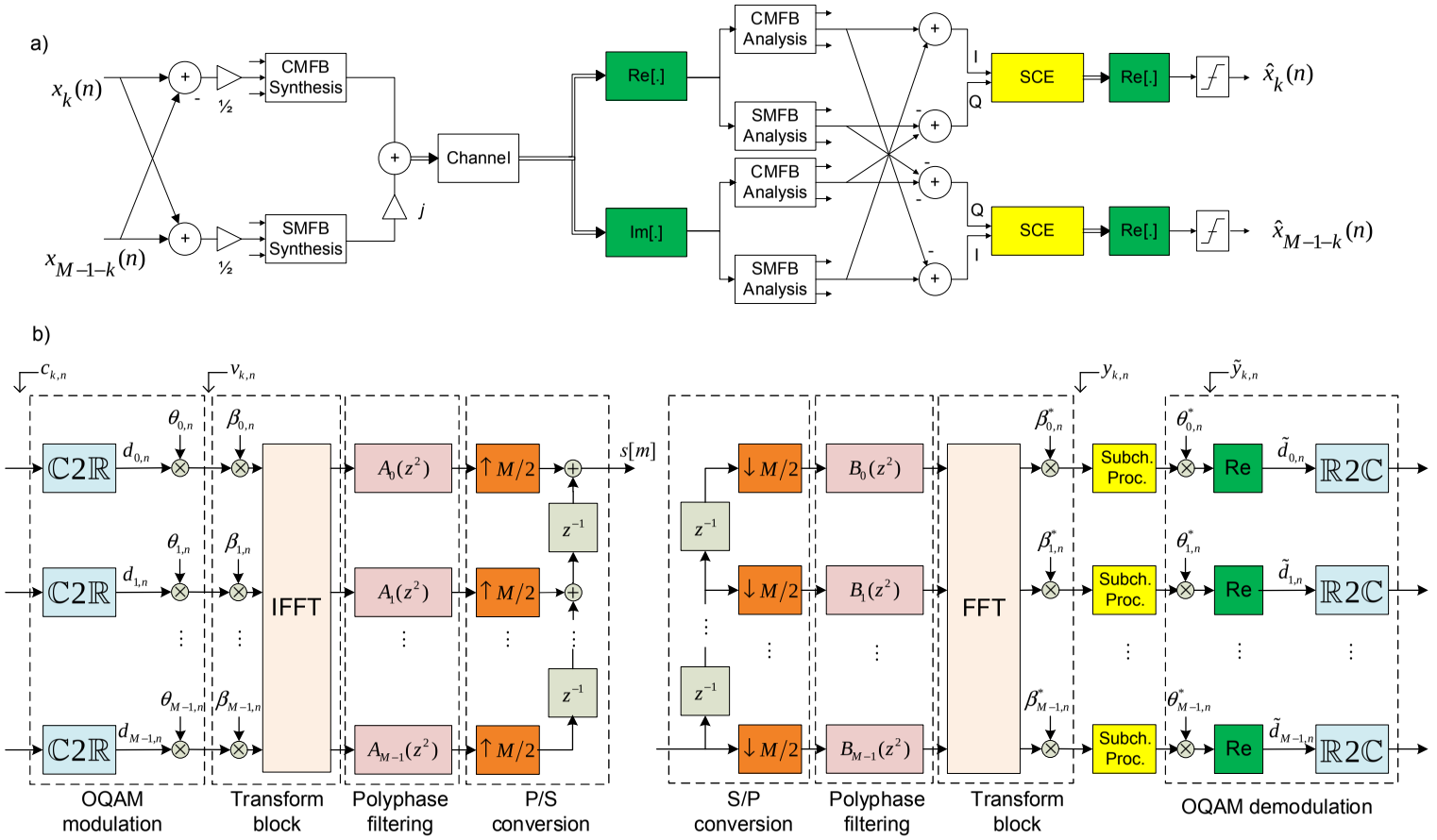

Figure 4.3: TMUX with oversampled analysis bank and per-subcarrier equalizers in (a) EMFB implementation and (b) FBMC/OQAM implementation.

The oversampled receiver is essential for the equalization studied in [P2]. In case of roll-off $\rho = 1.0$ or lower, non-aliased versions of the subchannel signals are obtained in the 2x-oversampled receiver, when complex (I/Q) signals are sampled at the symbol-rate, and complete channel equalization in an optimal manner is possible. As a result of the high stopband attenuation of the subchannel filters, there is practically no aliasing of the subchannel signals in the receiver bank. Thus, perfect equalization of the distorting channel within the subchannel passband and transition band regions would restore the orthogonality of the subchannel signals [91], completely eliminating ICI and the intersymbol interference (ISI).

4.1.1 Conditions for ISI and ICI Cancellation

The detailed derivation for canceling ISI and ICI can be found in [P2]. There, the analysis was performed for the odd stacked EMFB but the general results are valid for any of the related FBMC implementations with an oversampled receiver, taking into account the different subchannel filter definitions. Only the main results will be concisely summarized here.

With ideal sampling and no channel or with channel and ideal equalization, the desired subchannel signal, carried by the real part of the complex subchannel output, is orthogonal to the contiguous subchannel signal components occupying the imaginary part. The orthogonality between the subchannels is introduced when the linear-phase lowpass prototype $h_p[m]$ is exponentially frequency shifted as a bandpass filter, with 90-degree phase-shift between the carriers of the contiguous subchannels. This is the reason for taking the real part at the receiver to recover the desired signal, free from interference from the neighboring subchannels.

In practice, the non-ideal channel causes amplitude and phase distortion. ISI is mainly caused by the amplitude distortion. The phase distortion results in rotation between the I- and Q-components of the neighboring subchannel signals causing ICI or cross-talk between the subchannels. Limiting the sources of interference to the closest neighboring subchannels is justified if the filter bank design provides sufficiently high stopband attenuation, as visualized in Figure 4.4 for the first subband ($k = 0$).

The analysis in [P2], valid for PR filter banks and approximately for NPR designs, provides proof for this statement, yielding the following results for ICI and ISI cancellation at subchannel level:

Looking at Figure 4.3, the equalizer for subchannel k can be identified

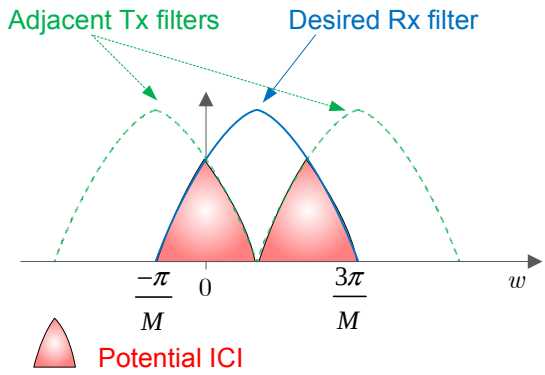

Figure 4.4: Potential ICI spectrum affecting subchannel $k = 0$ in the odd stacked EMFB implementation.

after the oversampled analysis bank and can be defined by $w_k[n]$. Using the multirate identities in Figure 2.7, an upsampled and non-causal version of it is denoted by

$$\bar{w}_k[m] = \begin{cases} w_k[2m/M], & \text{if } m = nM/2,\ n \in \mathbb{Z} \\ 0, & \text{otherwise.} \end{cases} \tag{4.1}$$

After rearranging the subchannel filter blocks and the channel with instantaneous impulse response in the baseband model $h[m]$, the compensated, overall response of the channel and equalizer cascade is

$$c_k[m] = h[m] \star \bar{w}_k[m], \tag{4.2}$$

and its version translated to baseband

$$\tilde{c}_k[m] = c_k[m] e^{-jmk2\pi/M}, \tag{4.3}$$

Cancellation of ICI is achieved when simultaneously

$$\begin{aligned} &\mathrm{Im}\left[\tilde{c}_k[m]\right] = 0 \\ &\mathrm{Im}\left[\tilde{c}_k[m] e^{-jm2\pi/M}\right] = 0. \end{aligned} \tag{4.4}$$

In frequency domain, the equalized channel frequency response is required to have symmetric amplitude and anti-symmetric phase with respect to both of the frequencies $k2\pi/M$ and $(k+1)2\pi/M$ to suppress both ICI components. Naturally, the ideal full-band channel equalization (resulting in constant amplitude and zero phase) implies both conditions. In our FBMC system, the

equalization is performed at low-rate, after filtering and decimation by $M/2$, and the mentioned two frequencies in the EMFB implementation correspond to 0 and π, i.e., the filtered and down-sampled portion of $H(e^{j\omega})$ in subchannel k multiplied by the equalizer $W_k(e^{j\omega})$ must fulfill the symmetry conditions for zero ICI. In this case, both symmetry conditions are equivalent (i.e, symmetric amplitude around 0 $\iff$ symmetric amplitude around π, and anti-symmetric phase around 0 $\iff$ anti-symmetric phase around π).

The intersymbol interference is suppressed when additionally

$$\mathrm{Re}\left[\tilde{c}_k[m]\right] = \delta[m] = \begin{cases} 1, & \text{if } m = 0 \\ 0, & \text{otherwise.} \end{cases} \tag{4.5}$$

The above conditions were derived in the high-rate, full-band case, and if the conditions are fully satisfied, ISI within the subchannel and ICI from the lower and upper adjacent subchannels are completely eliminated. In practice, the equalization takes place at the decimated low sampling rate, and the target of the subchannel equalizer is to approximate ideal channel equalization over the subchannel passband and transition bands (assuming roll-off $\rho \leq 1.0$) with sufficient accuracy. The ICI and ISI components outside the equalization band are proportional to the stopband attenuation of the subchannel filters and can be ignored.

Interference Optimization Criteria

The analysis that led to the ICI and ISI cancellation criteria can be used for optimizing the parameters of the equalizer in order to minimize the interference. With a given equalizer, the ICI power in subchannel k is well approximated by

$$P_k^{ICI} = \frac{M^2}{16} \int_{\frac{-\pi}{M}}^{\frac{\pi}{M}} \left| H_p\left(e^{j(\omega - \frac{\pi}{M})}\right) H_p\left(e^{j(\omega + \frac{\pi}{M})}\right) \right|^2 \left(\left| \tilde{C}_k^Q\left(e^{j\omega}\right) \right|^2 + \left| \tilde{C}_k^Q\left(e^{j(\omega + \frac{2\pi}{M})}\right) \right|^2 \right) d\omega, \tag{4.6}$$

where

$$H_p(e^{j\omega}) = \mathfrak{F}\{h_p[m]\} \tag{4.7}$$

$$\tilde{C}_k^Q(e^{j\omega}) = \mathfrak{F}\{\tilde{c}_k^Q[m]\} \tag{4.8}$$

are the Fourier transforms of the prototype filter $h_p[m]$ and the imaginary part of $\tilde{c}_k[m]$ from equation (4.3), i.e.,

$$\tilde{c}_k^Q[m] = \mathrm{Im}\left[\tilde{c}_k[m]\right]. \tag{4.9}$$

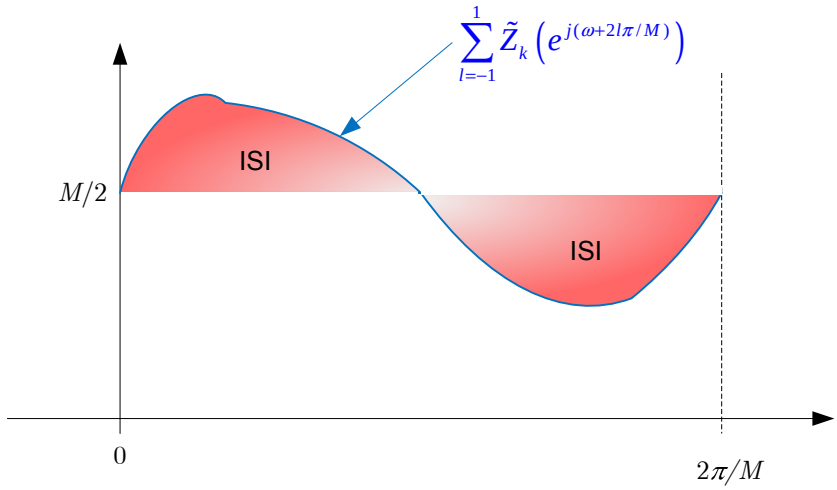

Figure 4.5: ISI from the folded spectrum of the overall transfer function $\tilde{z}_k[m]$.

Only the residual imaginary part of $c_k[m]$ is relevant for the ICI. We can see the cross-talk spectra (shaded in Figure 4.4) represented in the multiplication of the shifted frequency responses of the prototype filter.

The ISI power can be calculated with the help of the aliased spectrum of the overall transfer function

$$\tilde{z}_k[m] = \mathrm{Re}\left[t_{0,0}[m] \star \tilde{c}_k[m]\right] \tag{4.10}$$

as

$$P_k^{ISI} = \int_0^{\frac{2\pi}{M}} \left| \frac{M}{2} - \sum_{l=-1}^{1} \tilde{Z}_k(e^{j(\omega+\frac{l2\pi}{M})}) \right|^2 d\omega. \tag{4.11}$$

In equation (4.10), $t_{0,0}[m]$ is the TMUX transfer function for subchannel 0, obtained from convolving the synthesis filter $f_0[m]$ and the non-causal zero-phase form of the analysis filter $g_0[m]$ (see also Section 2.1.2). The Nyquist criterion in frequency domain is used: in ISI-free conditions, the folded spectrum of the overall subchannel response $\tilde{Z}_k(e^{j\omega}) = \mathfrak{F}\{\tilde{z}_k[m]\}$ adds up to a constant level $M/2$, a condition equivalent to the overall impulse response being a unity impulse. By calculating the difference between this ideal reference level and the actual spectrum, the spectrum resulting from the residual ISI can be extracted. Integration over this residual spectrum gives the ISI power, according to equation (4.11), as sketched in Figure 4.5.

Finally, the noise enhancement introduced by the equalizer is calculated as

$$\beta_k^{\eta} = \frac{1}{2\pi} \int_{-\pi}^{\pi} \left| W_k(e^{j\omega}) H_p(e^{j\frac{\omega \mp \frac{\pi}{2}}{M/2}}) \right|^2 d\omega, \tag{4.12}$$

where $W_k(e^{j\omega})$ is the response of the subchannel equalizer. The $-$ and $+$ signs are valid for even and odd subchannel indexes of the EMFB, respectively.

4.1.2 Low Complexity Subcarrier Equalization

Having developed a tool for evaluating the equalizer performance, we focused on the design of the low complexity equalizer. Early channel equalization solutions for FBMC suffered from insufficient performance when the channel is even mildly frequency selective, as in the case of a single complex multiplier [50]. Alternative solutions had relatively high implementation complexity, as in the FIR based approach described, e.g., by Hirosaki in [49]. To overcome these problems, specific equalizers that concentrate on a few chosen frequency points are considered. The point-wise equalization principle proceeds from the consideration that the subchannel equalizers are designed to equalize the channel optimally at certain frequency points within the subband. At those frequency points, the equalization aims to invert the channel, i.e., the coefficients of the equalizer are set such that the equalizer amplitude response optimally approaches the inverse of the determined channel amplitude response and the equalizer phase response optimally approaches the negative of the determined channel phase response. Between these considered points, the optimal linear equalizer is approximated and the residual ICI and ISI interference powers depend on the degree of inaccuracy with respect to the zero ICI/ISI conditions. On the other hand, the level of inaccuracy depends on how much the channel frequency response varies within the subchannel, i.e., the relation of the channel coherence bandwidth [99] to the size of the filter bank, and on the order of the point-wise per-subcarrier equalizer. For mildly frequency selective subband responses low-order equalizers are sufficient to keep the residual ICI and ISI at tolerable levels.

A complex FIR (CFIR) of a few taps is a straightforward solution for point-wise equalization. Another choice is the amplitude and phase subcarrier equalizer (AP-SCE) introduced in [P2]. The AP-SCE independently equalizes the channel phase with allpass IIR filters and the channel amplitude with a linear-phase FIR filter. An example CFIR and AP-SCE that are able to equalize at three frequency points are shown in Figures 4.6 and 4.7, respectively.

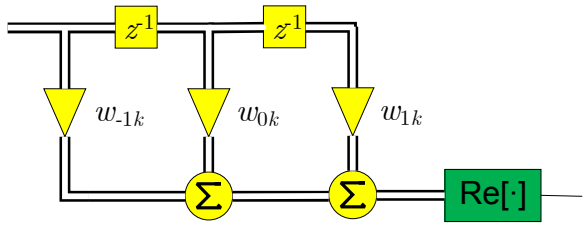

Figure 4.6: Complex FIR subcarrier equalizer for equalization at 3 frequency points.

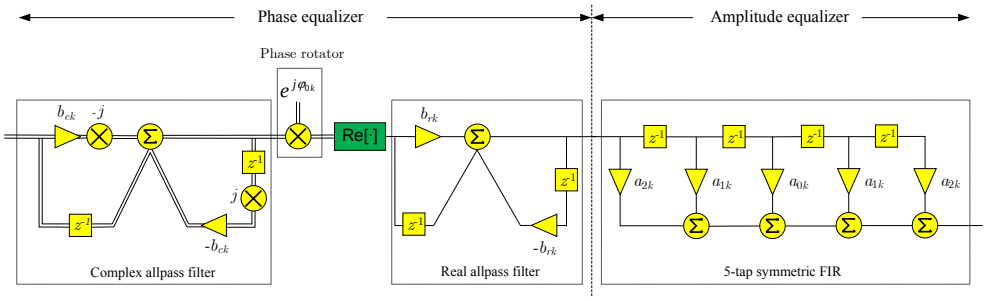

Figure 4.7: Amplitude and phase subcarrier equalizer for equalization at 3 frequency points.

Note that in the AP-SCE the operation of taking the real part of the signal for detection is moved before the real allpass phase correction stage. This does not affect the output of the AP-SCE, but reduces its implementation complexity. In the figures, the double lines indicate that the signal on them is complex valued, whereas the single line indicates real valued signals.

The equalizer coefficients can be calculated by evaluating the frequency responses of the equalizer at the desired frequencies and forcing the equalizer to adopt desired target values there. The target values optimally equalize the channel at their frequency locations in the zero forcing (ZF) or mean squared error sense (MSE) [73], [99]. With three frequency points, the most convenient and computationally least complex choice is to equalize at the center of the subchannel and at the subband edges.

Figure 4.8 presents the working principle of a three point ZF equalizer in which the channel is inverted with the target equalizer amplitude points ϵ_i and phase points ξ_i.

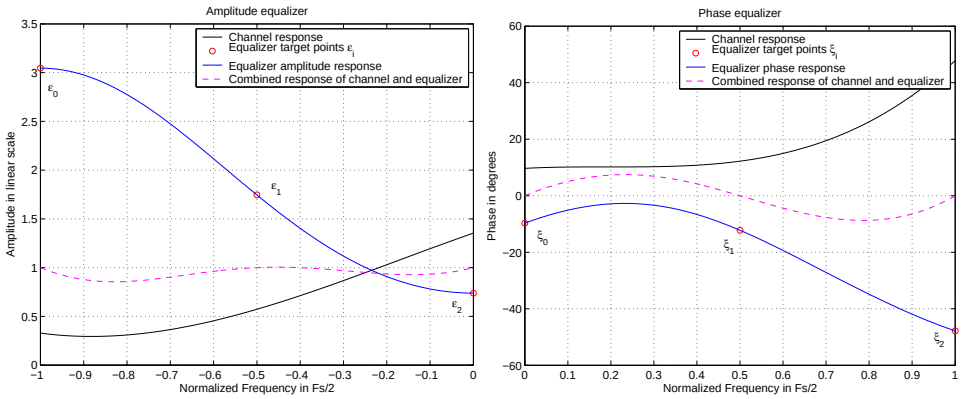

(a) Zero forcing amplitude equalization (b) Zero forcing phase equalization

Figure 4.8: Three point equalization working principle.

The results in [P2] showed an excellent match between system simulations with these equalizers and semianalytical predictions based on the derivations presented above in Section 4.1.1. The introduced equalizers present very good equalization performance for subchannels of the order of 100 kHz and the ITU Vehicular-A channel model [61]. This permits the design of MC communication systems with a fraction of the subchannel number used in OFDM systems, allowing for significant complexity reduction, especially in the downlink.

Doctoral candidate Tero Ihalainen is currently experimenting on increasing the number of points to equalize (=increasing the number of taps of the equalizer) to improve performance with severe fractional time delay (FTD) or strongly frequency selective fading at subchannel level. Moreover, he has extended the point-wise equalization concept to the multiantenna case in FBMC [55]. Also other equalization strategies, such as a different distribution of the frequency points within the subchannel band are possible. In fact, the flexibility and expandability is a definite virtue of the applied frequency sampling approach. Furthermore, the AP-SCE has the advantage over the CFIR that it can be optimized in a more flexible manner, since the amplitude and phase sections are independent of each other.

4.2 Narrowband Interference Suppression

The point-wise equalization introduced in the previous chapter can be applied to interference mitigation by placing notches at the equalization points. The

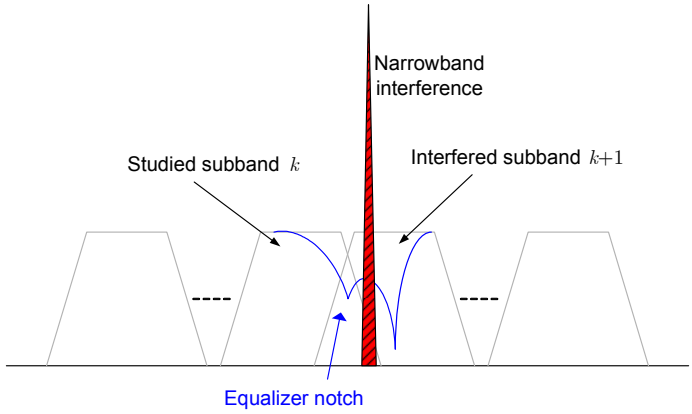

Figure 4.9: NBI mitigation in the adjacent subchannel.

main objective is to partially save information from the subchannels that are affected by the NBI. Successful achievement of this objective makes it possible to consider wider subchannel spacing in NBI scenarios. Publication [P4] explores this application in the case of adjacent subchannel interference, as seen in Figure 4.9, in which the NBI falls on the roll-off band of the studied subchannel. Mitigation within the subchannel directly hit by the interferer is expected to be only successful if it is very narrow and falls exactly on an equalization point. Mitigation at other than these two subchannels is not necessary if the subchannel filters are highly selective, as we have assumed so far in our FBMC models.

Since only the roll-off band is affected by the interferer, the notch is applied on the subband edge equalization point. However, we showed in [P4] that best performance is obtained if the notch does not completely null out the equalization frequency, but is scaled according to the NBI power. In absence of interference, the equalizing MSE target amplitude in subchannel k is

$$\epsilon_{ik} = \frac{|h_{ik}|}{|h_{ik}|^2 + \sigma_{\mathrm{N}}^2}, \tag{4.13}$$

where h_{ik} is the channel response at the considered frequency point i and σ_{N}^2 is the noise power. If a NBI is distorting the neighboring subchannel, the MSE criterion can be slightly modified to improve the BER performance by updating equation (4.13) into

$$\epsilon_{ik} = \frac{|h_{ik}|}{|h_{ik}|^2 + \sigma_{\mathrm{N}}^2 + \sigma_{\mathrm{I}}^2}, \tag{4.14}$$

where σ_{I}^2 is the NBI power. In both equations we assume that the signal is normalized to unity power. Note that this modification does not suppose any additional complexity for the equalizer. Obviously, in practice σ_{I}^2 needs to be calculated, adding some complexity to the estimation subsystem.

Publication [S3] develops this idea considering the interference power estimation problem. The system in which the subband equalizer and NBI mitigation are applied is of the single carrier type with frequency domain equalization. Nevertheless, the NBI estimation approach can be used similarly in the FBMC context. The idea is that if the channel gains in subchannel k are known at the subband edges (subindex $i = 0, 2$) and at the center of the subband (subindex $i = 1$), then one can estimate the expected signal and noise power present in the subband as

$$\hat{P}_k = \frac{|h_{0k}|^2 + 2|h_{1k}|^2 + |h_{2k}|^2}{4} + \sigma_{\mathrm{N}}^2. \tag{4.15}$$

The estimates of the channel gains could be obtained for example by interpolating from the gains estimated in neighboring, interference-free subbands. In case the measured power P_k exceeds $\hat{P}_k$ by a certain amount determined by an NBI detection threshold, the subband can be considered as affected by interference. A good estimate for the NBI power present in subchannel k is

$$\hat{\sigma}_{\mathrm{I}k}^2 = P_k - \hat{P}_k, \tag{4.16}$$

and the total NBI power to be used as the attenuation factor in equation (4.14) can be calculated as

$$\hat{\sigma}_{\mathrm{I}}^2 = \sum_k \hat{\sigma}_{\mathrm{I}k}^2. \tag{4.17}$$

Here k indexes the subbands affected by the interferer, normally two adjacent subbands, as in Figure 4.9.

Furthermore, the approximate interferer location within the subchannels can be estimated with help of $\hat{\sigma}_{\mathrm{I}k}^2$ from equation (4.16) and the frequency response of the prototype filter as the low rate $\omega = \hat{\omega}_{\mathrm{I}}$ that fulfills

$$\frac{\left|H_p\left(e^{j2\omega/M}\right)\right|^2}{\left|H_p\left(e^{j2\omega/M - 2\pi/M}\right)\right|^2} = \frac{\hat{\sigma}_{\mathrm{I}k}^2}{\hat{\sigma}_{\mathrm{I}k+1}^2}. \tag{4.18}$$

Here, the prototype filter H_p is assumed to be symmetric and the obtained $\hat{\omega}_{\mathrm{I}}$ is the distance from the center frequency of the analysis subchannel filter k to the interference, assuming it to be located between subchannel k and $k + 1$. Figure 4.10 clarifies this concept.

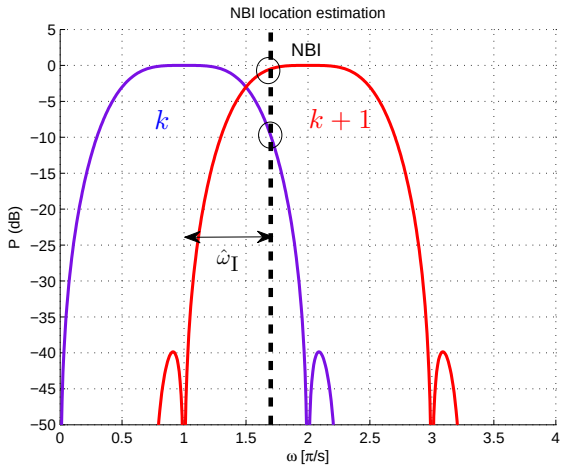

Figure 4.10: Locating NBI affecting two subbands.

The presented approach for NBI mitigation in FBMC is capable of reducing the impact of the interferer so that the adjacent subchannel does not need to be discarded for reception. In the FBMC case studied in the previous section we have seen that the subchannel bandwidth can be in the order of 100 kHz, which is a considerable amount of bandwidth that is saved for transmission. An FBMC system could now be dimensioned to have wider subcarrier spacing without sacrificing a whole subchannel in NBI scenarios. Furthermore, if subchannel equalizers such as the low complexity CFIR or AP-SCE are implemented in the receiver, they can be readily used to perform the NBI mitigation, without adding complexity to the equalization stage.

4.3 Channel Estimation and Synchronization

After understanding how to efficiently and effectively equalize the channel in our FBMC proposal, the logical continuation was to research the means for obtaining the channel information that the equalizer needs in order to perform its task. Closely related to channel estimation is the synchronization problem because again propagation parameters are estimated. Often, channel estimation and synchronization parameter estimation is done with the same means. Actual synchronization and equalization can then be performed separately, or up to a certain degree jointly, for example with the help of the subcarrier equalizers presented in Section 4.1.2.

In order to synchronize and equalize the channel, there are methods to perform timing, carrier frequency offset (CFO) and channel estimation. In the MC context, timing estimation involves locating the start of a transmission burst, finding the first multicarrier symbol, and estimating the fractional time delay (FTD), which is a fraction of the multicarrier symbol period. Since OFDM is the most widespread MC technique, many methods for synchronization and channel estimation can be found for it. They are based on scattered pilots and training sequences [83, 100], on exploiting the redundancy of the CP [132] or even blind methods that do not make use of overheads in the signal [100].

Due to the different nature of the FB waveforms, some of the OFDM methods can be applied to FBMC and others, such as the CP based ones, cannot. Although there exist preamble based [9, 38, 67, 76] and blind [16, 32, 80] approaches, we focus our interest here towards low rate training sequence and scattered pilot based approaches [63, 77]. In the context of this thesis, it is interesting to note that the authors of [63] present an approach to perform full synchronization in both FBMC/OQAM and OFDM/QAM systems based on scattered pilots. There, the time domain properties of the regularly scattered pilots are exploited and synchronization takes place in the time domain, instead of subcarrier-wise. Further, the preamble based approach in [9] performs synchronization of FBMC signals in a setup with parameters similar to the well established IEEE 802.11a [3] standard.

When using efficient FB implementations, as for example FBMC/OQAM [118], the application of low rate training sequence and scattered pilot based approaches for synchronization and channel estimation is not as straightforward as in OFDM. The reason is the imaginary interference, inherent to the filter bank, that a real-valued low-rate symbol suffers from adjacent symbols in time and frequency. This has motivated different proposals for generating pilots [64, 76] compatible with the filter bank class of interest. In our research, we first investigated the training sequence approach in the EMFB case [P5] and then built a synchronization and channel estimation subsystem for FBMC/OQAM based on pilots and auxiliary pilots similarly to [64] because of good estimation performance [P3]. It should be noted, however, that since both FB implementations are closely related, the estimation approaches can both be applied with simple updates in the signal models to the implementation for which they were not originally conceived.

The general receiver concept with the estimation, synchronization and equalization subsystems can be summarized in Figure 4.11. It includes the

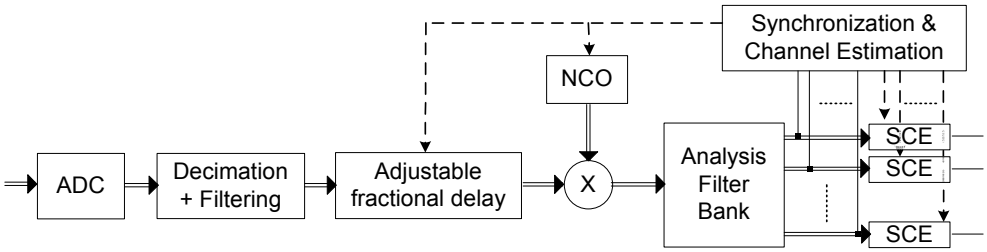

Figure 4.11: Complex TMUX receiver with oversampled analysis bank and per-subcarrier equalizers.

possible feedback before the AFB to compensate large CFOs and FTDs by tuning the numerically controlled oscillator and the correct sampling moment.

When studying the effect of a linear multipath channel with AWGN, fractional time delay and carrier frequency offset, the baseband signal model at the receiver input can be written as

$$r(t) = (s(t) \star h(t,\tau) \star \delta(t - \tau_{FTD}T))e^{j2\pi\frac{\varepsilon}{T}t} + \eta(t), \tag{4.19}$$

where $\star$ represents the convolution operation, $s(t)$ is the continuous time version of the SFB output at the transmitter, $h(t,\tau)$ is the time-varying transmission channel, and δ is the Dirac delta. The transmitter output $s(t)$ varies slightly depending on the FBMC implementation selected. Moreover, τ_{FTD} is the fractional time delay as a fraction of the signalling interval T, ε is the CFO as a fraction of the subcarrier spacing Δf, and $\eta(t)$ is complex valued AWGN. At the receiver, $r(t)$ is sampled at $T_s = \frac{T}{M}$ into $r[m]$ and then passes the analysis bank. Here it should be noted that in the following derivations a slight change in notations is introduced to match the more compact notation from [P3], in which the FBMC/OQAM implementation is applied. The time index at low sampling rate n is now placed as a subindex of the considered variable, i.e, $x_{k,n} \equiv x_k[n]$, next to the subchannel subindex k. With this in mind, the k-th subchannel sequence $y_{k,n}$ before the subchannel processing stage (estimation and synchronization/equalization in our case) can be expressed as

$$y_{k,n} = [r[m] \star f_k[m]]_{\downarrow\frac{M}{2}} = \sum_{i=k-1}^{k+1} v_{i,n} \star q_{i,k,n} + \eta_{k,n}, \tag{4.20}$$

where

$$q_{i,k,n} = \left[((g_i[m] \star h[n,m] \star \delta[m - \tau_{FTD}\frac{T}{T_s}])e^{j2\pi \frac{\varepsilon}{M} m}) \star f_k[m] \right]_{\downarrow \frac{M}{2}}. \quad (4.21)$$

Above, $q_{i,k,n}$ is the subchannel-dependent 2-dimensional impulse response, including the channel effects, from subchannel i to subchannel k, and $v_{i,n}$ is the input to the synthesis bank. In the FBMC/OQAM implementation (see Fig. 4.3 b)),

$$v_{i,n} = \theta_{i,n} d_{i,n}, \quad (4.22)$$

where

$$\theta_{k,n} = e^{j\frac{\pi}{2}(k+n)} = j^{k+n}. \quad (4.23)$$

The discrete-time time-varying channel is $h[n,m]$, the delay $\tau_{FTD}\frac{T}{T_s} = \tau_{FTD}M$ is assumed to be an integer number of samples, for simplicity, and $\downarrow \frac{M}{2}$ represents the downsampling by $\frac{M}{2}$ of the preceding expression included in the brackets. The sampled and filtered noise is $\eta_{k,n}$. Equation (4.20) assumes a sufficiently frequency selective prototype filter and roll-off $\rho \leq 1$. Therefore only adjacent subchannels overlap and have an effect on subchannel k of interest. Further, we also assume here a reasonably small frequency offset ε, in which case the overlaps with subchannels $i = k \pm 2$ remain insignificant.

4.3.1 Data Aided Channel Estimation

In the following sections the term pilot is used to designate a transmitted symbol that is known beforehand at the receiver, in order to sample the channel by evaluating its effect on the pilot symbol.

In efficient modulated filter banks the use of scattered (in time and frequency) pilot symbols or training sequences of pilot symbols at the low rate is not that simple as in OFDM, as a closer look into equation (4.21) reveals. Indeed, if we first remove all the channel effects in that equation, i.e., $\tau_{FTD} = 0$, $\varepsilon = 0$ and $h[n,m] = \delta[n]$, $q_{i,k,n}$ becomes the time- and frequency invariant 2-dimensional impulse response of the TMUX (see also Section 2.1.2), relating the real valued input $d_{i,n}$ with the received k-th subchannel signal before the operation of taking its real part, $\tilde{y}_{k,n}$. After multiplying in the FBMC/OQAM model by $\theta^*_{k,n}$, we can rewrite (4.20) as

$$\tilde{y}_{k,n} = d_{k,n} + \sum_{i=k-1}^{k+1} \sum_{\substack{l=-\infty \\ (i,l)\neq(k,n)}}^{\infty} j^{i-k} d_{i,l} q_{i,k,n-l} + \eta_{k,n} \quad (4.24)$$

$$= d_{k,n} + \left(\eta^{\mathrm{NPR}}_{k,n} + j u_{k,n}\right) + \eta_{k,n}. \quad (4.25)$$

Table 4.1: Interference weights for data surrounding the symbol in the center of the table.

	$n=-4$	$n=-3$	$n=-2$	$n=-1$	$n=0$	$n=1$	$n=2$	$n=3$	$n=4$
$k=-2$	0	0.0006	-0.0001	0	0	0	-0.0001	0.0006	0
$k=-1$	0.0054	j0.0429	-0.1250	-j0.2058	0.2393	j0.2058	-0.1250	-j0.0429	0.0054
$k=0$	0	-0.0668	0.0002	0.5644	1	0.5644	0.0002	-0.0668	0
$k=1$	0.0054	-j0.0429	-0.1250	j0.2058	0.2393	-j0.2058	-0.1250	j0.0429	0.0054
$k=2$	0	0.0006	-0.0001	0	0	0	-0.0001	0.0006	0

The elements $\eta_{k,n}^{\mathrm{NPR}}$ and $u_{k,n}$ within the parentheses of equation (4.25) are obtained by respectively taking the real and imaginary part of the summation term in equation (4.24) above. They can be considered interference on the desired symbol $d_{k,n}$. Now, even in a PR TMUX, in which the real-valued term $\eta_{k,n}^{\mathrm{NPR}} = 0$, the imaginary-valued interference $ju_{k,n}$ does not add up to 0. The transmultiplexer orthogonality is only obtained after taking the real part, i.e., this interference summation has only imaginary values [118]. In a good NPR design, $\eta_{k,n}^{\mathrm{NPR}}$ is a small real-valued contribution, generally well below the level of $\eta_{k,n}$, and can safely be ignored. Another property of the imaginary-valued interference $ju_{k,n}$ that can be deduced from equation (4.24) is that it is time-varying, since it depends on the data in the adjacent channels and on the symbols preceding and following $d_{k,n}$, weighted by the transfer function of the TMUX.

Table 4.1 presents the interference weights that multiply neighboring symbols in the case of an NPR prototype designed with the frequency sampling method in [14] and with an overlapping factor $K = 4$. We can see that the interference from subchannels not adjacent to the subchannel of interest have negligible effect and that in time direction the interference goes K symbols from the symbol of interest in both directions. With this NPR design, the residual distortion on the real part is less than -65 dB compared to the actual data.

It is clear that a known data symbol located at subcarrier k_p and time n_p cannot be immediately recovered even if the channel at that subcarrier is a simple complex coefficient H_{k_p,n_p} (flat fading), because the pilot information and the complex-valued, time-varying and data-dependent interference will be mixed by the channel. In the following paragraphs we point out several

alternative methods that can be used to handle the described complex-valued interference in order to make data-aided channel parameter estimation feasible. The interested reader is referred to the cited references for detailed description of the methods.

Auxiliary Pilots

This approach is based on an elegant idea presented in [64]: An auxiliary pilot located at k_a, n_a, adjacently to the pilot k_p, n_p, cancels the interference u_{k_p,n_p} of equation (4.24). We further develop and apply this idea in Publication [P3] to generate scattered pilots. The advantage of eliminating the interference is that the pilots can be used at the receiver in a similar fashion as OFDM pilots are used: the estimate of the channel at the pilot location is the received symbol normalized by the known transmitted symbol, i.e,

$$\hat{H}_{k_p,n_p} = \tilde{y}_{k_p,n_p}/d_{k_p,n_p}. \tag{4.26}$$

This assumes that the channel is constant over the whole subchannel bandwidth. The auxiliary pilot is indeed one element of the sum in equation (4.25) and has to be calculated on-line with data transmission every time a pilot is inserted since the interference terms vary with the data. In [64], the auxiliary pilot is chosen to cancel the interference from the 8 surrounding symbols. This is a good approximation in well time-frequency localized prototype filters, such as the ones based on the isotropic orthogonal transform algorithm (IOTA) function [72]. In [P3] we chose to include more terms in the calculation of the interference because also symbols located further away can significantly contribute to it.

In typical filter bank designs it is wise to locate the auxiliary pilot immediately preceding or following the pilot, i.e., $n_a = n_p - 1$ or $n_a = n_p + 1$. This is because when computing the auxiliary pilot, its expression is normalized by the interference weight of the auxiliary pilot affecting the actual pilot. In Table 4.1 we see that with this choice the magnitude of the auxiliary pilot amplitude is minimized on the average (the interference weight next to the pilot at $(k_p, n_p) = (0, 0)$ is the highest). Consequently, less transmission energy is wasted on the pilot/auxiliary pilot pair and possible negative effects on the peak to average power ratio (PAPR) due to excessively strong auxiliary pilots are prevented.

As an example, with the prototype filter presented above, it is sensible to use the shaded area of Table 4.1 for the computation of the interference and

the auxiliary pilot. This leaves the residual imaginary interference power −38 dB below the average level of data. Further, if the auxiliary pilot is chosen to precede or succeed the pilot, then the auxiliary pilot power is on the average 3.3 dB stronger than the data surrounding the pilot/auxiliary pilot pair. The next best choice for the auxiliary pilot location adds almost 6 dB to its average power.

Note that the use of two real-valued symbols as pilots does not mean a penalty in overhead with respect to OFDM, since there the pilot is complex-valued. This observation also applies to the next technique for FBMC pilot design.

Pair of Pilots

The pair of real pilots (POP) [76] method also uses two consecutive OQAM subsymbols within a subchannel to send known pilots, i.e., at locations (k_p, n_p) and $(k_p, n_p + 1)$. In the simplest case the pilots are similar. Ignoring the noise and assuming that the channel remains unchanged during both subsymbols, an equation system yields the equalizer coefficient (the same for both pilots) that restores the pilots to their original phase and amplitude. The estimate for the channel at the positions of the POP is obtained by inverting the computed equalizer coefficient. This method places the computational complexity on the receiver part and has the advantage that it is independent of the prototype filter design, since the interference term is not used explicitly in the equations. However, if the noise is not negligible, it will be enhanced in a random fashion, depending on the data surrounding the pilots, which makes the performance unpredictable and generally worse.

Interference Approximation Method

The authors of [76] also present the interference approximation method (IAM). The philosophy here is that most of the symbols surrounding the pilot in time and frequency are fixed and known at the receiver. In this case, the interference u_{k_p,n_p} can be approximatively calculated with equation (4.24), which leads to the channel estimate

$$\hat{H}_{k_p,n_p} = \tilde{y}_{k_p,n_p} / \left(d_{k_p,n_p} + j u_{k_p,n_p} \right). \tag{4.27}$$

The more symbols in the shaded area of Table 4.1 are fixed, the better is the approximation of u_{k_p,n_p}. Unfortunately, this approach leads to an unacceptable overhead if a good approximation of the interference, necessary for

accurate channel estimates, is desired. Therefore, it is practical only in situations in which pilots are packed closely together, e.g., in training sequences, such as in Publication [P5], where the fixed symbols can be simultaneously utilized by nearby located pilots. Of course, the symbols closer to the edge of the training sequence will be more exposed to the effect of the following random data and the approximation of u_{k_p,n_p} on them is worse.

Other Pilot Approaches

More sophisticated methods for scattered pilot-based channel estimation in FBMC/OQAM are presented in [77]. By means of an orthonormal transformation of the data around the pilot, the imaginary-valued term can be nulled while simultaneously avoiding the use of an auxiliary pilot with increased power. This implies an advantage in the transmit power efficiency compared to the auxiliary pilot approach, at the cost of increasing the computational complexity. Nevertheless, it is still necessary to fix one of the surrounding symbols, which cannot be used for data transmission. Another approach in [77] and in [78] consists of iteratively approximating u_{k_p,n_p} at the receiver with help of the detected data. At first, it is considered that $u_{k_p,n_p} = 0$, and the channel is estimated based on this assumption. The equalization and detection then yield estimates of the data surrounding the pilot, which, in turn, permit calculating a better estimate of u_{k_p,n_p}. The authors in [78] show that the technique converges in 3-4 iterations.

The methods presented above provide a way of sampling the time-varying frequency response of the transmission channel. The estimates required at the remaining subchannels and time-instants can be obtained by interpolating between the estimates obtained at the pilot locations. Note that for the 3-tap subcarrier equalizer presented in Section 4.1.2, the interpolation has to return estimates not only at the center frequencies of the subcarriers, but also at the subband edges in the middle of those frequencies. In general, if a higher order frequency sampling equalizer is used, the estimation and interpolation solution needs to provide estimates at the frequency locations at which the equalizer is designed to optimally invert the channel. Studying how improved interpolation techniques [100] affect the FBMC channel estimation performance is an interesting subject for future research.

4.3.2 Timing Synchronization

Timing synchronization can be divided into frame location and fine timing synchronization. The frame location aims to find the start of the transmitted frame in order to continue with the remaining synchronization operations. The objective of the fine timing synchronization is to estimate and correct the possible fractional time delay.

Frame Synchronization

Frame synchronization usually relies on correlating the received signal with a known training sequence [100, 115]. The transmitter sends the sequence embedded in the transmitted frame and the receiver correlates the received sample stream with the known sequence and uses the peak of the correlation to detect the beginning of the frame. The same sequence can be used to perform also FTD estimation [37, 124]. Often, these methods are time-domain methods [37, 38], i.e., they are performed before the AFB. In publication [P5], we transmit known training sequences on each subchannel and perform the correlation subcarrier-wise, i.e., after the AFB. Therefore, each subchannel correlation returns a peak that indicates the start of the frame:

$$n_{k,0} = \arg\max_{n} \left(\sum_{r=0}^{L_{\mathrm{TR}}} d_{k,n}^{\mathrm{TR}} \tilde{y}_{k,n+r} \right). \tag{4.28}$$

Here, $d_{k,n}^{\mathrm{TR}}$ is the training sequence of length L_{TR} in subchannel k. Note that the filter bank interference has to be taken into account, for example by including the known interference (see IAM method above in 4.3.1) to $d_{k,n}^{\mathrm{TR}}$.

Selecting a sufficient amount of strong subcarriers (not attenuated by the channel) and selecting the most frequently appearing peak position in these subcarriers, the estimation can be made more robust. In [P5] we achieved also certain robustness against CFO when the absolute values of the received signal and training sequence were used in the correlation.

The training sequences utilized here are a few times longer than the sequences used in time domain synchronization. However, the training sequences from [P5] not only synchronize the frame, but also perform CFO and channel estimation at subcarrier level, and therefore implicit FTD estimation, as presented in Section 4.3.4.

FTD Synchronization and Correction

Assuming that the coarse location of a transmission frame is obtained for example as described in the previous subsection, the effect of fractional time delay, can be understood with help of equation (4.21). In the frequency domain it can be expressed as equation (4.29), which shows that the FTD introduces a phase term that linearly varies with the frequency:

$$\begin{aligned} Q_{i,k}\left(e^{j\omega}\right) &= \left[\left(\left(G_i\left(e^{j\omega}\right) H_n\left(e^{j\omega}\right) e^{-j\omega\tau_{FTD}M}\right) \star \delta\left(\omega - 2\pi\varepsilon\right)\right) F_k\left(e^{j\omega}\right)\right]_{\downarrow\frac{M}{2}} \\ &= \left[\left(G_i\left(e^{j(\omega-2\pi\varepsilon)}\right) H_n\left(e^{j(\omega-2\pi\varepsilon)}\right) e^{-j(\omega-2\pi\varepsilon)\tau_{FTD}M}\right) F_k\left(e^{j\omega}\right)\right]_{\downarrow\frac{M}{2}} \\ &= \left[G_i\left(e^{j(\omega-2\pi\varepsilon)}\right) H_n\left(e^{j(\omega-2\pi\varepsilon)}\right) F_k\left(e^{j\omega}\right) e^{-j(\omega-2\pi\varepsilon)\tau_{FTD}M}\right]_{\downarrow\frac{M}{2}}. \end{aligned} \tag{4.29}$$

This frequency-dependent phase term destroys the orthogonality of the subchannels and causes the appearance of ICI.

For estimation purposes, let us first assume that there is neither channel distortion nor CFO present. In this case it seems straightforward to estimate the FTD from a transmitted pilot at k_p, n_p, allowing for some uncertainty caused by the ICI. In practice, the estimate is obtained from the phase difference between two pilots separated by Δk subcarriers, since the signal can have a constant random phase rotation that is eliminated when calculating the phase difference. If $\hat{H}_{k_p,n_p}$ is the estimated channel or, equivalently, the normalized transmitted pilot if no channel is considered, at the location k_p, n_p following equation (4.26) or (4.27), then

$$\hat{\tau}_{FTD} = \frac{\angle\left(\hat{H}_{k_p,n_p}\right) - \angle\left(\hat{H}_{k_p+\Delta k,n_p}\right)}{2\pi\Delta k} \tag{4.30}$$

where $\angle(\cdot)$ is the phase of $(\cdot)$.

This result limits the carrier separation for the pilots, if unambiguous phase differences are to be calculated. The phase difference becomes ambiguous, that is it exceeds π, if $\tau_{FTD}\Delta k > \frac{1}{2}$. For example, if pilot subcarriers are separated by $\Delta k = 10$, only a delay of $\pm\lfloor\frac{M}{20}\rfloor$ samples ($\lfloor\cdot\rfloor$ rounds to the closest smaller integer) can be estimated without phase ambiguity. If the pilot separation is expected to exceed the non-ambiguous FTD estimation range, phase disambiguation techniques have to be applied.

The estimate can be improved by averaging techniques such as least squares linear curve fitting over all pilot pairs that are sufficiently closely placed within

a frame. In case of CFO, consecutive symbols within a subcarrier are rotated with respect to each other, as discussed in the coming Section 4.3.3. This forces the estimation averaging to be independently done over the subchannels for every MC symbol time to avoid more complex estimation solutions that take into account the CFO-induced rotation in the time direction. The CFO additionally increases the additive distortion. Finally, in presence of the transmission channel, the (flat-fading) channel coefficient within the subchannel of interest also multiplies the transmitted signal, introducing additional rotation. Since in general this rotation is different at different subcarriers, it would be expected that this method cannot be used anymore with practical transmission channels. Nevertheless, if the effect of the FTD on the phase is predominant, the phase difference introduced by the channel coefficients will add up as noise at the end. Consequently, we can consider $\angle\left(\hat{H}_{k_p+\Delta k,n_p}\right) = \angle\left(\hat{H}_{k_p,n_p}\right) + 2\pi\Delta k\tau_{FTD} + \eta_\varphi$, where η_φ is an additive phase term, which depends on how much the channel is correlated in frequency direction at the pilot distance. Again, averaging over a sufficient number of pilots reduces the harmful effect of this additional phase term. In general, the FTD estimation can be seen as a problem of phase slope estimation over the active subcarriers.

The training sequences utilized in [P5] additionally permit estimating the mildly selective fading channel within the subchannel. This makes it possible to calculate the FTD within each subchannel, without need of resorting to the phase difference between subchannels with pilots.

The equalizers presented in Section 4.1.2 are well suited for compensating the FTD, since they can be designed to reverse the effect of the frequency-varying phase by including the FTD effect on the phase of the channel estimates at the subband edges.

Joint FTD and Channel Estimation Based on Iterative Interference Cancellation

The analysis above shows a clear interplay between the quality of the estimates and the presence of FTD and CFO. Therefore, it is desirable to apply the information of the estimated synchronization parameters to the estimated pilots in order to improve the quality of all the pilot-based estimates. One way to achieve this is by estimating both the subcarrier-wise channel coefficients and the phase slope in a joint manner. This is done in [P3], where we presented a new iterative interference canceling approach that utilizes the

FTD-induced linear phase slope within each pilot subcarrier. For the derivation of the joint FTD estimator and channel equalizer, we assume a simplified signal model where the amplitude response is assumed to be constant within each subchannel and the phase is assumed to be a linear function of frequency. This is motivated by equation (4.29) and by the observation that, in system configurations with high M, a 1-tap equalizer is able to equalize the channel quite well in the absence of timing offsets. The joint channel-FTD estimation includes two parts: estimation of the complex channel coefficient for each pilot, and estimation of the phase slope jointly for all pilots participating in the estimation window Ω_{JE}.

In the FBMC/OQAM model, in which the downsampled signal is centered around DC, the FTD-compensating target response of the 3-tap subcarrier equalizer presented in Section 4.1.2 can be written as

$$\begin{aligned} W_{k,n}\left(e^{-j\frac{\pi}{2}}\right) &= w_{k,n}e^{j\psi} \\ W_{k,n}\left(e^{j0}\right) &= w_{k,n} \\ W_{k,n}\left(e^{j\frac{\pi}{2}}\right) &= w_{k,n}e^{-j\psi}, \end{aligned} \tag{4.31}$$

where the equalizer phase difference correction between the subchannel center frequency and the edge is

$$\psi = -\pi\tau_{FTD}. \tag{4.32}$$

Deriving the transfer function of the equalizer and applying a simplification assuming small ψ, the equalized signal can be approximated as

$$\tilde{d}_{k,n} + j\tilde{u}_{k,n} \simeq w_{k,n}\tilde{y}_{k,n} + \psi w_{k,n}\widetilde{\Delta y}_{k,n}, \tag{4.33}$$

where we define

$$\widetilde{\Delta y}_{k,n} = -j\left(\tilde{y}_{k,n-1} + \tilde{y}_{k,n+1}\right)/2. \tag{4.34}$$

If the EMFB implementation is used, equation (4.31) has to be modified to accommodate the odd stacking of the filter bank. For even subchannels, the evaluation points are $0, \pi/2$ and π, and for odd subchannels $-\pi, -\pi/2$ and 0. This leads to a slightly different definition of $\widetilde{\Delta y}_{k,n}$ for EMFB:

$$\widetilde{\Delta y}_{k,n} = \pm j\left(\tilde{y}_{k,n-1} + \tilde{y}_{k,n+1}\right)/2, \tag{4.35}$$

where the sign depends on whether the subchannel k under consideration is even (+) or odd (−).

At the pilot locations, the 3-tap equalizer can be adjusted to approximate the transmitted known symbol $\tilde{d}_{k,n} + j\tilde{u}_{k,n}$, with known $\tilde{u}_{k,n}$ in the IAM

method or $\tilde{u}_{k,n} = 0$ using auxiliary pilots. Taking this case as example, for the pilot symbols the ideal output is $d_{k,n}$ (the subindices $(\cdot)_p$ are dropped here for readability) and the channel equalization problem can be formulated as:

$$\left\{\hat{\psi}, \hat{w}_{k,n}\right\} = \arg\min_{\psi, w_{k,n}} \left\{ \sum_{k,n\in\Omega_{JE}} \left| d_{k,n} - (w_{k,n}\tilde{y}_{k,n} + \psi w_{k,n}\widetilde{\Delta y}_{k,n}) \right|^2 \right\}, \quad (4.36)$$

where Ω_{JE} is the set of subcarrier symbols used in the joint estimation. The objective is to optimize ψ and $w_{k,n}$ in such a way that the difference between the equalizer output and the known pilot $d_{k,n}$ is minimized in the least-squares sense. This is a nonlinear optimization problem, which can be solved for example by iterating the following two steps:

1) Assuming that the phase slope is known from the previous iteration (0 in the beginning), $\left\{w^i_{k,n}\right\}$ are solved from pilots $\tilde{y}_{k,n} + \psi^{i-1}\widetilde{\Delta y}_{k,n}$ in equation (4.33). Note that the index i here represents the iteration number.

2) Assuming that $\left\{w^i_{k,n}\right\}$ are known, the observation is a linear function of ψ and the optimum $\hat{\psi}$ can easily be calculated with the derivative of the expression in brackets in equation (4.36) with respect to ψ and setting the result to 0, yielding

$$\hat{\psi} = \frac{\sum_{k,n\in\Omega_{JE}} d_{k,n}\,\mathrm{Re}\left[w_k\widetilde{\Delta y}_{k,n}\right] - |w_k|^2\,\mathrm{Re}\left[\tilde{y}_{k,n}\widetilde{\Delta y}^*_{k,n}\right]}{\sum_{k,n\in\Omega_{JE}} \left|w_k\widetilde{\Delta y}_{k,n}\right|^2}, \quad (4.37)$$

which, from equation (4.32), yields $\hat{\tau}_{FTD} = -\hat{\psi}/\pi$. Note that w_k is here the average of $w_{k,n}$ within subchannel k.

In Publication [P3] we saw that this process converges typically in 5-10 iterations, depending on the FTD and Ω_{JE}. Moreover, the estimates $\hat{\psi}$ are quite accurate even for higher values of ψ, exceeding greatly the estimation range imposed by the pilot separation in a scattered pilot setting. However, with higher mobility or lower SNR, the performance suffers more than the classical FTD estimation presented in the previous subsection. Therefore, this iterative approach could be better suited for initial locking to the correct timing and then the fine tuning can be done with the classical estimation.

4.3.3 Frequency Synchronization

Carrier frequency offsets have several effects on the transmitted signal. These effects can be analyzed with help of equations (4.19), (4.21) and (4.29). The main observation is that before the AFB, the complex exponential representing the frequency shift induces a linearly time-varying phase rotation of $2\pi\frac{\varepsilon}{M}$ on consecutive high-rate samples. Recall that ε is the normalized CFO with respect to the subcarrier separation Δf. After the receiver bank and downsampling by $M/2$, the phase rotation between two consecutive symbols at rate $2/T$ is $\pi\varepsilon$ radians. This leads to ISI from symbols in the same subchannel and ICI from symbols in neighboring subchannels at earlier and later time-instants. The neighboring symbols located at the same time instant n have the same phase rotation as the symbol under study, so they do not contribute to ICI. The linearly time-varying phase rotation is the property exploited in the following pilot-based CFO estimation and permits also to implement the basic compensation scheme.

A further effect of the CFO that can be deduced from equation (4.29) is that the subchannel filter at the AFB is not frequency-aligned with the corresponding subchannel filter of the transmitter SFB anymore. This distorts the effective impulse response of the synthesis-analysis cascade by a factor

$$F_{CFO}\left(e^{j\omega}\right) = \frac{H_p\left(e^{j(2\omega/M+2\pi\varepsilon/M)}\right)}{H_p\left(e^{j2\omega/M}\right)}, \tag{4.38}$$

where ω is the normalized angular frequency at subchannel sample rate and $H_p\left(e^{j2\omega/M}\right)$ is the prototype filter frequency response in the filter bank design. In filter banks with linear-phase channel filters in the analysis (and synthesis) filter banks and in the zero-phase subchannel processing model, only the magnitude of the distorting frequency response is significant, the phase is constant over the subchannel band (but still dependant on ε). The magnitude of the described distortion on the frequency response for the prototype filter introduced above is shown in Figure 4.12 for some selected CFO values. In the figure, the subband edges correspond to the normalized frequencies ± 0.5.

Finally, there are some effects like aliasing effects close to the subband edges and the appearance of distortion from the subchannel located 2 subcarrier spacings away. These effects can be considered minor with reasonable CFOs expected in a pilot-based estimation and tracking scenario.

Based on the CFO effects described above, pilot-based frequency offset estimation is straightforward: If a pilot at k_p, n_p is followed by another one Δn samples later at $k_p, n_p + \Delta n$, the phase rotation between them will cover

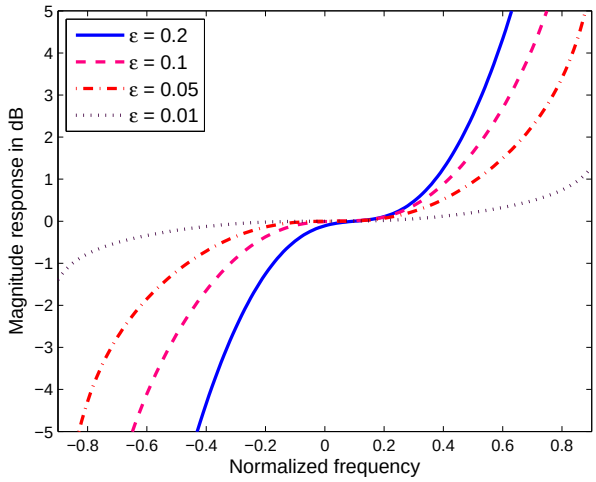

Figure 4.12: Subchannel frequency response distortion due to CFO for normalized frequency offsets $\varepsilon = 0.01$, 0.05, 0.1, and 0.2.

$\Delta\varphi = \pi\varepsilon\Delta n$ radians, assuming that the ISI introduced by equation (4.38) can be neglected and the channel does not vary in time. This yields an estimate

$$\hat{\varepsilon} = \frac{\Delta\varphi}{\pi\Delta n}$$
$$\hat{\varepsilon} = \frac{\angle\left(\hat{H}_{k_p,n_p}\right) - \angle\left(\hat{H}_{k_p,n_p+\Delta n}\right)}{\pi\Delta n}. \tag{4.39}$$

The performance of the estimation can be improved by averaging over many pilots to reduce the effect of the distortion. For example, if pilots are all separated by the same number of samples, the following expression [68] can be used for estimating the CFO, while simultaneously weighting the subcarrier pilots according to their powers:

$$\hat{\varepsilon} = \frac{\angle\left(\sum\limits_{(k,n)\in\Omega_{CFO}} \hat{H}_{k,n+\Delta n}\hat{H}^*_{k,n}\right)}{\pi\cdot\Delta n}. \tag{4.40}$$

This way, stronger subcarriers are favored over weaker ones. Again, the subindices $(\cdot)_p$ indicating pilot locations are not included in the equation for readability. Here, Ω_{CFO} is the set of pilot locations used for CFO estimation. Note that the same problem of phase-ambiguity appears as in the FTD

estimation above, when $\varepsilon\Delta n \geq 1$. Clearly, if a training sequence is used instead of scattered pilots, the range, in which the estimated CFO remains non-ambiguous is maximized. This is because the known data comes as a continuous stream ($\Delta n = 1$).

If the CFO is moderate, e.g., in CFO tracking scenarios, or the subchannel signal modulation is robust, then the offset compensation can be performed subchannel-wise, as sketched in Fig. 4.13a) with the multiplication by the complex exponential sequence that undoes the frequency shift, that is, $e^{-j\pi n\varepsilon}$. The frequency correction at subchannel level will obviously not recover the information leaked to the neighboring channel nor get rid of the distortion coming from 2 subchannels away, since the frequency shift is circular when performed at subchannel level. Further, the amplitude distortion due to the subchannel filter misalignments depicted in Fig. 4.12 also remains.

It is possible, however, to compensate for this amplitude distortion in a simple way with the help of the low complexity frequency sampling equalizers presented above. Similarly as with the phase slope in the presence of FTD, the low complexity equalizer can approximatively correct the amplitude distortion given by equation (4.38) setting the desired target responses to

$$W_{k,n}\left(e^{j\omega}\right) = \frac{1}{F_{CFO}\left(e^{j\omega}\right)}. \tag{4.41}$$

In the FBMC/OQAM implementation, the equation is evaluated at $\omega = -\frac{\pi}{2}, 0, \frac{\pi}{2}$, whereas in the EMFB structure $\omega = 0, \frac{\pi}{2}, \pi$ and $\omega = -\pi, -\frac{\pi}{2}, 0$, for the even and odd subchannels, respectively.

Figure 4.13 presents the subchannel model with the effect of the first two mentioned distortion types, which are the predominant ones. It includes also the basic subchannel-wise CFO correction that undoes the CFO phase rotation according to the estimated frequency shift $\hat{\varepsilon}$. In the equivalent model (b), the effect of inaccurate CFO estimation is represented by the residual frequency modulation $e^{j\pi n(\varepsilon-\hat{\varepsilon})}$.

Under serious carrier frequency deviations, the degradation of the received subchannel signal advocates for time domain solutions (before the AFB) for correcting and possibly also for estimating the CFO. In our research we observed that the compensation performance degrades faster than the estimation performance: With high values of CFO, the subcarrier-wise compensation cannot recover enough of the signal of interest that has leaked to the neighboring subchannel and eliminate the interference. In [48] and [P3] we conclude that the detection performance for 64-QAM, after CFO estimation and compensation, degrades severely when $|\varepsilon| > 0.05\Delta f$, even in low noise scenarios. With

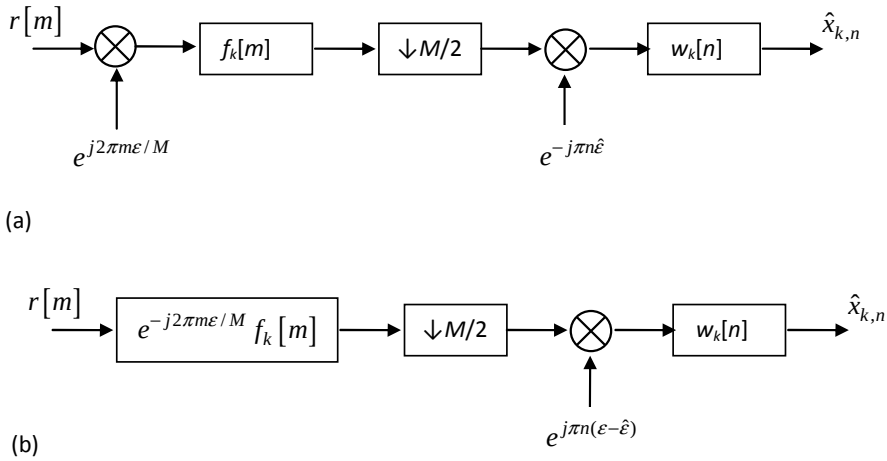

Figure 4.13: Subchannel receiver signal model in the presence of CFO, with CFO compensation and subchannel equalization. (a) Basic model. (b) Equivalent form.

more robust modulations such as 4-QAM, the range with acceptable detection performance is extended to over 20% of Δf and the bottleneck becomes the pilot separation. Usually, several pilots are used for CFO estimation and they are generally sent on a robust modulation, such as BPSK with power boost with respect to data. Because of this, it is possible that the CFO estimate is still acceptable at CFOs at which the BER performance of 64-QAM data transmission is unacceptable. In this case, the CFO may still be estimated at subcarrier level, but compensation has to take place before the analysis filter bank.

4.3.4 Applied Synchronization and Estimation Schemes

Our research group has applied two synchronization and estimation approaches during our studies: Training sequence based channel parameter estimation was reported in [P5]. In [P3] we presented channel parameter estimation based on scattered pilots. Both approaches make use of the low-complexity frequency sampled subband equalizers introduced in Section 4.1.2. It is worth underlining here that when multipath channel, FTD and CFO concur in a communication link, these equalizers can compensate for the three distortions at the desired frequency locations by combining (multiplying) the target frequency responses needed for correcting each of the estimated distortions.

Training Sequences

After the success of the low complexity equalizers in the TMUX with moderate number of subchannels M, our focus was on providing channel estimates to the equalizer that could resolve the mildly fading channel response within the subchannels. Scattered pilots are limited in this sense because they provide at most the information of the average complex gain of that subchannel at the pilot moment. Thus, training sequences were used at the beginning of a transmission burst. In the EMFB implementation, where even subchannels alias at baseband to the positive side of DC and odd ones to the negative side, we applied the repetition of following subsequences:

$$\begin{aligned} d_k^{\mathrm{Tr}} &= ..., 1, 1, 0, 0, ..., \text{ if } k \text{ even}, \\ d_k^{\mathrm{Tr}} &= ..., 0, 0, -1, 1, ..., \text{ if } k \text{ odd}. \end{aligned} \tag{4.42}$$

Shifting the training sequences by $\pi/2$, they could be used in a similar way in FBMC/OQAM configuration.

The spectral content of these training sequences is concentrated on the points of equalization for which we want to obtain the estimates, as shown in Figure 4.14. These sequences have the advantage that the intercarrier interference (ICI) is reduced, since even channels don't transmit when odd channels transmit their training sequence active symbols and viceversa. At the receiver side, after correlation for burst location, a 4-point FFT is taken on the centermost symbols of the training sequence of each subchannel, to minimize interference coming from random data symbols preceding or following the training sequence symbols. Obviously, the training sequence length has to be at least 4 low rate symbols for performing the 4-point FFT. This way, the estimates at the frequency points required by the equalizer are obtained. This is very convenient from the complexity point of view, since only multiplications by ± 1 and $\pm j$ are needed to implement the FFT.

When developing this model, we were not fully aware of the properties of the interference coming from symbols further away than the immediately neighboring ones. In practice, we measured this interference in the case of training sequences not embedded in data and then removed this interference. This practically amounts to applying the IAM pilot technique from [76] and explained above in Section 4.3.1.

There are several ways of improving the estimates obtained with the training sequence by enhancing their signal to noise ratio. For example, one can

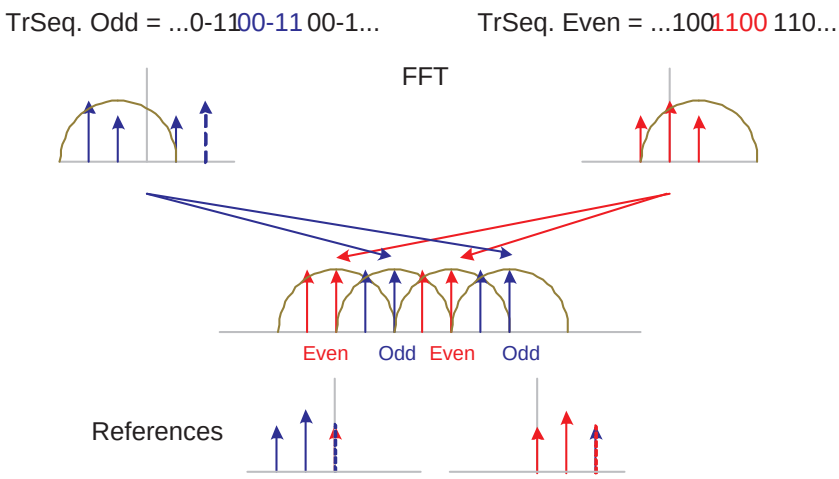

Figure 4.14: Training sequence behavior in the frequency domain.

average the estimates at the overlap location between subchannels. Further averaging is possible if the channel variation is so slow in time, that the estimates at two consecutive training sequences practically do not change. A third approach, and the one that delivered best results in our simulations consist in frequency domain windowing, to make the overall channel frequency response smooth. Ideally, the window weights should follow the shape of the spaced-frequency channel correlation function [99], but if the coherence bandwidth is large enough compared to the subcarrier separation, a simple averaging window performs well and avoids having to gain knowledge about the spaced-frequency channel correlation function.

Scattered Pilots

Within the European Commission FP7 research program PHYDYAS, we refocused our interest on the FBMC/OQAM implementation of the complex filter banks. The project set a defined target to improve WiMAX [154] performance, so it was natural to use it as a reference system. The same pilot configuration as in WiMAX was used in our research, i.e., scattered pilots at the same locations. Since $M = 1024$, the channel was assumed flat fading at subchannel level in most of the cases. We applied the auxiliary pilot principle to implement the scattered pilots and exploit the estimation techniques described here.

Although the auxiliary pilot approach performs as well as the pilots in OFDM, the pilot location has to be considered carefully to avoid appearance of other auxiliary pilots in the region of interference of a given pilot (see Table 4.1). If an auxiliary pilot falls into the shaded area of another pilot (e.g., at $k = -1$ and $n = 2$), not the one corresponding to the auxiliary pilot, the calculation of the auxiliary pilots gets increasingly complicated. This is because the auxiliary pilots cannot be computed independently anymore, first the 'overlapped' auxiliary pilot has to be calculated before being able to compute the auxiliary pilot that nulls the interference of the pilot under consideration, at the center of the shaded area. With the pilot scattering defined in WiMAX we easily achieved the separation of auxiliary pilots by alternatively placing the auxiliary pilot before and after the pilot, as was more convenient for simple computation. However, in more dense pilot configurations the placement can become increasingly difficult, if interdependent auxiliary pilot calculations are to be avoided.

The most striking result from our FBMC/OQAM research was that the throughput can be up to 20% higher than in WiMAX, as results obtained from an advanced simulator ready to be implemented into an actual demonstrator unit showed in [105]. Our synchronization and channel estimation results for the single antenna case are summarized in [P3]. All synchronization operations can be performed after the analysis filter bank, at least in the tracking mode, if the initial errors are not too large. The FBMC system was also capable of taking advantage of MIMO multiantenna transmission, including synchronization and channel estimation in a WiMAX-like MIMO environment.

Additional Considerations

An interesting research topic, for which we unfortunately lacked resources, is how to interpolate to obtain channel parameter estimates at all time and frequency locations needed within a transmitted frame.

In the scattered pilot approach, when computing these estimates for all subcarriers and time instants, the correct interpolation of the channel from the estimates at the pilots is not a trivial problem in the case of FTD due to the modulo 2π phase ambiguity. For example, if amplitude and phase are interpolated separately, in order to include the FTD estimation for compensating the phase, 2π hops can result in a very unsmooth 2-D channel interpolation. In our studies using very basic linear interpolation we obtained the smoothest results by first eliminating the phase slope from the center frequencies of the

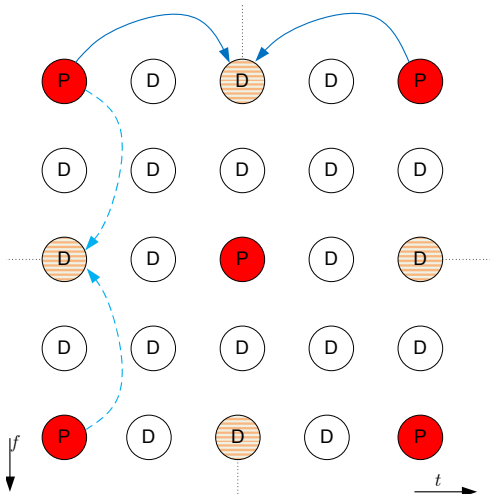

Figure 4.15: Extending the non-ambiguity ranges.

pilots. Then, 2-D complex interpolation to obtain the channel estimates for the data symbols both at the center and edge frequencies is performed, and finally the phase slope is restored to the whole estimation matrix for final calculation of the equalizer coefficients.

Also in the scattered pilot approach, the interpolation of the pilots could be used to increase the non-ambiguity ranges discussed in the synchronization sections above. Looking at Figure 4.15, consecutive pilots (marked with 'P') in frequency direction can be interpolated to estimate a pilot at the central subcarrier on the figure (circle filled with stripes), at the instant of the current pilots. Now the CFO estimation range within that subchannel is increased, because the interpolation has put an (interpolated) pilot closer to the actual pilot. Obviously, the pilot separation in frequency direction has to be within the FTD non-ambiguity range to yield a correct interpolated pilot. Exchanging frequency and time directions, the same holds for extending the FTD estimation range based on scattered pilots.

In the training sequence approach, the frequency direction did not need interpolation, but could take advantage of windowing, as mentioned above. However, in case of mobility or varying channel conditions, time domain interpolation between two training sequences is needed. We experimented with linear interpolation, but it remained an open question for us to study the trade-off among the interpolation method, the channel speed and the sepa-

ration between training sequences. For example, if an efficiency similar as in WiMAX is envisioned, 1/9 of the transmitted symbols are pilot overhead. How well can the training sequences track changes in practical channel models if they occupy 1/9 of the transmission time?

Another consideration when designing the data-aided estimation symbols is the peak to average power ratio (PAPR). All MC systems generate high signal peaks if the subchannel signals add coherently when synthesizing the high-rate MC signal. These peaks are likely to be affected by the non-linear elements such as the power amplifier, distorting the signal and inducing spectral regrowth. Strong spectral regrowth threatens the very purpose of using filter banks and their good spectral containment. In [P2] we study the effect of the non-linear power amplifier on OFDM and FBMC signals, concluding that both MC signals suffer similar spectral regrowth due to similar PAPR characteristics of both waveforms.

Furthermore, the regular pattern in which pilots are arranged within a transmitted symbol increases the probability of generating peaks in the signal after the synthesis bank. Thus, randomizing the pilots or training sequence is a utilized approach for example in WiMAX [2] to avoid high PAPR due to the training sequences. In [P3] we apply the pilot randomization of the IEEE 802.16e standard. In the training sequence based approach of [P5] the training sequences are multiplied with sequences that were optimized to minimize the resulting PAPR. The optimization was performed with a brute force algorithm, trying out different sequences and selecting the ones with reduced PAPR. During our research we also considered the cubic metric [127] as an optimization parameter, but the spectral regrowth did not vary much from the case with PAPR optimization.

Regarding the general MC signal obtained from random data, we have started to study other methods to reduce the PAPR in the FBMC signal in [S4]. The methods presented there study the trade-off in BER and spectral regrowth of different signal limitation methods to reduce the PAPR. Most recent simulation results indicate that, in combination with a realistic power amplifier model, feedforward linearization [40] of the PA produces the most promising distortion reduction compared to PAPR reduction techniques based on signal limiting. The PA model utilized is an adaptation of Rapp's narrowband solid state PA [102] based on actual simulations. More sophisticated broadband PA models with memory and the mitigation of its effects, for example in the receiver [151], are a subject for future research.

Chapter 5

Conclusions

The first part of this thesis presented the motivation and background to the research that resulted in the included publications. The research was performed as part of several research projects and in cooperation with other research groups. Publication [P1] was the result of the work funded by the National Technology Agency of Finland (Tekes) "Digital and Analog Techniques in Flexible Receivers" with the cooperation of Insta Group (formerly Instrumentointi). Publications [P2,P4] were partly funded by Nokia and [P4] was also supported by the Academy of Finland in the project "Advanced Multicarrier Techniques for Wireless Communications." The efforts in [P3] were partly funded by the European Commission under Project PHYDYAS (FP7-ICT-2007-1-211887).

Since the main tool applied in the research was the complex modulated filter bank in the EMFB and FBMC/OQAM implementations, basics on filter banks were introduced as a launcher for the remainder of the thesis. Chapters 3 and 4 paved the way towards the publications by presenting actual problems in digital communications and how they can be solved by means of filter bank based processing. First the case of narrowband interference suppression in a direct sequence spread spectrum was presented. Then the main transmission channel impairments and how they can be estimated and corrected in FBMC communications were introduced.

The main results of the research of the thesis are presented in the publications [P1]-[P5] at the end of the thesis. They comprise successful narrowband interference detection and mitigation with help of a subband system. In the context of FBMC, the problem of channel equalization in an oversampled system is analyzed and solved with low complexity subcarrier-wise equalizers.

These equalizers are applied in different scenarios with subcarriers spanning from a few kHz up to 100 kHz giving good equalization results. Furthermore, the equalizers are useful in the synchronization of fractional time delay, they can improve performance when correcting carrier frequency offsets and are useful for mitigating in-subband narrowband interference. In order to feed the subcarrier equalizers with required information to tune their coefficients, channel impairment estimation methods for FBMCs were applied. We adapted training sequence and scattered pilot based estimation to the filter bank particularities and showed that they produce useful timing and frequency offset estimates, along with accurate channel state information. With the help of the low complexity equalizer, the estimation range of fractional time delay can be expanded well beyond the ambiguity limits imposed by the pilot separation in the scattered pilot-aided approach. One important detail not to be missed is that all processing takes place at the low rate, after the analysis filter bank. Although synchronization may have to be coarsely performed before the AFB, the results of this work show in what range the system can obtain good estimates and correct synchronization errors subcarrier-wise. This enables exploiting the high selectivity of the subchannel filters to take care of the channelization filtering, i.e., separating different user bands.

5.1 Summary of the Main Differences between OFDM and FBMC

In general, the results contributed in this thesis show that filter banks are becoming a ripe technology that can offer the significant benefits sought after in modern wireless communications: robustness and spectral efficiency. Filter bank based multicarrier enjoys the advantages of multicarrier communications, namely simple wideband channel estimation and equalization, synchronization, robustness to narrowband interference and the option to configure the communication link with flexibility and scalability. The main enabler of further advantages over simple FFT based solutions is the possibility of designing the subchannels with desired stopband attenuation. This leads to gains in throughput due to the reduction of needed subcarriers acting as guard band and also because spectral leakage from strong adjacent non-synchronous signals is better under control. Another reason for better throughput is the lack of the cyclic prefix typical of OFDM. In the PHYDYAS project, WiMAX was taken as a reference for an advanced OFDM-based wireless communi-

cation system. A filter bank upgrade based on our research, together with other PHYDYAS partners, showed in complete link-level simulations a gain of around 20% [105] and a slow decay of the gain with increasing number of uplink users [114]. Within the typical number of uplink multiplexed users in WiMAX, the FBMC throughput still outperforms OFDM.

The reason for the capacity decrease with growing number of uplink users lies in one of the main disadvantages of the filter banks: The overlapping nature of the FB waveforms. This causes the transmission blocks to have preceding and trailing 'tails' with a length depending on the overlapping factor K. These tails are nevertheless important for correct transmission at subcarrier level. Shortening them artificially or allowing overlap with other asynchronous communications on the same band to increase efficiency can lead to degradation of performance in the first and/or last symbols of the burst. Additionally, cutting the tails also induces spectral leakage into neighboring subchannels, causing spectral regrowth. Optimization of the FBMC signal in the time direction is actually an interesting challenge for future research. Initial studies have been carried out within the PHYDYAS program and reported in [57].

The advantage of applying only one subchannel for separating signal multiplexes can be regarded as a disadvantage if it is compared to a quasi-synchronous OFDM system, in which no guard band is needed. The more users share a given bandwidth, the more unused subchannels appear in the bandwidth, as also reported in the submission [114] mentioned above. However, if the OFDM system is not synchronized within the cyclic prefix length, it would need a significantly higher number of subbands to separate the frequency multiplexes.

With regard to advanced and sophisticated communication techniques, current research is proving that FBMC can be applied in the MIMO context, for example exploiting multiple transmit and receive antennas to obtain spatial diversity gain [55, 58], or spatial multiplexing [29]. Nevertheless, not all MIMO methods that work in OFDM are directly applicable to FBMC. This is because of the characteristics of the FBMC subchannel signals, mainly the data-dependent complex interference on a symbol at a certain time and frequency locations, caused by the symbols surrounding it. For example, [58, 103] show that the Alamouti space-time coding scheme [6] is not directly applicable, turning this problem into an appealing research topic. In [103] a block-wise Alamouti approach is proposed as a viable alternative for moderate mobilities.

A final shortcoming of the filter banks compared to plain FFT systems is that FBs have a higher computational complexity. However, regarding the

total system complexity, i.e., taking into account all the other functions such as for example advanced channel decoding, it has been found to be only moderately higher in the filter bank case [105]. More detailed numerical analysis is expected to be presented in the closing PHYDYAS project documents.

The research presented here strongly focuses on filter banks and uses simple FFT-based references to benchmark the achieved improvements of the FBs. There are also modifications that can be applied to OFDM systems, in order to combat its disadvantage of slowly decaying sidelobes. The simplest and commonly used solution is additional filtering of the OFDM signal to better contain it to a certain frequency band. Typical solutions assume still a relatively wide transition band, in the order of 10 to 20 % of the signal band, to achieve low implementation complexity. Filter banks have, no doubt, higher complexity than the traditional basic approach, but on the other hand they offer the highest possible flexibility in composing the used, possibly non-contiguous signal band for transmission and reception, with the resolution of subband bandwidth. Further, filter banks implement the channel filtering jointly with subcarrier multiplexing. To achieve similar filtering characteristics and similar implementation complexity, highly-optimized multirate signal processing solutions would be needed for channel filtering. To achieve this together with high flexibility is an active topic in software radio oriented studies.

Other approaches increase their transmission overhead in order to obtain lower sidelobes. For example, the authors of [156] propose precoding the data before the IFFT at the transmitter. The method involves a precoding overhead and also a complex optimization task to obtain the coding matrix. Further, this matrix has to be calculated every time the configuration of active channels varies, losing therefore the simplicity of OFDM. Additionally, the transition band is still considerably wider than what can be achieved in a filter bank design with similar stopband attenuation and relatively low overlapping factor.

One well-known method to reduce OFDM sidelobes is raised-cosine windowing [150]. Our conclusion in [54] was that to obtain similar out of band radiation as with FBs, the required length of the cosine window tails, which is pure overhead, becomes prohibitive.

5.2 Suggestions for Future Research

The research within the PHYDYAS project chose WiMAX as the OFDM-based reference. Now it seems that LTE is getting wider acceptance. Because the LTE downlink is also based on OFDMA, similar conclusions as in the

WiMAX studies can be drawn. Moreover, the minimal uplink allocation for a user contains more subcarriers and more symbols in time domain than the minimal WiMAX allocation (uplink PUSC):12 subcarriers x 7 OFDM symbols, as compared to 4x3. A direct consequence is that in LTE there are less allocations within one multiplex, leading to less guard band and guard time overhead in a hypothetical LTE evolution based on FBs (i.e., uplink throughput gain in the FBMC approach is not so much degraded by multiplexes with full number of active users). Furthermore, LTE appears to prefer frequency division duplexing (FDD) to the time division duplexing (TDD) favored in WiMAX. In FDD mode, the tails around the main signal energy do not need protection by guard times or in uplink are needed less frequently, again reducing the FB overhead.

At this point it is also interesting to mention publication [53], in which our research group studies a filter bank based uplink waveform similar to LTE's SC-FDMA waveform. The synthesization of a filter bank-spread-FBMC waveform is possible, although the reduction in the PAPR of the signal compared to the MC implementation is somewhat lower as in the DFT-spread-OFDMA technique.

As a final comment regarding the comparison between the current contenders in the race to 4G and FBMC, it is important to notice that in our research we have tried to adapt the FBMC system to comply with WiMAX parameters as much as possible. Developing an FBMC system optimized from scratch according to its own peculiarities might be an interesting continuation topic and might possibly return better throughput gains.

Regarding other future studies involving filter banks, a current and hot field of research today is cognitive radio. The spectral properties of the filter bank based systems are a great match to the requirements of the cognitive radio paradigm. Our research group has proposed methods to perform spectral sensing, exploiting the selectivity of the filter banks [51, 52]. Sensing bands are introduced within the secondary user signal to sniff for the primary user, without suffering from the distortion of the surrounding secondary user signal.

There are more exciting future research possibilities linking with the work presented in this thesis and also the more extensive research performed at our department and in the PHYDYAS project. One interesting direction is to perfect the advanced simulators that were produced during this work, including more elements that appear in actual transmission and how they affect the filter bank based system. For example, the analysis and inclusion of the non-linearities or IQ-imbalances of the transmission chain, and how these elements

interact with the other subsystems. It would be a fantastic opportunity to obtain feedback from the hardware demonstrator [59, 105] that resulted from the PHYDYAS project in order to advance knowledge of practical issues in FBMC transmission.

Finally, it would be exciting to surf the wave of cognitive radio and be able to establish some day the supremacy of filter banks in this concept. Spectral sensing and monitoring (detection of reappearance of a primary user during secondary transmission) in the oversampled receiver is still an immature issue. In this case it is particularly important to exploit the good selectivity of the filter bank and to study the impairments that can negatively affect its properties. An example is the non-linearity of the power amplifier, which can easily degrade the good spectral containment of the FBMC signal and impair spectral sensing.

As always when future interesting research topics are considered: Your imagination is the limit.

Chapter 6

Summary of Publications

The second part of this thesis consists of five publications: Three articles ([P1]-[P3]) published in peer-reviewed scientific journals and two conference papers ([P4,P5]). From these, [P2] is going to be used also in the dissertation of doctoral candidate Tero Ihalainen and was mentioned in the thesis of Dr. Tech. Mika Rinne as part of his extensive publication list. In Section 6.2 the contribution of the author of this thesis to [P2] is clearly differentiated. All the other publications are exclusively part of this thesis. In this chapter, the results of the publications and the contributions of the author of the thesis are summarized.

6.1 Overview of the Publication Results

In [P1] we study the application of an efficient, complex and critically decimated PR filter bank in the subband system configuration to mitigate narrowband interference in a DSSS communication signal in AWGN. The complex exponentially modulated filter bank permits efficient complex baseband processing of the interfered signal. The high selectivity of the prototype filter prevents the energy of the narrowband interference from leaking to adjacent subbands even at very high interference-to-signal ratios, which is the main problem in FFT based NBI suppression. Without the leakage of the NBI energy, the interference distorts only the subbands that correspond to its spectral location and only they undergo mitigation processing. An improved adaptive threshold NBI detection algorithm is introduced that leads to better identification of the interfered subbands. Furthermore, a shortened despreading approach is proposed to fight the transients appearing due to the block pro-

cessing nature of the algorithm. This improves the BER of the bits affected by the transients almost to the performance obtained with the help of guard bits. The results match very well with the predictions of a simplified SNR reduction analysis due to elimination of useful signal bands. We also explore the needed amount of data to obtain useful NBI estimates, which is interesting for knowing how fast an interferer can change its frequency location and still be excised by our NBI mitigation technique.

Publication [P2] addresses channel equalization in FB-based communications. At the moment of the research, the equalization in FBMC was not well understood. Equalization is performed at a $2\times$ oversampled AFB of the transmultiplexer system, in order to place the desired information onto the real part of the signal. Then final critical sampling by taking the real part of the complex subband signal takes place. The paper presents the expressions for calculating the ISI and ICI powers of the equalized system when selective prototype filters with overlapping factor $\rho = 1$ are used. This enables simple semianalytic modeling of the PR TMUX with different equalizers. Since FBMC does not use a CP like OFDM, the channel response in the subchannels may be mildly fading, especially if M is relatively small. For this case, we derive low-complexity equalizers and the calculation of their coefficients to obtain the desired response in a frequency sampled manner. The amplitude and phase subchannel equalizer (AP-SCE) provides a flexible means to independently equalize amplitude and phase of the distorted signal. Moreover, some advantage with respect to a complex FIR equalizer can be gained from equalizing the phase independently when the reception suffers from fractional time delay. This equalization concept was rewarded with a patent [104]. Extensive simulations show a good match between the analytic and the simulated results. Moreover, scenarios with frequency and timing offsets, error control coding and the effect of the power amplifier non-linearity are studied. The BER performance and computational complexity of this approach is compared to OFDM, showing a promising alternative to FFT based MC, especially because most of the synchronization and equalization processing takes place after the analysis bank.

The logical evolution of the research of [P2] is reported in [P3], which concentrates on channel estimation and synchronization matters. Although the FBMC/OQAM NPR filter bank is different from the one used in [P2], the results are also applicable for that type of implementation. The research that led to these results was part of a common effort of a multinational and multidisciplinary research consortium within the European Commission FP7

research program. One of its objectives was to prove the viability of a filter bank based WiMAX substitute, maintaining as much compatibility as possible. In [P3], channel estimation and synchronization based on pilots arranged in a similar way as in WiMAX is tested, after providing an analysis of both problems and their interactions. Special pilot constructions are needed due to the inherent interference arising from the filter bank. The auxiliary pilot approach is chosen because it has the same bandwidth efficiency as common OFDM pilots, and we suggest ways to arrange the pilot pair to minimize computations. Also, a new iterative interference cancellation approach for jointly estimating the channel and the FTD is introduced, overcoming the limitations of the pilot separation for unambiguous FTD estimation. This technique can prove especially useful when sparse pilot allocations are used, such as in the MIMO scenario. In the multiantenna case, the pilot allocations have to be shared by the antennas, so the pilots for each transmitter-receiver stream are more separated, if the overhead due to the pilots is to remain the same. Simulations in quite a number of different scenarios show that the filter bank based WiMAX can perform as well as OFDM while providing a higher throughput.

The filter bank based multicarrier implementation presented in the conference papers [P4] and [P5] is the same as in [P2]: a PR EMFB TMUX with $2\times$ oversampling at the receiver processing. In [P4], the same problem as in [P1] is addressed, i.e., narrowband interference mitigation. However, now the interference is affecting one or two subchannels in a MC transmission over a multipath channel and the AP-SCE is applied to notch out the interference. The equalizer gain closest to the NBI is tuned in an MSE-like way to provide simultaneously channel equalization and NBI mitigation.

Finally, [P5] was published before [P3], although here we also discuss channel synchronization and estimation. In [P5] the EMFB-based FBMC system is dimensioned so that the channel response at subchannel level is mildly frequency selective and the advantages of the frequency sampled equalizer of [P2] are better exploited. Contrasting with the scattered pilot methods of [P3], in [P5] the estimation of the channel parameters is based on a training sequence (preamble) in each subchannel. This is more convenient in the case of wider subchannel bandwidths. With the proposed preambles, a low complexity approach to estimating the channel parameters needed by the AP-SCE is obtained. This publication also includes a study on how to perform frame synchronization by correlation of the training sequence. A main result of [P5] is that all the synchronization and channel estimation and equalization oper-

ations are done in the frequency domain, after the AFB. This motivated our team to pursue the same objective in the research with the narrower subbands and the scattered pilot based estimation approach of [P3].

An important common factor in all the publications is that all processing (detection, estimation, distortion correction) takes place after analysis filtering, at low rate. The highly selective subchannel filters are able to provide sufficient attenuation of non-synchronous signals so as to take care of the channelization filtering.

6.2 Author's Contribution to the Publications

The research that resulted in this thesis was carried out at the Department of Communications Engineering of the Tampere University of Technology in Tampere, Finland, with the support of Tekes, the Academy of Finland, the European Commission, Insta Oy and Nokia. The author has been a member of an active filter bank research group under close supervision of Prof. Markku Renfors. The core of the research group was formed by Dr. Ari Viholainen, M.Sc. Tero Ihalainen and the author of this thesis, but also Dr. Yuan Yang, M.Sc. Juuso Alhava, M.Sc. Toni Levänen and M.Sc. Usman Rahim participated in the common efforts. Therefore, the author's contribution cannot be separated completely and precisely from the co-author's contributions, since the work was performed under close interaction. Nevertheless, the author's contribution to the publications included in this thesis has been essential developing the theoretical models and building the simulation environments, performing the simulations and analyzing their results. The author has written most part of each of the publications, in which he is the main author, and has contributed with several passages in [P2]. The following paragraphs summarize the main contributions to the publications. The co-authors of these publications have seen these descriptions and agree with the author.

In publication [P1] the author applied the EMFB, which he helped to develop in [S1] to the NBI excision problem. He came up with the idea of iteratively setting the NBI detection threshold. Furthermore, he discovered the degradation introduced by the transients and proposed a means to combat them efficiently. The NBI mitigation method presented in [P1] was eventually implemented on hardware, as reported in [S2]. Furthermore, the author continued the research in the context of frequency-domain equalized single-carrier transmission contributing to the NBI power estimation and location techniques in [S3].

The theoretical model for complete ISI and ICI equalization in the 2× oversampled AFB in [P2] was postulated by Prof. Renfors and validated by M.Sc. Tero Ihalainen and the author of this thesis. Together they created the testbed on which the low-complexity AP-SCE was thoroughly examined in different environments, such as error control coding, presence of non-linearities and time and frequency offsets. The author of this thesis especially contributed to the CFO results and also to the study of the effect of the high PAPR of the MC signal with a non-linear PA. This original investigation seeded the research on PAPR reduction methods reported in [S4].

The author was responsible for the analysis of the channel impairments and their interactions in [P3]. The core of the WiMAX-like FBMC simulator was developed by him, and he implemented the channel parameter estimation functionalities in the FBMC/OQAM environment. Prof. Markku Renfors proposed the iterative interference cancellation idea for joint FTD and channel estimation, and the author of this thesis perfected and successfully implemented the idea. Convenient scattering of the pilots for channel parameter estimation was suggested by the author to avoid unnecessary nesting of the auxiliary pilot calculations.

In [P4] the author tuned the AP-SCE for NBI suppression in the FBMC case. After extensive simulations of different equalizer gain weighting approaches, he came up with the MSE-like expression for considering the interference power when calculating the desired frequency gains of the equalizer. This approach, including a means for estimating the power of the NBI was also used in [S3].

Publication [P5] considers the preamble based synchronization of the EMFB TMUX. Prof. Markku Renfors designed the preambles to concentrate their energy in the optimum frequency locations for channel parameter estimation for the AP-SCE. The author came up with the idea for low complexity estimation of the frequency sampled equalizer gains with help of the preambles. The author also overcame the difficulty of the self interference in the oversampled filter bank, which was not so well understood at the moment of this research.

Bibliography

[1] "Physical layer standard for cdma2000 spread spectrum systems, release C," *3GPP2 doc. C.S0002-C, v. 1.0*, May 2002. [Online]. Available: http://www.3gpp2.org/public_html/specs/C.S0002-A-1.pdf

[2] "IEEE standard for local and metropolitan area networks. Part 16: Air interface for fixed and mobile broadband wireless access systems. Amendment 2: Physical and medium access control layers for combined fixed and mobile operation in licensed bands and corrigendum 1," *IEEE Std 802.16e-2005 and IEEE Std 802.16-2004/Cor 1-2005 (Amendment and Corrigendum to IEEE Std 802.16-2004)*, pp. 1–822, 2006.

[3] "IEEE standard for Part 11: Wireless LAN medium access control (MAC) and physical layer (PHY) specifications," *IEEE Std 802.11-2007*, pp. 1–1233, 2007.

[4] "IEEE standard for Part 15.4: Wireless MAC and PHY specifications for low rate WPANs. amendment 1: Add alternate phys," *IEEE Std 802.15.4a-2007 (Amendment to IEEE Std 802.15.4-2006)*, pp. 1–203, 2007.

[5] A. N. Akansu and M. J. Medley, *Wavelet, Subband, and Block Transforms in Communications and Multimedia*. Springer-Verlag, Apr. 1999.

[6] S. Alamouti, "A simple transmit diversity technique for wireless communications," *IEEE J. Select. Areas Commun.*, vol. 16, no. 8, pp. 1451 –1458, Oct. 1998.

[7] J. Alhava and M. Renfors, "Complex lapped transforms and modulated filter banks," in *Proc. Int. Workshop on Spectral Methods and Multirate Signal Processing*, Toulouse, France, Sep. 2002, pp. 87–94.

[8] ——, "Exponentially-modulated filter bank-based transmultiplexer," in *Proc. IEEE Int. Symp. Circuits and Systems*, vol. IV, Bangkok, Thailand, May 2003, pp. 233–236.

[9] P. Amini and B. Farhang-Boroujeny, "Packet format design and decision directed tracking methods for filter bank multicarrier systems," *EURASIP Journal on Advances in Signal Processing*, vol. 2010, pp. 7–7, 2010.

[10] ANS/TIA/EIA-95-B-99, "Mobile station-base station compatibility standard for wideband spread spectrum cellular systems,," Feb. 1999.

[11] H. Atarashi, N. Maeda, S. Abeta, and M. Sawahashi, "Broadband packet wireless access based on VSF-OFCDM and MC/DS-CDMA," in *Proc. IEEE Int. Symp. Personal, Indoor and Mobile Radio Communications*, vol. 3, Lisbon, Portugal, Sep. 2002, pp. 992–997.

[12] L. Baltar, D. Waldhauser, and J. Nossek, "MMSE subchannel decision feedback equalization for filter bank based multicarrier systems," in *Proc. IEEE Int. Symp. Circuits and Systems*, Taipei, Taiwan, May 2009, pp. 2802 –2805.

[13] M. Bellanger and J. Daguet, "TDM-FDM transmultiplexer: Digital polyphase and FFT," *IEEE Trans. Commun.*, vol. 22, no. 9, pp. 1199 – 1205, Sep. 1974.

[14] M. Bellanger, "Specification and design of a prototype filter for filter bank based multicarrier transmission," in *Proc. IEEE Int. Conf. Acoustics, Speech, and Signal Processing*, vol. 4, Salt Lake City, USA, May 2001, pp. 2417–2420.

[15] A. Berni and W. Gregg, "On the utility of chirp modulation for digital signaling," *IEEE Trans. Commun.*, vol. 21, no. 6, pp. 748 – 751, Jun. 1973.

[16] H. Bölcskei, "Blind estimation of symbol timing and carrier frequency offset in wireless OFDM systems," *IEEE Trans. Commun.*, vol. 49, no. 6, pp. 988–999, Jun. 2001.

[17] G. Bongiovanni, P. Corsini, and G. Frosini, "One-dimensional and two-dimensional generalised discrete fourier transforms," *IEEE Trans. Acoust., Speech, Signal Processing*, vol. 24, no. 1, pp. 97 – 99, Feb. 1976.

[18] R. Bregović, "Optimal design of perfect-reconstruction and nearly perfect-reconstruction multirate filter banks," Ph.D. dissertation, Tampere University of Technology, Aug. 2003, TUT Publications 428, ISBN 952-15-1055-2.

[19] S. Buzzi and M. Lops, "Symbol synchronization and data detection in DS/CDMA systems affected by multiple narrowband interferers," in *Proc. IEEE Radio and Wireless Symp.*, San Diego, USA, Jan. 2006, pp. 371–374.

[20] S. Buzzi, M. Lops, and H. Poor, "Code-aided interference suppression for DS/CDMA overlay systems," *Proceedings of the IEEE*, vol. 90, no. 3, pp. 394 –435, Mar. 2002.

[21] X. Caijie, W. Aihua, A. Jianping, and G. Yongzheng, "Rejection of frequency sweeping interference in DSSS systems using improved polar exciser algorithm," in *Proc. WiCom 2007*, Shanghai, China, Oct. 2007, pp. 1228 –1231.

[22] J. Calvert, "The electromagnetic telegraph," revised, Dec. 2008. [Online]. Available: http://mysite.du.edu/~jcalvert/tel/morse/morse.htm

[23] R. W. Chang, "Synthesis of band-limited orthogonal signals for multichannel data transmission," *Bell Syst. Tech. J.*, vol. 45, pp. 1775–1796, Dec. 1966.

[24] C. Crochiere and R. Rabiner, *Multirate Digital Signal Processing*. Prentice-Hall, 1983.

[25] R. Crochiere and L. Rabiner, "Interpolation and decimation of digital signals - A tutorial review," *Proc. IEEE*, vol. 69, no. 3, pp. 300 – 331, Mar. 1981.

[26] A. Croisier, D. Esteban, and C. Galand, "Perfect channel splitting by use of interpolation, decimation, tree decomposition techniques," in *Proc. Int. Conf. on Information Sciences and Systems*, Patras, Greece, Aug. 1976, pp. 443–446.

[27] P. Diniz, E. da Silva, and S. Netto, *Digital Signal Processing: System Analysis and Design*. Cambridge University Press, 2002.

[28] F. Dominique and P. Petrus, "Spectral redundancy exploitation in narrow band interference rejection for a PN-BPSK system," in *Proc. IEEE Milcom*, vol. 2, Fort Monmouth, USA, Oct. 1994, pp. 405–409.

[29] M. El Tabach, J.-P. Javaudin, and M. Helard, "Spatial data multiplexing over OFDM/OQAM modulations," in *Proc. IEEE Int. Conf. Communications*, Glasgow, Scotland, Jun. 2007, pp. 4201 –4206.

[30] D. Falconer, S. Ariyavisitakul, A. Benyamin-Seeyar, and B. Eidson, "Frequency domain equalization for single-carrier broadband wireless systems," *IEEE Commun. Mag.*, vol. 40, no. 4, pp. 58–66, Apr. 2002.

[31] B. Farhang-Boroujeny, "Analysis of post-combiner equalizers in cosine-modulated filterbank-based transmultiplexer systems," *IEEE Trans. Commun.*, vol. 51, pp. 3249–3262, Dec. 2003.

[32] ——, "Multicarrier modulation with blind detection capability using cosine modulated filter banks," *IEEE Trans. Commun.*, vol. 51, pp. 2057–2070, Dec. 2003.

[33] ——, "Filter bank spectrum sensing for cognitive radios," *IEEE Trans. Signal Processing*, vol. 56, no. 5, pp. 1801 –1811, May 2008.

[34] B. Farhang-Boroujeny and R. Kempter, "Multicarrier communication techniques for spectrum sensing and communication in cognitive radios," *IEEE Commun. Mag.*, vol. 46, no. 4, pp. 80–85, Apr. 2008.

[35] K. Fazel and S. Kaiser, *Multi-Carrier and Spread Spectrum Systems: From OFDM and MC-CDMA to LTE and WiMAX, 2nd edition.* John Wiley & Sons, 2008.

[36] N. J. Fliege, *Multirate Digital Signal Processing.* John Wiley & Sons, 1994.

[37] T. Fusco, A. Petrella, and M. Tanda, "Data-aided time domain synchronization for filter-bank multicarrier systems," in *Proc. European Signal Processing Conf.*, Lausanne, Switzerland, Aug. 2008.

[38] ——, "Data-aided symbol timing and CFO synchronization for filter bank multicarrier systems," *IEEE Trans. Wireless Commun.*, vol. 8, no. 5, pp. 2705–2715, May 2009.

[39] J. Gevargiz, M. Rosenmann, P. Das, and L. B. Milstein, "A comparison of weighted and non-weighted transform domain processing systems for narrowband interference excision," in *Proc. IEEE Milcom*, vol. 3, Los Angeles, USA, Oct. 1984, pp. 474–477.

[40] A. Gokceoglu, A. Ghadam, and M. Valkama, "Effects of power amplifier memory on adaptive feedforward linearizers," in *Proc. IEEE Int. Symp. Wireless Communication Systems (ISWCS 2008*, Reykjavik, Iceland, Dec. 2008, pp. 304 –308.

[41] S. Haykin, "Cognitive radio: brain-empowered wireless communications," *IEEE J. Select. Areas Commun.*, vol. 23, no. 2, pp. 201–220, Feb. 2005.

[42] S. Haykin, D. Thomson, and J. Reed, "Spectrum sensing for cognitive radio," *Proc. IEEE*, vol. 97, no. 5, pp. 849 –877, May 2009.

[43] S. Haykin, *Adaptive Filter Theory (4th edition)*. Prentice-Hall, September 2001.

[44] P. Henttu, A. Pouttu, and M. Raustia, "Performance of PIE interference suppressor using FFT, DCT and ELT transformations in FH/DS communications," in *Proc. of IEEE EUROCOMM*, München, Germany, May 2000.

[45] P. Henttu and H. Saarnisaari, "Method for estimating power in a CDMA receiver," EP Patent EP 1 347 587 B1, Nov. 10, 2004. [Online]. Available: http://www.patentlens.net/patentlens/patent/EP_1347587_B1/en/

[46] ——, "Telecommunications system and receiver," US Patent US Pat. 7 173 960, Feb. 06, 2007. [Online]. Available: http://www.patentlens.net/patentlens/patent/US_7173960/en/

[47] ——, "Telecommunications system and receiver," US Patent US Pat. 7 426 244, Sep. 16, 2008. [Online]. Available: http://www.patentlens.net/patentlens/patent/US_7426244/en/

[48] T. Hidalgo Stitz, A. Viholainen, T. Ihalainen, and M. Renfors, "CFO estimation and correction in a WiMAX-like FBMC system," in *Proc. IEEE Workshop on Signal Processing Advances in Wireless Communications*, Perugia, Italy, Jun. 2009.

[49] B. Hirosaki, "An analysis of automatic equalizers for orthogonally multiplexed QAM systems," *IEEE Trans. Commun.*, vol. 28, pp. 73–83, Jan. 1980.

[50] T. Ihalainen, T. Hidalgo Stitz, and M. Renfors, "On the performance of low-complexity ASCET-equalizer for a complex transmultiplexer in wireless mobile channel," in *Proc. Int. OFDM-Workshop*, Hamburg, Germany, Sep. 2002.

[51] T. Ihalainen, A. Viholainen, T. Hidalgo Stitz, and M. Renfors, "Reappearing primary user detection in FBMC/OQAM cognitive radios," in *Int. Conf. on Cognitive Radio Oriented Wireless Networks and Communications*, Cannes, France, Jun. 2010.

[52] ——, "Spectrum monitoring scheme for filter bank based cognitive radios," in *Proc. Future Network & Mobile Summit (FNMS 2010)*, Florence, Italy, Jun. 2010.

[53] T. Ihalainen, A. Viholainen, T. Hidalgo Stitz, M. Renfors, and M.Bellanger, "Filter bank based multi-mode multiple access scheme for wireless uplink," in *Proc. European Signal Processing Conf.*, Glasgow, Scotland, Aug. 2009, pp. 1354–1358.

[54] T. Ihalainen, A. Viholainen, and M. Renfors, "On spectrally efficient multiplexing in cognitive radio systems," in *Proc. Int. Symp. on Wireless Pervasive Computing*, May 2008, pp. 675 –679.

[55] T. Ihalainen, A. Ikhlef, J. Louveaux, and M. Renfors, "Channel equalization for multi-antenna FBMC/OQAM receivers," *IEEE Trans. Veh. Technol.*, 2010, submitted.

[56] INFSO-ICT-211887 Project PHYDYAS, *Deliverable 5.1: Prototype filter and structure optimization*, Jan. 2009. [Online]. Available: http://www.ict-phydyas.org/delivrables/PHYDYAS-D5-1.pdf/at_download/file

[57] ——, *Deliverable 2.2: Synchronization and initialization with single antenna. Blind techniques*, Jan. 2009. [Online]. Available: http://www.ict-phydyas.org/delivrables/Phydyas-D2-2.pdf/at_download/file

[58] ——, *Deliverable 4.1: MIMO channel matrix estimation and tracking*, Jan. 2009. [Online]. Available: http://www.ict-phydyas.org/delivrables/Phydyas-D4.1.pdf/at_download/file

[59] ——, *Deliverable 9.2: WiMAX simulation results Lab setup and measurements*, Jul. 2009. [Online]. Available: http://www.ict-phydyas.org/delivrables/PHYDYAS-D9-2.pdf/at_download/file

[60] ITU-R, "300 bits per second duplex modem standardized for use in the general switched telephone network," Recommendation V.21, original draft, 1964.

[61] ——, "Guidelines for evaluation of radio transmission technologies for IMT-2000," Recommendation M.1225, 1997.

[62] ——, "International mobile telecommunications-2000 (IMT-2000)," Recommendation M.687-2, 1997.

[63] B. Jahan, M. Lanoiselée, G. Degoulet, and R. Rabineau, "Full synchronization method for OFDM/OQAM and OFDM/QAM modulations," in *Proc. IEEE Int. Symp. Spread Spectrum Techniques and Applications*, Bologna, Italy, Aug. 2008, pp. 344–348.

[64] J.-P. Javaudin, D. Lacroix, and A. Rouxel, "Pilot-aided channel estimation for OFDM/OQAM," *Proc. IEEE Vehicular Technology Conf.*, vol. 3, pp. 1581–1585, Apr. 2003.

[65] E. Kanterakis, "A novel technique for narrowband/broadband interference excision in DS-SS communications," in *Proc. IEEE Milcom*, vol. 2, Fort Monmouth, USA, Oct. 1994, pp. 628–632.

[66] T. Karp and N. J. Fliege, "Modified DFT filter banks with perfect reconstruction," *IEEE Trans. Circuits Syst. II*, vol. 46, pp. 1404–1414, Nov. 1999.

[67] D. Katselis, E. Kofidis, A. Rontogiannis, and S. Theodoridis, "Preamble-based channel estimation for CP-OFDM and OFDM/OQAM systems: A comparative study," *IEEE Trans. Signal Processing*, vol. 58, no. 5, pp. 2911 –2916, May 2010.

[68] S. Kay, "A fast and accurate single frequency estimator," *IEEE Trans. Acoust., Speech, Signal Processing*, vol. 37, no. 12, pp. 1987–1990, Dec. 1989.

[69] T. Kumpumäki, M. Isohookana, and J. Juntti, "Narrow-band interference rejection using transform domain signal processing in a hybrid

DS/FH spread-spectrum system," in *Proc. IEEE Milcom*, vol. 1, Monterey, USA, Nov. 1997, pp. 89–93.

[70] R. Laroia, S. Uppala, and J. Li, "Designing a mobile broadband wireless access network," *IEEE Signal Processing Mag.*, vol. 21, no. 5, pp. 20 – 28, Sep. 2004.

[71] J. Laster and J. Reed, "Interference rejection in digital wireless communications," *IEEE Signal Processing Mag.*, vol. 14, no. 3, pp. 37 –62, May 1997.

[72] B. Le Floch, M. Alard, and C. Berrou, "Coded orthogonal frequency division multiplex," *Proc. IEEE*, vol. 83, pp. 982–996, Jun. 1995.

[73] E. A. Lee and D. G. Messerschmitt, *Digital Communication, 2nd edition.* Kluwer Academic Publishers, 2000.

[74] J.-N. Lee and J.-T. Yuan, "Interpolation lattice filters for narrowband interference cancellation in pn spread spectrum communication systems," in *Proc. IEEE Int. Symp. Spread Spectrum Techniques and Applications*, vol. 1, Sep. 2000, pp. 107–111.

[75] Y. Lee, D. Kang, H. Park, and W. Oh, "Tone-interference cancellation algorithm for direct-sequence spread-spectrum systems," in *Proc. ASID*, Hong Kong, China, Oct. 2009, pp. 25–28.

[76] C. Lélé, J.-P. Javaudin, R. Legouable, A. Skrzypczak, and P. Siohan, "Channel estimation methods for preamble-based OFDM/OQAM modulations," in *Proc. European Wireless 2007*, Paris, France, Apr. 2007.

[77] C. Lélé, R. Legouable, and P. Siohan, "Channel estimation with scattered pilots in OFDM/OQAM," in *Proc. IEEE Workshop on Signal Processing Advances in Wireless Communications*, Recife, Brazil, Jul. 2008, pp. 286 –290.

[78] ——, "Iterative scattered pilot channel estimation in OFDM/OQAM," in *Proc. IEEE Workshop on Signal Processing Advances in Wireless Communications*, Jun. 2009, pp. 176–180.

[79] C.-N. Li, G.-R. Hu, and M.-J. Liu, "Narrow-band interference excision in spread-spectrum systems using self-orthogonalizing transform-domain adaptive filters," *IEEE J. Select. Areas Commun.*, vol. 18, no. 3, pp. 403–406, Mar. 2000.

[80] L. Lin and B. Farhang-Boroujeny, "Convergence analysis of blind equalizer in a filter-bank-based multicarrier communication system," *IEEE Trans. Signal Processing*, vol. 54, no. 10, pp. 4061 –4067, Oct. 2006.

[81] H. S. Malvar, *Signal Processing with Lapped Transforms*. Artech House, 1992.

[82] H. Malvar, "Modulated QMF filter banks with perfect reconstruction," *Electronics Letters*, vol. 26, no. 13, pp. 906–907, 1990. [Online]. Available: http://link.aip.org/link/?ELL/26/906/1

[83] J. Manton, "Optimal training sequences and pilot tones for OFDM systems," *IEEE Commun. Lett.*, vol. 5, no. 4, pp. 151–153, Apr. 2001.

[84] H. Markey and G. Antheil, "Secret communication sytsem," Patent US Pat. 2 292 387, Aug., 1942.

[85] M. Medley, G. Saulnier, and P. Das, "Applications of the wavelet transform in spread spectrum communications systems," in *Proc. SPIE*, vol. 2242, 1994.

[86] L. Milstein and P. Das, "An analysis of a real-time transform domain filtering digital communication system–Part I: Narrow-band interference rejection," *IEEE Trans. Commun.*, vol. 28, no. 6, pp. 816–824, Jun. 1980.

[87] L. Milstein, "Interference rejection techniques in spread spectrum communications," *Proc. IEEE*, vol. 76, no. 6, pp. 657 –671, Jun. 1988.

[88] J. Mitola III and G. Maguire, Jr., "Cognitive radio: Making software radios more personal," *IEEE Personal Commun. Mag.*, vol. 6, no. 4, pp. 13–18, Aug. 1999.

[89] H. G. Myung, J. Lim, and D. J. Goodman, "Single carrier FDMA for uplink wireless transmission," *IEEE Veh. Technol. Mag.*, vol. 1, no. 3, pp. 30–38, Sep. 2006.

[90] K. Nayebi, T. P. Barnwell, and M. J. T. Smith, "Time-domain filter bank analysis: A new design theory," *IEEE Trans. Signal Processing*, vol. 40, pp. 1412–1429, Jun. 1992.

[91] S. Nedic, "An unified approach to equalization and echo cancellation in OQAM-based multicarrier data transmission," in *Proc. IEEE Globecom*, Phoenix, USA, Nov. 1997, pp. 1519–1523.

[92] T. Nguyen, T. Laakso, and T. Tuncer, "On perfect-reconstruction allpass-based cosine-modulated IIR filter banks," in *Proc. IEEE Int. Symp. Circuits and Systems*, vol. 2, May-Jun 1994, pp. 33–36.

[93] H. Nyquist, "Certain topics in telegraph transmission theory," *Trans. AIEE*, vol. 47, no. 2, pp. 617 –644, Apr. 1928.

[94] S. Phoong, Y. Chang, and C. Chen, "DFT-modulated filterbank transceivers for multipath fading channels," *IEEE Trans. Signal Processing*, vol. 53, pp. 182–192, Jan. 2005.

[95] H. Poor and L. Rusch, "A promising multiplexing technology for cellular telecommunications: Narrowband interference suppression in spread spectrum CDMA," *IEEE Personal Commun. Mag.*, vol. 1, no. 3, pp. 14–27, Mar. 1994.

[96] A. Pouttu, J. Juntti, and T. Kumpumaki, "Adaptive transform domain interference suppression in a hybrid DS/FH-system," in *Proc. IEEE Int. Symp. Spread Spectrum Tech. Appl.*, vol. 1, Sun City, South Africa, Sep. 1998, pp. 351–355.

[97] A. Pouttu, J. Juntti, T. Kumpumaki, and M. Raustia, "Bit pattern matched phase interference suppression in a hybrid DS/FH-system," in *Proc. IEEE Milcom*, vol. 2, Atlantic City, USA, Oct-Nov 1999, pp. 841–845.

[98] R. Price, "Further notes and anecdotes on spread-spectrum origins," *IEEE Trans. Commun.*, vol. 31, no. 1, pp. 85 – 97, Jan. 1983.

[99] J. G. Proakis, *Digital Communications, 4th edition.* McGraw-Hill, 2001.

[100] M. Pun, M. Morelli, and C. Jay Kuo, *Multi-Carrier Techniques for Broadband Wireless Communications. A Signal Processing Perspective.* Imperial College Press, 2007.

[101] K. Raju, T. Ristaniemi, J. Karhunen, and E. Oja, "Jammer suppression in DS-CDMA arrays using independent component analysis," *Wireless Communications, IEEE Transactions on*, vol. 5, no. 1, pp. 77–82, Jan. 2006.

[102] C. Rapp, "Effect of HPA-nonlinearity on 4-DPSK/OFDM-signal for a digital sound broadcasting system," in *Proc. 2nd European Conf. Satellite Communications*, Liege, Belgium, Oct. 1991, pp. 179–184.

[103] M. Renfors, "A block-Alamouti scheme for filter bank based multicarrier transmission," in *Proc. European Wireless 2010*, Lucca, Italy, Apr. 2010.

[104] M. Renfors, T. Ihalainen, and T. Hidalgo Stitz, "Channel equalization," EP Patent EP 1 716 681 B1, Nov. 26, 2008. [Online]. Available: http://www.patentlens.net/patentlens/patent/EP_1716681_B1/en/

[105] V. Ringset, H. Rustad, F. Schaich, J. Vandermot, and M. Najar, "Performance of a filterbank multicarrier (FBMC) physical layer in the WiMAX context," in *Proc. Future Network & Mobile Summit (FNMS 2010)*, Florence, Italy, Jun. 2010.

[106] A. Roy and J. Doherty, "Locally optimum detection performance analysis for narrowband interference rejection in spread spectrum communications," in *Proc. IEEE Globecom*, vol. 1, Nov-Dec 2005, pp. 220–224.

[107] ——, "Robust interference suppression in spread spectrum systems using locally optimum detection," in *Proc. IEEE Milcom*, Oct. 2006, pp. 1–5.

[108] H. Ryu, "Design and performance analysis of FH/MFSK system using jammer side information in the combined jammer and Rayleigh fading channel," *Journal of the Research Institute for Computer and Information Communication*, vol. 14, no. 2, Oct. 2006.

[109] H. Saarnisaari, H. Puska, and P. Lilja, "Interference mitigation techniques for single and multi antenna receivers," in *Proc. EuCAP*, Nice, Nov. 2006, pp. 1–8.

[110] B. R. Saltzberg, "Performance of an efficient parallel data transmission system," *IEEE Trans. Commun.*, vol. 15, pp. 805–811, Dec. 1967.

[111] S. D. Sandberg and M. A. Tzannes, "Overlapped discrete multitone modulation for high speed copper wire communications," *IEEE J. Select. Areas Commun.*, vol. 13, pp. 1171–1183, Dec. 1995.

[112] T. Saramäki, "Designing prototype filters for perfect reconstruction cosine modulated filter banks," in *Proc. IEEE Int. Symp. Circuits and Systems*, vol. 3, San Diego, USA, May 1992, pp. 1606–1608.

[113] G. Saulnier, K. Yum, and P. Das, "Narrow-band jammer suppression using an adaptive lattice filter," in *Proc. IEEE Int. Conf. Acoustics, Speech, and Signal Processing*, vol. 12, Apr. 1987, pp. 2113–2116.

[114] F. Schaich, T. Hidalgo Stitz, T. Ihalainen, A. Viholainen, and M. Renfors, "Spectrally efficient transmission over evolved filter bank based WiMAX with forward error correction," *IET Communications*, 2010, submitted.

[115] T. Schmidl and D. Cox, "Robust frequency and timing synchronization for OFDM," *IEEE Trans. Commun.*, vol. 45, no. 12, pp. 1613–1621, Dec. 1997.

[116] R. Scholtz, "The origins of spread-spectrum communications," *IEEE Trans. Commun.*, vol. 30, no. 5, pp. 822 – 854, May 1982.

[117] C. Shannon, "Communication in the presence of noise," *Proc IRE*, vol. 37, no. 1, pp. 10–21, Jan. 1949.

[118] P. Siohan, C. Siclet, and N. Lacaille, "Analysis and design of OFDM/OQAM systems based on filterbank theory," *IEEE Trans. Signal Processing*, vol. 50, pp. 1170–1183, May 2002.

[119] M. J. T. Smith and T. P. Barnwell, "A procedure for designing exact reconstruction filter banks for tree-structured subband coders," in *Proc. IEEE Int. Conf. Acoustics, Speech, and Signal Processing*, San Diego, USA, Mar. 1984, pp. 27.1.1–27.1.4.

[120] ——, "Exact reconstruction techniques for tree-structured subband coders," *IEEE Trans. Acoust., Speech, Signal Processing*, vol. 34, no. 3, pp. 434–441, Jun. 1986.

[121] F. Takawira and L. B. Milstein, "Error propagation in decision feedback interference rejection DS spread spectrum systems," in *Proc. IEEE Milcom*, vol. 3, Washington DC, USA, Oct. 1987, pp. 934–937.

[122] R. Tandra and A. Sahai, "SNR walls for signal detection," *IEEE J. Select. Topics Signal in Processing*, vol. 2, no. 1, pp. 4–17, Feb. 2008.

[123] D. Thomson, "Spectrum estimation and harmonic analysis," *Proc. IEEE*, vol. 70, no. 9, pp. 1055–1096, Sep. 1982.

[124] A. Tonello and F. Rossi, "Synchronization and channel estimation for filtered multitone modulation," in *Proc. WPMC*, vol. 2, Abano Terme, Italy, Sep. 2004, pp. 590–594. [Online]. Available: http://web.diegm.uniud.it/tonello/PAPERS/CONFERENCES/WPMC2004_1.pdf

[125] TSG-RAN 3GPP TS 02.02, "Bearer services (BS) supported by a GSM public land mobile network (PLMN)," Version 3.1.1, Jan. 1990. [Online]. Available: http://www.3gpp.org/ftp/Specs/archive/02_series/02.02/0202-311.zip

[126] TSG-RAN 3GPP TS 36.211, "Physical channels and modulation," Release 8, Feb. 2009.

[127] TSG-RAN 3GPP WG1 LTE, "Cubic metric in 3GPP-LTE. Motorola Tdoc R1-060023," Jan. 2006. [Online]. Available: ftp://ftp.3gpp.org/tsg_ran/WG1_RL1/TSGR1_AH/LTE_AH_January-06/Docs/R1-060023.zip

[128] A. Vahlin and N. Holte, "Optimal finite duration pulses for OFDM," *IEEE Trans. Commun.*, vol. 44, pp. 10–14, Jan. 1996.

[129] P. P. Vaidyanathan, *Multirate Systems and Filter Banks*. Prentice-Hall, 1993.

[130] P. Vaidyanathan, T. Nguyen, Z. Doganata, and T. Saramäki, "Improved technique for design of perfect reconstruction FIR QMF banks with lossless polyphase matrices," *IEEE Trans. Acoust., Speech, Signal Processing*, vol. 37, no. 7, pp. 1042 –1056, Jul. 1989.

[131] K. van Acker, G. Leus, M. Moonen, O. van de Wiel, and T. Pollet, "Per tone equalization for DMT-based systems," *IEEE Trans. Commun.*, vol. 49, pp. 109–119, Jan. 2001.

[132] J. J. van de Beek, M. Sandell, and P. O. Borjesson, "ML estimation of time and frequency offset in OFDM systems," *IEEE Trans. Signal Processing*, vol. 45, no. 7, pp. 1800–1805, 1997.

[133] R. van Nee and R. Prasad, *OFDM for Wireless Multimedia Communications*. Artech House, 2000.

[134] B. Van Veen and K. Buckley, "Beamforming: a versatile approach to spatial filtering," *IEEE ASSP Mag.*, vol. 5, no. 2, pp. 4 –24, Apr. 1988.

[135] L. Vandendorpe, L. Cuvelier, F. Deryck, J. Louveaux, and O. Van de Wiel, "Fractionally spaced linear and decision-feedback detectors for transmultiplexers," *IEEE Trans. Signal Processing*, vol. 46, pp. 996–1011, Apr. 1998.

[136] J. Vartiainen, J. Lehtomaki, H. Saarnisaari, and M. Juntti, "Interference suppression in several transform domains," in *Proc. IEEE Milcom*, vol. 4, Atlantic City, USA, Oct. 2005, pp. 2294–2300.

[137] M. Vetterli, "Perfect transmultiplexers," in *Proc. IEEE Int. Conf. Acoustics, Speech, and Signal Processing*, vol. 4, Tokyo, Japan, Sep. 1986, pp. 2567–2570.

[138] ——, "Filter banks allowing perfect reconstruction," *Signal Processing*, vol. 10, no. 3, pp. 219–244, 1986.

[139] ——, "A theory of filter banks," in *Proc. European Signal Processing Conf.*, Den Haag, Netherlands, Sep. 1986, pp. 61–64.

[140] ——, "A theory of multirate filter banks," *IEEE Trans. Acoust., Speech, Signal Processing*, vol. 35, no. 3, pp. 356–372, 1987.

[141] A. Viholainen, J. Alhava, and M. Renfors, "Efficient implementation of 2× oversampled exponentially modulated filter banks," *IEEE Trans. Circuits Syst. II*, vol. 53, no. 10, pp. 1138–1142, Oct. 2006.

[142] A. Viholainen, T. Ihalainen, T. Hidalgo Stitz, M. Renfors, and M. Bellanger, "Prototype filter design for filter bank based multicarrier transmission," in *Proc. European Signal Processing Conf.*, Glasgow, Scotland, Aug. 2009, pp. 1359–1363.

[143] A. Viholainen, "Modulated filter bank design for communications signal processing," Ph.D. dissertation, Tampere University of Technology, Nov. 2004, TUT Publications 500, ISBN 952-15-1255-5.

[144] E. Viscito and J. Allebach, "The design of tree-structured M-channel filter banks using perfect reconstruction filter block," in *Proc. IEEE Int. Conf. Acoustics, Speech, and Signal Processing*, New York, USA, Apr. 1988, pp. 1475–1478.

[145] D. Waldhauser, L. Baltar, and J. Nossek, "MMSE subcarrier equalization for filter bank based multicarrier systems," in *Proc. IEEE Workshop on Signal Processing Advances in Wireless Communications*, Jul. 2008, pp. 525–529.

[146] ——, "Adaptive decision feedback equalization for filter bank based multicarrier systems," in *Proc. IEEE Int. Symp. Circuits and Systems*, Taipei, Taiwan, may 2009, pp. 2794 –2797.

[147] C. Wang, R. Ying, and Y. Yang, "Code-aided interference suppression in direct sequence spread spectrum systems with eigenvector sign spreading code," *Journal of Shanghai Jiaotong University (Science)*, vol. 14, no. 3, pp. 350–353, 2009.

[148] Y. Wei and G. Bi, "Interference suppression in DS-SS systems with modified discrete fourier transform," in *Proc. IEEE Asia Pacific Conf. Circuits and Systems*, Singapore, Dec. 2006, pp. 1192–1195.

[149] Y. Wei, G. Bi, and G. Li, "Tone interference suppression in DS-SS systems with modified DFT," *Signal Processing*, vol. 88, no. 11, pp. 2817 – 2824, 2008.

[150] T. Weiss, J. Hillenbrand, A. Krohn, and F. Jondral, "Mutual interference in OFDM-based spectrum pooling systems," in *Proc. IEEE Vehicular Technology Conf.*, vol. 4, Milan, Italy, May 2004, pp. 1873 – 1877.

[151] S. Werner, F. Gregorio, J. Cousseau, J. Figueroa, and R. Wichman, "Broadband power amplifier nonlinearity cancellation in OFDM systems," *Acta Technica Napocensis - Electronics and Telecommunications*, vol. 49, no. 4/2008, pp. 19–22, 2008.

[152] J. Whitehead and F. Takawira, "Code-aided blind adaptive cyclic multiuser detection," in *Proc. Satnac*, Western Cape, South Africa, Sep. 2004. [Online]. Available: http://www.satnac.org.za/proceedings/2004/AccessNetworks/No%2080%20-%20Whitehead.pdf

[153] T. Wiegand and N. J. Fliege, "Equalizers for transmultiplexers in orthogonal multiple carrier data transmission," in *Proc. European Signal Processing Conf.*, vol. 2, Trieste, Italy, Sep. 1996, pp. 1211–1214.

[154] WiMAX Forum, "Mobile system profile," Release 1.0 Approved Specification, Revision 1.5.0, Nov. 2007.

[155] A. M. Wyglinski, P. Kabal, and F. Labeau, "Adaptive filterbank multicarrier wireless systems for indoor environments," in *Proc. IEEE Vehicular Technology Conf.*, Vancouver BC, Canada, Sep. 2002, pp. 336–340.

[156] R. Xu and M. Chen, "A precoding scheme for DFT-based OFDM to suppress sidelobes," *IEEE Commun. Lett.*, vol. 13, no. 10, pp. 776–778, Oct. 2009.

[157] Y. Yang, T. Ihalainen, M. Rinne, and M. Renfors, "Frequency-domain equalization in single-carrier transmission: Filter bank approach," *EURASIP Journal on Applied Signal Processing*, vol. 2007, no. 1, pp. 135–135, 2007.

Publications

Publication P1

T. Hidalgo Stitz, and M. Renfors, "Filter-bank-based narrowband interference detection and suppression in spread spectrum systems" in *EURASIP Journal on Applied Signal Processing*, 2004 (Jan. 2004), pp. 1163-1176.

DOI= http://dx.doi.org/10.1155/S1110865704312102

EURASIP Journal on Applied Signal Processing 2004:8, 1163–1176

Filter-Bank-Based Narrowband Interference Detection and Suppression in Spread Spectrum Systems

Tobias Hidalgo Stitz

Institute of Communications Engineering, Tampere University of Technology, P.O. Box 553, 33101 Tampere, Finland
Email: tobias.hidalgo@tut.fi

Markku Renfors

Institute of Communications Engineering, Tampere University of Technology, P.O. Box 553, 33101 Tampere, Finland
Email: markku.renfors@tut.fi

Received 29 October 2002; Revised 27 October 2003; Recommended for Publication by Xiang-Gen Xia

A filter-bank-based narrowband interference detection and suppression method is developed and its performance is studied in a spread spectrum system. The use of an efficient, complex, critically decimated perfect reconstruction filter bank with a highly selective subband filter prototype, in combination with a newly developed excision algorithm, offers a solution with efficient implementation and performance close to the theoretical limit derived as a function of the filter bank stopband attenuation. Also methods to cope with the transient effects in case of frequency hopping interference are developed and the resulting performance shows only minor degradation in comparison to the stationary case.

Keywords and phrases: narrowband interference cancellation, complex PR filter banks, DS-SS.

1. INTRODUCTION

Direct sequence spread spectrum (DS-SS) systems have several applications, for example, CDMA communications and advantages, low power spectral density, privacy of the communications, and an inherent immunity to narrowband interferences, due to the processing gain [1]. Nevertheless, this immunity is only effective up to certain interference power, making it necessary to apply additional techniques to suppress the effect of strong narrowband interferences if a degradation of the performance is to be avoided. Several interference suppression techniques have been proposed to process the signal in the time domain (e.g., adaptive transversal filtering) [2, 3, 4, 5, 6] and in the transform domain [2, 7, 8, 9]. These techniques take advantage of the knowledge of the wide spectral shape of the desired signal's spectrum as compared to the interferer's narrow spectrum. There are also methods in the spatial domain, using techniques like antenna diversity or beamforming [2, 10], although these methods are not exclusive to narrowband interference on a wideband SS signal. There exist more advanced approaches in the time-frequency domain [11, 12], like wavelet transformation-based methods. In situations in which the interfering environment changes quickly, time-domain techniques are too slow to work correctly. In these cases, frequency-domain techniques like the FFT-based or the filter-bank-based methods perform better [8, 12].

The purpose of this paper is to analyse the performance of a filter-bank-based interference suppression system. To eliminate the effects of narrowband interference, a perfect reconstruction (PR) filter bank with interference detection and subband suppression logic is used. Efficient implementation of the complex, critically sampled filter bank is based on an extension of the extended lapped transform (ELT) to the complex case. Based on detection and excision algorithms that can be found in the literature [8], a new, improved recursive algorithm is developed. Simulations have been run with different types of narrowband interference sources (jammers), demonstrating promising performance even in high jammer power cases.

The structure of the paper is as follows. Section 2 introduces the idea of filter-bank-based interference suppression and proposes an efficient implementation for the filter bank. Also the novel excision algorithm is presented and methods to relieve the transient effects in case of frequency hopping interference are introduced. Section 3 presents a theoretical performance analysis of the system. In Section 4 a detailed system model is presented and performance simulation results are shown and discussed in Section 5. Finally, Section 6 summarizes the conclusions obtained from this research work.

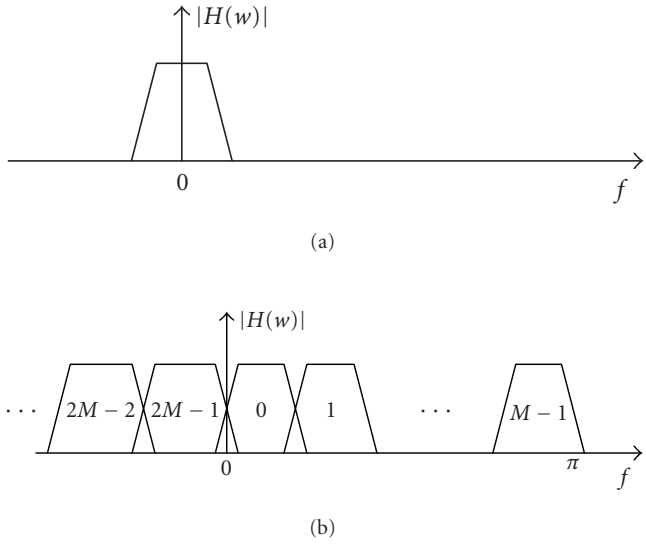

FIGURE 1: Modulated filter bank. (a) Prototype filter. (b) Complex modulated subband filters.

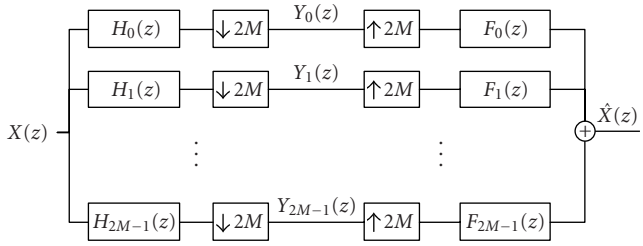

FIGURE 2: Maximally decimated $2M$-channel analysis-synthesis filter bank system.

2. FILTER BANKS FOR INTERFERENCE SUPPRESSION

2.1. Detection and suppression principle

The interference suppressor presented in this paper is based on a complex modulated filter bank (MFB). In a complex MFB, a prototype filter $h_p(n)$ is modulated by a complex exponential function to yield $2M$ bandpass filters in the form

$$h_k(n) = h_p(n) \cdot e^{jn(2k+1)\pi/2M}. \tag{1}$$

As shown in Figure 1, the whole sampled frequency range can be divided into subbands by lining up consecutive filters. In the following, the terms "subchannel" and "subband" will be used interchangeably.

MFBs can be used to form analysis-synthesis filter banks that divide the received signal into several subchannels (analysis part), and reconstruct the original signal from the subchannels (synthesis part), after some optional processing. One benefit of this type of filter banks is that the processing can be done at a lower sampling rate, taking advantage

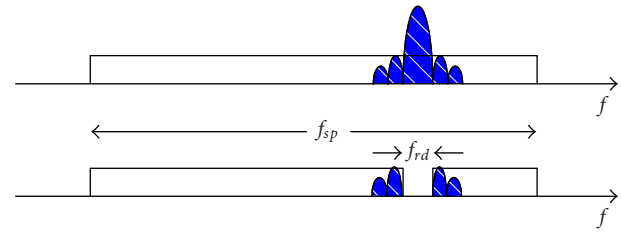

FIGURE 3: Application of the filter bank to the elimination of narrowband interference.

of the reduced bandwidth due to the subband filtering [13]. Figure 2 presents a maximally decimated filter bank, which means that, if the filter bank consists of $2M$ channels, the factor by which the down- and upsampling is performed is also $2M$.

If the filter design parameters are chosen correctly, the filter bank can offer PR, meaning that the output signal is just a scaled and delayed version of the input signal [13]:

$$\hat{x}(n) = cx(n - n_0). \tag{2}$$

Applying the filter banks to the narrowband interference suppression problem, the subbands affected by the interference are not included in the synthesis part of the filter, resulting in notch filtering, as sketched in Figure 3 [2, 12].

Since the FFT can also be regarded as a filter bank, it can be used as an approach to remove the interference. However, each subchannel of the FFT filter bank has strong sidelobes, the first ones at −13 dB. Thus, the power of the narrowband jammer is very likely to leak to adjacent subchannels, affecting a relatively high portion of the signal bandwidth. To fight this limitation, windowing can be applied to the signal before taking the FFT [14]. Although this is an effective solution to lower the sidelobes, the conditions for sufficient aliasing cancellation in an efficient, maximally decimated system are not so well understood as in PR filter bank systems. It should also be emphasized that a straightforward application of the complex modulation principle does not provide a PR system in the maximally decimated case [15]. Our implementation of the filter bank overcomes these problems by using the novel maximally decimated filter bank structure [16] shown in Figure 4, based on the ELT [17]. Using a PR filter bank, we also assure that the signal does not suffer any additional distortion by the processing. This is especially important in the case in which there is no interference present and no subband processing takes place. Further, the PR filter banks have efficient implementation methods based on ELT that are not applicable in the non-PR case [18]. However, properly designed nearly-perfect-reconstruction (NPR) CMFB/SMFB filter banks can be used in the same configuration (Figure 4) to implement a complex NPR filter bank suitable for our application. Depending on the used hardware architecture and allowed performance degradation in the interference free case, such a design could be slightly more efficient than the PR bank.

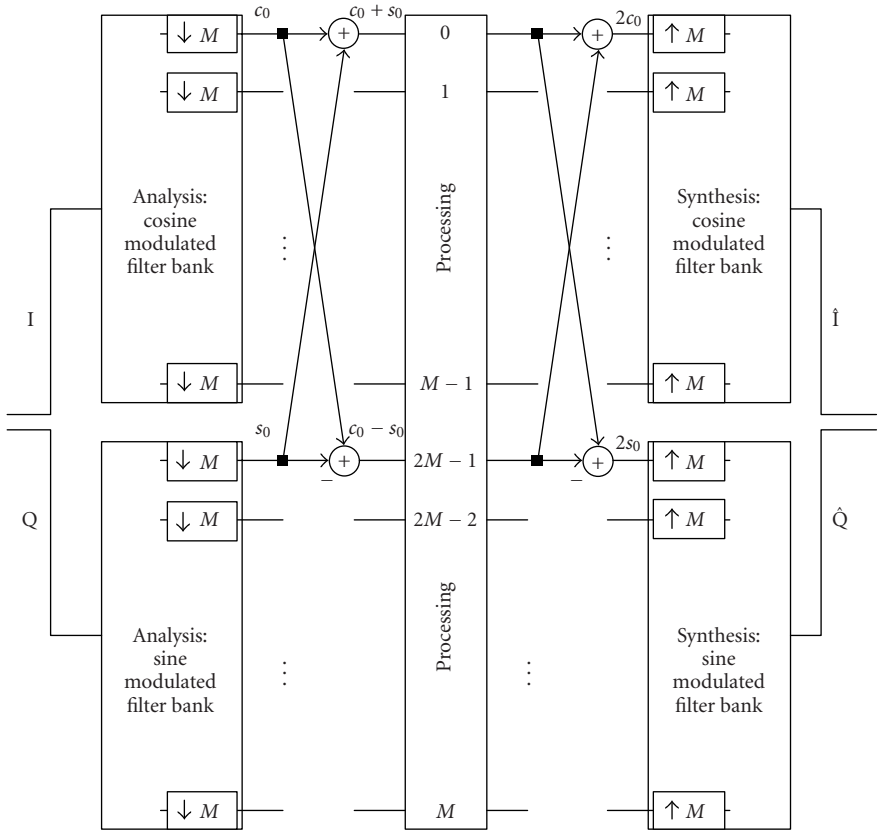

FIGURE 4: Realisation of the $2M$-channel complex MFB using sine and cosine MFBs that can be implemented with real-valued ELTs.

2.2. *Complex critically sampled PR filter bank structure*

Some papers have appeared proposing complex modulated lapped transforms for different applications, such as audio processing [19] and image motion estimation [20]. However, these papers use real-valued input signals to which the transform is applied.

The method chosen here to implement the complex MFB for the interference detection and suppression system with complex (I/Q) input signal is illustrated in Figure 4. The inputs are the real (I, in-phase) and imaginary (Q, quadrature) parts of the complex signals. The PR cosine and sine MFBs and the following butterfly structures effectively allow obtaining real subband signals by separating the positive and negative parts of the spectrum corresponding to each real subband, as sketched in Figure 5. If we observe the subsampled signals of Figure 4, we can see that, due to the butterfly structures, at the entrance of the synthesis banks we have, for the kth subchannel in the upper branch (CMFB),

$$(c_k + s_k) + (c_k - s_k) = 2c_k, \tag{3}$$

and, in the lower branch (SMFB),

$$(c_k + s_k) - (c_k - s_k) = 2s_k, \tag{4}$$

where c_k and s_k are the outputs of the analysis CMFB and SMFB for subchannel k, respectively (time index omitted). From the point of view of the filter bank, the signal remains unchanged (except for a scaling factor of 2), but in between the butterflies, the positive and negative sides of the spectra of the original signal at the entrance of the filter bank are separated. We can see this process in Figure 5. At the beginning we have a complex signal with different positive and negative frequency spectra. A certain spectral region and its corresponding symmetric negative counterpart are highlighted for better understanding. Next, the real and imaginary parts of the complex signal are separated and their corresponding spectra are shown. We then apply the filter bank and follow the changes suffered by the highlighted sections of the spectrum, sections that for simplicity coincide with the kth subchannel of the filter bank. The real part of the signal is filtered by the CMFB and the imaginary by the SMFB and then decimated and combined by the first butterfly. This is reflected in the spectra of Figure 5 by the spectral expansion inherent to decimation and by the fact that in the upper branch $(c_k + s_k)$ we now have a signal corresponding to the positive side of the filtered spectrum section of the original signal x. In a same manner, the lower branch $(c_k - s_k)$ carries a signal corresponding to the negative side of the filtered spectrum section of the original signal x. Ignoring the processing stage,

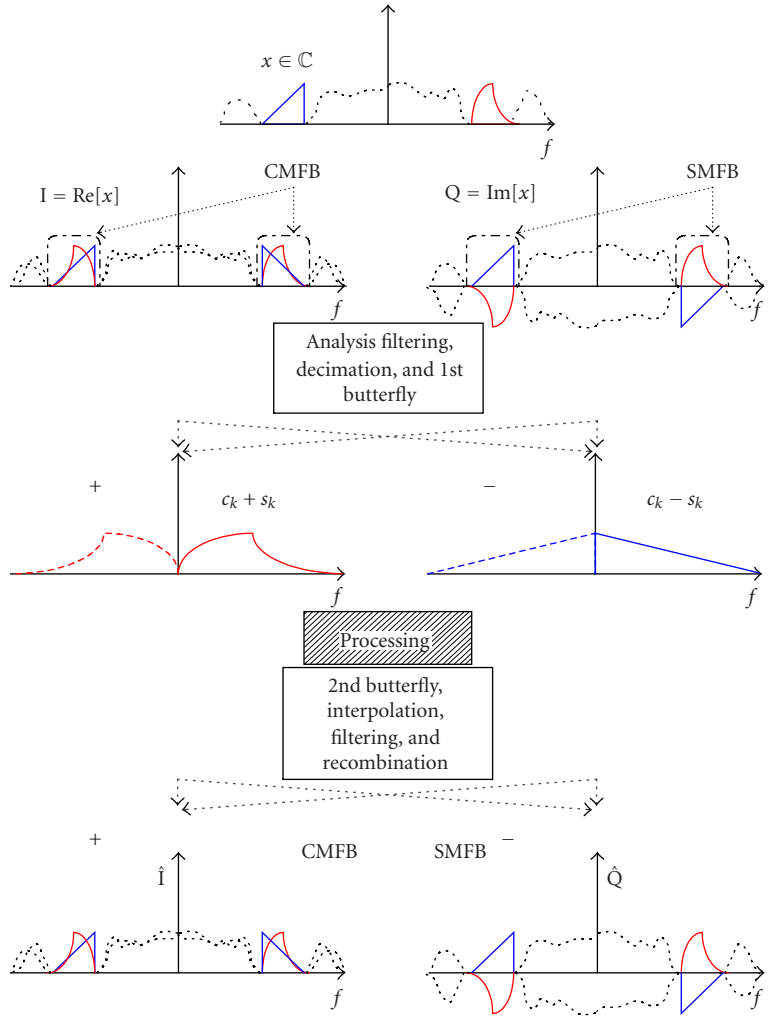

Figure 5: Separating and combining the spectral components using the structure of Figure 4.

after the second butterfly we recover the signals as they were before the first one (except for the scaling factor). Upsampling (spectral contraction) and recombining with the other subband signals yields Î and Q̂, similar to I and Q, assuming there was no further processing of the signals involved.

In other words, the analysis subchannel filtering function is equivalent to applying the corresponding complex subband filter of the complex MFB to the input signal, taking the real part of the output and decimating by M. Thus, the subband signals of the basically complex bank are used in real format at the processing stage. Finally, after the synthesis bank, the filtered in-phase and quadrature high-rate signals are obtained, with perfect reconstruction if no processing has taken place.

In the proposed structure, all the operations at the processing stage take place with real instead of complex signals and arithmetic. In fact, it can be shown that perfect reconstruction can be achieved in a critically sampled system only if the subsampled signals are real. If the subsampled signals are complex, the necessary aliasing cancellation for achieving PR cannot be obtained [16].

The implementation of the cosine and sine MFBs with efficient algorithms has been well studied; lattice, polyphase, and ELT structures can be used [17, 21]. We use the ELT-based approach, based on DCT-IV and DST-IV, leading to an efficient implementation of the filter bank. In [16], it is shown that a complex PR system can be obtained from an ELT-based real PR system using the proposed approach.

2.3. The excision principle

The detection of the jammer is based on thresholds, taking into consideration the uniform shape of the DS-SS signal spectrum. Different adaptive threshold calculation methods for FFT-based systems have been studied and presented in [8]. The simplest effective one measures the powers of the subbands, obtains a mean of them, and multiplies it by a factor t_f (threshold factor, $t_f > 1$) to set up the threshold θ. If

we define the signals after the first butterflies as

$$b_k = \begin{cases} c_k + s_k, & k = 0, \ldots, M-1, \\ c_{2M-1-k} - s_{2M-1-k}, & k = M, \ldots, 2M-1, \end{cases} \tag{5}$$

we can write

$$\theta = \frac{t_f}{2M} \sum_{k=0}^{2M-1} E(b_k^2), \tag{6}$$

considering that the signals b_k have zero mean. The subbands with higher powers are eliminated, so after the processing,

$$\hat{b}_k = \begin{cases} b_k, & E(b_k^2) < \theta, \\ 0, & E(b_k^2) \geq \theta. \end{cases} \tag{7}$$

However, there might be some jammer energy present in the neighbouring subchannels that is not detected in the first sweep, so our algorithm was built out to be recursive, as sketched in Figure 6. A similar excision algorithm has been developed independently in [22].

Once the subbands with detected jammer presence are removed, the same process is repeated without the removed subchannels. This can be described by rewriting (6) into the form

$$\theta = \frac{t_f}{M_r} \sum_{\substack{k=0 \\ k \notin R}}^{2M-1} \operatorname{var}(b_k), \tag{8}$$

where M_r is the number of active subbands that has not been set to 0 and R represents the indices of the removed subbands. Thus, the algorithm checks if there are subchannels that could have passed the previous threshold but could still be affected by jammer power and exceed a newly set averaging threshold. This can happen if the jammer is very powerful, pulling the threshold up in such a way that the leaking to the neighbouring subbands is not detected in the first sweep. A possible further jammer with lower power would also not be detected. Setting a too low threshold factor to accelerate or even avoid the recursive algorithm could be counterproductive, especially if we have few signal samples at our disposal to calculate the subband signal power. In this case, there might be great variations in the subband power estimates, which would lead to wrong decisions if the threshold is low.

2.4. Mitigating transient effects in case of frequency hopping interference

We here consider mostly the case where the interference frequency may be changing or the interference may appear or disappear instantaneously. In such a case, it is natural to use relatively short processing blocks, the length of which is an integer multiple of the symbol interval. In this situation, one important source of errors is the transients that appear at the beginning and at the end of the processing blocks. In our work, different methods have been tried to mitigate the transient effects. The most effective one from the performance point of view is the use of a guard symbol at the end of the block, where the transients cause more errors. Nevertheless, there is a more efficient way to fight the transients and to save the last bit for information: the guard interval. In this approach, the despreading of the last bit does not happen with the whole spreading code, only the last chips are discarded because of their distorted values due to the transients.

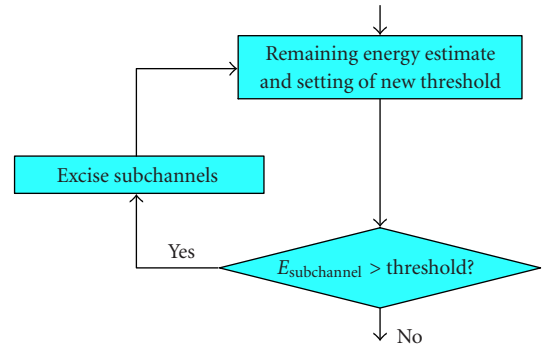

Figure 6: Recursive jammer detection principle.

3. PERFORMANCE ANALYSIS

In a BPSK system with AWGN channel, the bit error rate (BER), as a function of the energy per bit to noise power spectral density ratio, can be estimated with the help of the Q-function as follows [1]:

$$p_b = \text{BER} = Q\left(\sqrt{2\frac{E_b}{N_0}}\right). \tag{9}$$

In the case of a spread spectrum communication system with interference present in the channel, the BER can be estimated as

$$\text{BER} = Q\left(\sqrt{\frac{2g_p S}{J+N}}\right) = Q\left(\sqrt{\frac{2g_p (S/N)(S/J)}{S/N + S/J}}\right), \tag{10}$$

where g_p is the processing gain introduced by the despreading of the signal, and S, J, and N are the powers of the signal, the jammer, and the noise, respectively. The quotient S/N can be calculated from the energy per bit to noise power spectral density ratio as

$$\frac{S}{N} = \frac{1}{g_p} \frac{E_b}{N_0}. \tag{11}$$

To estimate the effect of removing some of the filter bank subbands of a BPSK signal, E_b/N_0 should be reduced by the factor $(f_{sp} - f_{rd})/f_{sp}$ (see Figure 3) [8]. Thus, the effective S/N becomes

$$\frac{S}{N} = \frac{1}{g_p} \frac{E_b}{N_0} \frac{f_{sp} - f_{rd}}{f_{sp}}. \tag{12}$$

Here, f_{sp} is the bandwidth of the spread signal and f_{rd} is the part of it that is being removed. It is assumed that the remaining jammer power is clearly below the noise power level.

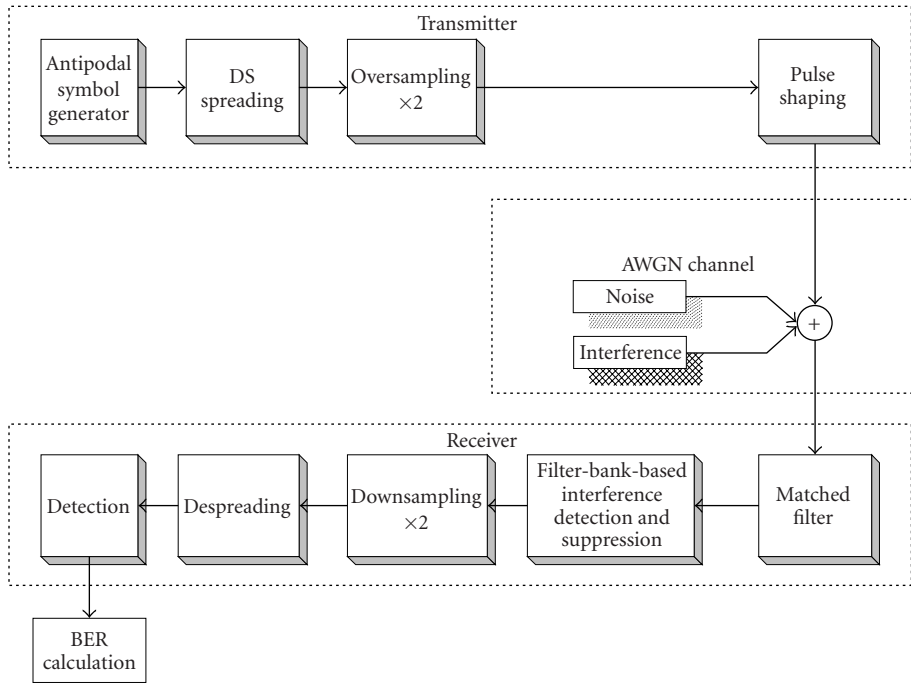

Figure 7: Block diagram of the general baseband system model.

Equation (12) permits to predict the expected performance if the bandwidth that is removed to fight the jammer is known. The bandwidth to be removed can be estimated from the bandwidth and power of the jammer and from the spectral characteristics of the prototype filter in the filter bank, since its stopband edge and attenuation determine how much jammer power can leak to neighbouring subchannels.

4. SYSTEM MODEL

The system used to model the narrowband interference suppressor is presented in Figure 7.

The figure shows a transmitter that sends information through a channel to a receiver, modelled in the baseband domain. At the transmitter, the antipodal signal generator generates a random sequence of 1's and −1's. The generated binary sequence is spread by a pseudorandom m-sequence by multiplying each information bit by this sequence in the DS spreading block. Next, the sampling frequency is doubled and the obtained signal is filtered by a pulse shaping filter of the root-raised cosine type with a roll of factor of 22%.

The channel is an AWGN channel with additive interference. The signals that model the noise and the interference are both complex. The jammer is either a single tone or a 10% BPSK-type interferer, pulse shaped with a roll of factor of 35%. It occupies 10% of the desired signals bandwidth and can have either a fixed spectral position or hops in the range $[-f_s/2, f_s/2]$, where f_s is the sampling rate, at regular intervals.

At the receiver, the signal is filtered by a digital matched filter at twice the chip rate. The interference detection and suppression block performs an estimation of the jammer location in the frequency axis and suppresses the bands that contain it. To achieve this goal, an ELT-based filter bank is used, dividing, respectively, the real part and the imaginary part of the received signal among $2M$ real subbands.

Next, the inverse operations to the ones performed at the transmitter are completed: the jammer-free signal is downsampled and despread following the integrate-and-dump principle. Ideal code synchronization is assumed. The received signal is converted to a sequence of bits after the decisions have been made at the detector. The obtained sequence is compared with the original bit sequence to obtain the BER.

As an alternative to the two-times oversampled system, we consider also the case where the filter bank processing is done at the chip rate. Perfect code synchronization is assumed in both cases.

The frequency responses of the fourth subchannel filters that are used for the filter bank with $2M = 64$ complex channels are plotted in Figure 8. The figure shows a frequency modulated ELT prototype with overlapping factor $K = 4$ and another more frequency selective one with $K = 6$. In both cases, the roll-off in the filter bank design is 100%, meaning that each subchannel transition band is overlapping with the closest transition band and passband of the adjacent subchannel, but not with the more distant ones.

Knowing the elements of this model, the number of affected and eliminated subbands can be estimated for each jammer power and a prediction for the expected performance based on (12) can be plotted. Depending on the stopband attenuation of the prototype filter in the suppressor, the number of affected subchannels varies with the power of

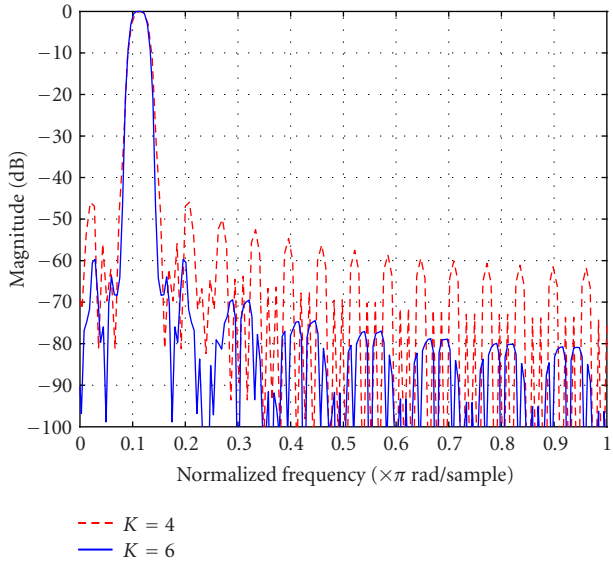

FIGURE 8: Frequency response for the analysis and synthesis banks of one of the subchannel filters with $K = 4$ and $K = 6$ where $2M = 64$ subbands.

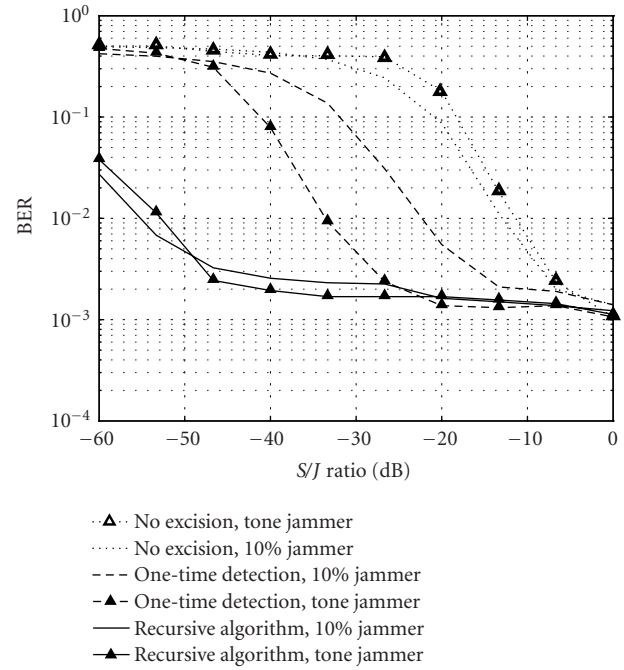

FIGURE 9: Performance without excision, with one-time excision, and using the proposed recursive excision algorithm. $E_b/N_0 = 7$ dB, $2M = 32$ subbands with $K = 4$, spreading factor = 127, 10% and single tone jammers at fixed position. Guard-interval-based transient mitigation is applied.

the jammer. Thus, if the filter characteristics are known, the number of affected subbands can be predicted and the effective S/N from (12) can be calculated to obtain the estimated BER for the two filter bank designs. An application of this idea is presented in Figure 13.

5. PERFORMANCE EVALUATION

Simulations with the previously described model were run with the following parameters: the spreading factor/processing gain of the spread spectrum system was $g_p = 127$ and the spread signal was oversampled by 2. The filter bank was an ELT-based complex bank with $2M$ complex channels (M on the positive and M on the negative sides of the frequency band), decimation, and interpolation by M and perfect reconstruction. The threshold factor used in the jammer detection block was 2. For each point in the simulation results, at least 10000 data bits were used to check the BER. In the case of a randomly hopping jammer, the interferer hopped every 16 information bits and the simulations were done with $E_b/N_0 = 7$ dB. The results below extend the ones presented in [23].

Figure 9 compares the results applying the recursive algorithm with those that do not apply it with a 10% jammer and a single tone jammer at a fixed position. The improvement in the performance using the recursive algorithm is evident.

The previously mentioned effect of the transients is studied in Figure 10. The curves present the performance of a filter bank with $2M = 32$ subbands and with different prototype filters $K = 4$ and $K = 6$. It can be seen that without mitigating the transients, the results for both prototypes are very similar and we are not completely taking advantage of the higher stopband attenuation of the filter with higher overlapping factor K. However, when the guard interval method

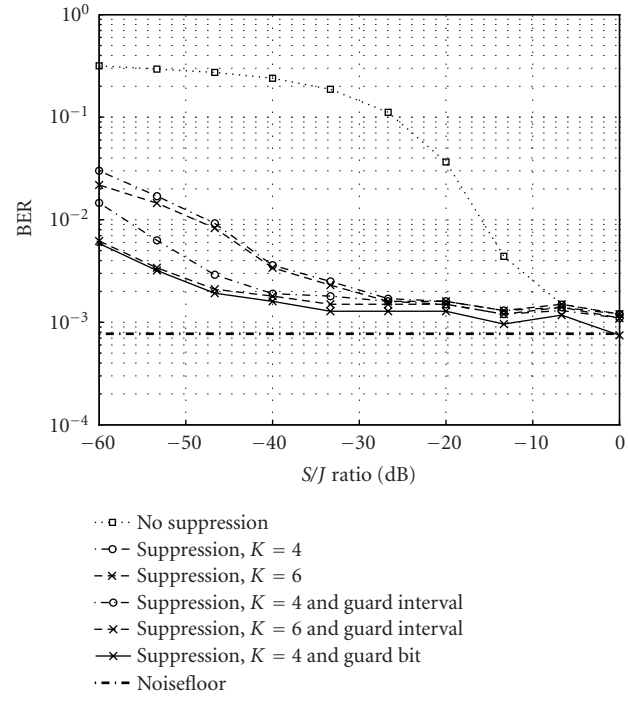

FIGURE 10: Fighting the transients with guard interval and guard bit. Filter prototypes with overlapping factors $K = 4$ and $K = 6$, where $E_b/N_0 = 7$ dB, $2M = 32$ subbands, spreading factor = 127, 10% jammer at randomly hopping positions.

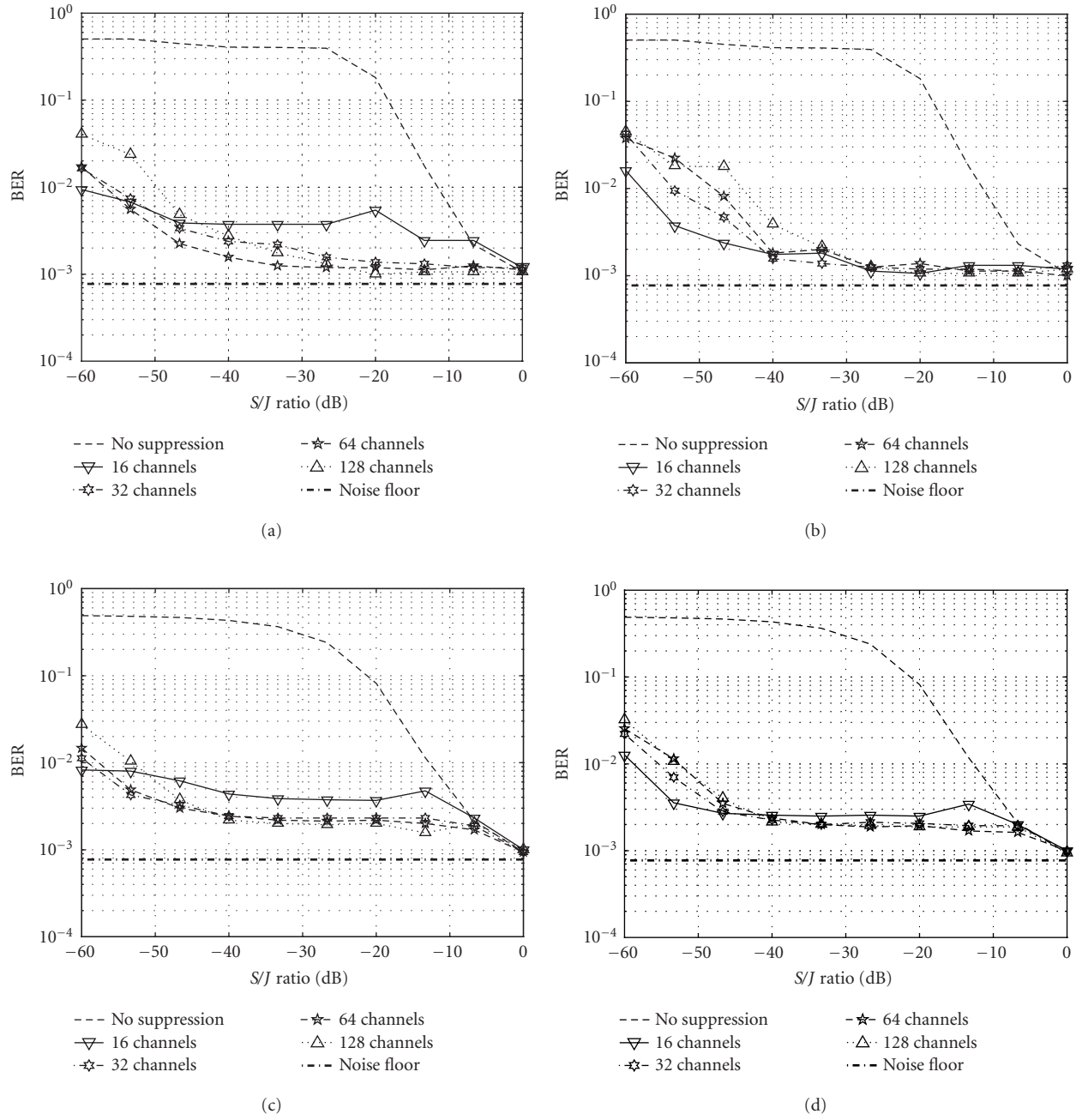

FIGURE 11: Performance with oversampled (a, c) and chip rate (b, d) processing using different filter bank sizes with $2M = 16$ to 128, where $K = 6$, $E_b/N_0 = 7$ dB, spreading factor = 127. (a, b) represent the single tone and (c, d) represent the 10% jammers at fixed positions. Guard-interval-based transient mitigation is applied.

is applied, apart from an improvement in the performance in both designs, we can see that the difference between the performances grows. The figure also includes the guard bit approach as a lower BER bound for the guard interval method. With a guard interval of 20 chips, the performance of the guard interval idea is close to the performance of the guard bit approach. In the figure we also include the noise floor, representing the performance of the system when no jammer is present.

Several parameters have been modified during the simulations to investigate their effect on the performance of the system. For instance, the number of subchannels varied and the downsampling by two was performed before the filter bank (see the model in Figure 6), resulting in chip rate processing at the filter bank. Figures 11 and 12 combine the results of these variations. We can see that using $2M = 32$ gives a good performance with a reasonably low number of subbands. For the case $2M = 16$, the performance worsens,

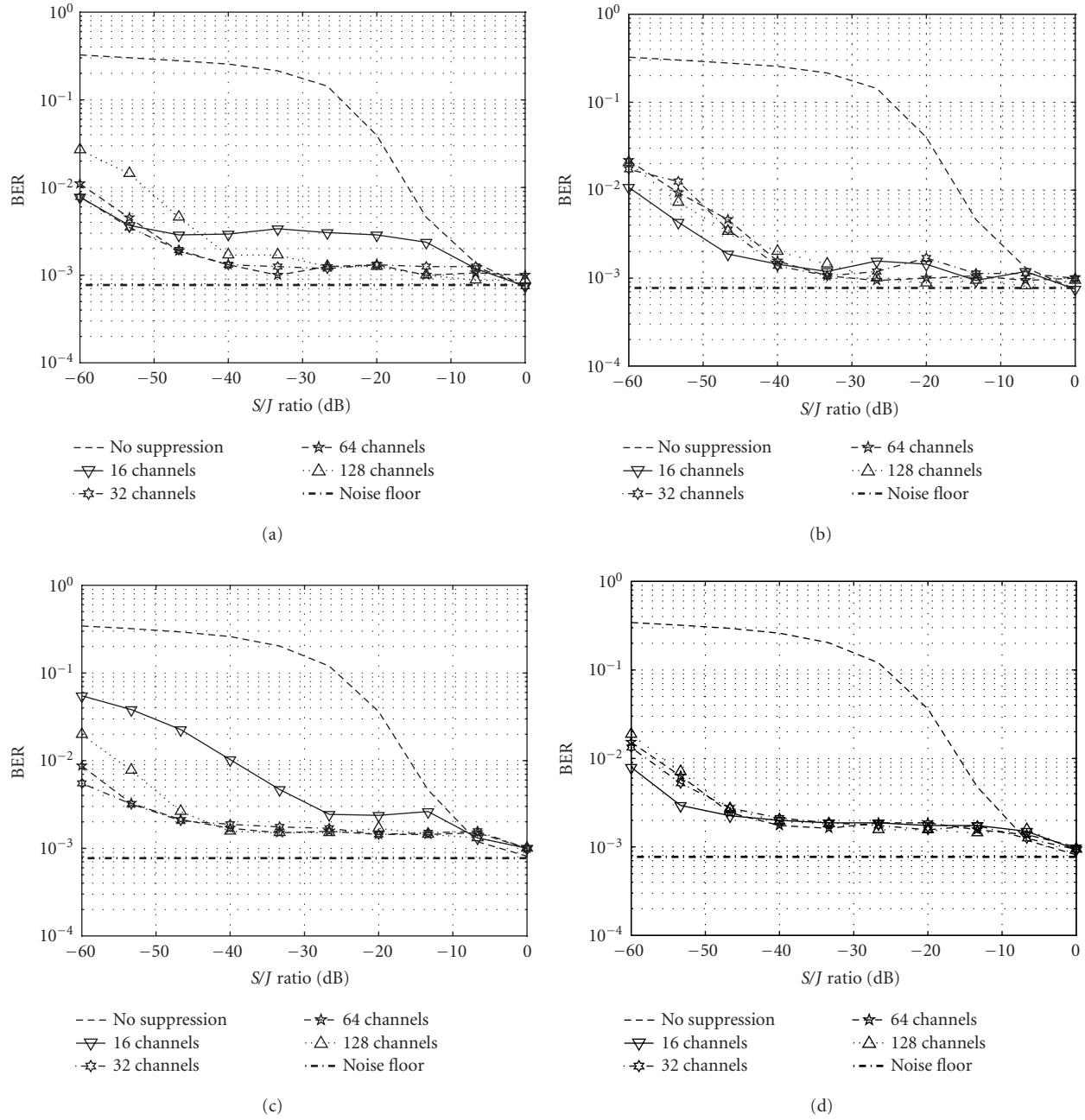

FIGURE 12: Performance with oversampled (a, c) and chip rate (b, d) processing using different filter bank sizes with $2M = 16$ to 128, where $K = 6$, $E_b/N_0 = 7$ dB, spreading factor = 127. (a, b) represent the single tone and (c, d) represent the 10% jammers at randomly hopping positions. Guard-interval-based transient mitigation is applied.

and the difference with higher number of subchannels is especially high in the case of low-to-medium power jammers. Considering the case of chip rate processing, the width of the spectrum relative to the sampling frequency at the filter bank input is doubled, and this could allow having a filter bank with fewer subbands. The processing load can thus also be reduced in two ways, first by handling half the number of samples, second by using a smaller filter bank. In this case we see that also the filter bank with $2M = 16$ subbands achieves acceptable performance. Overall, using chip rate processing results only in a minor degradation in performance if the filter banks size is chosen appropriately.

The size of the filter bank affects the length of the prototype filter in its design: the larger M is used, the more coefficients are needed for each subchannel filter. Longer subchannel filters cause also longer lasting transients, so a good trade-off between the length of the guard interval and the number of subbands in the bank has to be found.

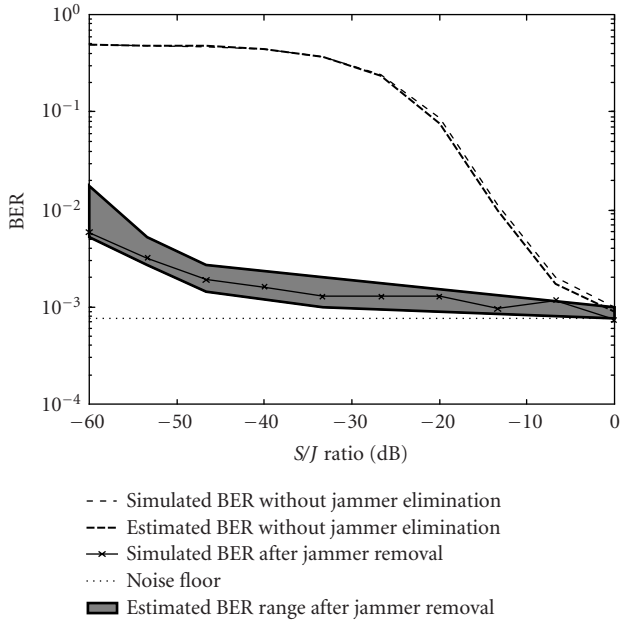

Figure 13: Expected BER range and obtained BER values over S/J ratio in the optimised system with $2M = 32$, $K = 6$, oversampled processing, guard bit, $E_b/N_0 = 7$ dB, spreading factor = 127, different interference parameters.

We can compare the obtained results with the expected performance of the derivations of Section 3, taking into account the filter bank design proposed in Section 4. Figure 13 shows the estimated and simulated BER performances in the cases in which the jammer is not removed and also when it is removed. For the estimation of the BER range after the jammer removal, the range in the numbers of removed subbands at each S/J ratio was considered. Knowing the type of interference and its power and the noise level, it is possible to predict how much the interference will stick out of the uniform DS-SS signal spectrum. Based on the stopband attenuation of the filters in the filter bank, we can then estimate how many subbands will be affected by the jammer, that is, get enough jammer energy to modify the uniformity of the desired signal. With the number of affected and therefore eliminated subbands and (12), we can calculate the expected degradation of the E_b/N_0 ratio and consequently the expected BER. Testing this idea on empirical measurements and counting the maximum and minimum number of affected subbands with different interference parameters, at each S/J ratio, we were able to obtain the shaded area of Figure 13. The figure shows that the expected results match quite well with the obtained ones.

In another experiment, the processing was shortened into blocks of 2 to 8 information bits, instead of 16 as in the previous results. Shorter processing blocks permit the tracking and elimination of more quickly hopping jammers. The aim was to see how short the blocks could be made before the performance of the system decreased too much. Figures 14 and 15 reflect the results of this research. For a system of $K = 6$, $2M = 128$ subbands at chip rate processing and using guard bits, the conclusion is that the degradation in performance is negligible for block lengths down to 6 bits, but beyond that point it starts to be significant.

The results shown in this section are clearly better than the ones presented in the reference method [8] using a 1024-point FFT, as far as a direct comparison can be made. Apparently, the 10% BPSK jammer in [8] did not have any kind of pulse shaping, hence resulting in a more wideband signal with sinc spectrum. We present in Figure 16 a comparison between a filter bank with 32 subchannels and a 1024-point FFT (no windowing) under a 10% fixed positioned jammer.

6. CONCLUSIONS

In this paper, a filter-bank-based interference detection and excision method for a DS-SS system has been studied and evaluated. The interfered subbands were removed from the signal to eliminate the jammers. The system worked with interference at a fixed position and with interference that randomly changed its position, with continuous wave interference and with BPSK type of interference taking up to 10% of the desired signal bandwidth.

The main strengths of the system presented in this paper are the perfect reconstruction property of the filter bank used and its affordable complexity requirements. It was shown through simulations that the performance is close to the theoretical limit when all aspects of the system are carefully optimised. The proposed system works quite well with far greater S/J ratios than any of the transform domain techniques reported in the literature. We can take the results of [12, Figure 3.14] as a reference. They show the performance of different frequency domain excision methods in the case of 10% jammer bandwidth and indicate best performance for the ELT-based approach. In those results, the performance degrades drastically (BER > 0.1) for S/J ratios lower than about −45 dB. For comparison, we repeated our simulations with similar parameters (5 dB E_b/N_0, almost the same spreading code length, 63 instead of 64, but different spreading code). These results, with properly optimised filter bank and recursive jammer detection algorithm, indicate smoother degradation with low S/J ratios providing tolerable performance (BER < 0.1) for S/J above −75 dB with $K = 6$ (−55 dB with $K = 4$).

Implementing the perfect reconstruction filter bank with ELTs, an efficient system is obtained, allowing the system to work at high data rates. In [24], it was shown that the whole excision system with overlapping factor $K = 5$ can be implemented with a single TMS320C6414 DSP with sampling rate in the order of 6–9 MHz, depending on the size of the filter bank.

One significant aspect when comparing with most of the other frequency domain approaches is that the needed number of subchannels is very low. Even with 16 subchannels, the performance is close to the theoretical one.

All in one, the narrowband interference suppression method presented is a good compromise between complexity, efficiency, and performance at relatively high jammer powers. In [9], a similar conclusion is drawn when

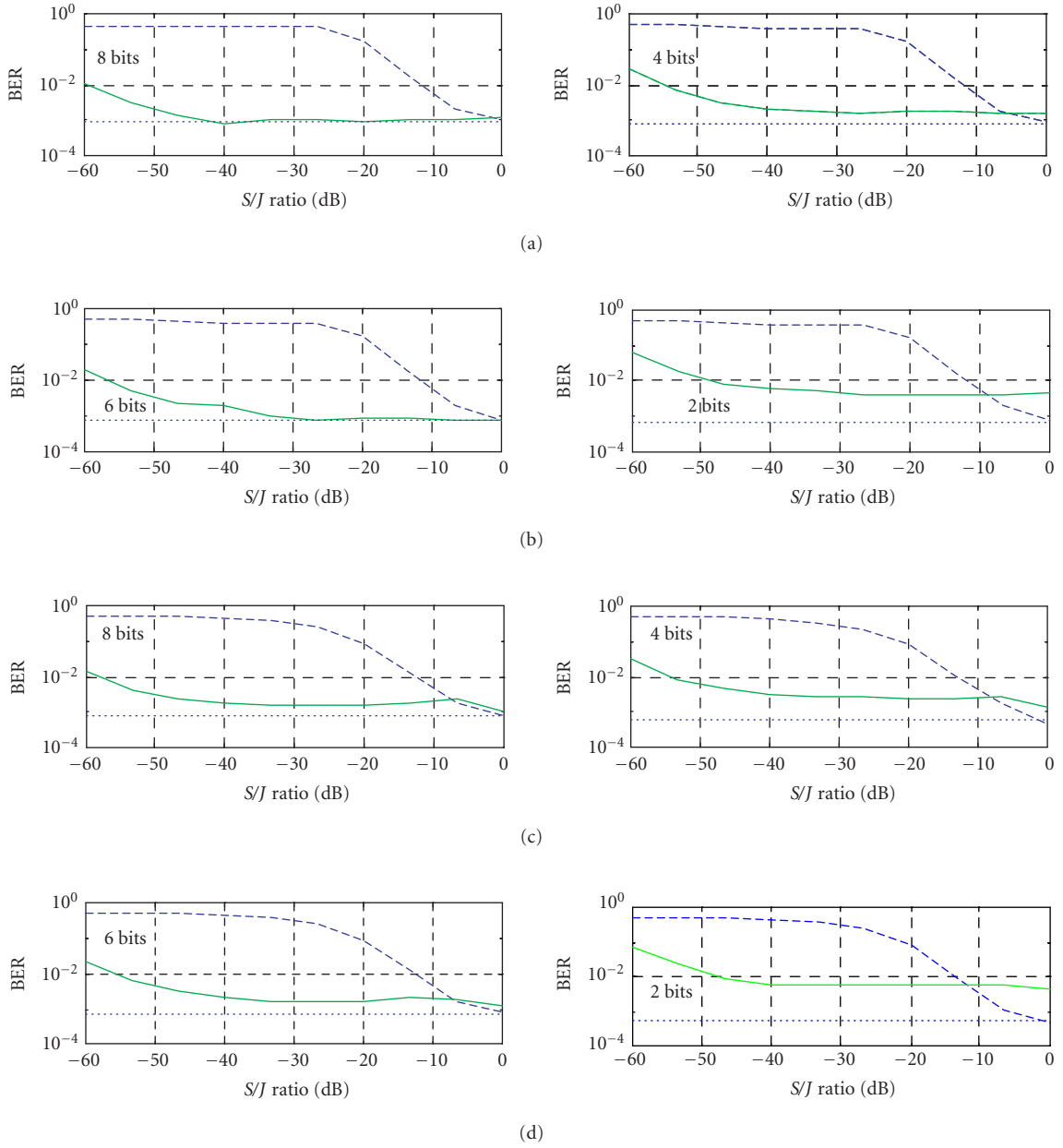

FIGURE 14: Different processing block lengths of 2 to 8 bits. Filter bank with $2M = 128$, $K = 6$, chip rate processing, guard bit, $E_b/N_0 = 7$ dB, and spreading factor $= 127$. (a), (b) represent the single tone and (c), (d) represent the 10% jammers at fixed positions. Dashed lines represent simulated BER without jammer removal, solid lines represent simulated BER after jammer removal, and dotted lines represent noise floor.

comparing ELT, FFT, and DCT methods. Better performance at increasing jammer powers can be obtained by using prototype filters that are more frequency selective and have higher stopband attenuation. However, the limiting factors can be at earlier stages in the receiver. For example, the resolution of the A/D converter has to be good enough to represent a desired signal that is, for instance, 70 dB weaker than the interfering signal that is also being sampled simultaneously.

We have studied the performance of the proposed method only in the single-user case. In multiuser CDMA environment, the effect of the notch filtering due to filter bank excision on the multiple access interference (MAI) is a serious concern. Considering the case of very strong narrowband interference, it is obvious that the best thing to do also from the MAI point of view is to remove the interfered frequency band completely since it could not include any useful information for detection. However, in this context, the use of higher number of subchannels than needed in the single-user case could be favourable. In case of modest jammer levels, subband excision is clearly a suboptimal solution and

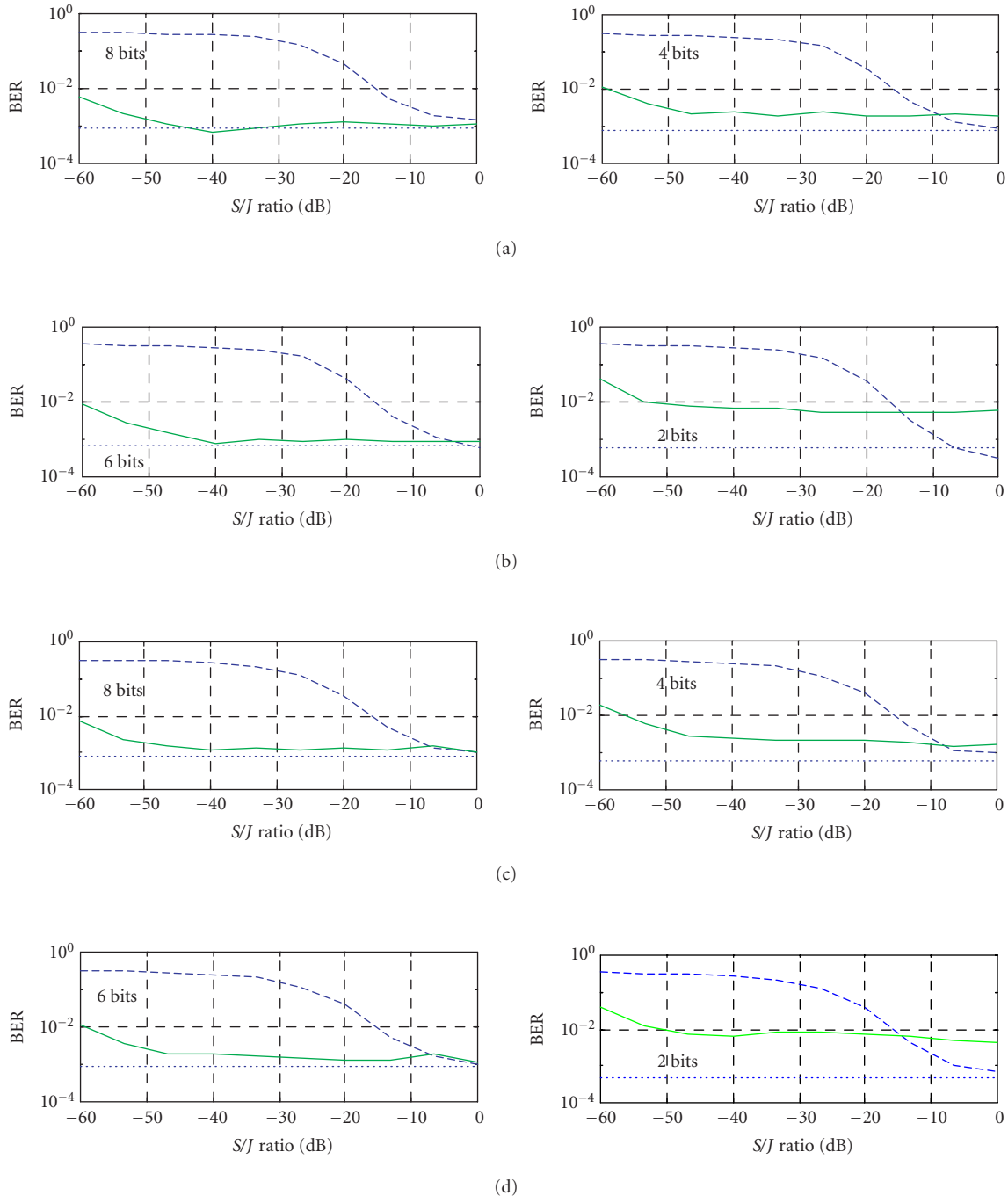

FIGURE 15: Different processing block lengths of 2 to 8 bits. Filter bank with $2M = 128$, $K = 6$, chip rate processing, guard bit, $E_b/N_0 = 7$ dB, and spreading factor = 127. (a), (b) represent the single tone and (c), (d) represent the 10% jammers at randomly hopping positions. Dashed lines represent simulated BER without jammer removal, solid lines represent simulated BER after jammer removal, and dotted lines represent noise floor.

its performance comparisons against other interference suppression methods are a topic for future studies. Also a more analytical study of the recursive jammer detection methods is included in the future plans.

ACKNOWLEDGMENT

This work was carried out in the project "Digital and Analog Techniques in Flexible Receivers" funded by the National Technology Agency of Finland (Tekes).

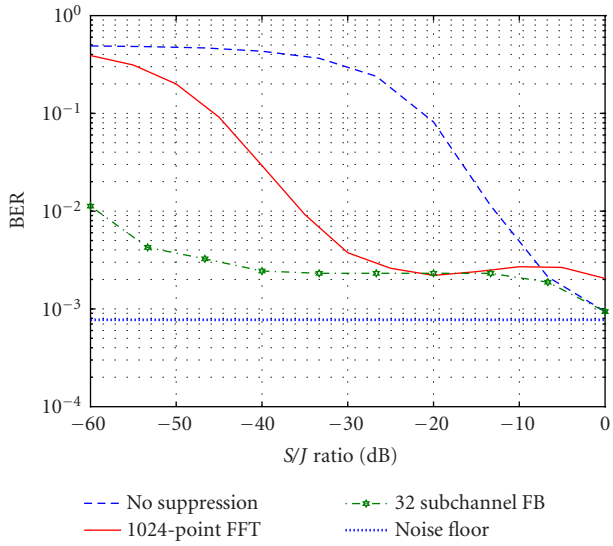

FIGURE 16: Comparison between a filter bank with $2M = 32$, $K = 6$ and oversampled processing and a 1024-point FFT, where $E_b/N_0 = 7$ dB, spreading factor = 127 and the 10% jammer is at a fixed position. Guard-interval-based transient mitigation is applied.

REFERENCES

[1] J. G. Proakis, *Digital Communications*, Electrical Engineering Series. McGraw-Hill International Editions, New York, NY, USA, 4th edition, 2001.

[2] L. B. Milstein, "Interference rejection techniques in spread spectrum communications," *Proceedings of the IEEE*, vol. 76, no. 6, pp. 657–671, 1988.

[3] F. Hsu and A. Giordano, "Digital whitening techniques for improving spread spectrum communications performance in the presence of narrowband jamming and interference," *IEEE Trans. Communications*, vol. 26, no. 2, pp. 209–216, 1978.

[4] J. W. Ketchum and J. G. Proakis, "Adaptive algorithms for estimating and suppressing narrow-band interference in PN spread-spectrum systems," *IEEE Trans. Communications*, vol. 30, no. 5, pp. 913–924, 1982.

[5] R. A. Iltis and L. B. Milstein, "Performance analysis of narrow-band interference rejection techniques in DS spread-spectrum systems," *IEEE Trans. Communications*, vol. 32, no. 11, pp. 1169–1177, 1984.

[6] P. Henttu, H. Saarnisaari, and S. Aroinaa, "Interference suppression in DS/FH system using modified two sided adaptive filter," in *Proc. IEEE Military Communications Conference*, pp. 1429–1433, McLean, Va, USA, October 2001.

[7] M. J. Medley, G. J. Saulnier, and P. K. Das, "Narrow-band interference excision in spread spectrum systems using lapped transforms," *IEEE Trans. Communications*, vol. 45, no. 11, pp. 1444–1455, 1997.

[8] A. Pouttu, J. K. Juntti, and T. J. Kumpumäki, "Adaptive transform domain interference suppression in a hybrid DS/FH-system," in *Proc. IEEE 5th International Symposium on Spread Spectrum Techniques and Applications*, pp. 351–355, Sun City, South Africa, September 1998.

[9] P. Henttu, A. Pouttu, and M. Raustia, "Performance of PIE interference suppressor using FFT, DCT and ELT transformations in FH/DS communications," in *Proc. Information Systems for Enhanced Public Safety and Security. IEEE/AFCEA*, pp. 126–130, Munich, Germany, May 2000.

[10] R. A. Monzingo and T. W. Miller, *Introduction to Adaptive Arrays*, John Wiley & Sons, New York, NY, USA, 1980.

[11] M. V. Tazebay and A. N. Akansu, "Adaptive subband transforms in time-frequency excisers for DSSS communications systems," *IEEE Trans. Signal Processing*, vol. 43, no. 11, pp. 2776–2782, 1995.

[12] A. N. Akansu and M. J. Medley, *Wavelet, Subband, and Block Transforms in Communications and Multimedia*, Kluwer Academic, Boston, Mass, USA, 1999.

[13] P. P. Vaidyanathan, *Multirate Systems and Filter Banks*, Prentice-Hall Signal Processing Series. Prentice-Hall, Englewood Cliffs, NJ, USA, 1993.

[14] T. J. Kumpumäki, M. A. Isohookana, and J. K. Juntti, "Narrow-band interference rejection using transform domain signal processing in a hybrid DS/FH spread spectrum system," in *Proc. IEEE Military Communications Conference*, pp. 89–93, Monterey, Calif, USA, November 1997.

[15] T. Karp and N. J. Fliege, "Modified DFT filter banks with perfect reconstruction," *IEEE Trans. on Circuits and Systems II: Analog and Digital Signal Processing*, vol. 46, no. 11, pp. 1404–1414, 1999.

[16] A. Viholainen, T. H. Stitz, J. Alhava, T. Ihalainen, and M. Renfors, "Complex modulated critically sampled filter banks based on cosine and sine modulation," in *Proc. IEEE Int. Symp. Circuits and Systems*, pp. 833–836, Scottsdale, Ariz, USA, May 2002.

[17] H. S. Malvar, *Signal Processing with Lapped Transforms*, Artech House, Boston, Mass, USA, 1992.

[18] J. Alhava, A. Viholainen, and M. Renfors, "Efficient implementation of complex exponentially-modulated filter banks," in *Proc. IEEE Int. Symp. Circuits and Systems*, pp. 157–160, Bangkok, Thailand, May 2003.

[19] H. S. Malvar, "A modulated complex lapped transform and its applications to audio processing," in *Proc. IEEE Int. Conf. Acoustics, Speech, Signal Processing*, pp. 1421–1424, Phoenix, Ariz, USA, March 1999.

[20] R. W. Young and N. G. Kingsbury, "Frequency-domain motion estimation using a complex lapped transform," *IEEE Trans. Image Processing*, vol. 2, no. 1, pp. 2–17, 1993.

[21] A. Viholainen, J. Alhava, and M. Renfors, "Implementation of parallel cosine and sine modulated filter banks for equalized transmultiplexer systems," in *Proc. IEEE Int. Conf. Acoustics, Speech, Signal Processing*, pp. 3625–3628, Salt Lake City, Utah, USA, May 2001.

[22] P. Henttu, "Signaalikomponenttien erottaminen radiojärjestelmän vastaanottimessa," in *Suomalainen Pattentihakemus nro. 20010952*, Nokia Networks Oy, Finland, 2001.

[23] T. H. Stitz and M. Renfors, "Filter bank based narrowband interference detection and suppression in spread spectrum systems," in *Proc. IEEE Int. Symp. Circuits and Systems*, pp. 516–519, Phoenix-Scottsdale, Ariz, USA, May 2002.

[24] Y. Yang, T. H. Stitz, and M. Renfors, "Implementation of a filter bank based narrowband interference suppression algorithm on a DSP processor," in *Proc. International Conference on Telecommunications*, Beijing, China, June 2002.

Tobias Hidalgo Stitz was born in 1974 in Eschwege, Germany. He obtained the M.S. degree in telecommunications engineering from the Polytechnic University of Madrid (UPM) in 2001, after writing his Master's thesis at the Institute of Communications Engineering of the Tampere University of Technology (TUT). From 1999 to 2001, he was a Research Assistant at TUT and is now

working towards his doctoral degree there. His research interests include wireless communications based on multicarrier systems, especially focusing on filter-bank-based systems and other filter bank applications for signal processing.

Markku Renfors was born in Suoniemi, Finland, on January 21, 1953. He received the Diploma Engineer, Licentiate of Technology, and Doctor of Technology degrees from Tampere University of Technology (TUT) in 1978, 1981, and 1982, respectively. He held various research and teaching positions at TUT from 1976 to 1988. In the years 1988–1991, he was working as a Design Manager in the area of video signal processing, especially for HDTV, at Nokia Research Centre and Nokia Consumer Electronics. Since 1992, he has been a Professor and Head of the Institute of Communications Engineering at TUT. His main research areas are multicarrier systems and signal processing algorithms for flexible radio receivers and transmitters.

Publication P2

T. Ihalainen, T. Hidalgo Stitz, M. Rinne, and M. Renfors, "Channel equalization in filter bank based multicarrier modulation for wireless communications" in *EURASIP Journal on Advances in Signal Processing*, vol. 2007, Article ID 49389, 18 pages, 2007.

DOI= http://dx.doi.org/10.1155/2007/49389

Hindawi Publishing Corporation
EURASIP Journal on Advances in Signal Processing
Volume 2007, Article ID 49389, 18 pages
doi:10.1155/2007/49389

Research Article

Channel Equalization in Filter Bank Based Multicarrier Modulation for Wireless Communications

Tero Ihalainen,[1] Tobias Hidalgo Stitz,[1] Mika Rinne,[2] and Markku Renfors[1]

[1] *Institute of Communications Engineering, Tampere University of Technology, P.O. Box 553, Tampere FI-33101, Finland*
[2] *Nokia Research Center, P.O. Box 407, Helsinki FI-00045, Finland*

Received 5 January 2006; Revised 6 August 2006; Accepted 13 August 2006

Recommended by See-May Phoong

Channel equalization in filter bank based multicarrier (FBMC) modulation is addressed. We utilize an efficient oversampled filter bank concept with 2x-oversampled subcarrier signals that can be equalized independently of each other. Due to Nyquist pulse shaping, consecutive symbol waveforms overlap in time, which calls for special means for equalization. Two alternative linear low-complexity subcarrier equalizer structures are developed together with straightforward channel estimation-based methods to calculate the equalizer coefficients using pointwise equalization within each subband (in a frequency-sampled manner). A novel structure, consisting of a linear-phase FIR amplitude equalizer and an allpass filter as phase equalizer, is found to provide enhanced robustness to timing estimation errors. This allows the receiver to be operated without time synchronization before the filter bank. The coded error-rate performance of FBMC with the studied equalization scheme is compared to a cyclic prefix OFDM reference in wireless mobile channel conditions, taking into account issues like spectral regrowth with practical nonlinear transmitters and sensitivity to frequency offsets. It is further emphasized that FBMC provides flexible means for high-quality frequency selective filtering in the receiver to suppress strong interfering spectral components within or close to the used frequency band.

1. INTRODUCTION

Orthogonal frequency division multiplexing (OFDM) [1] has become a widely accepted technique for the realization of broadband air-interfaces in high data rate wireless access systems. Indeed, due to its inherent robustness to multipath propagation, OFDM has become the modulation choice for both wireless local area network (WLAN) and terrestrial digital broadcasting (digital audio and video broadcasting; DAB, DVB) standards. Furthermore, multicarrier transmission schemes are generally considered candidates for the future "beyond 3 G" mobile communications.

All these current multicarrier systems are based on the conventional cyclic prefix OFDM modulation scheme. In such systems, very simple equalization (one complex coefficient per subcarrier) is made possible by converting the broadband frequency selective channel into a set of parallel flat-fading subchannels. This is achieved using the inverse fast Fourier transform (IFFT) processing and by inserting a time domain guard interval, in the form of a cyclic prefix (CP), to the OFDM symbols at the transmitter. By dimensioning the CP longer than the maximum delay spread of the radio channel, interference from the previous OFDM symbol, referred to as inter-symbol-interference (ISI), will only affect the guard interval. At the receiver, the guard interval is discarded to elegantly avoid ISI prior to transforming the signal back to frequency domain using the fast Fourier transform (FFT).

While enabling a very efficient and simple way to combat multipath effects, the CP is pure redundancy, which decreases the spectral efficiency. As a consequence, there has recently been a growing interest towards alternative multicarrier schemes, which could provide the same robustness without requiring a CP, that is, offering improved spectral efficiency. Pulse shaping in multicarrier transmission dates back to the early work of Chang [2] and Saltzberg [3] in the sixties. Since then, various multicarrier concepts based on the Nyquist pulse shaping idea with overlapping symbols and bandlimited subcarrier signals have been developed by Hirosaki [4], Le Floch et al. [5], Sandberg and Tzannes [6], Vahlin and Holte [7], Wiegand and Fliege [8], Nedic [9], Vandendorpe et al. [10], Van Acker et al. [11], Siohan et al. [12], Wyglinski et al. [13], Farhang-Boroujeny [14, 15], Phoong et al. [16], and others. One central ingredient in the

later developments is the theory of efficiently implementable, modulation-based uniform filter banks, developed by Vetterli [17], Malvar [18], Vaidyanathan [19], and Karp and Fliege [20], among others. In this context, the filter banks are used in a transmultiplexer (TMUX) configuration.

We refer to the general concept as filter bank based multicarrier (FBMC) modulation. In FBMC, the subcarrier signals cannot be assumed flat-fading unless the number of subcarriers is very high. One approach to deal with the fading frequency selective channel is to use waveforms that are well localized, that is, the pulse energy both in time and frequency domains is well contained to limit the effect on consecutive symbols and neighboring subchannels [5, 7, 12]. In this context, a basic subcarrier equalizer structure of a single complex coefficient per subcarrier is usually considered. Another approach uses finite impulse response (FIR) filters as subcarrier equalizers with cross-connections between the adjacent subchannels to cancel the inter-carrier-interference (ICI) [6, 10]. A third line of studies applies a receiver filter bank structure providing oversampled subcarrier signals and performs per-subcarrier equalization using FIR filters [4, 8, 9, 11, 13]. The main idea here is that equalization of the oversampled subcarrier signals restores the orthogonality of the subcarrier waveforms and there is no need for cross-connections between the subcarriers. This paper contributes to this line of studies by developing low-complexity linear per-subcarrier channel equalizer structures for FBMC. The earlier contributions either lack connection to the theory of efficient multirate filter banks, use just a complex multiplier as subcarrier equalizer or, in case of non trivial subcarrier equalizers, lack the analysis of needed equalizer length in practical wireless communication applications (many of such studies have focused purely on wireline transmission). Also various practical issues like peak-to-average power ratio and effects of timing and frequency offsets have not properly been addressed in this context before.

The basic model of the studied adaptive sine modulated/cosine modulated filter bank equalizer for transmultiplexers (ASCET) has been presented in our earlier work [21–23]. This paper extends the low-complexity equalizer of [23, 24], presenting comprehensive performance analysis, and studies the tradeoffs between equalizer complexity and number of subcarriers required to achieve close-to-ideal performance in a practical broadband wireless communication environment. A simple channel estimation-based calculation of the equalizer coefficients is presented. The performance of the studied equalizer structures is compared to OFDM, taking into account various practical issues.

In a companion paper [25], a similar subband equalizer structure is applied to the filter bank approach for frequency domain equalization in single carrier transmission. In that context, filter banks are used in the analysis-synthesis configuration to replace the traditional FFT-IFFT transform-pair in the receiver.

The rest of the paper is organized as follows. Section 2 briefly describes an efficient implementation structure for the TMUX based on exponentially modulated filter banks (EMFB) [26]. The structure consists of a critically sampled synthesis and a 2x-oversampled analysis bank. The problem of channel equalization is addressed in Section 3. The theoretical background and principles of the proposed compensation method are presented. The chosen filter bank structure leads to a relatively simple signal model that results in criteria for perfect subcarrier equalization and formulas for FBMC performance analysis in case of practical equalizers. A complex FIR filter-based subcarrier equalizer (CFIR-SCE) and the so-called amplitude-phase (AP-SCE) equalizer are presented. Especially, some low-complexity cases are analyzed and compared in Section 4. In Section 5, we present a semianalytical and a full time domain simulation setup to evaluate the performance of the equalizer structures in a broadband wireless communication channel. Furthermore, the effects of timing and frequency offsets, nonlinearity of a power amplifier, and overall system complexity are briefly investigated. Finally, the conclusions are drawn in Section 6.

2. EXPONENTIALLY MODULATED PERFECT RECONSTRUCTION TRANSMULTIPLEXER

Figure 1 shows the structure of the complex exponentially modulated TMUX that can produce a complex inphase/quadrature (I/Q) baseband signal required for spectrally efficient radio communications [23]. It has real format for the low-rate input signals and complex I/Q-presentation for the high-rate channel signal. It should be noted that FBMC with (real) m-PAM as subcarrier modulation and OFDM with (complex) m^2-QAM ideally provide the same bit rate since in general the subcarrier symbol rate in FBMC is twice that of OFDM for a fixed subchannel spacing. In this structure, there are $2M$ low-rate subchannels equally spaced between $[-F_s/2, F_s/2]$, F_s denoting the high sampling rate.

EMFBs belong to a class of filter banks in which the subfilters are formed by frequency shifting the lowpass prototype $h_p[n]$ with an exponential sequence [27]. Exponential modulation translates $H_p(e^{j\omega})$ (lowpass frequency response) around the new center frequency determined by the subcarrier index k. The prototype $h_p[n]$ can be optimized in such a manner that the filter bank satisfies the perfect-reconstruction (PR) condition, that is, the output signal is a delayed version of the input signal [27, 28]. In the general form, the synthesis and analysis filters of EMFBs can be written as

$$f_k[n] = \sqrt{\frac{2}{M}} h_p[n] \exp\left(j\left[n + \frac{M+1}{2}\right]\left[k + \frac{1}{2}\right]\frac{\pi}{M}\right), \quad (1)$$

$$h_k[n] = \sqrt{\frac{2}{M}} h_p[n] \exp\left(-j\left[N - n + \frac{M+1}{2}\right]\left[k + \frac{1}{2}\right]\frac{\pi}{M}\right), \quad (2)$$

respectively, where $n = 0, 1, \ldots, N$ and $k = 0, 1, \ldots, 2M-1$. Furthermore, it is assumed that the filter order is $N = 2KM-1$. The overlapping factor K can be used as a design parameter because it affects on how much stopband attenuation can be achieved. Another essential design parameter is the stopband edge of the prototype filter $\omega_s = (1+\rho)\pi/2M$, where

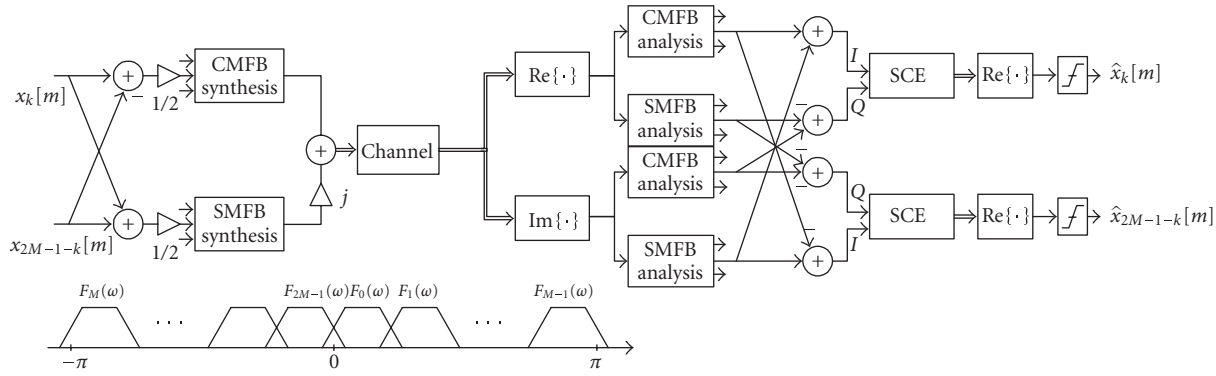

Figure 1: Complex TMUX with oversampled analysis bank and per-subcarrier equalizers.

the roll-off parameter ρ determines how much adjacent subchannels overlap. Typically, $\rho = 1.0$ is used, in which case only the contiguous subchannels are overlapping with each other, and the overall subchannel bandwidth is twice the subchannel spacing.

In the approach selected here, the EMFB is implemented using cosine and sine modulated filter bank (CMFB/SMFB) blocks [28], as can be seen in Figure 1. The extended lapped transform (ELT) is an efficient method for implementing PR CMFBs [18] and SMFBs [28]. The relations between the synthesis and analysis filters of the $2M$-channel EMFB and the corresponding M-channel CMFB and SMFB with the same real FIR prototype $h_p[n]$ are

$$f_k[n] = \begin{cases} f_k^c[n] + j f_k^s[n], & k \in [0, M-1] \\ -\left(f_{2M-1-k}^c[n] - j f_{2M-1-k}^s[n]\right), & k \in [M, 2M-1], \end{cases} \tag{3}$$

$$h_k[n] = \begin{cases} h_k^c[n] - j h_k^s[n], & k \in [0, M-1] \\ -\left(h_{2M-1-k}^c[n] + j h_{2M-1-k}^s[n]\right), & k \in [M, 2M-1], \end{cases} \tag{4}$$

respectively. A specific feature of the structure in Figure 1 is that while the synthesis filter bank is critically sampled, the subchannel output signals of the analysis bank are oversampled [26] by a factor of two. This is achieved by using the symbol-rate complex (I/Q) subchannel signals, instead of the real ones that are sufficient for detection after the channel equalizer, or in case of a distortion-free channel.

We consider here the use of EMFBs which have odd channel stacking, that is, the center-most pair of subchannels is symmetrically located around the zero frequency at the baseband. We could equally well use a modified EMFB structure [26] with even stacking (the center-most subchannel located symmetrically about zero). The latter form has also a slightly more efficient implementation structure, based on DFT-processing. The proposed equalizer structure can also be applied with modified DFT (MDFT) filter banks [20], with modified subchannel processing. However, for the following analysis EMFB was selected since it results in the most straightforward system model.

Further, although the discussion here is based on the use of PR filter banks, also nearly perfect-reconstruction (NPR) designs could be utilized. In the critically sampled case, the implementation benefits of NPR designs are limited because the efficient ELT structures cannot be utilized [29]. However, in the 2x-oversampled case, having two parallel CMFB and SMFB blocks, the implementation benefits of NPR designs could be more significant.

3. CHANNEL EQUALIZATION

The problem of channel equalization in the FBMC context is not so well understood as in the DFT-based systems. Our equalizer concept can be applied to both real and complex modulated baseband signal formats; here we focus on the complex case. In its simplest form, the subcarrier equalizer structure consists only of a single complex coefficient that adjusts the amplitude and phase responses of each subchannel in the receiver [22]. Higher-order SCEs are able to equalize each subchannel better if the channel frequency response is not flat within the subchannel. As a result, the use of higher-order SCEs enables to increase the relative subchannel bandwidth because the subchannel responses are allowed to take mildly frequency selective shapes. As a consequence, the number of subchannels to cover a given signal bandwidth by FBMC can be reduced. In general, higher-order equalizer structures provide flexibility and scalability to system design because they offer a tradeoff between the number of required subchannels and complexity of the subcarrier equalizers.

The oversampled receiver is essential for the proposed equalizer structure. In case of roll-off $\rho = 1.0$ or lower, nonaliased versions of the subchannel signals are obtained in the 2x-oversampled receiver when complex (I/Q) signals are sampled at the symbol rate. Consequently, complete channel equalization in an optimal manner is possible. As a result of the high stopband attenuation of the subchannel filters, there is practically no aliasing of the subchannel signals in the receiver bank. Thus perfect equalization of the distorting channel within the subchannel passband and transition band regions would completely restore the orthogonality of the subchannel signals [9].

3.1. Theoretical background and principles

Figure 2(a) shows a subchannel model of the complex TMUX with per-subcarrier equalizer. A more detailed model that includes the interference from the contiguous subchannels is shown in Figure 2(b). Limiting the sources of interference to the closest neighboring subchannels is justified if the filter bank design provides sufficiently high stopband attenuation. Furthermore, in this model the order of downsampling and equalization is interchanged based on the multirate identities [19]. The latter model is used as a basis for the cross-talk analysis that follows. It is also convenient for semianalytical performance evaluations. The equalizer concept is based on the property that with ideal sampling and equalization, the desired subchannel signal, carried by the real part of the complex subchannel output, is orthogonal to the contiguous subchannel signal components occupying the imaginary part. The orthogonality between the subchannels is introduced when the linear-phase lowpass prototype $h_p[n]$ is exponentially frequency shifted as a bandpass filter, with 90-degree phase-shift between the carriers of the contiguous subchannels.

In practice, the nonideal channel causes amplitude and phase distortion. The latter results in rotation between the I-and Q-components of the neighboring subchannel signals causing ICI or cross-talk between the subchannels. ISI, on the other hand, is mainly caused by the amplitude distortion. The following set of equations provides proofs for these statements. We derive them for an arbitrary subchannel k on the positive side of the baseband spectrum and the results can easily be extended for the subchannels on the negative side using (3) and (4). In the following analysis we use a noncausal zero-phase system model, which is obtained by using, instead of (2), analysis filters of the form

$$\overline{h}_k[n]=\sqrt{\frac{2}{M}}h_p[n+N]\exp\left(-j\left[-n+\frac{M+1}{2}\right]\left[k+\frac{1}{2}\right]\frac{\pi}{M}\right). \tag{5}$$

By referring to the equivalent form, shown in Figure 2(b), and adopting the notation from there, we can express the cascade of the synthesis and analysis filters of the desired subchannel k as

$$\begin{aligned} f_k[n]*\overline{h}_k[n] &= \sum_{l=a}^{b}\overline{h}_k^c[l]f_k^c[n-l]+\sum_{l=a}^{b}\overline{h}_k^s[l]f_k^s[n-l] \\ &\quad + j\cdot\left(\sum_{l=a}^{b}\overline{h}_k^c[l]f_k^s[n-l]-\sum_{l=a}^{b}\overline{h}_k^s[l]f_k^c[n-l]\right) \\ &= t_k^I[n]+j\cdot t_k^Q[n]=t_k[n], \end{aligned} \tag{6}$$

where $*$ denotes the convolution operation, summation indexes are $a=-N+\max(n,0)$ and $b=\min(n,0)$, and $n\in[-N,\ldots,N]$.

3.1.1. ICI analysis

For the potential ICI terms from the contiguous subchannels $k-1$ and $k+1$ (below and above) to the subchannel k of interest, we can write

$$\begin{aligned} &f_{k-1}[n]*\overline{h}_k[n] \\ &\quad=\sum_{l=a}^{b}\overline{h}_k^c[l]f_{k-1}^c[n-l]+\sum_{l=a}^{b}\overline{h}_k^s[l]f_{k-1}^s[n-l] \\ &\qquad+j\cdot\left(\sum_{l=a}^{b}\overline{h}_k^c[l]f_{k-1}^s[n-l]-\sum_{l=a}^{b}\overline{h}_k^s[l]f_{k-1}^c[n-l]\right) \\ &\quad=v_k^I[n]+j\cdot v_k^Q[n]=v_k[n], \\ &f_{k+1}[n]*\overline{h}_k[n] \\ &\quad=\sum_{l=a}^{b}\overline{h}_k^c[l]f_{k+1}^c[n-l]+\sum_{l=a}^{b}\overline{h}_k^s[l]f_{k+1}^s[n-l] \\ &\qquad+j\cdot\left(\sum_{l=a}^{b}\overline{h}_k^c[l]f_{k+1}^s[n-l]-\sum_{l=a}^{b}\overline{h}_k^s[l]f_{k+1}^c[n-l]\right) \\ &\quad=u_k^I[n]+j\cdot u_k^Q[n]=u_k[n], \end{aligned} \tag{7}$$

respectively.

Due to PR design, the real parts $v_k^I[m]$ and $u_k^I[m]$ (m being the sample index at the low rate) of the downsampled subchannel signals are all-zero sequences (or close to zero sequences in the NPR case). So ideally, when the real part of the signal is taken in the receiver, no crosstalk from the neighboring subchannels is present in the signal used for detection. Channel distortion, however, causes phase rotation between the I- and Q-components breaking the orthogonality between the subcarriers. Channel equalization is required to recover the orthogonality of the subcarriers.

The ICI components from other subcarriers located further apart from the subchannel of interest are considered negligible. This is a reasonable assumption because the extent of overlapping of subchannel spectra and the level of stopband attenuation can easily be controlled in FBMC. In fact, they are used as optimization criteria in filter bank design, as discussed in the previous section.

The cascade of the distorting channel with instantaneous impulse response (in the baseband model) $h_{\mathrm{ch}}[n]$ and the upsampled version of the per-subcarrier equalizer $\overline{c}_k[n]$ (see Figure 2) applied to the subchannel k of interest can be expressed as

$$h_{\mathrm{ch}}[n]*\overline{c}_k[n]=r_k[n]. \tag{8}$$

In the analysis, a noncausal high-rate impulse response $\overline{c}_k[n]$ is used for the equalizer, although in practice the low-rate causal form $c_k[m]$ is applied.

Next we analyze the ICI components potentially remaining in the real parts of the subchannel signals that are used for detection. Figure 3 visualizes the two ICI bands for subchannel $k=0$. We start from the lower-side ICI term and use an equivalent baseband model, where the potential ICI energy

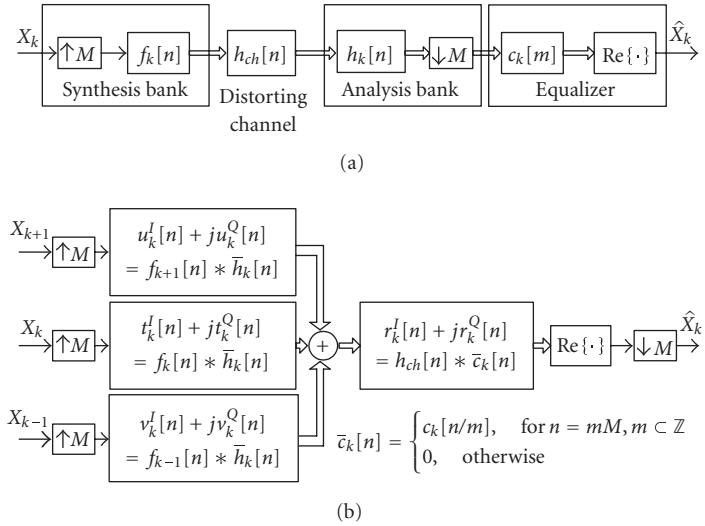

Figure 2: Complex TMUX with per-subcarrier equalizer. (a) System model for subchannel k. (b) Equivalent form including also contiguous subchannels for crosstalk analysis.

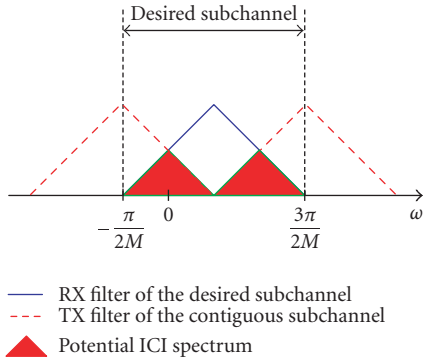

Figure 3: Potential ICI spectrum for subchannel $k = 0$.

is symmetrically located about zero frequency. We can write the baseband cross-talk impulse response from subchannel $k-1$ to subchannel k in case of an ideal channel as

$$\tilde{v}_k[n] = \tilde{v}_k^I[n] + j\tilde{v}_k^Q[n] = v_k[n]e^{-jnk\pi/M}. \quad (9)$$

In the appendix, it is shown that this impulse response is purely imaginary, that is, $\tilde{v}_k^I[n] \equiv 0$ and $\tilde{v}_k[n] = v_0[n]$. In case of nonideal channel with channel equalization, the baseband cross-talk impulse response can now be written as

$$\tilde{g}_k^{k-1}[n] = jv_0^Q[n] * \tilde{r}_k[n], \quad (10)$$

where $\tilde{r}_k[n] = r_k[n]e^{-jnk\pi/M}$. Here the upper index denotes the source of ICI. Now we can see that if the equalized channel impulse response is real in the baseband model, then the cross-talk impulse response is purely imaginary, and there is no lower-side ICI in the real part of the subchannel signal that is used for detection.

At this point we have to notice that the lower-side ICI energy is zero-centered after decimation only for the even-indexed subchannels, and for the odd subchannels the above model is not valid as such. However, we can establish a simple relation between the actual decimated subchannel output sequence $z_k[mM]$ in the filter bank system and the sequence obtained by decimating in the baseband model. It is straightforward to see that the following relation holds:

$$z_k[n]e^{-jnk\pi/M}\Big|_{n=mM} = (-1)^{mk}z_k[mM]. \quad (11)$$

Thus, for odd subchannels, the actual decimated ICI sequence is obtained by lowpass-to-highpass transformation (i.e., through multiplication by an alternating ± 1-sequence) from the ICI sequence of the baseband model. Then the actual ICI is guaranteed to be zero if it is zero in the baseband model. Therefore, a sufficient condition for zero lower-side ICI in all subchannels is that the equalized baseband channel impulse response is purely real.

For the upper-side ICI, we can first write the baseband model as

$$\tilde{u}_k[n] = \tilde{u}_k^I[n] + j\tilde{u}_k^Q[n] = u_k[n]e^{-jn(k+1)\pi/M}. \quad (12)$$

Again, it is shown in the appendix that this baseband impulse response is purely imaginary, that is, $\tilde{u}_k^I[n] \equiv 0$ and $\tilde{u}_k[n] = u_{2M-1}[n]$. With equalized nonideal channel, the cross-talk response is now

$$\tilde{g}_k^{k+1}[n] = ju_{2M-1}^Q[n] * \left(\tilde{r}_k[n]e^{-jn\pi/M}\right) \quad (13)$$

and the upper-side ICI vanishes if the equalized channel impulse response is real in this baseband model. Now the relation between the decimated models is

$$z_k[n]e^{-jn(k+1)\pi/M}\Big|_{n=mM} = (-1)^{m(k+1)}z_k[mM] \quad (14)$$

and a sufficient condition also for zero upper-side ICI is that the equalized baseband channel impulse response is purely real. However, the baseband models for the two cases are slightly different, and both conditions

$$\begin{aligned} \mathrm{Im}\left[\widetilde{r}_k[n]\right] &\equiv 0, \\ \mathrm{Im}\left[\widetilde{r}_k[n]e^{-jn\pi/M}\right] &\equiv 0 \end{aligned} \tag{15}$$

have to be simultaneously satisfied to achieve zero overall ICI. In frequency domain, the equalized channel frequency response is required to have symmetric amplitude and antisymmetric phase with respect to both of the frequencies $k\pi/M$ and $(k+1)\pi/M$ to suppress both ICI components. Naturally, the ideal full-band channel equalization (resulting in constant amplitude and zero phase) implies both conditions. In our FBMC system, the equalization is performed at low rate, after filtering and decimation by M, and the mentioned two frequencies correspond to 0 and π, that is, the filtered and downsampled portion of $H_{\mathrm{ch}}(e^{j\omega})$ in subchannel k multiplied by the equalizer $C_k(e^{j\omega})$ must fulfill the symmetry condition for zero ICI. In this case, the two symmetry conditions are equivalent (i.e., symmetric amplitude around 0 implies symmetric amplitude around π, and antisymmetric phase around 0 implies antisymmetric phase around π). The target is to approximate ideal channel equalization over the subchannel passband and transition bands with sufficient accuracy.

3.1.2. ISI analysis

In case of an ideal channel, the desired subchannel impulse response of the baseband model can be written as

$$\widetilde{t}_k[n] = \widetilde{t}^I_k[n] + j\widetilde{t}^Q_k[n] = t_k[n]e^{-jnk\pi/M}. \tag{16}$$

For odd subchannels, a lowpass-to-highpass transformation has to be included in the model to get the actual response for the decimated filter bank, but the model above is suitable for analyzing all subchannels. Now the real part of the subchannel response with actual channel and equalizer can be written (see the appendix) as

$$\begin{aligned} \widetilde{g}_k[n] &= \mathrm{Re}\left[\widetilde{t}_k[n] * \widetilde{r}_k[n]\right] = \mathrm{Re}\left[t_0[n] * \widetilde{r}_k[n]\right] \\ &= t^I_0[n] * \mathrm{Re}\left[\widetilde{r}_k[n]\right] - t^Q_0[n] * \mathrm{Im}\left[\widetilde{r}_k[n]\right]. \end{aligned} \tag{17}$$

The conditions for suppressing ICI are also sufficient for suppressing the latter term of this equation. Furthermore, in case of PR filter bank design, $t^I_0[n]$ is a Nyquist pulse. Designing the channel equalizer to provide unit amplitude and zero-phase response, a condition equivalent of having

$$\mathrm{Re}\left[\widetilde{r}_k[n]\right] = \delta[n] = \begin{cases} 1, & n = 0, \\ 0, & \text{otherwise}, \end{cases} \tag{18}$$

would suppress the ISI within the subchannel.

The above conditions were derived in the high-rate, full-band case, and if the conditions are fully satisfied, ISI within the subchannel and ICI from the lower and upper adjacent subchannels are completely eliminated. In practice, the equalization takes place at the decimated low sampling rate, and can be done only within the passband and transition band regions (assuming roll-off $\rho = 1.0$). However, the ICI and ISI components outside the equalization band are proportional to the stopband attenuation of the subchannel filters and can be ignored.

3.2. Optimization criteria for the equalizer coefficients

Our interest is in low-complexity subcarrier equalizers, which do not necessarily provide responses very close to the ideal in all cases. Therefore, it is important to analyze the ICI and ISI effects with practical equalizers. This can be carried out most conveniently in frequency domain. In the baseband model, the lower and upper ICI spectrum magnitudes are

$$\begin{aligned} &\left|\widetilde{V}^Q_k(e^{j\omega})\widetilde{R}^Q_k(e^{j\omega})\right| \\ &\quad = \left|V^Q_0(e^{j\omega})\widetilde{R}^Q_k(e^{j\omega})\right| \\ &\quad = \frac{M}{2}\left|H_p\left(e^{j(\omega-(\pi/2M))}\right)H_p\left(e^{j(\omega+(\pi/2M))}\right)\right| \cdot \left|\widetilde{R}^Q_k(e^{j\omega})\right|, \\ &\left|\widetilde{U}^Q_k(e^{j\omega})\widetilde{R}^Q_k\left(e^{j(\omega+(\pi/M))}\right)\right| \\ &\quad = \left|U^Q_{2M-1}(e^{j\omega})\widetilde{R}^Q_k\left(e^{j(\omega+(\pi/M))}\right)\right| \\ &\quad = \frac{M}{2}\left|H_p\left(e^{j(\omega-(\pi/2M))}\right)H_p\left(e^{j(\omega+(\pi/2M))}\right)\right| \cdot \left|\widetilde{R}^Q_k\left(e^{j(\omega+(\pi/M))}\right)\right|, \end{aligned} \tag{19}$$

respectively. Here the upper-case symbols stand for the Fourier transforms of the impulse responses denoted by the corresponding lower-case symbols. The terms involving the two frequency shifted prototype frequency responses are the overall magnitude response for the crosstalk. $H_p(e^{j(\omega-(\pi/2M))})$ appears here as the receive filter for the desired subchannel and $H_p(e^{j(\omega+(\pi/2M))})$ denotes the response of the transmit filter of the contiguous (potentially interfering) subchannel. The actual frequency response includes phase terms, but based on the discussion in the previous subsection we know that, in the baseband model of the ideal channel case, all the cross-talk energy is in the imaginary part of the impulse response. The residual imaginary part of the equalized channel impulse response $\widetilde{r}^Q_k[n]$ determines how much of this cross-talk energy appears as ICI in detection. It can be calculated as a function of frequency for a given set of equalizer coefficients, assuming the required knowledge on the channel response is available. Now the ICI power for subchannel k can be obtained with good accuracy by integrating over the transition bands in the baseband

model

$$P_k^{ICI} = \int_{-\pi/2M}^{\pi/2M} \frac{M^2}{4} \left| H_p\left(e^{j(\omega-(\pi/2M))}\right) H_p\left(e^{j(\omega+(\pi/2M))}\right) \right|^2 \cdot \left| \widetilde{R}_k^{Q}(e^{j\omega}) \right|^2 d\omega + \int_{-\pi/2M}^{\pi/2M} \frac{M^2}{4} \left| H_p\left(e^{j(\omega-(\pi/2M))}\right) H_p\left(e^{j(\omega+(\pi/2M))}\right) \right|^2 \cdot \left| \widetilde{R}_k^{Q}\left(e^{j(\omega+(\pi/M))}\right) \right|^2 d\omega. \tag{20}$$

Also the ISI power can be calculated, as soon as the channel and equalizer responses are known, from the aliased spectrum of $\widetilde{G}_k(e^{j\omega})$, as

$$P_k^{ISI} = \int_0^{\pi/M} \left| M - \sum_{l=-1}^{1} \widetilde{G}_k(e^{j(\omega+(l\pi/M))}) \right|^2 d\omega. \tag{21}$$

Here, the Nyquist criterion in frequency domain is used: in ISI-free conditions, the folded spectrum of the overall subchannel response $\widetilde{G}_k(e^{j\omega})$ adds up to a constant level M, a condition equivalent to overall impulse response being unity impulse. By calculating the difference between this ideal reference level and the actual spectrum, the spectrum resulting from the residual ISI can be extracted. Integration over this residual spectrum gives the ISI power, according to (21).

Typically, the pulse shape applied to the symbol detector, the slicer, is constrained to satisfy the Nyquist criterion. In the presence of ISI, this often requires from the receive filter (in this context, the term "receive filter" is assumed to include both the analysis filter and the equalizer) a gain that compensates for the channel loss and causes the noise power to be amplified. This is called noise enhancement. The subchannel noise gain can be calculated as

$$\beta_k^n = \frac{1}{2\pi} \int_{-\pi}^{\pi} \left| C_k(e^{j\omega}) H_p\left(e^{j((\omega\mp\pi/2)/M)}\right) \right|^2 d\omega, \tag{22}$$

where $C_k(e^{j\omega})$ is the response of the subchannel equalizer. The $-$ and $+$ signs are valid for even and odd subchannel indexes, respectively.

3.3. Semianalytical performance evaluation

The performance of the studied FBMC, using per-subcarrier equalization to combat multipath distortion, can be evaluated semianalytically according to the discussion above. The term "semianalytically" refers, in this context, to the fact that no actual signal needs to be generated for transmission. Instead, a frequency domain analysis of the distorting channel and the equalizer can be applied to derive the ICI and ISI power spectra and the noise enhancement involved. Based on P_k^{ICI}, P_k^{ISI}, and β_k^n, the overall signal to interference plus noise ratio(s) (SINR) for given E_b/N_0-value(s) can be obtained. Then, well-known formulas based on the Q-function [30] and Gray-coding assumption can be exploited to estimate the uncoded bit error-rate (BER) performance. This can further be averaged over a number of channel instances corresponding to a given power delay profile.

4. LOW-COMPLEXITY POINTWISE PER-SUBCARRIER EQUALIZATION

The known channel equalization solutions for FBMC suffer from insufficient performance, as in the case of the 0th-order ASCET [22], and/or from relatively high implementation complexity, as in the FIR filter based approach described, for example, by Hirosaki in [4]. To overcome these problems, a specific structure that equalizes at certain frequency points is considered. The pointwise equalization principle proceeds from the consideration that the subchannel equalizers are designed to equalize the channel optimally at certain frequency points within the subband. To be more precise, the coefficients of the equalizer are set such that, at all the considered frequency points, the equalizer amplitude response optimally approaches the inverse of the determined channel amplitude response and the equalizer phase response optimally approaches the negative of the determined channel phase response. Optimal equalization at all frequencies would implicitly fulfill the zero ICI conditions of (15), and the zero ISI condition of (18). In pointwise equalization, the optimal linear equalizer is approximated between the considered points and the residual ICI and ISI interference powers depend on the degree of inaccuracy with respect to the zero ICI/ISI conditions and can be measured using (20) and (21), respectively. On the other hand, the level of inaccuracy depends on the relation of the channel coherence bandwidth [31] to the size of the filter bank and the order of the pointwise per-subcarrier equalizer. For mildly frequency selective subband responses, low-complexity structures are sufficient to keep the residual ICI and ISI at tolerable levels.

Alternative optimization criteria are possible for the equalizer coefficients from the amplitude equalization point of view, namely, zero-forcing (ZF) and mean-squared error (MSE) criteria [30, 31]. The most straightforward approach is ZF, where the coefficients are set such that the achieved equalizer response compensates the channel response exactly at the predetermined frequency points. The ZF criterion aims to minimize the P_k^{ICI} and P_k^{ISI}, but ignores the effect of noise. Ultimately, the goal is to minimize the probability of decision errors. The MSE criterion tries to achieve this goal by making a tradeoff between the noise enhancement and residual ISI at the slicer input. The MSE criterion thus alleviates the noise enhancement problem of ZF and could provide improved performance for those subchannels that coincide with the deep notches in the channel frequency response. For high SNR, the MSE solution of the amplitude equalizer converges to that obtained by the ZF criterion.

4.1. Complex FIR equalizer

A straightforward way to perform equalization at certain frequency points within a subband is to use complex FIR filter (CFIR-SCE), an example structure of which is shown in Figure 4, that has the desired frequency response at those given points. In order to equalize for example at three

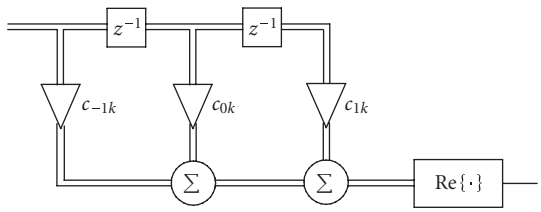

Figure 4: An example structure of the CFIR-SCE subcarrier equalizer.

frequency points, a 3-tap complex FIR with noncausal transfer function

$$H_{\text{CFIR-SCE}}(z) = c_{-1}z + c_0 + c_1 z^{-1} \tag{23}$$

offers the needed degrees of freedom. The equalizer coefficients are calculated by evaluating the transfer function, which is set to the desired response, at the chosen frequency points and setting up an equation system that is solved for the coefficients.

4.2. Amplitude-phase equalizer

We consider a linear equalizer structure consisting of an allpass phase correction section and a linear-phase amplitude equalizer section. This structure is applied to each complex subchannel signal for separately adjusting the amplitude and phase. This particular structure makes it possible to independently design the amplitude equalization and phase equalization parts, leading to simple algorithms for optimizing the equalizer coefficients. The orders of the equalizer stages are chosen to obtain a low-complexity solution. A few variants of the filter structure have been studied and will be described in the following.

An example structure of the AP-SCE equalizer is illustrated in detail in Figure 5. In this case, each subchannel equalizer comprises a cascade of a first-order complex allpass filter, a phase rotator combined with the operation of taking the real part of the signal, and a first-order real allpass filter for compensating the phase distortion. The structure, moreover, consists of a symmetric 5-tap FIR filter for compensating the amplitude distortion. Note that the operation of taking the real part of the signal for detection is moved before the real allpass phase correction stage. This does not affect the output of the AP-SCE, but reduces its implementation complexity.

The transfer functions of the real and complex first-order allpass filters are given by

$$H_r(z) = \frac{1 + b_r z}{1 + b_r z^{-1}}, \tag{24}$$

$$H_c(z) = \frac{1 - jb_c z}{1 + jb_c z^{-1}}, \tag{25}$$

respectively. In practice, these filters are realized in the causal form as $z^{-1}H_\cdot(z)$, but the above noncausal forms simplify the following analysis. For the considered example structure, the overall phase response of the AP-SCE phase correction section (for the kth subchannel) can be derived from (24) and (25)

$$\begin{aligned}\arg\left[H_{\text{peq}}(e^{j\omega})\right] &= \arg\left[e^{j\varphi_{0k}} \cdot H_c(e^{j\omega}) \cdot H_r(e^{j\omega})\right] \\ &= \varphi_{0k} + 2\arctan\left(\frac{-b_{ck}\cos\omega}{1 + b_{ck}\sin\omega}\right) \\ &\quad + 2\arctan\left(\frac{b_{rk}\sin\omega}{1 + b_{rk}\cos\omega}\right).\end{aligned} \tag{26}$$

In a similar manner, we can express the transfer function of the amplitude equalizer section in a noncausal form as

$$H_{\text{aeq}}(z) = a_2 z^2 + a_1 z + a_0 + a_1 z^{-1} + a_2 z^{-2}, \tag{27}$$

from which the equalizer magnitude response for the kth subchannel is obtained

$$\left|H_{\text{aeq}}(e^{j\omega})\right| = \left|a_{0k} + 2a_{1k}\cos\omega + 2a_{2k}\cos 2\omega\right|. \tag{28}$$

4.3. Low-complexity AP-SCE and CFIR-SCE

Case 1. The subchannel equalization is based on a single frequency point located at the center frequency of a specific subchannel, at $\pm\pi/2$ at the low sampling rate. Here the + sign is valid for the even and the − sign is valid for the odd subchannel indexes, respectively. In this case, the associated phase equalizer only has to comprise a complex coefficient $e^{j\varphi_{0k}}$ for phase rotation. The amplitude equalizer is reduced to just one real coefficient as a scaling factor. This case corresponds to the 0th-order ASCET or a single-tap CFIR-SCE.

Case 2. Here, equalization at two frequency points located at the edges of the passband of a specific subchannel, at $\omega = 0$ and $\omega = \pm\pi$, is expected to be sufficient. The + and − signs are again valid for the even and odd subchannels, respectively. In this case, the associated equalizer has to comprise, in addition to the complex coefficient $e^{j\varphi_{0k}}$, the first-order complex allpass filter as the phase equalizer, and a symmetric 3-tap FIR filter as the amplitude equalizer. Compared to the equalizer structure of Figure 5, the real allpass filter is omitted and the length of the 5-tap FIR filter is reduced to 3. In the CFIR-SCE approach, two taps are used.

Case 3. Here, three frequency points are used for channel equalization. One frequency point is located at the center of the subchannel frequency band, at $\omega = \pm\pi/2$, and two frequency points are located at the passband edges of the subchannel, at $\omega = 0$ and $\omega = \pm\pi$. In this case, the associated equalizer has to comprise all the components of the equalizer structure depicted in Figure 5. In the CFIR-SCE structure of Figure 4, all three taps are used.

Mixed cases of phase and amplitude equalization. Naturally, also mixed cases of AP-SCE are possible, in which a different number of frequency points within a subband are considered for the compensation of phase and amplitude distortion. For

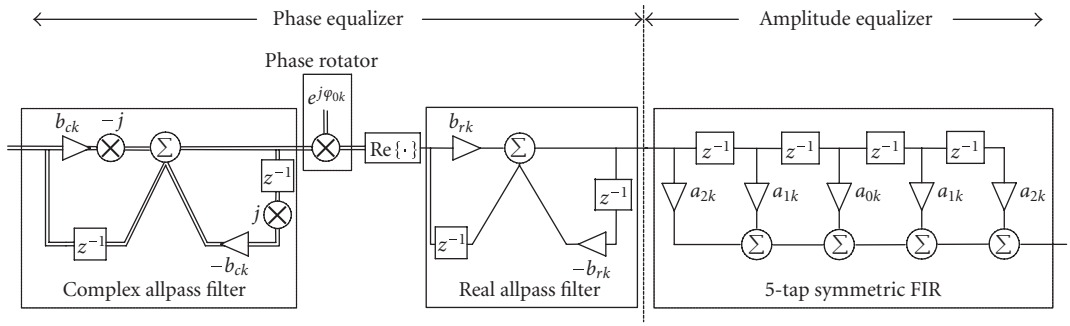

Figure 5: An example structure of the AP-SCE subcarrier equalizer.

example, Case 3 phase equalization could be combined with Case 2 amplitude correction and so forth. Ideally, the number of frequency points considered within each subchannel is not fixed in advance, but can be individually determined for each subchannel based on the frequency domain channel estimates of each data block. This enables the structure of each subchannel equalizer to be controlled such that the associated subchannel response is equalized optimally at the minimum number of frequency points which can be expected to result in sufficient performance. The CFIR-SCE cannot provide such mixed cases.

Also further cases could be considered since additional frequency points are expected to result in better performance when the subband channel response is more selective. However, this comes at the cost of increased complexity in processing the data samples and much more complicated formulas for obtaining the equalizer coefficients.

For Case 3 structure, CFIR-SCE and AP-SCE equalizer coefficients can be calculated by evaluating (23) and (26), and (28), respectively, at the frequency points of interest, setting them equal to the target values, and solving the resulting system of equations for the equalizer coefficients:
CFIR-SCE:

$$\begin{aligned} c_{-1k} &= \frac{\gamma}{4}\Big((\chi_{0k}-\chi_{2k}) \mp j(2\chi_{1k}-\chi_{0k}-\chi_{2k})\Big),\\ c_{0k} &= \frac{\gamma}{2}(\chi_{0k}+\chi_{2k}),\\ c_{1k} &= \frac{\gamma}{4}\Big((\chi_{0k}-\chi_{2k}) \pm j(2\chi_{1k}-\chi_{0k}-\chi_{2k})\Big); \end{aligned} \tag{29}$$

AP-SCE:

$$\begin{aligned} \varphi_{0k} &= \frac{\xi_{0k}+\xi_{2k}}{2}, & a_{0k} &= \frac{\gamma}{4}(\epsilon_{0k}+2\epsilon_{1k}+\epsilon_{2k}),\\ b_{ck} &= \pm\tan\left(\frac{\xi_{2k}-\xi_{0k}}{4}\right), & a_{1k} &= \pm\frac{\gamma}{4}(\epsilon_{0k}-\epsilon_{2k}),\\ b_{rk} &= \pm\tan\left(\frac{\xi_{1k}-\varphi_{0k}}{2}\right), & a_{2k} &= \frac{\gamma}{8}(\epsilon_{0k}-2\epsilon_{1k}+\epsilon_{2k}). \end{aligned} \tag{30}$$

Here the $\pm$ signs are again for the even/odd subchannels, respectively, and χ_{ik}, ξ_{ik}, and ϵ_{ik}, $i = 0,\ldots,2$, are the complex target response, the target phase, and amplitude response values at the three considered frequency points for subchannel k. The value $i = 1$ corresponds to the subchannel center frequency whereas values $i = 0$ and $i = 2$ refer to the lower and upper passband edge frequencies, respectively. With MSE criterion,

$$\begin{aligned} \chi_{ik} &= \frac{H_{\text{ch}}\left(e^{j(2k+i)(\pi/2M)}\right)^*}{\left|H_{\text{ch}}\left(e^{j(2k+i)(\pi/2M)}\right)\right|^2+\eta},\\ \xi_{ik} &= \arg(\chi_{ik}), \quad \epsilon_{ik} = |\chi_{ik}|, \end{aligned} \tag{31}$$

where H_{ch} is the channel frequency response in the baseband model of the overall system. The effect of noise enhancement is incorporated into the solution of the equalizer parameters using the noise-to-signal ratio η and a scaling factor $\gamma = 3/\sum_{i=0}^{2}\chi_{ik}H_{\text{ch}}(e^{j(2k+i)(\pi/2M)})$ that normalizes the subchannel signal power to avoid any scaling in the symbol values used for detection. In the case of ZF criterion, $\eta = 0$ and $\gamma = 1$.

The operation of the ZF-optimized amplitude and phase equalizer sections of Case 3 AP-SCE are illustrated with randomly selected subchannel responses in Figures 6 and 7, respectively.

In Case 2, MSE-optimized coefficients for CFIR-SCE and AP-SCE amplitude equalizer can be calculated as

$$\begin{aligned} c_{0k} &= \frac{\gamma}{2}(\chi_{0k}+\chi_{2k}), & a_{0k} &= \frac{\gamma}{2}(\epsilon_{0k}+\epsilon_{2k}),\\ c_{1k} &= \pm\frac{\gamma}{2}(\chi_{0k}-\chi_{2k}), & a_{1k} &= \pm\frac{\gamma}{4}(\epsilon_{0k}-\epsilon_{2k}), \end{aligned} \tag{32}$$

where $\gamma = 2/(\chi_{0k}H_{\text{ch}}(e^{j(k\pi/M)}) + \chi_{2k}H_{\text{ch}}(e^{j(2k+2)(\pi/2M)}))$. The AP-SCE phase equalizer coefficients φ_{0k} and b_{ck} can be obtained as in Case 3.

Case 1 equalizers are obtained as special cases of the used structures, including only a single complex coefficient for CFIR-SCE and an amplitude scaling factor and a phase rotator for AP-SCE. It is natural to calculate these coefficients based on the frequency response values at the subchannel center frequencies, that is,

$$\begin{aligned} c_{0k} &= \chi_{1k},\\ a_{0k} &= |\chi_{1k}|, \qquad \varphi_{0k} = \arg(\chi_{1k}), \end{aligned} \tag{33}$$

with $\eta = 0$, since MSE and ZF solutions are the same.

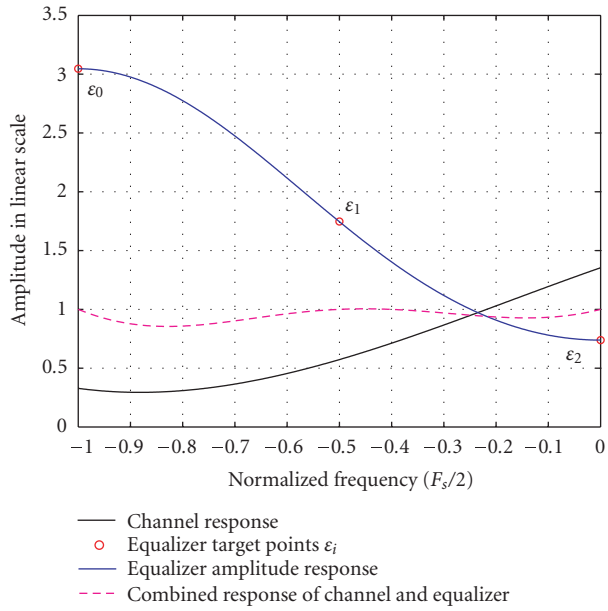

Figure 6: Operation of the ZF-optimized Case 3 amplitude equalizer section.

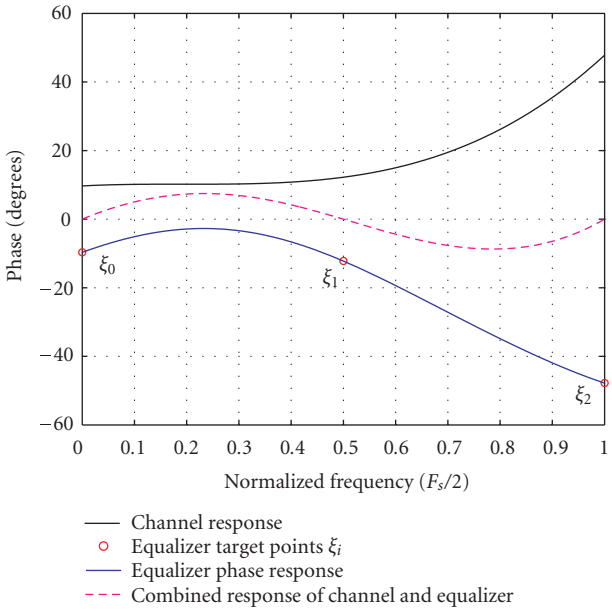

Figure 7: Operation of the Case 3 phase equalizer section.

5. NUMERICAL RESULTS

The performance of the low-complexity subcarrier equalizers was evaluated with different number of subchannels both semianalytically and using full simulations in time domain. First, basic results are reported to illustrate how the performance depends on the number of subcarriers and the equalizer design case. Also the reliability of the semianalytical model is examined and the differences between ZF and MSE criteria are compared. Finally, more complete simulations with error control coding are reported and compared to an OFDM reference in a realistic simulation environment. Also sensitivity to timing and frequency offsets and performance with practical transmitter power amplifiers are investigated. We consider equally spaced real 2-PAM, 4-PAM, and 8-PAM constellations for FBMC and complex square-constellations QPSK, 16-QAM, and 64-QAM in the OFDM case.

5.1. Semianalytical performance evaluation

Semianalytical simulations were carried out with the Vehicular-A power delay profile (PDP), defined by the recommendations of the ITU [32], for a 20 MHz signal bandwidth. These simulations were performed in quasi-static conditions, that is, the channel was time-invariant during each transmitted frame. Perfect channel information was assumed. In all the simulations, the average channel power gain was scaled to unity. Performance was tested with filter banks consisting of $2M = \{64, 128, 256\}$ subchannels. The filter bank designs used roll-off $\rho = 1.0$ and overlapping factor $K = 5$ resulting in about 50 dB stopband attenuation. The statistics are based on 2000 frame transmissions for each of which an independent channel realization was considered. The semianalytical results were obtained by calculating the subcarrierwise ICI and ISI powers P_k^{ICI} and P_k^{ISI}, respectively, together with noise gains β_k^n for $k = 0, 1, \ldots, 2M-1$. These were then used to determine the subcarrierwise SINR-values, as a function of channel E_b/N_0-values, for all the channel instances. The uncoded BER results were obtained for 2-, 4-, and 8-PAM modulations by evaluating first the theoretical subcarrierwise BERs based on the SINR-values using the Q-function and Gray-coding assumption, and finally averaging the BER over all the subchannels and 2000 channel instances.

5.1.1. Basic results for AP-SCE

The comparison in Figure 8(a) for ZF 4-PAM shows that the time domain simulation-based (Sim) and semi-analytic model-based (SA) results match quite well. This encourages to carry out system performance evaluations, especially in the algorithm development phase, mostly using the semianalytical approach, which is computationally much faster. Time domain simulation results in Figure 8(b) for 4-PAM indicate that the performance difference of ZF and MSE criteria is rather small. Figures 8(c) and 8(d) show the semi-analytic results for 2-PAM and 8-PAM, respectively, using the ZF criterion. It can be observed that higher-order AP-SCE improves the equalizer performance significantly, allowing the use of a lower number of subcarriers. Also ideal OFDM performance (without guard interval overhead) is shown as a reference. With the aid of the AP-SCE equalizer, the performance of FBMC with a modest number of subcarriers can be made to approach that of the ideal OFDM.

5.1.2. Comparison of CFIR-FBMC and AP-FBMC

In the other simulations, it is assumed that the receiver is time-synchronized such that the first path corresponds to

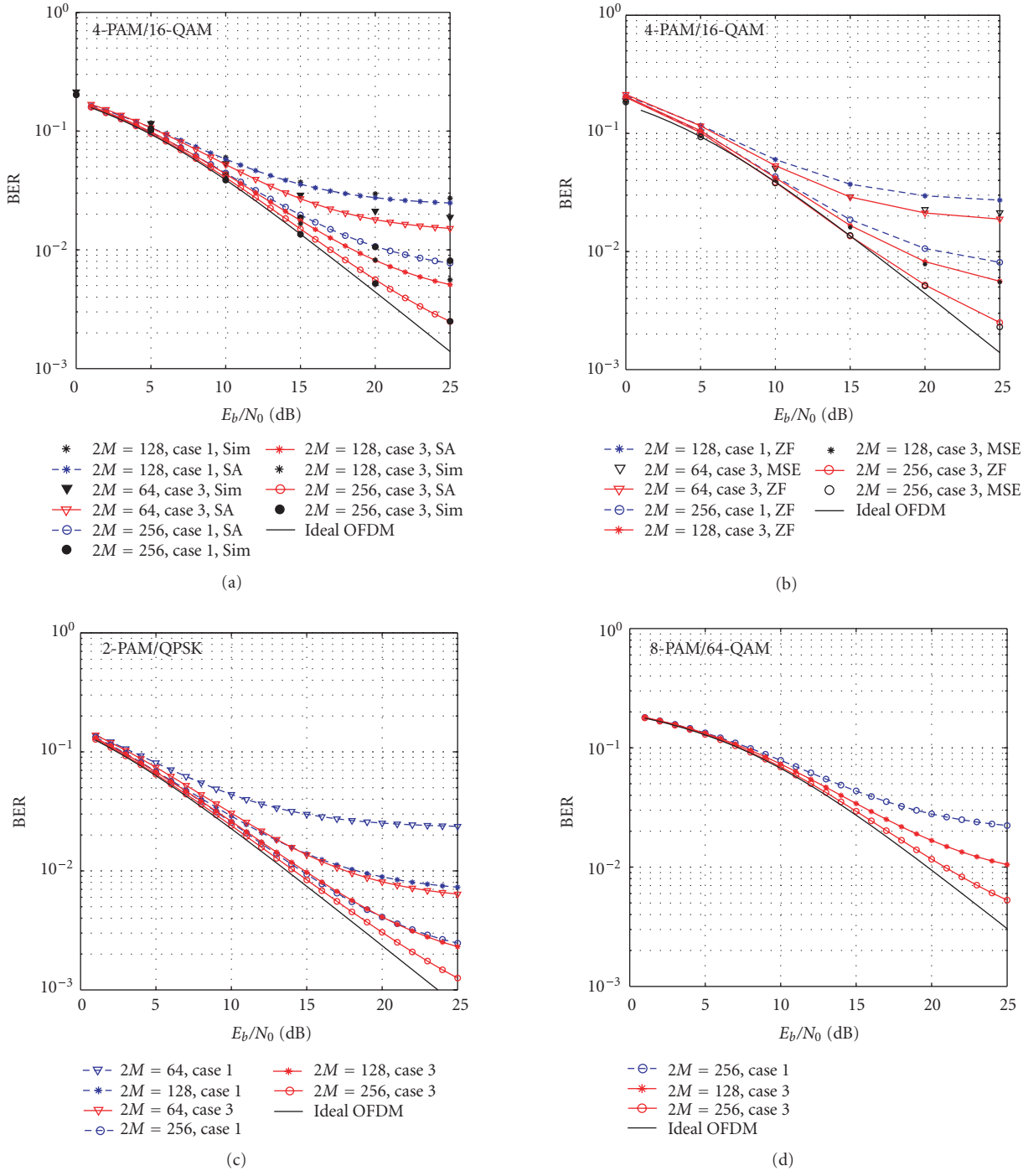

FIGURE 8: Uncoded BER results for AP-SCE with a quasi-static ITU-R Vehicular-A channel model and 20 MHz bandwidth. (a) Comparison of time domain simulations (Sim) and semi-analytic model (SA) for ZF 4-PAM. (b) Comparison of ZF and MSE criteria with 4-PAM based on time domain simulations. (c) Semi-analytic performance of ZF 2-PAM. (d) Semi-analytic performance of ZF 8-PAM. Ideal OFDM (using corresponding square-constellation QAM, without guard interval overhead) included in all figures as a reference.

zero delay. Figure 9, however, shows a semi-analytic BER comparison of the two subcarrier equalizer structures for $2M = 256$ subchannels when the effect of time synchronization error is considered. Simulations were carried out with a quasi-static channel model based on the extended ITU-R Vehicular-A PDP [33]. Simulation result statistics are based on 2000 independent channel instances of this model and the MSE criterion was used in the derivation of the amplitude equalizer coefficients. Figure 9 shows the performance in two cases: with delays of 0 and 64 samples, corresponding to 0

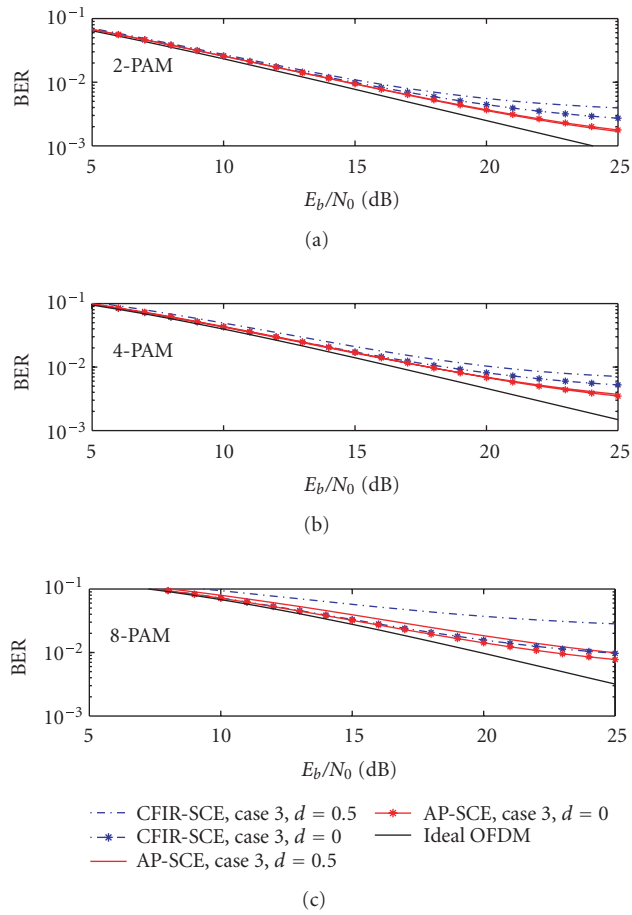

Figure 9: Semi-analytic BER in AP-SCE and CFIR-SCE. Parameter d = timing offset/subcarrier symbol interval.

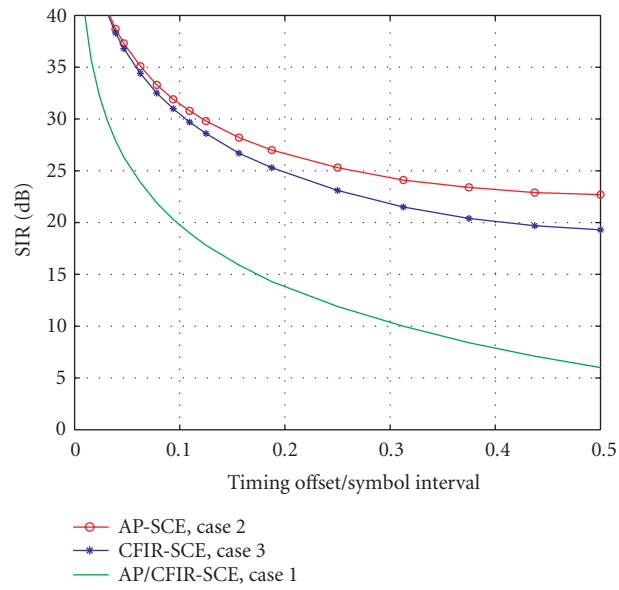

Figure 10: Semi-analytic SIR due to timing phase offset in AP-SCE and CFIR-SCE in an ideal channel.

and 50% of the subcarrier symbol interval, respectively. It is seen that with 0 timing offset, CFIR-SCE and AP-SCE have very similar performance. However, AP-SCE is clearly more robust in the presence of timing offset. Especially with high-order modulations, the performance of CFIR-SCE is significantly degraded when the timing error approaches half of the subcarrier symbol interval. AP-SCE is very robust in this sense, and the results demonstrate that FBMC with AP-SCE can be operated without timing synchronization prior to the receiver filter bank.

Figure 10 shows the signal-to-interference ratio (SIR) performance in case of an ideal channel with timing offset only. Here, Case 2 AP-SCE includes only the first-order complex allpass and phase rotation; the real allpass does not have any effect in this case. Figure 10 was obtained in the $2M = 256$ subcarrier case, but it was observed that with other filter bank sizes, the behavior in terms of relative timing offset is very similar. It is seen that Case 3 CFIR-SCE gives clearly better performance than simple phase rotation (Case 1), and with timing offsets approaching half of the symbol interval, Case 2 AP-SCE has 3 dB better performance than Case 3 CFIR-SCE. This is in accordance with the findings in [34], where it is observed that allpass IIR structures provide performance gain in fractional delay compensation compared to FIR structures with similar complexity.

5.2. Performance comparisons with channel coding

5.2.1. Channel model, system parameters, and OFDM reference

We have also carried out full simulations in time domain comparing cyclic prefix OFDM and FBMC. It was of particular interest to evaluate the performance of FBMC with AP-SCE and CFIR-SCE per-subcarrier equalizers and to explore the potential spectral efficiency gain. Time-variant radio channel impairments were modeled based on the extended ITU-R Vehicular-A PDP [33] (maximum excess delay of 2.51 μs). This upgraded channel model has been shown to improve the frequency correlation properties when compared to the original PDP, making it better suited for evaluation of wideband transmission with frequency-dependent characteristics. Mobile velocity of 50 km/h and carrier frequency of 5 GHz were assumed. With sampling rate of 26.88 MHz (7× WCDMA chip rate), 616 subcarriers of 1024 in OFDM and 84/168/672 subchannels of 128/256/1024 in FBMC were activated to obtain systems with the same effective bandwidth of 18 MHz (at 40 dB below passband level). This corresponds to subchannel bandwidths of 26.25 kHz and 210/105/26.25 kHz, respectively. 2-, 4-, and 8-PAM modulations were considered for FBMC whereas QPSK, 16-QAM, and 64-QAM were used for OFDM. The FBMC design used roll-off $\rho = 1.0$ and overlapping factor $K = 5$ resulting in a stopband attenuation (defined as the level of the highest sidelobe) of about 50 dB (for 2-PAM/QPSK comparison also $K = 3$ was considered, giving stopband attenuation of about 38 dB). Channel coding

was performed using low-density parity check (LDPC) coding [35]. The maximum number of iterations in iterative decoding was set to ten. About 10% overhead for pilot carriers is assumed in OFDM and similar overhead for training sequences in FBMC. OFDM has 41.67 μs overall symbol duration, with 2.53 μs guard interval and 1.04 μs raised-cosine roll-off for spectral shaping. Both systems have a single zero power subcarrier in the middle of the spectrum to facilitate receiver implementation. The information bit rates in the two systems were approximately matched using code rates of $R = 3/4$ and $R = 2/3$ for OFDM and FBMC, respectively. Bits for a single frame to be transmitted were coded in blocks of 3348 and 3990 bits, respectively, after which all the coded bits of a frame were randomly interleaved before bits-to-symbols and symbols-to-subcarriers mappings. The resulting number of source bits in a fixed frame duration of 250 μs are 5022 and 5320 for QPSK/OFDM and 2-PAM/FBMC, respectively. Ideal channel estimation was assumed for both OFDM and FBMC modulations. Simulation result statistics are based on 5000 transmitted frames for each of which an independent realization of the channel model was applied. MSE optimization criterion was used to derive the amplitude equalizer parameters.

5.2.2. Coded results

Figures 11(a), 11(b), and 11(c) show the obtained results for 2-PAM/QPSK, 4-PAM/16-QAM, and 8-PAM/64-QAM comparisons, respectively. Coded frame error rate (FER) and BER are shown as a function of required energy per source bit to noise spectral density-ratio. Due to the absence of time domain guard interval and reduced frequency domain guardbands, higher spectral efficiency in FBMC is achieved. This excess transmission capacity can be used to transmit more redundant data (lower coding rate) while maintaining similar information data rate compared to OFDM. This turns into favor of FBMC in the FER/BER performance comparison as somewhat less energy in FBMC is sufficient to result in similar error probability compared to OFDM. Alignment of the performance curves for $K = 3$ and $K = 5$ in Figure 11(a) indicates that at least in narrowband interference-free conditions, FBMC design with $K = 3$ (and possibly even $K = 2$) provides sufficient performance with reduced complexity compared to $K = 5$.

5.2.3. Effect of AP-SCE structure and parameters

The ability of AP-SCE/CFIR-SCE equalizer to compensate for mildly frequency selective subchannel responses is clearly visible in the simulation results. FBMC of $2M = 256$ subchannels with Case 3 AP-SCE/CFIR-SCE follows the performance curves obtained with the structure consisting of $2M = 1024$ subchannels with Case 1 equalizer. So, great reduction in the number of subchannels required to cover the 18 MHz signal band can be achieved with higher-order AP-SCE/CFIR-SCE structures. In case of 2-PAM modulation even a filter bank with $2M = 128$ subchannels can be considered. For 4-PAM and 8-PAM, $2M = 256$ subchannels are required to keep the performance benefit with respect to the OFDM reference.

5.3. Performance with nonlinear power amplifier

The ratio between the maximum instantaneous power of a signal and its mean power (PAPR) is proportional to the number of subcarriers and also depends on the modulation constellation used. This is a matter of concern when the signal passes through a nonlinear device such as the power amplifier (PA). In this situation, signal components of different instantaneous power might be amplified differently, introducing distortion to the signal and causing spectral regrowth to the bands adjacent to the signal. In this section, we focus on the spectral regrowth caused by a PA on FBMC and OFDM with similar parameters as in the time domain BER simulations. We apply time domain raised-cosine windowing of 28 samples to the OFDM signal in order to assure attenuation of 40 dB for the signal at 9 MHz from the carrier frequency. Therefore, the overall 40 dB bandwidth for OFDM and FBMC is 18 MHz. The PA follows the solid state power amplifier (SSPA) model that can be found in [36]. Only amplitude nonlinearity is taken into account. The amplitude gain is given by

$$p_o = \frac{p_i}{\sqrt{1 + \left(p_i/p_{\text{sat}}\right)^2}}, \tag{34}$$

where p_i and p_o are the amplitude of the PA input signal and output signal, respectively, and p_{sat} denotes the saturation voltage of the PA. The spectral regrowth is measured as a function of the input back-off (IBO) of the input signal at the amplifier. In Figure 12 we show the regrowth of the spectra of FBMC (dashed lines) and OFDM (continuous lines). For FBMC we simulate IBOs that are 1.2 dB higher than for OFDM. This reflects the fact that for a similar coded BER performance we can use an FBMC signal with 1.2 dB less power than OFDM. We can see from the figure, that it is of advantage to be able to use a weaker signal, since close to the desired passband we obtain less spectral regrowth. At more distant frequencies, the OFDM spectrum decays faster because the useful bandwidth is smaller than the useful bandwidth in FBMC (16.2 MHz versus 17.6 MHz). OFDM with a comparable useful bandwidth (672 active subcarriers) has a spectral decay profile similar to FBMC's. Moreover, at the same IBOs and same useful bandwidths, both systems show very similar regrowth curves.

5.4. Frequency offset

In multicarrier transmissions, frequency offsets (e.g., due to Doppler and inaccuracy of local oscillators in the transmission chain) introduce ICI. In case of a fixed frequency offset in OFDM, the SIR due to the resulting ICI is given by [37]

$$\text{SIR} = \frac{1}{\left(\sin(\pi\Delta f)\right)^2 \sum_{p=0,\, p\neq N_c/2}^{N_c-1} 1/\left\{N_c \sin\left(\pi(p+\Delta f)/N_c\right)\right\}^2}, \tag{35}$$

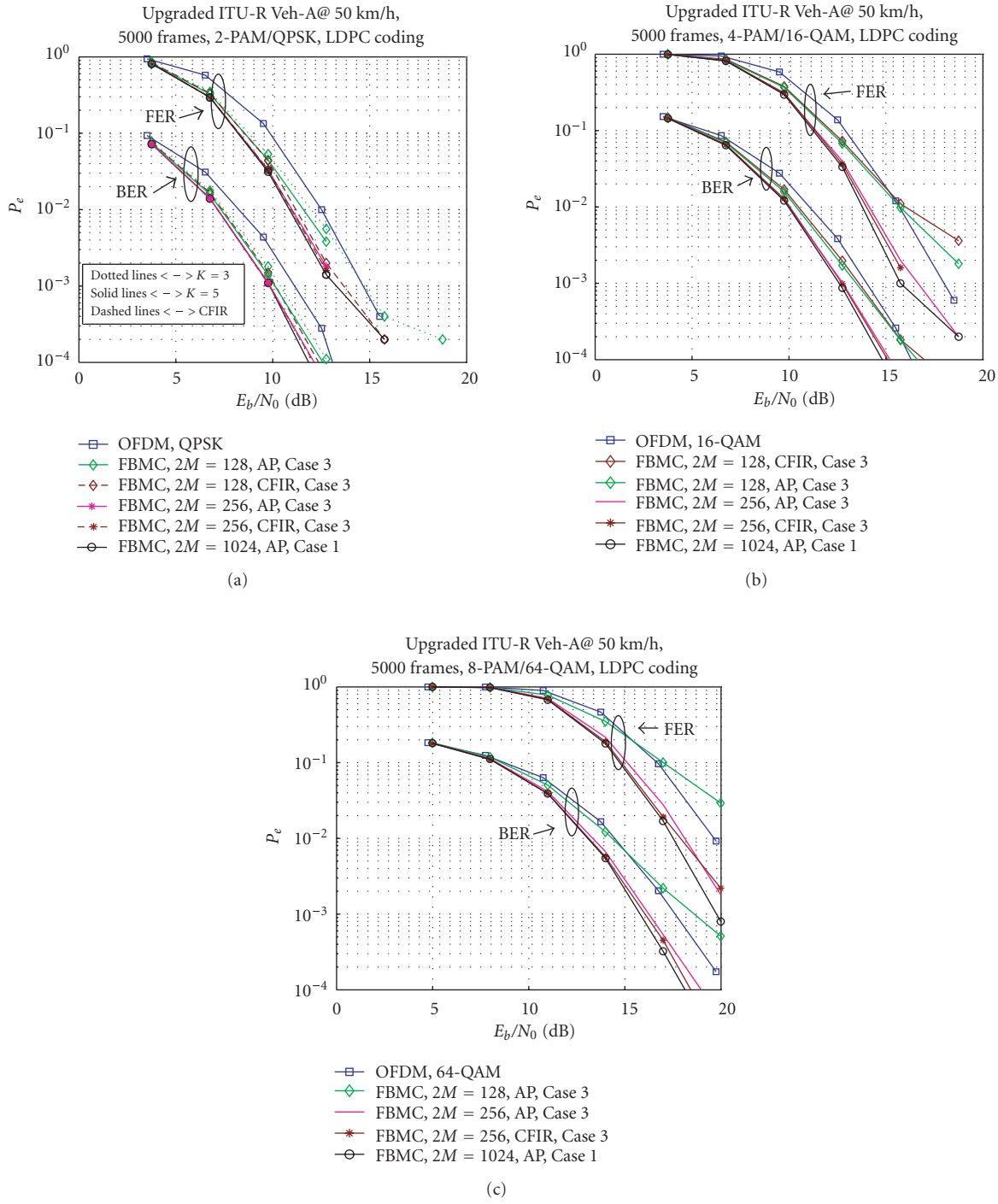

Figure 11: Coded FER and BER performance: (a) 2-PAM/FBMC and QPSK/OFDM; (b) 4-PAM/FBMC and 16-QAM/OFDM; and (c) 8-PAM/FBMC and 64-QAM/OFDM.

where N_c and Δf are the number of subcarriers and frequency offset, respectively. The effects of frequency offsets in FBMC were tested with a simple simulation experiment by measuring the mean squared error in symbol detection with a set of fixed frequency offsets. The results are shown and compared to the OFDM performance in Figure 13. Here $N_c = 256$ for both systems.

Basically, the frequency offset introduces a time-varying phase offset, which is common to all subcarriers. In the simulation, as well as in the analytical results for OFDM, the constant part of the common phase offset is assumed to be cancelled by the channel equalizer such that in the middle of each symbol the phase error of each subcarrier is zero.

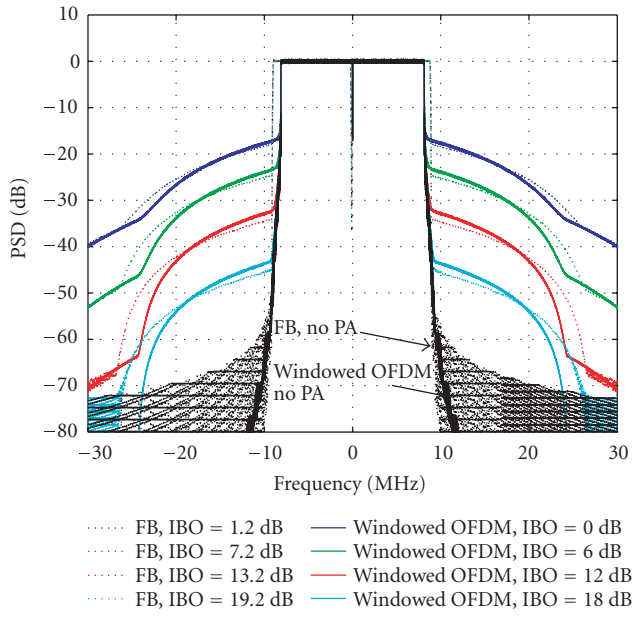

Figure 12: Spectral regrowth due to PA nonlinearity.

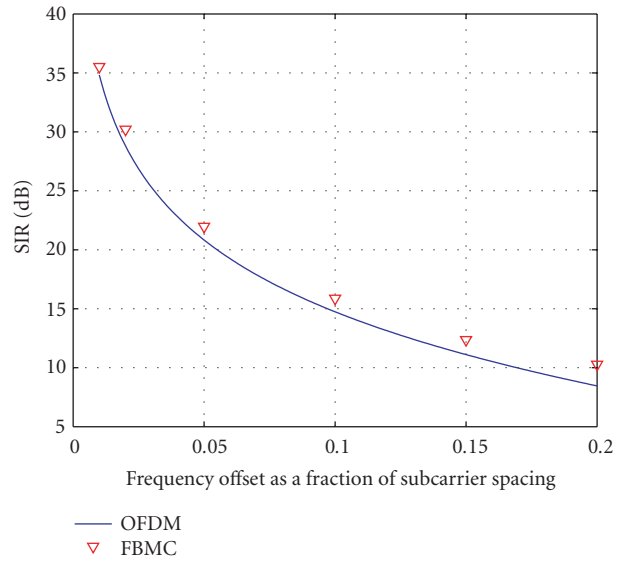

Figure 13: SIR due to frequency offset in OFDM and FBMC.

It can be seen from Figure 13 that for a given relative (with respect to subcarrier spacing) frequency offset, the FBMC SIR performance is slightly better but within 2 dB from the OFDM performance. Since FBMC allows significantly wider subcarrier spacing, the relative frequency offsets are smaller, and there is a clear performance benefit for FBMC in terms of frequency offset effects. This indicates also a potential for better performance in case of fast fading.

5.5. Complexity

In this subsection, a rough evaluation of the computational complexity of FBMC is presented, using a simple complexity measure: the number of real multiplications required to detect a symbol. We focus on the receiver side where the OFDM FFT or FBMC analysis bank and the equalizer are the main processing blocks. Channel estimation and calculation of the equalizer coefficients are not included in this evaluation.

One of the most efficient algorithms for implementing DFT is the split radix FFT algorithm [18], taking $M(\log_2(M) - 3) + 4$ real multiplications for a block of M complex samples. In the OFDM case, 3 real multipliers are enough to do the complex multiplication to equalize each of the used subcarriers.

In the FBMC case, the FFT-based algorithm presented in [26] is the most efficient one to implement the oversampled analysis bank in terms of multiplication rate. It requires $2M(2K - 2 + \log_2(M))$ real multiplications for a block of M high-rate samples. In an efficient implementation, the AP-SCE subcarrier equalizers take 2, 5, and 7 real multiplications in Cases 1, 2, and 3, respectively, per detected real symbol. Alternatively, the 3-tap CFIR-SCE structure takes 6 real multiplications per detected real symbol.

Table 1: Multiplications in receiver per one detected complex symbol in OFDM and per two detected real symbols in FBMC.

	Case 1	Case 3
OFDM, 1k-FFT	10	—
FBMC, $K = 2$, $2M = 128$, AP-SCE	20	30
FBMC, $K = 5$, $2M = 256$, AP-SCE	34	44
FBMC, $K = 2$, $2M = 128$, CFIR-SCE	20	28
FBMC, $K = 5$, $2M = 256$, CFIR-SCE	34	42

For a fair comparison, we calculate the overall number of multiplications per detected complex symbol in the OFDM case and per two detected real symbols in the FBMC case. For simplicity, it is assumed that all the subcarriers are in use. The resulting overall multiplication rates with the two extreme cases of FBMC-complexity are shown in Table 1.

It is observed that with this complexity measure, FBMC is more complex than the basic OFDM system. However, the implementation of FBMC is yet quite realistic with today's efficient digital signal processors or dedicated very large scale integration (VLSI) hardware. It is expected that there are a lot of possibilities to optimize the EMFB implementation in dedicated hardware, using short coefficient word-lengths, sums of powers of two implementations for coefficients, and so forth.

Furthermore, it can be noted that due to the larger block-size, OFDM requires significantly bigger data memory and coefficient storage in processor-based implementations.

One quite significant aspect is the needed baseband filtering in the receiver before the filter bank or FFT. The oversampled analysis bank acts as a high-quality channel selection filter, effectively suppressing adjacent channels and other interference components appearing in the range of the unused subcarriers. In the OFDM case, the attenuation capability

of the DFT is rather limited, regarding the adjacent channels and other out-of-band interference sources that are not synchronized to the guard interval structure. Therefore additional highly selective digital baseband filtering is usually needed in OFDM, especially if the frequency domain guard-bands between the adjacent frequency channels are to be minimized. Including the baseband filtering in the complexity comparison may change the measures significantly.

6. CONCLUSION

We have studied a new low-complexity per-subcarrier channel equalizer for FBMC transceiver for high-rate wideband communications over doubly-dispersive channel and analyzed its performance. It was shown that the coded error-rate performance of FBMC is somewhat better than that of the OFDM reference. It was also indicated that the performance of FBMC with a practical nonlinear power amplifier is similar to that of OFDM or even better. Further, FBMC is much less sensitive to frequency offsets than OFDM due to the possibility of using significantly lower number of subcarriers. The latter observation indicates also a potential for improved performance benefit in case of fast-fading channels. It was seen that an FBMC receiver can be operated without time synchronization prior to the receiver bank, also with higher-order modulations if AP-SCE is used. This leads to a simplified overall receiver structure.

The arithmetic complexity of FBMC is, no doubt, higher than that of the reference OFDM, but yet realistic with digital VLSI technologies. However, FBMC has various benefits over OFDM, like higher flexibility in choosing the design parameters. Especially, it can be emphasized that the receiver filter bank in FBMC acts as a high-quality frequency selective filter for all the signal components in the received band. This is in contrast to OFDM where transients are introduced to the signal components that are not synchronized to the guard interval structure, causing leakage of interference power also to noninterfered parts of the spectrum. Therefore, FBMC has the potential of providing sufficient attenuation for adjacent channels and other interferences, reducing the complexity of the baseband filtering of the receiver. On the other hand, this feature makes it feasible to have small frequency domain guard-bands between the asynchronous adjacent channel users, increasing the spectral efficiency. Selectivity provides also high robustness to narrowband interferences in the signal band, and a possibility to use multiple nonadjacent frequency slots for a single user in a flexible manner.

The numerical examples were mostly performed with high-end TMUX designs ($K = 5$) with relatively high stopband attenuation (about 50 dB). However, results with lower-complexity filter banks ($K = 3$) (about 38 dB) were also shown and even the case with $K = 2$ (about 30 dB) was tested. The conclusion is that even though the performance analysis assumed infinite attenuation for the subchannel stopbands, the performance degradation even with about 30 dB stopband attenuation is minor if the system does not need to suppress strong interfering signal components.

These results encourage further research on FBMC for beyond 3G communications. Such studies include development of robust synchronization and channel estimation techniques, as well as optimization of filter banks for low complexity with high flexibility. For example, efficient NPR filter bank designs form an interesting topic.

APPENDIX

ICI AND ISI RELATED IMPULSE RESPONSES IN THE BASEBAND MODEL

We first derive the equivalent baseband model for the lower ICI response using (1) and (5):

$$\begin{aligned}
\widetilde{v}_k[n] &= \left\{ f_{k-1}[n] * \overline{h}_k[n] \right\} e^{-j(nk\pi/M)} \\
&= \left\{ f_{k-1}[n] e^{-j(nk\pi/M)} \right\} * \left\{ \overline{h}_k[n] e^{-j(nk\pi/M)} \right\} \\
&= \left\{ f_{k-1}[n] e^{-j(nk\pi/M)} e^{-j((M+1)k\pi/2M)} \right\} \\
&\quad * \left\{ \overline{h}_k[n] e^{-j(nk\pi/M)} e^{+j((M+1)k\pi/2M)} \right\} \\
&= \left\{ f_{k-1}[n] e^{-j(n+(M+1)/2)(k\pi/M)} \right\} \\
&\quad * \left\{ \overline{h}_k[n] e^{j(-n+(M+1)/2)(k\pi/M)} \right\} \\
&= f_{2M-1}[n] * \overline{h}_0[n] = v_0[n].
\end{aligned} \tag{A.1}$$

Further,

$$\begin{aligned}
v_0[n] &= f_{2M-1}[n] * \overline{h}_0[n] \\
&= \left(-f_0^c[n] + j f_0^s[n] \right) * \left(\overline{h}_0^c[n] - j \overline{h}_0^s[n] \right) \\
&= -f_0^c[n] * \overline{h}_0^c[n] + f_0^s[n] * \overline{h}_0^s[n] \\
&\quad + j \left(f_0^s[n] * \overline{h}_0^c[n] + f_0^c[n] * \overline{h}_0^s[n] \right).
\end{aligned} \tag{A.2}$$

Applying the relationships between the sine/cosine modulated analysis/synthesis filters that can be found in [26] and which apply for a PR TMUX,

$$\begin{aligned}
h_k^s[n] &= (-1)^{k+K} f_k^c[n], \\
f_k^s[n] &= (-1)^{k+K} h_k^c[n],
\end{aligned} \tag{A.3}$$

we finally obtain

$$v_0[n] = j \left(f_0^s[n] * \overline{h}_0^c[n] + f_0^c[n] * \overline{h}_0^s[n] \right). \tag{A.4}$$

Although (A.2) and (A.4) use the noncausal form for the analysis filters, we can see that the introduced time delay does not affect (A.3) in any way. Further, since the delay is the same in both sine and cosine analysis filters, the real terms cancel each other out the same way they would do if causal expressions were used. Therefore, the lower ICI is purely imaginary in the baseband model. Likewise, we can write for the upper ICI response

$$\begin{aligned}
\widetilde{u}_k[n] &= \left\{ f_{k+1}[n] * \overline{h}_k[n] \right\} e^{-j(n(k+1)\pi/M)} \\
&= \left\{ f_{k+1}[n] e^{-j(n+(M+1)/2)((k+1)\pi/M)} \right\} \\
&\quad * \left\{ \overline{h}_k[n] e^{j(-n+(M+1)/2)((k+1)\pi/M)} \right\} \\
&= f_0[n] * \overline{h}_{2M-1}[n] = u_{2M-1}[n].
\end{aligned} \tag{A.5}$$

Now

$$\begin{aligned} u_{2M-1}[n] &= \left(f_0^c[n] + jf_0^s[n]\right) * \left(-\overline{h}_0^c[n] - j\overline{h}_0^s[n]\right) \\ &= -f_0^c[n] * \overline{h}_0^c[n] + f_0^s[n] * \overline{h}_0^s[n] \\ &\quad - j\left(f_0^c[n] * \overline{h}_0^s[n] + f_0^s[n] * \overline{h}_0^c[n]\right) \\ &= -j\left(f_0^c[n] * \overline{h}_0^s[n] + f_0^s[n] * \overline{h}_0^c[n]\right), \end{aligned} \tag{A.6}$$

so also the upper ICI response is purely imaginary.

For the impulse response of subchannel k, we can write in the baseband model

$$\begin{aligned} \widetilde{t}_k[n] &= \left\{f_k[n] * \overline{h}_k[n]\right\} e^{-j(nk\pi/M)} \\ &= \left\{f_k[n] e^{-j(n+(M+1)/2)(k\pi/M)}\right\} \\ &\quad * \left\{\overline{h}_k[n] e^{+j(-n+(M+1)/2)(k\pi/M)}\right\} \\ &= f_0[n] * \overline{h}_0[n] = t_0[n]. \end{aligned} \tag{A.7}$$

ACKNOWLEDGMENTS

The authors would like to thank the anonymous reviewers and the associate editor for their constructive comments and suggestions that helped to improve the manuscript, both in presentation and contents. This research was partly funded by Nokia.

REFERENCES

[1] R. van. Nee and R. Prasad, *OFDM for Wireless Multimedia Communications*, Artech House, Boston, Mass, USA, 2000.

[2] R. W. Chang, "Synthesis of band-limited orthogonal signals for multichannel data transmission," *Bell System Technical Journal*, vol. 45, pp. 1775–1796, 1966.

[3] B. R. Saltzberg, "Performance of an efficient parallel data transmission system," *IEEE Transactions on Communications*, vol. 15, no. 6, pp. 805–811, 1967.

[4] B. Hirosaki, "An analysis of automatic equalizers for orthogonally multiplexed QAM systems," *IEEE Transactions on Communications*, vol. 28, no. 1, pp. 73–83, 1980.

[5] B. Le Floch, M. Alard, and C. Berrou, "Coded orthogonal frequency division multiplex," *Proceedings of the IEEE*, vol. 83, no. 6, pp. 982–996, 1995.

[6] S. D. Sandberg and M. A. Tzannes, "Overlapped discrete multitone modulation for high speed copper wire communications," *IEEE Journal on Selected Areas in Communications*, vol. 13, no. 9, pp. 1571–1585, 1995.

[7] A. Vahlin and N. Holte, "Optimal finite duration pulses for OFDM," *IEEE Transactions on Communications*, vol. 44, no. 1, pp. 10–14, 1996.

[8] T. Wiegand and N. J. Fliege, "Equalizers for transmultiplexers in orthogonal multiple carrier data transmission," in *Proceedings of the European Signal Processing Conference (EUSIPCO '96)*, vol. 2, pp. 1211–1214, Trieste, Italy, September 1996.

[9] S. Nedic, "An unified approach to equalization and echo cancellation in OQAM-based multi-carrier data transmission," in *Proceedings of IEEE Global Telecommunications Conference (GLOBECOM '97)*, vol. 3, pp. 1519–1523, Phoenix, Ariz, USA, November 1997.

[10] L. Vandendorpe, L. Cuvelier, F. Deryck, J. Louveaux, and O. van de Wiel, "Fractionally spaced linear and decision-feedback detectors for transmultiplexers," *IEEE Transactions on Signal Processing*, vol. 46, no. 4, pp. 996–1011, 1998.

[11] K. Van Acker, G. Leus, M. Moonen, O. van de Wiel, and T. Pollet, "Per tone equalization for DMT-based systems," *IEEE Transactions on Communications*, vol. 49, no. 1, pp. 109–119, 2001.

[12] P. Siohan, C. Siclet, and N. Lacaille, "Analysis and design of OFDM/OQAM systems based on filterbank theory," *IEEE Transactions on Signal Processing*, vol. 50, no. 5, pp. 1170–1183, 2002.

[13] A. M. Wyglinski, P. Kabal, and F. Labeau, "Adaptive filterbank multicarrier wireless systems for indoor environments," in *Proceedings of the 56th IEEE Vehicular Technology Conference (VTC '02)*, vol. 1, pp. 336–340, Vancouver BC, Canada, September 2002.

[14] B. Farhang-Boroujeny, "Multicarrier modulation with blind detection capability using cosine modulated filter banks," *IEEE Transactions on Communications*, vol. 51, no. 12, pp. 2057–2070, 2003.

[15] B. Farhang-Boroujeny and L. Lin, "Analysis of post-combiner equalizers in cosine-modulated filterbank-based transmultiplexer systems," *IEEE Transactions on Signal Processing*, vol. 51, no. 12, pp. 3249–3262, 2003.

[16] S.-M. Phoong, Y. Chang, and C.-Y. Chen, "DFT-modulated filterbank transceivers for multipath fading channels," *IEEE Transactions on Signal Processing*, vol. 53, no. 1, pp. 182–192, 2005.

[17] M. Vetterli, "Perfect transmultiplexers," in *Proceedings of IEEE International Conference on Acoustics, Speech and Signal Processing (ICASSP '86)*, vol. 11, pp. 2567–2570, Tokyo, Japan, September 1986.

[18] H. S. Malvar, *Signal Processing with Lapped Transforms*, Artech House, Boston, Mass, USA, 1992.

[19] P. P. Vaidyanathan, *Multirate Systems and Filter Banks*, Prentice Hall, Englewood Cliffs, NJ, USA, 1993.

[20] T. Karp and N. J. Fliege, "Modified DFT filter banks with perfect reconstruction," *IEEE Transactions on Circuits and Systems II: Analog and Digital Signal Processing*, vol. 46, no. 11, pp. 1404–1414, 1999.

[21] J. Alhava and M. Renfors, "Adaptive sine-modulated/cosine-modulated filter bank equalizer for transmultiplexers," in *Proceedings of the European Conference on Circuit Theory and Design (ECCTD '01)*, vol. 3, pp. 337–340, Espoo, Finland, August 2001.

[22] T. Ihalainen, T. Hidalgo Stitz, and M. Renfors, "On the performance of low-complexity ASCET-equalizer for a complex transmultiplexer in wireless mobile channel," in *Proceedings of the 7th International OFDM-Workshop*, Hamburg, Germany, September 2002.

[23] T. Ihalainen, T. Hidalgo Stitz, and M. Renfors, "Efficient per-carrier channel equalizer for filter bank based multicarrier systems," in *Proceedings of IEEE International Symposium on Circuits and Systems (ISCAS '05)*, pp. 3175–3178, Kobe, Japan, May 2005.

[24] T. Ihalainen, T. Hidalgo Stitz, and M. Renfors, "Performance comparison of LDPC-coded FBMC and CP-OFDM in beyond 3G context," in *Proceedings of IEEE International Symposium*

on Circuits and Systems (ISCAS '06), pp. 2049–2052, Kos, Greece, May 2006.

[25] Y. Yuan, T. Ihalainen, M. Rinne, and M. Renfors, "Frequency domain equalization in single carrier transmission: filter bank approach," accepted to *EURASIP Journal on Applied Signal Processing*.

[26] A. Viholainen, J. Alhava, and M. Renfors, "Efficient implementation of 2x oversampled exponentially modulated filter banks," *IEEE Transactions on Circuits and Systems II*, vol. 53, pp. 1138–1142, 2006.

[27] J. Alhava and M. Renfors, "Complex lapped transforms and modulated filter banks," in *Proceedings of the 2nd International Workshop on Spectral Methods and Multirate Signal Processing (SMMSP '02)*, pp. 87–94, Toulouse, France, September 2002.

[28] A. Viholainen, T. Hidalgo Stitz, J. Alhava, T. Ihalainen, and M. Renfors, "Complex modulated critically sampled filter banks based on cosine and sine modulation," in *Proceedings of IEEE International Symposium on Circuits and Systems (ISCAS '02)*, vol. 1, pp. 833–836, Scottsdale, Ariz, USA, May 2002.

[29] A. Viholainen, J. Alhava, and M. Renfors, "Efficient implementation of complex modulated filter banks using cosine and sine modulated filter banks," *Eurasip Journal on Applied Signal Processing*, vol. 2006, Article ID 58564, 10 pages, 2006.

[30] E. A. Lee and D. G. Messerschmitt, *Digital Communication*, Kluwer Academic, Boston, Mass, USA, 2nd edition, 1994.

[31] J. G. Proakis, *Digital Communications*, McGraw-Hill, New York, NY, USA, 3rd edition, 1995.

[32] ITU-R, "Guidelines for evaluation of radio transmission technologies for IMT-2000," Recommendation M.1225, 1997.

[33] T. B. Sorensen, P. E. Mogensen, and F. Frederiksen, "Extension of the ITU channel models for wideband (OFDM) systems," in *Proceedings of the 62nd IEEE Vehicular Technology Conference (VTC '05)*, vol. 1, pp. 392–396, Dallas, Tex, USA, September 2005.

[34] T. I. Laakso, V. Välimäki, M. Karjalainen, and U. K. Laine, "Splitting the unit: delay tools for fractional delay filter design," *IEEE Signal Processing Magazine*, vol. 13, no. 1, pp. 30–60, 1996.

[35] R. G. Gallager, "Low-density parity-check codes," *IRE Transactions on Information Theory*, vol. 8, pp. 21–28, 1962.

[36] C. Rapp, "Effects of HPA-nonlinearity on a 4-DPSK/OFDM-signal for a digital sound broadcasting system," in *Proceedings of the 2nd European Conference on Satellite Communications*, pp. 179–184, Liege, Belgium, October 1991.

[37] P. H. Moose, "Technique for orthogonal frequency division multiplexing frequency offset correction," *IEEE Transactions on Communications*, vol. 42, no. 10, pp. 2908–2914, 1994.

Tero Ihalainen received his M.S. degree in electrical engineering from Tampere University of Technology (TUT), Finland, in 2005. Currently, he is a Researcher and a Postgraduate student at the Institute of Communications Engineering at TUT, pursuing towards the doctoral degree. His main research interests are digital signal processing algorithms for multicarrier and frequency domain equalized single-carrier modulation-based wireless communications, especially applications of multirate filter banks.

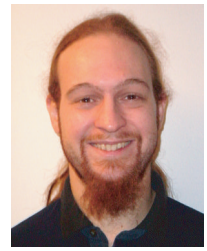

Tobias Hidalgo Stitz was born in 1974 in Eschwege, Germany. He obtained the M.S. degree in telecommunications engineering from the Polytechnic University of Madrid (UPM) in 2001, after writing his Masters Thesis at the Institute of Communications Engineering of the Tampere University of Technology (TUT). From 1999 to 2001, he was Research Assistant at TUT and is now working towards his doctoral degree there. His research interests include wireless communications based on multicarrier systems, especially focusing on filter bank based systems and other filter bank applications for signal processing.

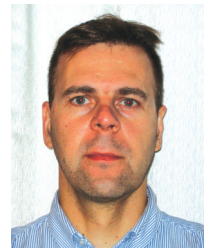

Mika Rinne received his M.S. degree from TUT in signal processing and computer science, in 1989. He acts as Principal Scientist in the Radio Technologies Laboratory of Nokia Research Center. His background is in research of multiple-access methods, radio resource management, and implementation of packet decoders for radio communication systems. Currently, his interests are in research of protocols and algorithms for wireless communications including WCDMA, long-term evolution of 3G and beyond 3G systems.

Markku Renfors was born in Suoniemi, Finland, on January 21, 1953. He received the Diploma Engineer, Licentiate of Technology, and Doctor of Technology degrees from (TUT), Tampere, Finland, in 1978, 1981, and 1982, respectively. From 1976 to 1988, he held various research and teaching positions at TUT. From 1988 to 1991, he was a Design Manager at the Nokia Research Center and Nokia Consumer Electronics, Tampere, Finland, where he focused on video signal processing. Since 1992, he has been a Professor and Head of the Institute of Communications Engineering at TUT. His main research areas are multicarrier systems and signal processing algorithms for flexible radio receivers and transmitters.

Publication P3

T. Hidalgo Stitz, T. Ihalainen, A. Viholainen, and M. Renfors, "Pilot-based synchronization and equalization in filter bank multicarrier communications" in *EURASIP Journal on Advances in Signal Processing*, vol. 2010, Article ID 741429, 18 pages, 2010.

DOI= http://dx.doi.org/10.1155/2010/741429

Hindawi Publishing Corporation
EURASIP Journal on Advances in Signal Processing
Volume 2010, Article ID 741429, 18 pages
doi:10.1155/2010/741429

Research Article

Pilot-Based Synchronization and Equalization in Filter Bank Multicarrier Communications

Tobias Hidalgo Stitz, Tero Ihalainen, Ari Viholainen, and Markku Renfors (EURASIP Member)

Department of Communications Engineering, Tampere University of Technology, P.O. Box 553, 33101 Tampere, Finland

Correspondence should be addressed to Tobias Hidalgo Stitz, tobias.hidalgo@tut.fi

Received 16 June 2009; Revised 21 October 2009; Accepted 30 December 2009

Academic Editor: Pierre Siohan

This paper presents a detailed analysis of synchronization methods based on scattered pilots for filter bank based multicarrier (FBMC) communications, taking into account the interplay of the synchronization, channel estimation, and equalization methods. We show that by applying pilots designed specifically for filter banks, the carrier frequency offset (CFO), fractional time delay (FTD), and channel response can be accurately estimated. Further, a novel joint FTD and channel estimation scheme, based on iterative interference cancelation, permits extending the FTD estimation range well beyond the limit imposed by the pilot separation. The channel parameter estimation and compensation are successfully performed totally in the frequency domain, in a subchannel-wise fashion, which is appealing in spectrally agile and cognitive radio scenarios. The performance evaluation is done in a hypothetical WiMAX scenario in which an FBMC system would substitute OFDM maintaining as much physical layer compatibility as possible.

1. Introduction

Research on increasing data transmission rates and the development of applications exploiting these improved rates, or requiring even more bandwidth, have been fueling each other for decades already, and it seems that this trend will continue. The challenge is therefore to boost high data rates in wireless communications.

Multicarrier (MC) techniques have proven to be a means to adequately overcome many challenges of wide bandwidth transmission while providing also high spectral efficiency. Using MC communications, a frequency selective channel can be divided into several parallel subchannels with flat or mildly selective fading, facilitating channel estimation and equalization (the terms "subchannel", "subband" and "subcarrier" are used interchangeably throughout the whole text, referring to the frequency subband centered at the subcarrier frequency). Timing synchronization is also easier and limited narrowband interference can be easily mitigated. In fact, the division of the whole bandwidth into many subchannels provides scalability and flexibility when configuring the communication link [1].

The flagship of MC techniques is orthogonal frequency division multiplexing (OFDM) with cyclic prefix (CP) [1]. A correctly chosen CP elegantly turns severely frequency selective channels into flat fading ones at subcarrier level, enabling very simple subcarrier-wise equalization (one complex coefficient per subcarrier). OFDM has become the MC technique of choice in a number of communication systems, including emerging cellular standards such as WiMAX [2] (based on the IEEE 802.16e [3] standard) and E-UTRA LTE (Evolved UMTS Terrestrial Radio Access Long Term Evolution) [4]. These two exploit the flexibility of OFDM to also provide multiple access in time and frequency through orthogonal frequency division multiple access(OFDMA).

Filter bank based multicarrier (FBMC) modulation can be considered an evolved OFDM due to the advantages it presents and also because it can easily be implemented

building on the core blocks of OFDM, that is, the IFFT/FFT pair [5]. The filter banks (FBs) display the following two highly desirable properties. Firstly, their subchannels can be optimally designed in the frequency domain to have desired spectral containment [6]. Secondly, FBMC systems do not make use of the CP, which is pure redundancy, enabling a more efficient use of channel resources. Basically, the subchannel filters are designed with the Nyquist pulse shaping principle, which means that the consecutive symbol waveforms are overlapping in time. Compared to OFDM, where the adjacent subbands are only attenuated 13 dB, the excellent spectral containment allowed by the FBs is crucial for avoiding distortion from asynchronous signals in adjacent bands. Further savings in spectral resources appear at the edges of the transmission band, where ideally only one subchannel can be used as guard band to the next transmission band. An OFDM system with slowly decaying sidelobes would need more subbands or very sharp additional filtering to provide similar attenuation outside the transmission band. In the context of cognitive radio [7, 8], where a secondary user scans the spectrum assigned to primary users for a transmission opportunity (spectral sensing), the high spectral definition of FBMC is especially valuable. The performance of Haykin's method of choice for radio scene analysis, the multitaper method [9], can be well approximated using FBs with greatly reduced complexity [10].

In order to synchronize and equalize the channel, there are methods to perform timing, frequency offset and channel estimation. In the MC context, timing estimation involves locating the start of a transmission burst, finding the first multicarrier symbol, and estimating the fractional time delay (FTD), which is a fraction of the multicarrier symbol period. Since OFDM is the most widespread MC technique, many methods for synchronization and channel estimation can be found for it. They are based on scattered pilots and training sequences [11, 12], on exploiting the redundancy of the CP [13] or even blind methods that do not make use of overheads in the signal [12].

Due to the different nature of the FB waveforms, some of the OFDM methods can be applied to FBMC and others, such as the CP-based ones, cannot. Although there exist preamble based [14], training sequence based [15] and blind [16] approaches, we focus our interest here towards scattered-pilot-based approaches. However, when using efficient filter bank implementations, as for example the FBMC/OQAM (offset quadrature amplitude modulation) [5], the application of scattered pilots is not as straightforward as in OFDM due to the complementary interference that a low-rate symbol suffers from adjacent symbols in time and frequency. This has motivated different proposals for generating pilots [17, 18] compatible with the filter bank class of interest. In this paper, we build our synchronization and channel estimation subsystem based on pilots and auxiliary pilots [19] similarly to [18] because of good estimation performance.

Here it is interesting to mention that the authors of [20] also present an approach to perform full synchronization in both FBMC/OQAM and OFDM/QAM systems based on scattered pilots. However, in that publication the time domain properties of the regularly scattered pilots are exploited and synchronization takes place in the time domain instead of subcarrier-wise, as is our goal in this paper. Both approaches complement each other and could be used together, for example, for performing coarse acquisition and fine tuning or to improve their respective performances.

In order to obtain results of practical relevance, we develop a testbed system that aims to maintain a certain resemblance and even compatibility up to a degree with the WiMAX profile. Also the channel model and distortion parameters are chosen to be typical of WiMAX communications. We use rather basic synchronization parameter estimation, and compensation methods, many of which are known from the literature in the OFDM context, and adapt them to the FBMC/OQAM system model. Our focus is on understanding the interplay of different synchronization and channel equalization functions. We also explore the possibilities to enhance the overall performance by iterating the estimation and compensation tasks. It is important to underline, that all the necessary synchronization, channel estimation and equalization operations take place after the analysis bank at the receiver, at the low sampling rate. This makes it possible to utilize the filter bank itself for efficient implementation of the needed frequency channelization selectivity for all signal processing functions. Further, the channelization can be done in a dynamically adjustable manner, efficiently suppressing immediately adjacent and even (narrow) in-band interference components.

The paper is structured as follows: first, we review the concept of efficient filter bank based multicarrier communications. In Section 2, we describe how to implement the filter banks and perform efficient subchannel-wise equalization. In Section 3, we first discuss the synchronization requirements in spectrally agile radios. Then we present the method for obtaining pilots for FBMC/OQAM and study the effect of the channel distortions on these pilots. In the end of this section, we present solutions for correcting the distortions, including a novel, iterative interference canceling, joint FTD, and channel estimating algorithm. In Section 4, we introduce the design of the WiMAX-like simulation testbed based on FBMC. Section 5 presents the estimation and correction performance of the studied methods. Finally, Section 6 draws the conclusions from this research.

2. FBMC and Efficient Subchannel-Wise Equalization

2.1. Filter Bank Based Multicarrier Communications. Exponentially modulated filter banks (EMFB) [21], modified DFT (MDFT) filter banks [22], and OFDM with offset QAM (OFDM/OQAM or FBMC/OQAM) [5], among others, are complex filter bank structures that can produce complex I/Q baseband signals for transmission, making them suitable for FBMC systems in spectrally efficient radio communications. In FBMC communications, the filter banks are used in the transmultiplexer (TMUX) configuration [23], with the synthesis filter bank (SFB) in the transmitter and the analysis filter bank (AFB) in the receiver. Figure 1 shows the filter banks in this configuration as fundamental part

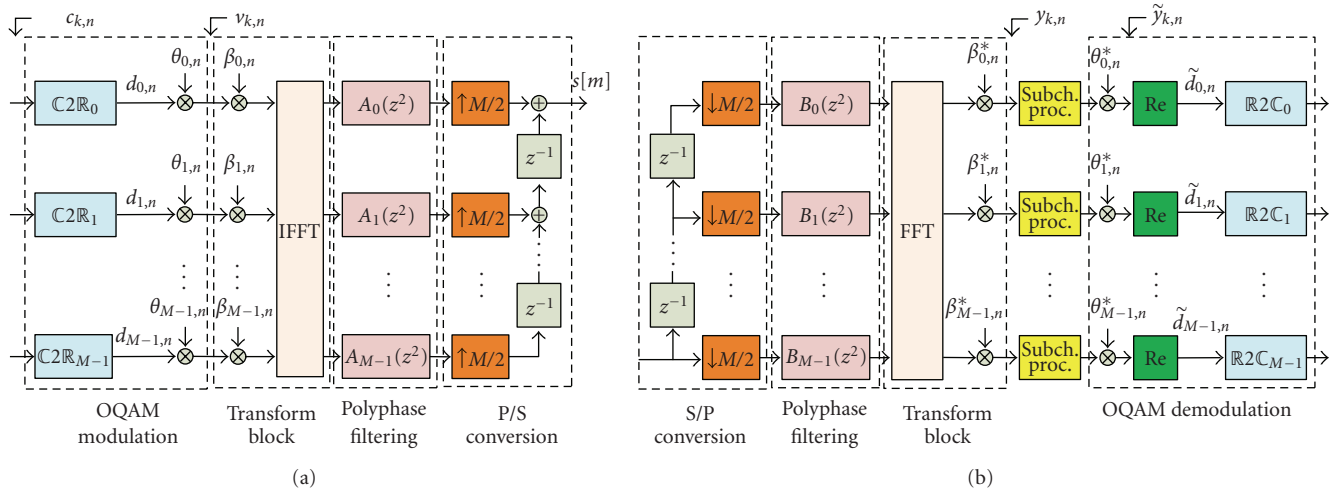

Figure 1: (a) Synthesis and (b) analysis filter banks for complex FBMC transmultiplexer (TMUX) with per-subchannel processing.

of a complete FBMC/OQAM transmission/reception system. This FB technique builds on uniform modulated filter banks [23], in which a prototype filter $p[m]$ of length L_p is shifted in frequency to generate subbands which cover the whole system bandwidth. The output of such a synthesis filter bank can be expressed by

$$s[m] = \sum_{k=0}^{M-1} \sum_{n=-\infty}^{\infty} d_{k,n}\theta_{k,n} p\left[m - \frac{nM}{2}\right] e^{j(2\pi/M)k(m-n(M/2)-((L_p-1)/2))}, \quad (1)$$

where

$$\theta_{k,n} = e^{j(\pi/2)(k+n)} = j^{k+n}, \quad (2)$$

m is the sample index at the output of the SFB (at high rate), M is the number of subchannels in the filter bank, and $d_{k,n}$ are the real-valued data symbols in subchannel k, transmitted at a rate $2/T$. The signaling interval is defined as $T = 1/\Delta f$, where Δf is the subcarrier spacing. The pair of symbols $d_{k,n}$ and $d_{k,n+1}$ can be interpreted as carrying the in-phase and quadrature information of a complex-valued symbol transmitted at rate $1/T$. Therefore, the filter bank presented in Figure 1 is critically sampled. The "$\mathbb{C}2\mathbb{R}_k$"-blocks indicate the conversion into real-valued data from the real and imaginary parts of the complex-valued input symbols $c_{k,n}$ and can be considered as introducing upsampling by 2. "$\mathbb{R}2\mathbb{C}_k$" carries out the inverse operation after the AFB in the receiver, effectively downsampling the signal by 2. In FBMC/OQAM, $c_{k,n}$ belongs to a QAM alphabet and the real and imaginary parts are interleaved with a relative time offset of $T/2$ (hence *offset* QAM) and $\mathbb{C}2\mathbb{R}_k$ performs the following mapping:

$$d_{k,2n} = \begin{cases} \mathrm{Re}[c_{k,n}], & k \text{ even} \\ \mathrm{Im}[c_{k,n}], & k \text{ odd}, \end{cases} \quad (3)$$

$$d_{k,2n+1} = \begin{cases} \mathrm{Im}[c_{k,n}], & k \text{ even} \\ \mathrm{Re}[c_{k,n}], & k \text{ odd}. \end{cases} \quad (4)$$

Note that the signs of the sequences in (2)–(4) could be chosen arbitrarily, but the pattern of real and imaginary symbols after multiplication by $\theta_{k,n}$ has to follow the above definitions to maintain orthogonality [5].

This type of filter bank pairs can be efficiently implemented using FFT and IFFT of size M aided by polyphase filtering structures. The different parts of the polyphase SFB structure of Figure 1(a) can be better identified by noting that $a_k[m] = p[m + kM]$ and rewriting (1) as

$$s[m] = \sum_{k=0}^{M-1} \sum_{n=-\infty}^{\infty} d_{k,n}\theta_{k,n}\beta_{k,n} p\left[m - \frac{nM}{2}\right] e^{j(2\pi/M)km}, \quad (5)$$

where

$$\beta_{k,n} = (-1)^{kn} \cdot e^{-j(2\pi k/M)((L_p-1)/2)}. \quad (6)$$

Here, the factor $(-1)^{kn}$ centers the low-rate output signal of each subchannel k of the analysis filter bank around DC.

The synthesis and analysis banks in Figure 1, between the OQAM modulation and the subchannel processing parts, respectively, can also be understood from the classical FB presentation: each subchannel k with its own up/downsampling and subchannel filters. The synthesis/analysis subchannel

filters are, respectively, obtained from the prototype filter $p[m]$ as

$$g_k[m] = p[m]e^{j(2\pi/M)k(m-(L_p-1)/2)},$$
$$f_k[m] = g_k^*\Big[L_p - 1 - m\Big], \tag{7}$$

where $m = 0, 1, \ldots, L_p - 1$ and $(\cdot)^*$ indicates complex conjugation.

Further, the length L_p of the prototype filter $p[m]$ depends on the size of the filter bank and the integer overlapping factor K as $L_p = KM$, where the factor K indicates the number of FBMC/OQAM symbol waveforms that overlap in time. In [24], other lengths of the prototype filter, close to $L_p = KM$, are explored. High values for K allow more freedom in designing the prototype filter, for example to achieve very high stopband attenuation. On the other hand, it increases the time required for processing each symbol. The prototype filter $p[m]$ can be designed in such a way that the filter bank pair yields perfect reconstruction (PR) of the transmitted data in case of an ideal channel, that is, the received data sequence $\widetilde{d}_{k,n}$ equals the transmitted data $d_{k,n}$ (except for the FB processing delay), if there is no additional processing involved. Methods to design PR prototype filters can be found in [25]. However, in practical communication systems, the channel will always introduce some distortion to the signal. Therefore, the design constraints can be somewhat relaxed and the prototype can be optimized to achieve nearly PR (NPR). The trade-off, when comparing with PR designs, is that for prototype filters of the same length, NPR designs can achieve higher stopband attenuations, or with fixed stopband attenuations, the NPR prototype filter can be shorter. This happens at the cost of allowing some marginal intersymbol (ISI) and intercarrier (ICI) interference from the filter bank, well under the noise level of the communication channel.

The NPR prototype can be designed using, among others, window-based techniques [26] or the frequency sampling approach [27, 28]. In the studies described here, the prototype is obtained using the latter method, in which the filter impulse response is obtained by the inverse Fourier transform of the desired frequency response at certain frequency locations. The design of such an NPR prototype filter under different optimization criteria has been addressed in [24].

2.2. Subchannel-Wise Equalization in FBMC. In OFDM, as long as the channel delay spread and the possible synchronization errors remain within the cyclic prefix time, equalization can simply be done with a complex coefficient multiplication at subcarrier level. This approach is also applicable to FBMC, if the ratio of channel delay spread in samples and number of subchannels is sufficiently low, since the frequency variation within a subchannel is then small enough that it can be considered flat fading. But as this is not the general case, more effective channel equalization methods have been developed for FBMC. The single complex coefficient is usually considered when the FB waveforms are well localized in time and frequency domains to limit the effect on consecutive symbols and neighboring subchannels [5, 29, 30]. Longer finite impulse response (FIR) filters as subcarrier equalizers with cross-connections between the adjacent subchannels to cancel the ICI are studied in [31, 32]. To avoid the cross-connections between subchannels, an oversampled receiver filter bank structure with per-subcarrier FIR equalizers can restore the orthogonality of the subcarrier waveforms. This approach is followed in [33–37] and more recently with MMSE equalizers explicitly for FBMC/OQAM in [38].

The authors of this paper have worked on a low-complexity, subcarrier-wise FBMC equalizer using oversampled subcarrier signals [39, 40]. The equalizers were considered earlier for the exponential modulation type of filter banks, which are basically a generalization of the sine and cosine modulated filter banks to complex-valued signals. Nevertheless, these equalizers can readily be applied to FBMC/OQAM receivers by noting that now the filter bank is even stacked, as compared to the odd stacking of the EMFB-based system. We base the equalization in the current study on this approach because it yields good equalization performance with practical channels and subcarrier spacings of up to 100 kHz, which is more than enough for the WiMAX-like system under consideration.

The working principle is based on frequency sampling: assuming a roll-off factor of the prototype filter $\alpha = 1$ or smaller, each subchannel overlaps only with the immediately neighboring subchannels. At the oversampled part of the receiver bank, before taking the real part of the subcarrier signals, the equalizer can perform equalization at a number of frequency points according to its complexity. For example, if the equalizer is a 3-tap complex FIR filter, 3 frequency points within the subchannel can be completely equalized, according to the zero-forcing (ZF) or the mean squared error (MSE) criterion. With the filter bank structure in Figure 1, all the subchannels alias to frequencies centered around DC, and a straightforward choice is to equalize at DC and at $\pm\pi/2$, that is, the center of the subchannel and the passband edge frequencies, respectively. Also other frequencies can be used, as well as longer filters, but the described solution is the computationally least demanding.

In the 3-tap complex FIR equalizer of subchannel k at time n with (noncausal) transfer function

$$W_{k,n}(z) = w_{k,n}^{(-1)}z + w_{k,n}^{(0)} + w_{k,n}^{(1)}z^{-1}, \tag{8}$$

the filter coefficients $w_{k,n}^{(d)}$, with $d = -1, 0, 1$, can be tuned in a way that the filter achieves at the mentioned frequency points the following target values:

$$\chi_{k,n}^{(i)} = \gamma\frac{\left(H_{k,n}^{(i)}\right)^*}{\left|H_{k,n}^{(i)}\right|^2 + \xi}. \tag{9}$$

Here, $i \in \{0, 1, 2\}$, where $i = 0$ corresponds to the lower subband edge, $i = 1$ to the subband center, and $i = 2$ to the upper subband edge frequency. $H_{k,n}^{(i)}$ is the channel frequency response in subchannel k and time n at frequency position given by i, and γ and ξ are scaling factors. If the equalizer

applies the ZF criterion, $\xi = 0$ and $\gamma = 1$. In the MSE case, ξ is the noise-to-signal power ratio and the choice of

$$\gamma = \frac{3}{\sum_{i=0}^{2}\left(\left|H_{k,n}^{(i)}\right|^2 / \left(\left|H_{k,n}^{(i)}\right|^2 + \xi\right)\right)} \tag{10}$$

removes the bias of the MSE solution.

Taking into account these assumptions, the equalizer coefficients can readily be derived from the target values in (9) above as [39]

$$\begin{aligned} w_{k,n}^{(-1)} &= \frac{-\chi_{k,n}^{(0)}(1-j) + 2\chi_{k,n}^{(1)} - \chi_{k,n}^{(2)}(1+j)}{4}, \\ w_{k,n}^{(0)} &= \frac{\chi_{k,n}^{(0)} + \chi_{k,n}^{(2)}}{2}, \\ w_{k,n}^{(1)} &= \frac{-\chi_{k,n}^{(0)}(1+j) + 2\chi_{k,n}^{(1)} - \chi_{k,n}^{(2)}(1-j)}{4}. \end{aligned} \tag{11}$$

Furthermore, it is worth mentioning here that this equalizer can perform also limited FTD and CFO correction in addition to channel equalization, as will be discussed in the next section.

3. Pilot-Based Synchronization in FBMC

3.1. Synchronization in Spectrally Agile Radios. Traditional wireless communication systems are characterized by dedicated frequency bands and well-defined frequency channels. After analog and digital receiver front-ends, the signal contains only the transmissions allocated to that channel, which have well-controlled dynamics under the radio resource management functionalities of the wireless network.

The scarcity of frequency spectrum which can be used in wireless communications is a significant factor that has given raise to the concepts of flexible dynamic spectrum use and cognitive radio. In this context, the used frequency band is not anymore dedicated to a specific service and specific waveforms. The band cannot be expected anymore to be free of other waveforms, the utilized frequency spectrum may be noncontiguous, and the dynamics of signal power levels are not well-controlled anymore. This calls for efficient means to dynamically separate the used portions of the frequency spectrum from other portions that are considered interference. Filter banks are ideal for this purpose. It should be noted that in OFDM, the plain FFT processing does not provide effective filtering to signal elements that are not synchronized to the CP structure, and the frequency channelization selectivity has to be implemented in the analog and digital front-end.

As for the synchronization functionalities in case of spectrally agile radios, it is clear that synchronization parameter estimation cannot be implemented in time domain before major part of the selectivity is implemented and strong interferers are suppressed. As the filter bank itself can be used effectively for implementing the selectivity, the feasibility of time domain synchronization becomes questionable. Therefore, in the context of cognitive radio, there is a strong motivation to develop synchronization methods which are operating in frequency domain, utilizing the subchannel signals only. However, for compensation of coarse synchronization errors, time domain methods are still favorable. In the following discussion, it is assumed that coarse timing and frequency offsets have been compensated in time domain. The required accuracy of coarse CFO and FTD estimates is an outcome of this study.

The primary use of these methods is for channel tracking. In normal tracking mode, with continuous flow of data packets, only small CFO and FTD values are expected, and it is enough to use only the estimation algorithms in conjunction with basic time domain compensation methods and some filtering to reduce the random variations of block-wise estimates. However, in advanced packet-based radio interfaces, there can be long gaps in the packet flow, especially when the terminal is in idle mode. This may result in significant drift of the CFO and FTD values, and it is advantageous to be able to compensate significant synchronization errors right away for the first received data packet.

For initial synchronization, the developed scheme could be a part of a search procedure, where different coarse CFO and FTD values are tested until synchronization can be established.

3.2. Signal Models. In order to perform channel equalization and synchronization with the presented equalizer, it has to be fed with channel estimates that provide information about the channel state and the possible synchronization errors. In this paper, we study only the effect of a linear multipath channel with additive white Gaussian noise (AWGN), fractional time delay, and carrier frequency offset. In this scenario, the baseband signal model at the receiver input can be expressed as

$$r(t) = (s(t) \star h(t,\tau) \star \delta(t - \tau_{\mathrm{FTD}}T))e^{j2\pi(\varepsilon/T)t} + \eta(t), \tag{12}$$

where $\star$ represents the convolution operation, $s(t)$ is the continuous time version of (1) (or (5)), $h(t,\tau)$ is the time-varying transmission channel, and δ is the Dirac delta. Moreover, τ_{FTD} is the fractional time delay as a fraction of the signalling interval T, ε is the CFO as a fraction of the subcarrier spacing Δf, and $\eta(t)$ is complex valued AWGN. At the receiver, $r(t)$ is sampled at $T_s = T/M$ into $r[m]$ and then passes the analysis bank. Before the subchannel processing stage (estimation and synchronization/equalization in our case), the kth subchannel sequence $y_{k,n}$ can be expressed as

$$y_{k,n} = \left[r[m] \star f_k[m]\right]_{\downarrow M/2} = \sum_{i=0}^{M-1} v_{i,n} \star q_{i,k,n} + \eta_{k,n}, \tag{13}$$

where

$$q_{i,k,n} = \left[\left(\left(g_i[m] \star h[n,m] \star \delta\left[m - \tau_{\mathrm{FTD}}\frac{T}{T_s}\right]\right)e^{j2\pi(\varepsilon/M)m}\right) \star f_k[m]\right]_{\downarrow M/2}. \tag{14}$$

Table 1: Interference weights for data surrounding the symbol in the center of the table

	$n=-4$	$n=-3$	$n=-2$	$n=-1$	$n=0$	$n=1$	$n=2$	$n=3$	$n=4$
$k=-2$	0	0.0006	−0.0001	0	0	0	−0.0001	0.0006	0
$k=-1$	0.0054	j0.0429	−0.1250	−j0.2058	0.2393	j0.2058	−0.1250	−j0.0429	0.0054
$k=0$	0	−0.0668	0.0002	0.5644	1	0.5644	0.0002	−0.0668	0
$k=1$	0.0054	−j0.0429	−0.1250	j0.2058	0.2393	−j0.2058	−0.1250	j0.0429	0.0054
$k=2$	0	0.0006	−0.0001	0	0	0	−0.0001	0.0006	0

Above, $q_{i,k,n}$ is the subchannel-dependent 2-dimensional impulse response, including the channel effects, from subchannel i to subchannel k, and (see Figure 1)

$$v_{i,n} = \theta_{i,n} d_{i,n}. \tag{15}$$

The discrete-time time varying channel is $h[n,m]$, the delay $\tau_{\mathrm{FTD}}(T/T_s) = \tau_{\mathrm{FTD}} M$ is assumed in this paper to be an integer number of samples, for simplicity, and $\downarrow M/2$ represents the downsampling by $M/2$ of the preceding expression. The sampled and filtered noise is $\eta_{k,n}$.

In an FB system with a sufficiently frequency selective prototype filter and roll-off $\alpha \leq 1$, only adjacent subchannels overlap and have an effect on subchannel k of interest. This implies that the sum in (13), which is basically a 2-dimensional convolution, can be limited to run from $i = k-1$ to $i = k+1$:

$$y_{k,n} = \sum_{i=k-1}^{k+1} v_{i,n} \star q_{i,k,n} + \eta_{k,n}. \tag{16}$$

This also assumes a reasonably small frequency offset ε, in which case the overlaps with subchannels $i = k \pm 2$ remain limited.

3.3. Pilots for FBMC. In a multicarrier system with sufficient number of subcarriers, it is just intuitive to obtain information about a doubly selective (in frequency and time) transmission channel by sampling it in frequency and time directions at certain intervals. The samples are obtained by known data symbols (pilots) that are transmitted at given time and frequency locations and from which the channel information at these locations is recovered. This information is extended to cover the whole signal domain by interpolating between the pilots. In OFDM the application and exploitation of the pilots is straightforward: the channel state in subchannel k at time instant n is just the received symbol divided by the transmitted symbol (this implies ignoring the additive noise). In efficient modulated filter banks it is not that simple, as a closer look into (14) reveals. Indeed, if we first remove all the channel effects in that equation, that is, $\tau_{\mathrm{FTD}} = 0$, $\varepsilon = 0$, and $h[n,m] = \delta[n]$, $q_{i,k,n}$ becomes the time- and frequency invariant 2-dimensional impulse response of the TMUX, relating $v_{i,n}$ with $y_{k,n}$ (or equivalently $d_{i,n}$ with the received kth subchannel signal before the operation of taking its real part, $\widetilde{y}_{k,n}$). In this case, (16) can be expressed as

$$\begin{aligned} y_{k,n} &= \sum_{i=k-1}^{k+1} \sum_{l=-\infty}^{\infty} v_{i,l} q_{i,k,n-l} + \eta_{k,n} \\ &= v_{k,n} + \sum_{i=k-1}^{k+1} \sum_{\substack{l=-\infty \\ (i,l)\neq(k,n)}}^{\infty} v_{i,l} q_{i,k,n-l} + \eta_{k,n}. \end{aligned} \tag{17}$$

Equivalently, we can write

$$\begin{aligned} \widetilde{y}_{k,n} &= \theta^*_{k,n} y_{k,n} \\ &= \theta^*_{k,n} v_{k,n} + \theta^*_{k,n} \sum_{i=k-1}^{k+1} \sum_{\substack{l=-\infty \\ (i,l)\neq(k,n)}}^{\infty} v_{i,l} q_{i,k,n-l} + \theta^*_{k,n} \eta_{k,n} \\ &= d_{k,n} + \sum_{i=k-1}^{k+1} \sum_{\substack{l=-\infty \\ (i,l)\neq(k,n)}}^{\infty} j^{i-k} d_{i,l} q_{i,k,n-l} + \theta^*_{k,n} \eta_{k,n} \end{aligned} \tag{18}$$

$$= d_{k,n} + \left(\eta^{\mathrm{NPR}}_{k,n} + j u_{k,n}\right) + \theta^*_{k,n} \eta_{k,n}. \tag{19}$$

The elements $\eta^{\mathrm{NPR}}_{k,n}$ and $u_{k,n}$ within the parentheses of (19) are obtained by, respectively, taking the real and imaginary part of the summation term in (18). They can be considered interference on the desired symbol $d_{k,n}$. Now, even in a PR TMUX, in which the real-valued term $\eta^{\mathrm{NPR}}_{k,n} = 0$, the imaginary-valued interference $j u_{k,n}$ does not add up to 0. The orthogonality is only obtained after taking the real part, that is, this interference summation has only imaginary values [5]. In an NPR design, $\eta^{\mathrm{NPR}}_{k,n}$ is a small real-valued contribution, generally well below the level of $\eta_{k,n}$, and will be ignored from now on. Another property of the imaginary-valued interference $j u_{k,n}$ is that it is time-varying, since it depends on the data in the adjacent channels and on the symbols preceding and following $d_{k,n}$.

For simplicity of notation, we define the noncausal TMUX response at subchannel k and instant n as $t_{k,n}$. It is assumed that it is normalized at $k = 0$ and $n = 0$ as $t_{0,0} = 1$. Table 1 presents the interference weights that multiply neighboring symbols in the case of an NPR prototype designed with the frequency sampling method in [28] and with an overlapping factor $K = 4$. Thus, we obtain at the location (k_0, n_0) of interest

$$\widetilde{y}_{k_0,n_0} = \theta^*_{k_0,n_0} y_{k_0,n_0} = d_{k_0,n_0} + j u_{k_0,n_0} + \eta_{k_0,n_0}, \tag{20}$$

where the imaginary interference is

$$u_{k_0,n_0} = \sum_{(k,n)\in\Omega_{k_0,n_0}} d_{k,n}\hat{t}_{k_0-k,n_0-n}, \tag{21}$$

with

$$\hat{t}_{k,n} = \mathrm{Im}\left[\theta^*_{k,n} t_{k,n}\right] \tag{22}$$

and Ω_{k_0,n_0} is the set of subcarrier and time indices that are considered to contribute to the interference on the symbol at (k_0, n_0). Without channel distortions, t and q are related as $q_{i,k,n} = t_{k-i,n}$.

Table 1 shows that the interference from subchannels not adjacent to the subchannel of interest have negligible effect and that in time direction the interference goes K symbols from the symbol of interest in both directions. With this design, the residual distortion on the real part is less than −65 dB compared to the actual data.

It is clear that a pilot located at subcarrier k_p and time n_p cannot be immediately recovered even if the channel at that subcarrier is a simple complex coefficient H_{k_p,n_p} (flat fading), because the pilot information and the complex-valued, time-varying, and data-dependent interference will be mixed by the channel. In the following paragraphs we describe the method we use to handle the described complex-valued interference in order to make pilot-based channel sampling feasible and briefly point out several alternative approaches. The interested reader is referred to the cited references for detailed description of the methods. We first consider a channel with neither FTD nor CFO.

3.3.1. Auxiliary Pilots. This approach is based on an elegant idea presented in [18] utilizing an auxiliary pilot located at k_a, n_a adjacently to the pilot k_p, n_p and which cancels the interference u_{k_p,n_p} of (21). The advantage of eliminating the interference is that the pilots can be used at the receiver in a similar fashion as OFDM pilots are used; the estimate of the channel at the pilot location is

$$\hat{H}_{k_p,n_p} = \frac{\theta^*_{k_p,n_p} y_{k_p,n_p}}{d_{k_p,n_p}}, \tag{23}$$

assuming that the channel is constant over the whole subchannel bandwidth. The auxiliary pilot is indeed one element of the sum (21) and has to be calculated on-line with data transmission every time a pilot is inserted since the interference terms vary with the data. In [18], the auxiliary pilot is chosen to cancel the interference from the 8 surrounding symbols. This is a good approximation in well time-frequency localized prototype filters, such as the ones based on the isotropic orthogonal transform algorithm (IOTA) function [29]. Here we chose to include more terms in the calculation of the interference because also symbols located further away can add significant interference. The auxiliary pilot that cancels the imaginary interference can be calculated as

$$d_{k_a,n_a} = -\frac{1}{\hat{t}_{k_p-k_a,n_p-n_a}} \sum_{\substack{(k,n)\in\Omega_{k_p,n_p} \\ (k,n)\neq(k_p,n_p) \\ (k,n)\neq(k_a,n_a)}} d_{k,n}\hat{t}_{k_p-k,n_p-n}. \tag{24}$$

In typical filter bank designs it is wise to locate the auxiliary pilot immediately preceding or following the pilot, that is, $n_a = n_p - 1$ or $n_a = n_p + 1$. This way, the absolute value of the denominator $\hat{t}_{k_p-k_a,n_p-n_a}$ is maximized (see Table 1) and the magnitude of the auxiliary pilot is minimized on the average, wasting less transmission energy on the pilot/auxiliary pilot pair and preventing possible strong effects on the peak-to-average-power ratio (PAPR) due to excessively strong auxiliary pilots. As an example, with the prototype filter presented above, it is sensible to use the shaded area of Table 1 for the computation of the interference and the auxiliary pilot. This leaves the residual imaginary interference below −38 dB level with respect to the data. Further, if the auxiliary pilot is chosen to precede or succeed the pilot, then the auxiliary pilot power is on the average 3.3 dB stronger than the data surrounding the pilot/auxiliary pilot pair. Note that the use of two real-valued symbols as pilots does not mean a penalty in overhead with respect to OFDM, since there the pilot is complex-valued.

3.3.2. Alternative Pilot Techniques for Channel Estimation. The pair of real pilots (POP) [17] method also uses two consecutive OQAM subsymbols to send known pilots, in the simplest case, similar pilots. Ignoring the noise and assuming that the channel remains unchanged during both subsymbols, an equation system yields the equalizer coefficient (the same for both pilots) that restores the pilots to their original phase. Its inverse is the estimate for the channel at the positions of the POP. This method places the computational complexity on the receiver part and has the advantage that it is independent from the prototype filter design, since the interference term is not used explicitly in the equations. However, if the noise is not negligible, it will be enhanced in a random fashion, depending on the data surrounding the pilots, which makes the performance unpredictable and generally worse.

The authors of [17] present also the interference approximation method (IAM). The philosophy here is that most of the symbols surrounding the pilot in time and frequency are fixed and known at the receiver. In this case, the interference u_{k_p,n_p} can be approximatively calculated with (21), which leads to the estimate $\hat{H}_{k_p,n_p} = \theta^*_{k_p,n_p} y_{k_p,n_p}/(d_{k_p,n_p} + j u_{k_p,n_p})$. The more symbols in the shaded area of Table 1 are fixed, the better is the approximation of u_{k_p,n_p}. Unfortunately, this approach leads to an unacceptable overhead if a good approximation of the interference, necessary for accurate channel estimates, is desired. Therefore, it is practical only in situations in which pilots are packed closely together, for example, in preambles, where the fixed symbols can be simultaneously utilized by nearby located pilots.

More sophisticated methods for scattered-pilot-based channel estimation in FBMC/OQAM are presented in [41]. By means of an orthonormal transformation of the data around the pilot, the imaginary-valued term can be nulled while avoiding the need of an auxiliary pilot with increased power. Nevertheless, it is still necessary to fix one of the surrounding symbols, which cannot be used for data transmission. Another approach in [41, 42] consists of iteratively

approximating u_{k_p,n_p} at the receiver with help of the demodulated data. At first, it is considered that $u_{k_p,n_p} = 0$, and the channel is estimated based on this assumption. The equalization and detection then yield estimates of the data surrounding the pilot, which, in turn, permit calculating a better estimate of u_{k_p,n_p}. This technique converges in 3-4 iterations.

The methods presented above provide a way of sampling the time-varying frequency response of the transmission channel. The estimates required at the remaining subchannels and time-instants can be obtained by interpolating between the estimates obtained at the pilot locations. Note that for the 3-tap subcarrier equalizer presented in Section 2.2, the interpolation has to return estimates not only at the center frequencies of the subcarriers, but also at the subband edges in the middle of those frequencies. Studying how improved interpolation techniques [12] affect the FBMC channel estimation performance is an interesting research subject but goes beyond the scope of this paper.

3.4. Timing Estimation and Correction. Assuming that the coarse location of a transmission frame is obtained by other means, the effect of not synchronizing exactly with the MC symbols, hence introducing a fractional time delay, can be understood with help of (14). In the frequency domain we can write

$$\begin{aligned} &Q_{i,k}\left(e^{j\omega}\right) \\ &= \left[\left(\left(G_i\left(e^{j\omega}\right)H_n\left(e^{j\omega}\right)e^{-j\omega\tau_{\mathrm{FTD}}M}\right)\star\,\delta(\omega-2\pi\varepsilon)\right)F_k\left(e^{j\omega}\right)\right]_{\downarrow M/2} \\ &= \left[\left(G_i\left(e^{j(\omega-2\pi\varepsilon)}\right)H_n\left(e^{j(\omega-2\pi\varepsilon)}\right)e^{-j(\omega-2\pi\varepsilon)\tau_{\mathrm{FTD}}M}\right)F_k\left(e^{j\omega}\right)\right]_{\downarrow M/2} \\ &= \left[G_i\left(e^{j(\omega-2\pi\varepsilon)}\right)H_n\left(e^{j(\omega-2\pi\varepsilon)}\right)F_k\left(e^{j\omega}\right)e^{-j(\omega-2\pi\varepsilon)\tau_{\mathrm{FTD}}M}\right]_{\downarrow M/2}, \end{aligned} \tag{25}$$

which shows that FTD introduces a phase term that linearly varies with the frequency. This frequency-dependent phase term destroys the orthogonality of the subchannels and causes the appearance of ICI.

For estimation purposes, let us first assume that there is neither channel distortion nor CFO present. In this case, (16) can be approximated as

$$y_{k,n} \simeq e^{-j2\pi k\tau_{\mathrm{FTD}}} \sum_{i=k-1}^{k+1} \nu_{i,n} \star t_{i-k,n} e^{j2\pi\tau_{\mathrm{FTD}}((k-i)/2)} + \eta_{k,n}, \tag{26}$$

where the term $e^{\pm j2\pi\tau_{\mathrm{FTD}}(1/2)}$ at $i = k-1$ and $i = k+1$, respectively, causes the interference $u_{k,n}$ not to be purely imaginary anymore (after compensation of the common phase rotation $e^{-j2\pi k\tau_{\mathrm{FTD}}}$ and multiplication by $\theta^*_{k,n}$), hence causing ICI. However, from (26) it seems straightforward to estimate the FTD from a transmitted pilot at k_p, n_p, allowing for some uncertainty caused by the ICI. In practice, the estimate is obtained from the phase difference between two pilots separated by Δk subcarriers, since the signal can have a constant random phase rotation that is eliminated when calculating the phase difference. Thus,

$$\begin{aligned} \hat{\tau}_{\mathrm{FTD}} &= \frac{\angle\left(\widetilde{y}_{k_p,n_p}\right) - \angle\left(\widetilde{y}_{k_p+\Delta k,n_p}\right)}{2\pi\Delta k} \\ &= \frac{\angle\left(y_{k_p,n_p}\right) - \angle\left(y_{k_p+\Delta k,n_p}\right) + \Delta k(\pi/2)}{2\pi\Delta k}, \end{aligned} \tag{27}$$

where $\angle(\cdot)$ is the phase of $(\cdot)$ and $\Delta k(\pi/2)$ comes from the $\theta_{k,n}$ that relate $\widetilde{y}_{k,n}$ and $y_{k,n}$. This result limits the carrier separation for the pilots, if unambiguous phase differences are to be calculated. The phase difference remains below π if $\tau_{\mathrm{FTD}}\Delta k < 1/2$. For example, if pilot subcarriers are separated by $\Delta k = 10$, only a delay of $\pm\lfloor M/20\rfloor$ samples ($\lfloor\cdot\rfloor$ rounds to the closest smaller integer) can be estimated without phase ambiguity.

The estimate can be improved by averaging techniques such as least squares linear curve fitting over all pilot pairs that are sufficiently closely placed within a frame. In case of CFO, consecutive symbols within a subcarrier are rotated with respect to each other, as will soon be discussed, forcing the averaging to be independently done over the subchannels for every MC symbol time. The CFO additionally increases the additive distortion. Finally, in presence of the transmission channel, the (flat-fading) channel coefficient within the subchannel of interest also multiplies the transmitted signal, introducing additional rotation. Since in general this rotation is different at different subcarriers, it would be expected that this method cannot be used anymore with practical transmission channels. Nevertheless, if the effect of the FTD on the phase is predominant, the phase difference introduced by the channel coefficients will add up as noise at the end. Consequently, we can consider $\angle(H_{k_p+\Delta k,n_p}) = \angle(H_{k_p,n_p}) + 2\pi\Delta k\tau_{\mathrm{FTD}} + \eta_\varphi$, where η_φ is an additive phase term, which depends on how much the channel is correlated in frequency direction at the pilot distance. Again, averaging over a sufficient number of pilots reduces the harmful effect of this additional phase term. In general, the FTD estimation can be seen as a problem of phase slope estimation over the active subcarriers.

To compensate for the FTD, an equalizer can be designed to reverse the effect of the frequency-varying phase. The 3-tap complex FIR equalizer presented in Section 2.2 is well suited for performing this task simply by including the FTD effect on the phase of the channel estimates at the subband edges. When computing these estimates for all subcarriers and time instants, the correct interpolation of the channel from the estimates at the pilots is not a trivial problem in the case of FTD due to the modulo 2π phase ambiguity. For example, if amplitude and phase are interpolated separately, in order to include the FTD estimation for compensating the phase, 2π hops can result in a very unsmooth 2-D channel interpolation. In our studies using very basic linear interpolation we obtained the smoothest results by first eliminating the phase slope from the center frequencies of the pilots. Then, 2-D complex interpolation to obtain the channel estimates for the data symbols both at the center and edge frequencies is performed, and finally the phase slope is

restored to the whole estimation matrix for final calculation of the equalizer coefficients.

3.5. Joint FTD and Channel Estimation Based on Iterative Interference Cancelation. The analysis above shows a clear interplay between the quality of the estimates and the presence of FTD and CFO. Therefore, it is desirable to apply the information of the estimated synchronization parameters to the estimated pilots in order to improve the quality of all the pilot-based estimates. One way to achieve this is by jointly estimating the subcarrier-wise channel coefficients and the phase slope. Here, we present a new approach that utilizes the FTD-induced linear phase slope within each pilot subcarrier. We assume a simplified signal model, where the amplitude response is assumed to be constant within each subchannel and the phase is assumed to be a linear function of frequency. This is motivated by the observation that, in many cases, a 1-tap equalizer is able to equalize the channel quite well in the absence of timing offsets. The joint channel-FTD estimation includes two parts: estimation of the complex channel coefficient for each pilot, and estimation of the phase slope jointly for all pilots participating in the estimation window Ω_{JE}.

Simplifying the notation for the 1-tap equalizer coefficient at k, n in (11) as $w_{k,n} = w_{k,n}^{(0)}$, the FTD-compensating target response of the 3-tap subcarrier equalizer presented in Section 2.2 can be written as

$$\begin{aligned} W_{k,n}\left(e^{-j(\pi/2)}\right) &= w_{k,n}e^{j\psi}, \\ W_{k,n}\left(e^{j0}\right) &= w_{k,n}, \\ W_{k,n}\left(e^{j(\pi/2)}\right) &= w_{k,n}e^{-j\psi}, \end{aligned} \tag{28}$$

where the equalizer phase difference correction between the subchannel center frequency and the edge is

$$\psi = -\pi\tau_{\mathrm{FTD}}. \tag{29}$$

The subcarrier equalizer in the frequency sampling design can now be written as

$$\begin{aligned} W_{k,n}(z) = {} & \left[0.5(1-\cos(\psi)-\sin(\psi))z+\cos(\psi)\right. \\ & \left.+0.5(1-\cos(\psi)+\sin(\psi))z^{-1}\right]w_{k,n}, \end{aligned} \tag{30}$$

resulting in the following signal model for the subcarrier equalizer output:

$$\begin{aligned} \overline{y}_{k,n}(\psi) = {} & \cos(\psi)w_{k,n}y_{k,n} \\ & + 0.5(1-\cos(\psi)+\sin(\psi))w_{k,n}y_{k,n-1} \\ & + 0.5(1-\cos(\psi)-\sin(\psi))w_{k,n}y_{k,n+1}. \end{aligned} \tag{31}$$

If small ψ is assumed we can approximate (31) as

$$\overline{y}_{k,n}(\psi) \simeq w_{k,n}y_{k,n} + \frac{\psi}{2}w_{k,n}(y_{k,n-1}-y_{k,n+1}). \tag{32}$$

This can be rewritten as

$$\begin{aligned} \widetilde{d}_{k,n} + j\widetilde{u}_{k,n} &= \theta_{k,n}^{*}\overline{y}_{k,n}(\psi) \\ &\simeq w_{k,n}\theta_{k,n}^{*}y_{k,n} + \frac{\psi}{2}w_{k,n}\theta_{k,n}^{*}(y_{k,n-1}-y_{k,n+1}) \\ &= w_{k,n}\widetilde{y}_{k,n} + \psi w_{k,n}\widetilde{\Delta y}_{k,n}, \end{aligned} \tag{33}$$

where we define

$$\widetilde{\Delta y}_{k,n} = \frac{\theta_{k,n}^{*}(y_{k,n-1}-y_{k,n+1})}{2}. \tag{34}$$

Using the auxiliary pilot scheme, for the pilot symbols the ideal output is $d_{k,n}$ (the subindices $(\cdot)_p$ are ignored here for readability). Now, the channel equalization problem can be formulated as

$$\begin{aligned} &\{\widehat{\psi}, \widehat{w}_{k,n}\} \\ &\quad = \arg\min_{\psi, w_{k,n}}\left\{\sum_{k,n\in\Omega_{\mathrm{JE}}}\left|d_{k,n}-\left(w_{k,n}\widetilde{y}_{k,n}+\psi w_{k,n}\widetilde{\Delta y}_{k,n}\right)\right|^2\right\}, \end{aligned} \tag{35}$$

where Ω_{JE} is the set of subcarrier symbols used in the joint estimation. The idea is to adjust ψ and $w_{k,n}$ in such a way that the difference between the equalizer output and the known pilot $d_{k,n}$ is minimized in the least-squares sense. This is a nonlinear optimization problem, which can be solved for example by iterating the following two steps.

(1) Assuming that the phase slope is known from the previous iteration (0 in the beginning), $\{w_{k,n}^{i}\}$ are solved from pilots $\widetilde{y}_{k,n} + \psi^{i-1}\widetilde{\Delta y}_{k,n}$. Note that here i is the iteration index.

(2) Assuming that $\{w_{k,n}^{i}\}$ are known, the observation is a linear function of ψ and the optimum $\widehat{\psi}$ can easily be calculated with the derivative of the expression in brackets in (35) with respect to ψ and setting the result to 0, yielding

$$\widehat{\psi} = \frac{\sum_{k,n\in\Omega_{\mathrm{JE}}} d_{k,n}\,\mathrm{Re}\left[w_k\widetilde{\Delta y}_{k,n}\right] - |w_k|^2\,\mathrm{Re}\left[\widetilde{y}_{k,n}\widetilde{\Delta y}_{k,n}^{*}\right]}{\sum_{k,n\in\Omega_{\mathrm{JE}}}\left|w_k\widetilde{\Delta y}_{k,n}\right|^2}, \tag{36}$$

which, from (29), yields $\widehat{\tau}_{\mathrm{FTD}} = -\widehat{\psi}/\pi$. Note that w_k is here the average of $w_{k,n}$ within subchannel k. This process converges typically in 5–10 iterations, depending on the FTD and Ω_{JE}. Moreover, the estimates $\widehat{\psi}$ are quite accurate even for higher values of ψ, as will be seen in Section 5.

Since this method relies on iteratively canceling the ICI, it will hereafter be referred to as iterative interference cancelation (IIC) approach.

3.6. CFO Estimation and Correction. The effect of carrier frequency offset can be analyzed with help of (12), (14), and (25). We observe that before the AFB, the complex exponential that represents the frequency shift induces a linearly time-varying phase rotation of $2\pi(\varepsilon/M)$ on consecutive high-rate samples. Recall that ε is the normalized CFO with respect to the subcarrier separation Δf. After the receiver bank and downsampling by $M/2$, the phase rotation between two consecutive symbols at rate $2/T$ is $\pi\varepsilon$ radians. This leads to ISI from symbols in the same subchannel and ICI from symbols in neighboring subchannels at earlier and later time-instants (the neighboring symbols located at the same timing instant have the same phase rotation as the symbol under study, so they do not contribute to ICI, if only CFO is present). The linearly time-varying phase rotation is the property exploited in the forthcoming pilot-based CFO estimation and permits also to implement the basic compensation scheme.

A further effect of the CFO that can be deduced from (25) is that the subchannel filter at the AFB is not frequency-aligned with the corresponding subchannel filter at the SFB. This distorts the effective impulse response of the synthesis-analysis cascade by a factor

$$F_{\mathrm{CFO}}\left(e^{j\omega}\right) = \frac{P\left(e^{j(2\omega/M+2\pi\varepsilon/M)}\right)}{P(e^{j2\omega/M})}, \tag{37}$$

where ω is the normalized angular frequency at subchannel sample rate and $P(e^{j2\omega/M})$ is the prototype filter frequency response in the filter bank design. In filter banks with linear-phase channel filters in the analysis (and synthesis) filter banks and in the zero-phase subchannel processing model, only the magnitude of the distorting frequency response is significant. The described distortion on the frequency response for the prototype filter introduced above is shown in Figure 2 for some selected CFO values.

Finally, there are some effects like aliasing effects close to the subband edges and the appearance of distortion from the subchannel located 2 subcarrier spacings away.

3.6.1. CFO Estimation. Based on the CFO effects described above, pilot-based frequency offset estimation is straightforward. If a pilot at k_p, n_p is followed by another one Δn samples later at $k_p, n_p + \Delta n$, the phase rotation between them will cover $\Delta\varphi = \pi\varepsilon\Delta n$ radians. This yields an estimate

$$\begin{aligned}\widehat{\varepsilon} &= \frac{\Delta\varphi}{\pi\Delta n} \\ &= \frac{\angle\left(\widetilde{y}_{k_p,n_p}\right) - \angle\left(\widetilde{y}_{k_p,n_p+\Delta n}\right)}{\pi\Delta n} \\ &= \frac{\angle\left(y_{k_p,n_p}\right) - \angle\left(y_{k_p,n_p+\Delta n}\right) + \Delta n(\pi/2)}{\pi\Delta n},\end{aligned} \tag{38}$$

where $\Delta n(\pi/2)$ comes from the $\theta_{k,n}$ that relate $\widetilde{y}_{k,n}$ and $y_{k,n}$.

The performance of the estimation can be improved by averaging over many pilots to reduce the effect of the distortion. For example, if pilots are all separated by the same number of samples, the following expression [43] can be used for estimating the CFO, while simultaneously weighting the subcarrier pilots according to their powers:

$$\widehat{\varepsilon} = \frac{\angle\left(\sum_{(k,n)\in\Omega_{\mathrm{CFO}}} j^{-\Delta n} y_{k,n+\Delta n} y^*_{k,n}\right)}{\pi\Delta n}. \tag{39}$$

This way, stronger subcarriers are favored over weaker ones. Again the subindices $(\cdot)_p$ indicating pilot locations are not included in the equation for readability. Here, Ω_{CFO} is the set of pilot locations used for CFO estimation. Note that the same problem of phase-ambiguity appears as in FTD estimation when $\varepsilon\Delta n \geq 1$.

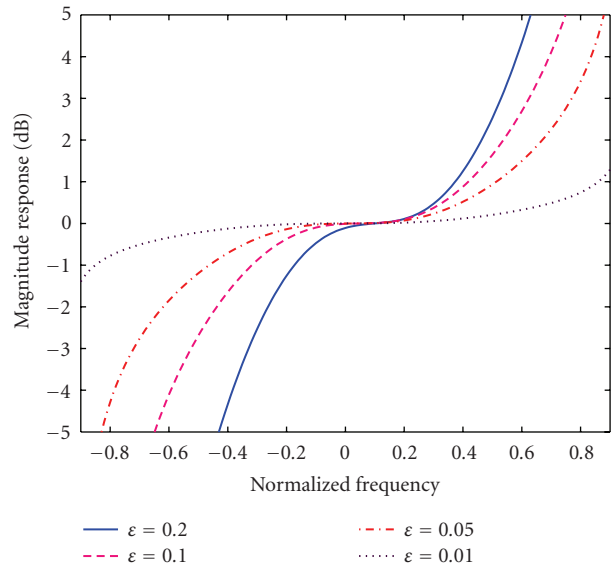

Figure 2: Subchannel frequency response distortion due to CFO for normalized frequency offsets $\varepsilon = 0.01, 0.05, 0.1$, and 0.2.

3.6.2. CFO Compensation. If the CFO is moderate, for example, in CFO tracking scenarios, or the subchannel signal modulation is robust, then the offset compensation can be performed subchannel-wise, as sketched in Figure 3(a) with the multiplication by the complex exponential sequence that undoes the frequency shift: $e^{-j\pi n\varepsilon}$. The performance of this CFO correction on a WiMAX-like FBMC system is presented in [19], although there no other synchronization tasks are considered. The frequency shifting correction will obviously not recover the information leaked to the neighboring channel nor get rid of the distortion coming from 2 subchannels away, since the frequency shift is circular when performed at subchannel level. Further, the amplitude distortion due to the subchannel filter misalignments, depicted in Figure 2, is also ignored when shifting the signal back to its original location subchannel-wise.

It is possible, however, to compensate for this amplitude distortion in a simple way with the help of the 3-tap equalizer presented above. Similarly as with the phase slope in the presence of FTD, the low complexity equalizer can approximatively correct the amplitude distortion given by

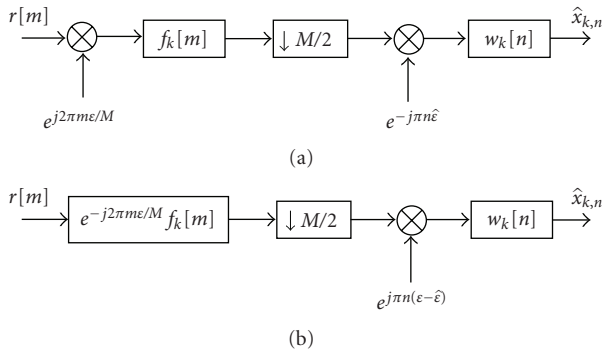

Figure 3: Subchannel receiver signal model in the presence of CFO, with CFO compensation and subchannel equalization. (a) Basic model. (b) Equivalent form.

(37). This is achieved by setting the desired target responses to

$$W_{k,n}\left(e^{j\omega}\right) = \frac{1}{F_{\mathrm{CFO}}(e^{j\omega})}, \tag{40}$$

for $\omega = -\pi/2, 0, \pi/2$.

Figure 3 presents the subchannel model with the effect of the first two mentioned distortion types, which are predominating. It includes also the basic subchannel-wise CFO correction that undoes the CFO phase rotation according to the estimated frequency shift $\hat{\varepsilon}$. In the equivalent model (b), the effect of inaccurate CFO estimation is represented by the residual frequency modulation $e^{j\pi n(\varepsilon-\hat{\varepsilon})}$.

When the frequency shift is too large, the degradation of the signal advocates for time domain solutions for correcting and possibly also for estimating the CFO. The compensation performance degrades faster than the estimation performance: At sufficiently high CFO, the subcarrier-wise compensation cannot recover enough of the signal of interest that has leaked to the neighboring subchannel and eliminate the interference. This logically affects higher order modulations most. However, since several pilots are used for CFO estimation, it is possible that the CFO estimate is still acceptable at the given CFO level. In this case, CFO estimation may still be done at subcarrier level, but compensation has to take place before the analysis filter bank.

It is also worth underlining that when multipath channel, FTD and CFO concur in a communication link, the low-complexity subband equalizer can compensate for the three distortions at the desired frequency locations by combining (multiplying) the target frequency responses needed for correcting each of the estimated distortions.

3.7. Synchronization Scheme with Iteration. In order to estimate and compensate the effect of CFO and FTD and the interplay between these effects shown in (14) and (25) we propose a receiver to jointly estimate and correct the channel impairments subchannel-wise. First, the pilots are recovered from the received signal and from them, the CFO is estimated and the frequency shift is reverted. Then, the synchronization block estimates the FTD and uses the obtained information when interpolating the channel between the pilots. Finally, at the equalization stage, the channel estimates at the equalization frequency points are weighted by the frequency-dependent amplitude distortion caused by the CFO (Figure 2) and the 3-tap equalizer then equalizes the signal. It is also possible to iterate this loop, since the 3-tap equalizer is able to remove a lot of distortion from the pilots, allowing for better estimates after the iteration.

4. FBMC for WiMAX

Next we describe the parameters and adjustments required for an FBMC communication system that aims to maintain a certain degree of compatibility with WiMAX specifications. We have aimed to design a system taking as much parameters from the mobile WiMAX specifications [2] and the underlying 802.16e standard [3] as possible. For our setup, we have selected the time division duplexing (TDD) specification for the 10 MHz bandwidth at sampling rate $f_s = 1/T_s = 11.2$ MHz. With a transform size $M = 1024$, the subcarrier spacing is $\Delta f = 10.94$ kHz. The frame duration of 5 ms allows for transmission of 47 OFDMA symbols with the cyclic prefixes permitted in the specifications. If the whole frame was to be used for a downlink (DL) transmission, FBMC could fit 53 FBMC symbols in the same time because of the absence of the CP. In a more realistic scenario including the uplink (UL) subframe, one or two FBMC symbols would have to be sacrificed for guard times between the forward and reverse links. WiMAX provides for different data configuration modes. Here, we observe two of the possible configurations: the downlink partial usage of subcarriers (DL-PUSC) and the adaptive modulation and coding (AMC23). PUSC and AMC23 use 840 and 864 active consecutive subcarriers, respectively, and have a null subcarrier at the center of the transmission band. Compared to AMC23 in OFDMA without additional filtering, if an attenuation of 40 dB outside the 10 MHz transmission band is desired, the FBMC design with the prototype filter presented above could transmit on around 50 additional subcarriers thanks to its good spectral containment. The configurations also define the size of the transmission slots and how the pilots are located within the frame. Figure 4 shows these pilot configurations for the mentioned cases. Here, each OFDMA symbol corresponds to two consecutive subcarrier samples in the FBMC model.

The auxiliary pilot scheme introduced in Section 3.3.1 can directly be applied to the AMC23 pilot configuration. However, if the auxiliary pilot is to be placed in the advantageous position preceding or succeeding the actual pilot, the proximity of the pilots in DL-PUSC poses a computational problem. As shown in Figure 5, directly allocating the pilot and auxiliary pilot fixes a previous auxiliary pilot inside the range used for calculating the complex interference needed for obtaining the auxiliary pilot of interest. If the contribution of this previous auxiliary pilot is not to be ignored, the calculation requires optimization of the auxiliary pilots over the whole burst duration, taking into account their interdependencies (basically, the first

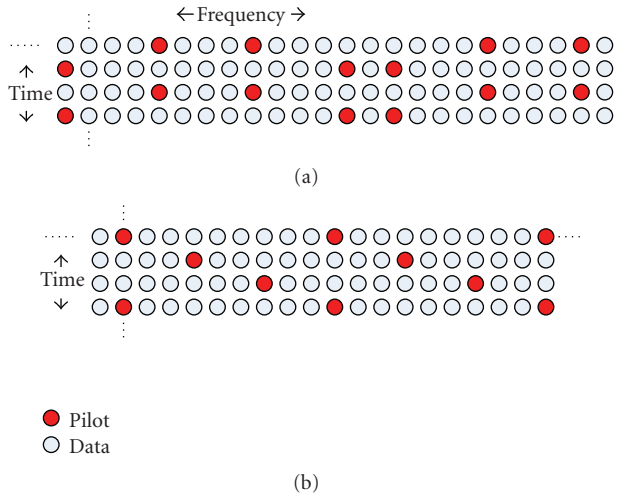

Figure 4: Pilot distribution in WiMAX (a) DL-PUSC and (b) AMC23 configurations.

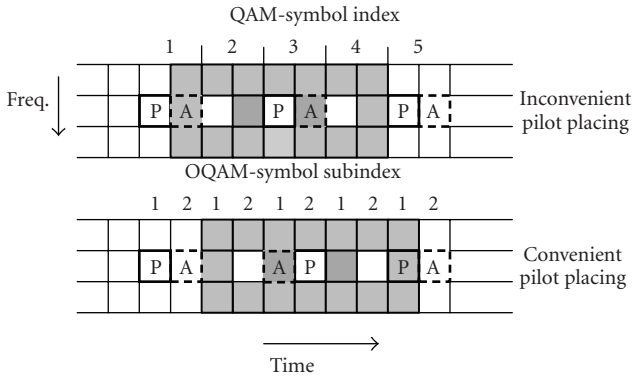

Figure 5: Alternative pilot and data allocations for FBMC with DL-PUSC-like pilot pattern. P: Pilot. A: Auxiliary Pilot.

auxiliary pilot would need to be calculated, then the next one and so on successively). It is more practical to be able to calculate the interference-nulling auxiliary pilots only from the surrounding data. This can be achieved by switching the positions of the pilot/auxiliary pilot pair every other pilot. The lower part of Figure 5 shows this convenient allocation, where the interference window extends only over data and a known pilot.

5. Simulation Setup and Results

We have tested the filter bank based multicarrier system with WiMAX-like parameters and using the synchronization and channel equalization methods that have been described above. The prototype filter is the NPR optimized design with $K = 4$ described in Section 3.3. The FBMC signal is sent through a quasistatic channel, if not indicated otherwise, modeled according to the International Telecommunication Union ITU-R Vehicular-A Channel guidelines [44]. This means, that for the duration of a transmission burst, the channel remains constant in time unless a certain mobility is indicated. In this case, the fading varies with time

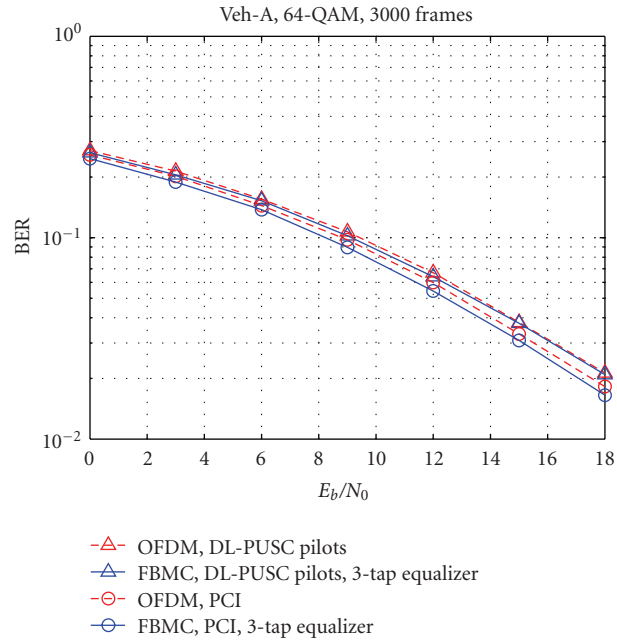

Figure 6: Comparison between OFDM-based WiMAX and FBMC-based WiMAX with 3-tap equalizers with respect to E_b/N_0. 64-QAM transmission with perfect channel information (PCI) and pilot-based estimation in a quasistatic channel.

according to the mobile velocity. For each simulation, 3000 independent burst transmissions with independent channel realizations are performed. The estimation of the synchronization parameters and the channel state relies on scattered pilots obtained with the auxiliary pilot technique. The combined pilot/auxiliary pilot symbol is boosted on average by 4.5 dB with respect to the data. The overall channel response is obtained from the scattered channel estimates by triangulation-based linear interpolation between the pilots. It is important to note that all the processing is done subcarrier-wise, after the AFB.

Extensive results presented in [45] justify favoring the 3-tap equalizer over the single tap solution. With perfect synchronization in the Veh-A channel model, the differences are hardly visible, but in channel models with longer delay spreads and especially when correcting synchronization errors, the performance advantage of the 3-tap equalizer is overwhelming. With respect to the OFDM-based WiMAX, Figure 6 shows the BER performance in the synchronized case of FBMC and OFDM in a system with around 1000 subcarriers that transmit during a whole frame of 5 ms. The OFDM pilots are boosted by 4.5 dB with respect to the data, that is, by the same boost applied to the FBMC pilot/auxiliary pilot pair. The obtained BER curves are quite similar. The better performance of FBMC with perfect knowledge of the channel (PCI) is due to the power that goes into the OFDM CP of length 1/8 of the OFDM symbol [2]. This advantage is almost completely used up when channel estimation takes place because in OFDM all the pilot power is used but in FBMC part of it is dedicated to the auxiliary pilot, which does not contribute to the actual estimation.

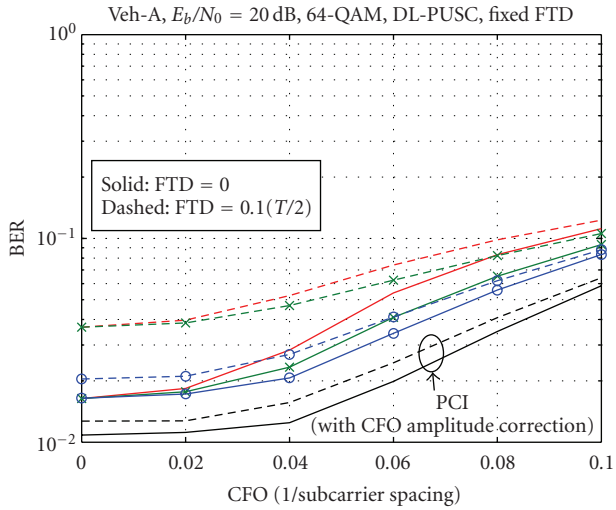

(a) BER versus CFO with fixed FTD $\tau_{\text{FTD}} = 0$ and $0.1(T/2)$

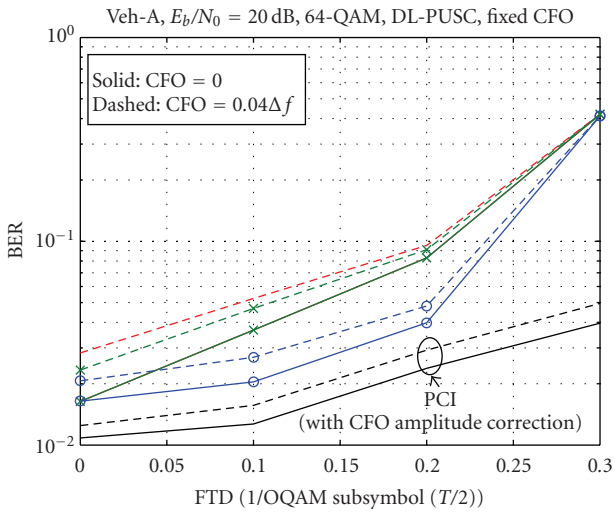

(b) BER versus FTD with fixed CFO $\varepsilon = 0$ and $0.04\Delta f$

Figure 7: BER performance for different synchronization options and equalization of a DL-PUSC zone consisting of 4 MC symbols within Vehicular-A channel at $E_b/N_0 = 20$ dB, 64-QAM modulation.

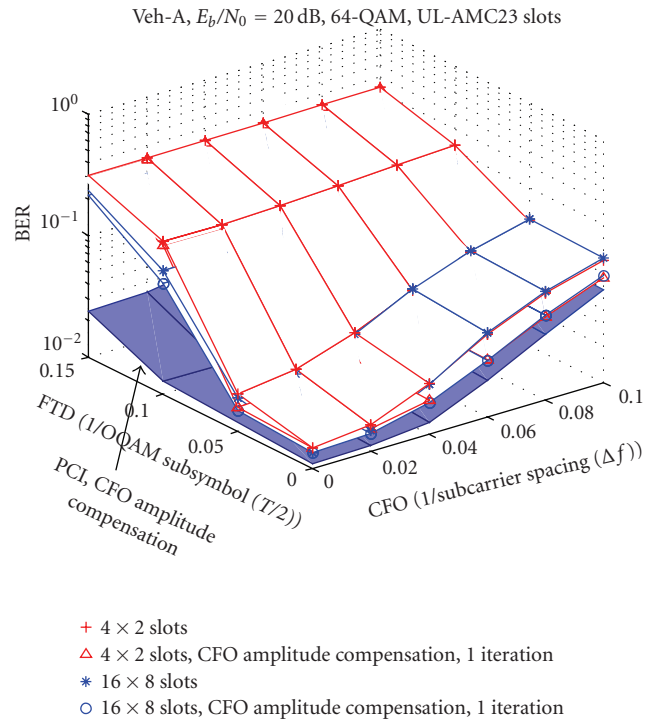

Figure 8: BER performance versus CFO and FTD for uplink transmission of 16×8 and 4×2 AMC23 slots in Vehicular-A channel at $E_b/N_0 = 20$ dB using 64-QAM. Different synchronization options.

In an actual communication system there are synchronization mismatches, and a receiver has to be able to cope with the joint effect of CFO and FTD. The approach detailed above in Section 4, including the iteration of the synchronization/equalization stage, is applied. In our simulations we have concluded that the described synchronization and equalization chain plus one iteration delivers nearly all the improvement, since the differences in offset estimates with additional iterations are marginal.

The first results in Figure 7 show the BER-performance of the mentioned system with 64-QAM at $E_b/N_0 = 20$ dB in a quasistatic Vehicular-A channel. All the subcarriers are used, and the pilots are in the DL-PUSC configuration, simulating a downlink scenario. The transmitted burst consists of 4 FBMC symbols. Until otherwise mentioned, the FTD is calculated through averaging the phase differences between pilots. Figure 7(a) presents the BER results with changing CFO for two fixed FTD values, while Figure 7(b) presents the BER as a function of the FTD for two fixed CFO values. These figures show a clear improvement in performance with respect to CFO due to the CFO amplitude compensation. Further, the iteration of the synchronization and equalization stages also improves the BER, especially with respect to τ_{FTD}. Because improvements in 4-QAM are not that visible (since the modulation is very robust by itself), these results are not shown here. Nevertheless, a slight improvement can still be achieved.

Next, a situation similar to an uplink is tested. The pilots are now placed according to the AMC23 configuration, as in Figure 4(b), and the user sends its data in AMC23 slots, each slot consisting of 18 consecutive subcarriers and 3 MC symbols. Within each slot there are 6 pilot/auxiliary pilot pairs, as can be seen from the figure. We have studied two sizes for the transmitted bursts: 4×2 and 16×8 slots, where the first number indicates the number of slots in frequency direction and the second number in time direction. The smaller burst includes 48 pilot/auxiliary pilot pairs, the larger one has 768. We assume that other users are separated by the required guard band and that they do not produce multiuser interference.

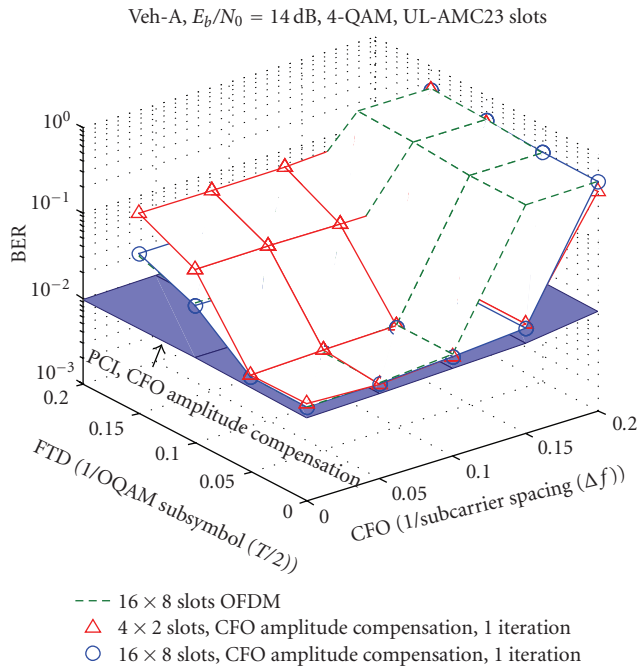

FIGURE 9: BER performance versus CFO and FTD for uplink transmission of 16 × 8 and 4 × 2 AMC23 slots in Vehicular-A channel at E_b/N_0 = 14 dB using 4-QAM. OFDM- and FBMC-based WiMAX. FBMC Synchronization performed with CFO amplitude compensation in the 3-tap equalizer and one synchronization iteration.

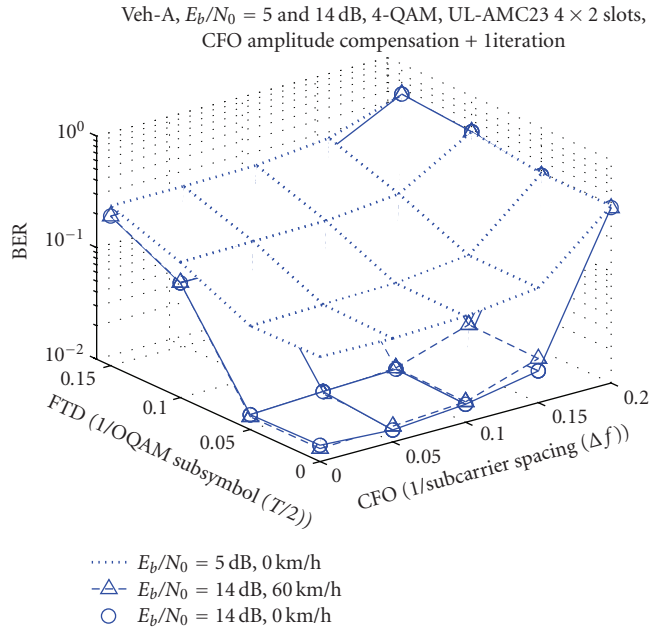

FIGURE 10: BER performance versus CFO and FTD for uplink transmission of 4 × 2 AMC23 slots in Vehicular-A channel at E_b/N_0 = 5 dB and E_b/N_0 = 14 dB using 4-QAM. Static user and user with 60 km/h mobility. Synchronization with CFO amplitude distortion correction and one iteration.

Figures 8 and 9 present the BER performances for 64-QAM and 4-QAM, respectively. The degradation that occurs when using a smaller burst size can be observed. This is due to the lower number of pilots available to perform synchronization and estimation. We further see that the range in which the synchronization is successful is much smaller than in the downlink case, but this is mainly due to the larger pilot separation. The effect of this is that the phase ambiguity when estimating FTD or CFO appears for τ_{FTD} between 0.05 to $0.1(T/2)$ and ε between 0.15 to $0.2\Delta f$ (at around $\varepsilon = 0.17$, because only every 6th symbol is a pilot in time direction). Figure 9 also compares the BER performance of an OFDM-based WiMAX system using the same synchronization and estimation methods as its FBMC counterpart. It occupies 16 × 8 AMC23 slots and the BER results are similar to the FBMC case. The main difference is that in the CFO axis the performance degradation commences earlier. Due to the CP extension of the OFDM symbols, effectively slightly "separating" the pilots in time, the phase ambiguity appears approximately when $\varepsilon = 0.14$. Further, Figure 10 shows the effects on the FBMC system of user mobility and low SNR on the smaller burst with robust subchannel modulation. The performance is barely affected at this speed and only when the CFO approaches the nonambiguity limit the difference becomes visible. On the other hand, the stronger noise is evidently worsening the BER, but still allowing for a certain synchronization range. The following simulation results prove this by taking a closer look at the estimation performance of the synchronization parameters.

The CFO estimator performance is evaluated with help of the root mean square (RMS) error with respect to the actual CFO. The RMS error of the previously presented simulation scenarios is shown for a fixed $\tau_{\text{FTD}} = 0.1(T/2)$ in Figure 11(a). The CFO estimation performance proves to be quite independent from the actual FTD, having only a minor degradation with increasing τ_{FTD}, as the interested reader can verify in [45]. In the low SNR scenario, even with the small burst and with FTD present, the estimate for the frequency offset is acceptable if the CFO stays below 7% of the subcarrier spacing. Also the user with vehicular mobility can be synchronized well by the base station. The other considered cases have a low variation of the performance with increasing CFO, until the ambiguity limit is reached. Although not presented here, the RMS CFO error of $\hat{\varepsilon}$ increases slightly if the synchronization procedure is iterated. Nevertheless, the estimates are still good enough for accurate synchronization within the WiMAX requirements for maximum CFO offset, specifically, ±2% of the subcarrier spacing [3].

Similar results, now for the FTD RMS estimation error at the fixed CFO $\varepsilon = 0.1\Delta f$, are summarized in Figure 11(b). Here the estimation error with iteration of the synchronization part is almost overlaying with the presented results. Also the case with the AMC23 mobile at 60 km/h has been omitted for readability, since the estimation RMS error is similar to the other AMC23 results. As in the CFO case, also here the FTD error is very much independent

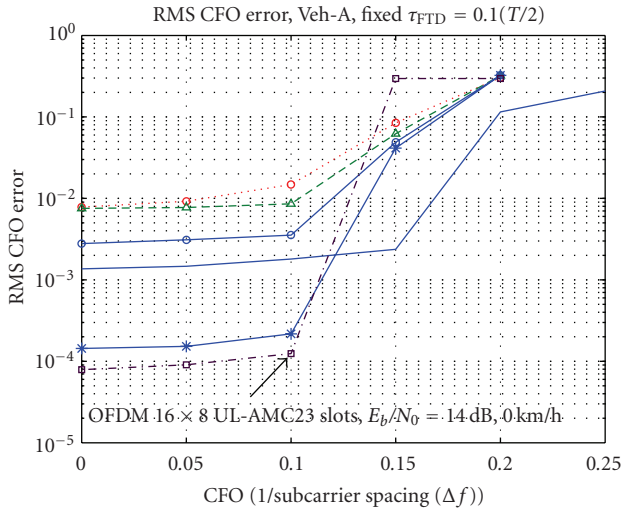

(a) RMS CFO error versus CFO at fixed FTD $\tau_{FTD} = 0.1(T/2)$

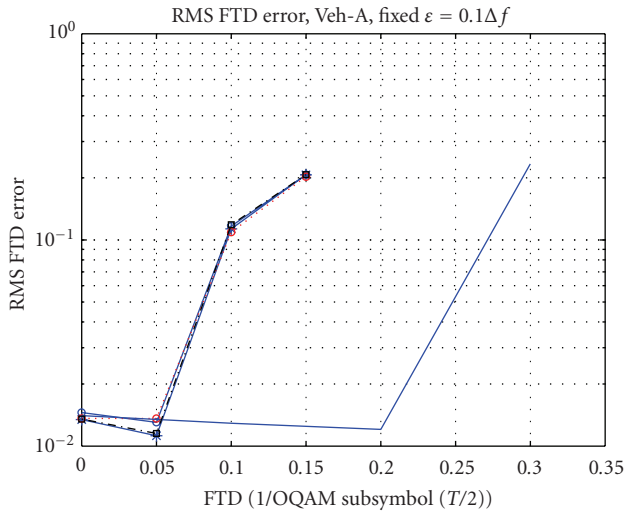

(b) RMS FTD error versus FTD at fixed CFO $\varepsilon = 0.1\Delta f$

Figure 11: RMS errors in CFO and FTD estimation in AMC23 and DL-PUSC transmission with different burst sizes. E_b/N_0 values are referred to 4-QAM modulation.

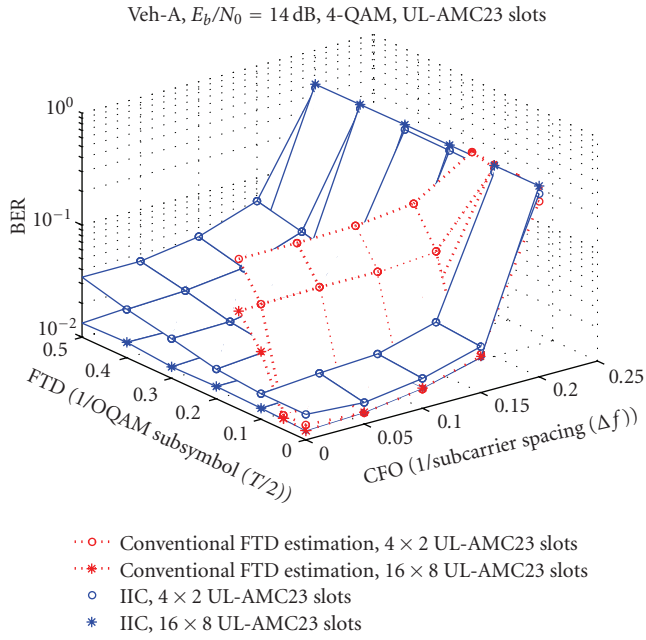

Figure 12: BER performance versus CFO and FTD of the IIC joint FTD and channel estimation method compared to classical FTD estimation. 4-QAM transmission of 4 × 2 and 16 × 8 AMC23 slots in Vehicular-A channel at $E_b/N_0 = 14$ dB. Static user. No additional synchronization iteration.

of the CFO (see again [45]) and is almost constant within the nonambiguous estimation range, between 5 and 10 high rate samples. This error floor for the different scenarios is caused by the inherent delay the channel introduces due to the delay spread distribution. Its effect is a mild slope in the phase with respect to the subcarrier index, even in the absence of proper FTD. This mild slope is also detected by the estimation methods as part of the FTD, inducing the error floor when comparing it to the actual FTD.

Figures 11(a) and 11(b) include the RMS estimation error performance of the OFDM-based system. It can be seen that due to the higher available power boost for the OFDM pilots, the CFO estimates are better than in the FBMC system in the nonambiguous region. The FTD estimation error almost matches the error in the FBMC system because the mild slope of the inherent channel delay mentioned in the previous paragraph is detected here, too. The better CFO estimation performance does not translate into a better BER performance, as can be verified above in Figure 9.

The FTD estimation range can be extended further than the limit imposed by the frequency separation of the pilots by applying the interference minimization approach described in Section 3.5, yielding (36). The BER performance of the IIC technique for the AMC23 transmission configuration is shown in Figure 12, where the novel method is iterated 10 times. Figure 13 presents the corresponding RMS FTD estimation error. The extension into longer delay operating ranges is evident, and the BER performance for this E_b/N_0 achieves the same level as the conventional technique when the larger bursts are compared. However, when a mobile user transmits using small bursts, and consequently few pilots, the BER and estimation performances of the IIC approach suffer greatly. If the interference cancelation method does not perform well enough in estimating the FTD because it has not enough pilots, it can, nevertheless, be applied for a coarse estimation within a wide FTD range to pin the delay

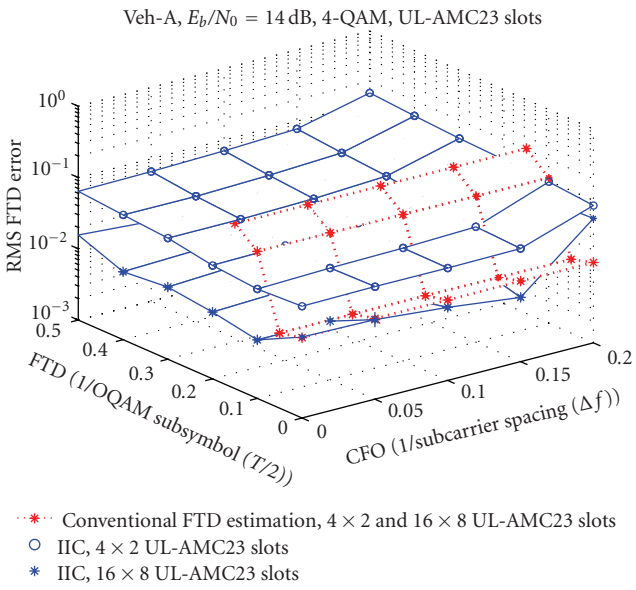

Figure 13: RMS error in FTD estimation versus CFO and FTD of the IIC FTD estimation method compared to classical FTD estimation. 4-QAM transmission of 4×2 and 16×8 AMC23 slots in Vehicular-A channel at $E_b/N_0 = 14$ dB. Static user. No additional synchronization iteration.

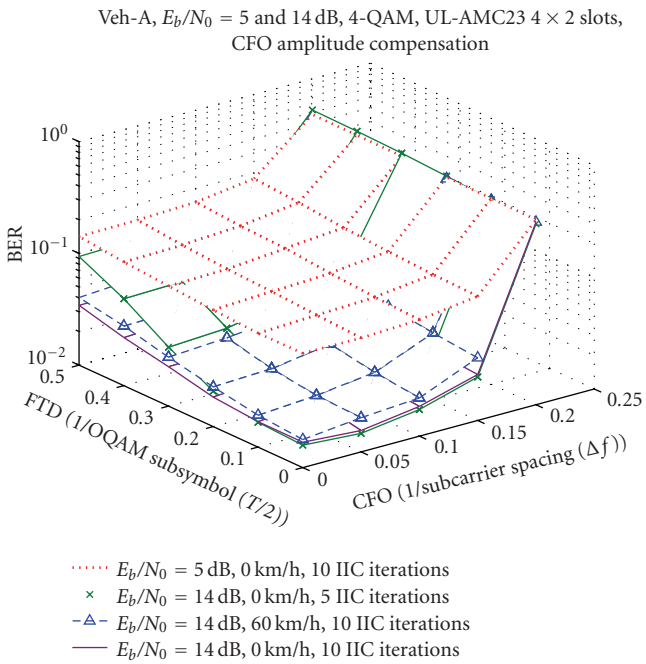

Figure 14: BER performance versus CFO and FTD of the IIC joint FTD and channel estimation method in different channel scenarios. 4-QAM transmission of 4×2 AMC23 slots in Vehicular-A channel at $E_b/N_0 = 5$ dB and $E_b/N_0 = 14$ dB and at different velocities. 5 and 10 iterations in the IIC technique. No additional synchronization iteration.

to a value from where the conventional FTD estimation can take over the task.

Figure 14 presents the performance of the IIC method for AMC23 transmission of 4×2 slots under different channel conditions. We see that this method is more sensitive to the mobility conditions than the conventional FTD and channel estimation method (see Figure 10). The BER performance with low SNR is also worse in this small burst case. If only 5 iterations in the IIC are performed, then the BER worsens for longer fractional time delays. Although not presented here, 5 iterations suffice if the larger burst of 16×8 slots is sent, since the performance is practically the same as with 10 iterations.

6. Conclusions

In this contribution we proposed an integrated synchronization subsystem for filter bank based multicarrier communications. If the dimensioning of the filter bank leads to approximately flat fading subchannels, scattered pilots can be used to perform the synchronization and channel estimation tasks. Spectrally efficient filter banks with efficient implementations, such as the FBMC/OQAM transmultiplexer, can provide well-contained communication channels with high isolation to adjacent, nonsynchronous signals. However, the orthogonality conditions between subchannels for this kind of systems require special solutions in pilot design. The auxiliary pilot approach permits creating pilots that can take advantage of the basic synchronization procedures for OFDM to estimate the fractional time delay, carrier offsets, and communication channel. More important, it enables the design of FBMC-specific synchronization and channel estimation methods taking into account the interplay of the different stages involved in estimating and compensating for the distortions experienced by the signal. The utilized low-complexity subchannel-wise equalizer for filter banks can use these estimates for equalizing the channel and also to correct distortions caused by incorrect timing or frequency tuning in an efficient way. We have also presented a novel iterative interference cancelation (IIC) approach that estimates the fractional time delay and can return channel estimates by iterating an optimization routine specific to the low-complexity equalizer.

The mentioned synchronization apparatus was put to test in a 10 MHz WiMAX-like communications scenario, where the discussed tools succeed in estimating and compensating the channel distortions. Special emphasis is put on maintaining as many compatible physical layer elements with WiMAX as possible. As a matter of fact, the FBMC system can be updated to send over more subchannels and more MC symbols within the given time frame and system bandwidth, compared to the OFDM-based WiMAX, while achieving similar BER performance. For example, if a whole frame is used for downlink transmission and a 40 dB attenuation is assumed at the transmission band limits, the additional MC symbols and subcarriers in the FBMC-based system permit transmitting 16% more QAM symbols.

Clever reuse of the subchannel equalizer leads to improved BER performance, compared to basic techniques, especially for higher order modulations, for example, 64-QAM. In this case, performance degradation with significant

synchronization offsets is due to insufficient compensation by the synchronization subsystem, whereas with more robust modulations, such as 4-QAM, the bottleneck is in the estimation performance, that is, the performance after compensation is satisfactory as long as estimation is acceptable, which mainly depends on the pilot distribution. In this sense, the introduced joint FTD and channel estimation approach can outperform the conventional method under favorable channel conditions (good SNR and low mobility) allowing acceptable reception under severe FTD. In adverse conditions, it provides sufficiently good estimates for a wide range of FTD, making it suitable for coarse estimation and synchronization of robust data signals.

This can also be exploited when multiple-input multiple-output (MIMO) techniques are used to improve the throughput. The pilots of one transmit antenna have to coincide with "silence" on the other antennas to enable MIMO channel estimation similar as in the single stream case. If the pilot (including the "silent pilots") overhead is to remain the same, as for example in the optional 2 antenna WiMAX AMC transmission [3], the density of active pilots that can be used for actual estimation of the MIMO channel diminishes. In this scenario of greater separation of active pilots, the new FTD estimation with its wider estimation range can prove itself very practical.

Some of the simulation results of Section 5 were obtained for small- and medium-sized transmission bursts. Since the FTD and CFO values are relatively slowly changing in most wireless communication scenarios, it is always possible to refine the estimates by filtering them over multiple transmission bursts to reduce the random variations of block-wise estimates.

An attractive aspect of the presented method is that it operates completely in the frequency domain, after the analysis filter bank. This is especially useful in cognitive radio scenarios, in which high spectral containment and resolution permit secondary users to exploit appearing and vanishing spectral time-frequency holes in the communications of the primary system. Processing after the AFB means that the signal has been well delimited in frequency domain.

In an uplink multiuser scenario, a base station using the presented synchronization, estimation, and equalization methods for FBMC can independently synchronize different users in different bands transmitting in an unsynchronized way, that is, with different FTDs, as long as they are separated by a guard band of at least one subchannel. The bands assigned to each user are processed subcarrier-wise and independently. It is not necessary for the users to transmit synchronously because the guard subchannel assures that the signals remain orthogonal to each other, independently of their relative timings.

A possible direction of future work is to examine the behavior of smaller filter banks in the same bandwidth, with higher subcarrier spacings. This situation poses challenges to the estimation part, since the use of scattered pilots is not that well justified when the subchannel channel is not flat fading anymore.

All in all, we conclude that FBMC can perform sufficiently well to offer an alternative to OFDM as modulation and multiple access technique, offering several advantages especially as a cognitive radio physical layer.

Acknowledgments

This research was supported in part by the European Commission under Project PHYDYAS (FP7-ICT-2007-1-211887). The authors would like to acknowledge the valuable contributions of their colleagues in the PHYDYAS project. They also wish to thank the reviewers and the editor for their comments that helped to improve the manuscript.

References

[1] R. van Nee and R. Prasad, *OFDM for Wireless Multimedia Communications*, Artech House, Boston, Mass, USA, 2000.

[2] WiMAX Forum, "Mobile system profile," Release 1.0 Approved Specification, Revision 1.5.0, November 2007.

[3] "IEEE standard for local and metropolitan area networks. Part 16: air interface for fixed and mobile broadband wireless access systems. Amendment 2: physical and medium access control layers for combined fixed and mobile operation in licensed bands and corrigendum 1," *IEEE Std 802.16e-2005 and IEEE Std 802.16-2004/Cor 1-2005 (Amendment and Corrigendum to IEEE Std 802.16-2004)*, pp. 1–822, 2006.

[4] TSG-RAN 3GPP TS 36.211, "Physical channels and modulation," Release 8, February 2009.

[5] P. Siohan, C. Siclet, and N. Lacaille, "Analysis and design of OFDM/OQAM systems based on filterbank theory," *IEEE Transactions on Signal Processing*, vol. 50, no. 5, pp. 1170–1183, 2002.

[6] H. S. Malvar, *Signal Processing with Lapped Transforms*, Artech House, Boston, Mass, USA, 1992.

[7] J. Mitola III and G. Q. Maguire Jr., "Cognitive radio: making software radios more personal," *IEEE Personal Communications*, vol. 6, no. 4, pp. 13–18, 1999.

[8] S. Haykin, "Cognitive radio: brain-empowered wireless communications," *IEEE Journal on Selected Areas in Communications*, vol. 23, no. 2, pp. 201–220, 2005.

[9] D. Thomson, "Spectrum estimation and harmonic analysis," *Proceedings of the IEEE*, vol. 70, no. 9, pp. 1055–1096, 1982.

[10] B. Farhang-Boroujeny and R. Kempter, "Multicarrier communication techniques for spectrum sensing and communication in cognitive radios," *IEEE Communications Magazine*, vol. 46, no. 4, pp. 80–85, 2008.

[11] J. H. Manton, "Optimal training sequences and pilot tones for OFDM systems," *IEEE Communications Letters*, vol. 5, no. 4, pp. 151–153, 2001.

[12] M. Pun, M. Morelli, and C. Jay Kuo, *Multi-Carrier Techniques for Broadband Wireless Communications. A Signal Processing Perspective*, Imperial College Press, London, UK, 2007.

[13] J.-J. van de Beek, M. Sandell, and P. O. Börjesson, "ML estimation of time and frequency offset in OFDM systems," *IEEE Transactions on Signal Processing*, vol. 45, no. 7, pp. 1800–1805, 1997.

[14] T. Fusco, A. Petrella, and M. Tanda, "Data-aided symbol timing and CFO synchronization for filter bank multicarrier systems," *IEEE Transactions on Wireless Communications*, vol. 8, no. 5, pp. 2705–2715, 2009.

[15] T. Hidalgo Stitz, T. Ihalainen, and M. Renfors, "Practical issues in frequency domain synchronization for filter bank based multicarrier transmission," in *Proceedings of the 3rd International Symposium on Communications, Control, and*

Signal Processing (ISCCSP '08), pp. 411–416, St. Julians, Malta, March 2008.

[16] H. Bölcskei, "Blind estimation of symbol timing and carrier frequency offset in wireless OFDM systems," *IEEE Transactions on Communications*, vol. 49, no. 6, pp. 988–999, 2001.

[17] C. Lélé, J.-P. Javaudin, R. Legouable, A. Skrzypczak, and P. Siohan, "Channel estimation methods for preamble-based OFDM/OQAM modulations," in *Proceedings of the European Wireless Conference*, Paris, France, April 2007.

[18] J.-P. Javaudin, D. Lacroix, and A. Rouxel, "Pilot-aided channel estimation for OFDM/OQAM," in *Proceedings of the 57th IEEE Semiannual Vehicular Technology Conference (VTC '03)*, vol. 3, pp. 1581–1585, April 2003.

[19] T. Hidalgo Stitz, A. Viholainen, T. Ihalainen, and M. Renfors, "CFO estimation and correction in a WiMAX-like FBMC system," in *Proceedings of IEEE Workshop on Signal Processing Advances in Wireless Communications (SPAWC '09)*, pp. 633–637, Perugia, Italy, June 2009.

[20] B. Jahan, M. Lanoiselée, G. Degoulet, and R. Rabineau, "Full synchronization method for OFDM/OQAM and OFDM/QAM modulations," in *Proceedings of IEEE International Symposium on Spread Spectrum Techniques and Applications (ISSSTA)*, pp. 344–348, Perugia, Italy, June 2008.

[21] J. Alhava and M. Renfors, "Exponentially-modulated filter bank-based transmultiplexer," in *Proceedings of IEEE International Symposium on Circuits and Systems (ISCAS)*, vol. 4, pp. 233–236, Bangkok, Thailand, May 2003.

[22] S. Mirabbasi and K. Martin, "Overlapped complex-modulated transmultiplexer filters with simplified design and superior stopbands," *IEEE Transactions on Circuits and Systems II*, vol. 50, no. 8, pp. 456–469, 2003.

[23] P. P. Vaidyanathan, *Multirate Systems and Filter Banks*, Prentice-Hall, Englewood Cliffs, NJ, USA, 1993.

[24] A. Viholainen, T. Ihalainen, T. Hidalgo Stitz, M. Renfors, and M. Bellanger, "Prototype filter design for filter bank based multicarrier transmission," in *Proceedings of European Signal Processing Conference (EUSIPCO)*, Glasgow, Scotland, August 2009.

[25] R. Bregović, *Optimal design of perfect-reconstruction and nearly perfect-reconstruction multirate filter banks*, Ph.D. dissertation, Tampere University of Technology, TUT Publications 428, Tampere, Finland, 2003.

[26] P. Martín-Martín, R. Bregović, A. Martín-Marcos, F. Cruz-Roldán, and T. Saramäki, "A generalized window approach for designing transmultiplexers," *IEEE Transactions on Circuits and Systems I*, vol. 55, no. 9, pp. 2696–2706, 2008.

[27] K. W. Martin, "Small side-lobe filter design for multitone data-communication applications," *IEEE Transactions on Circuits and Systems II*, vol. 45, no. 8, pp. 1155–1161, 1998.

[28] M. G. Bellanger, "Specification and design of a prototype filter for filter bank based multicarrier transmission," in *Proceedings of IEEE International Conference on Acoustics, Speech and Signal Processing (ICASSP '01)*, vol. 4, pp. 2417–2420, May 2001.

[29] B. Le Floch, M. Alard, and C. Berrou, "Coded orthogonal frequency division multiplex," *Proceedings of the IEEE*, vol. 83, no. 6, pp. 829–996, 1995.

[30] A. Vahlin and N. Holte, "Optimal finite duration pulses for OFDM," *IEEE Transactions on Communications*, vol. 44, no. 1, pp. 10–14, 1996.

[31] S. D. Sandberg and M. A. Tzannes, "Overlapped discrete multitone modulation for high speed copper wire communications," *IEEE Journal on Selected Areas in Communications*, vol. 13, no. 9, pp. 1571–1585, 1995.

[32] L. Vandendorpe, L. Cuvelier, F. Deryck, J. Louveaux, and O. Van de Wiel, "Fractionally spaced linear and decision-feedback detectors for transmultiplexers," *IEEE Transactions on Signal Processing*, vol. 46, no. 4, pp. 996–1011, 1998.

[33] B. Hirosaki, "An analysis of automatic equalizers for orthogonally multiplexed QAM systems," *IEEE Transactions on Communications Systems*, vol. 28, no. 1, pp. 73–83, 1980.

[34] T. Wiegand and N. J. Fliege, "Equalizers for transmultiplexers in orthogonal multiple carrier data transmission," in *Proceedings of European Signal Processing Conference (EUSIPCO)*, vol. 2, pp. 1211–1214, Trieste, Italy, September 1996.

[35] S. Nedic, "An unified approach to equalization and echo cancellation in OQAM-based multi-carrier data transmission," in *Proceedings of the IEEE Global Telecommunications Conference*, vol. 3, pp. 1519–1523, Phoenix, Ariz, USA, November 1997.

[36] K. van Acker, G. Leus, M. Moonen, O. van de Wiel, and T. Pollet, "Per tone equalization for DMT-based systems," *IEEE Transactions on Communications*, vol. 49, no. 1, pp. 109–119, 2001.

[37] A. M. Wyglinski, P. Kabal, and F. Labeau, "Adaptive filterbank multicarrier wireless systems for indoor environments," in *Proceddings of IEEE Vehicular Technology Conference*, pp. 336–340, Vancouver, Canada, September 2002.

[38] D. S. Waldhauser, L. G. Baltar, and J. A. Nossek, "MMSE subcarrier equalization for filter bank based multicarrier systems," in *Proceedings of IEEE Workshop on Signal Processing Advances in Wireless Communications (SPAWC '08)*, pp. 525–529, July 2008.

[39] T. Ihalainen, T. Hidalgo Stitz, M. Rinne, and M. Renfors, "Channel equalization in filter bank based multicarrier modulation for wireless communications," *EURASIP Journal on Advances in Signal Processing*, vol. 2007, Article ID 49389, 18 pages, 2007.

[40] M. Renfors, T. Ihalainen, and T. Hidalgo Stitz, "Channel equalization," Patent EP1 716 681, November 2008.

[41] C. Lélé, *OFDM/OQAM modulation: channel estimation methods, and applications to multicarrier CDMA and multi-antenna transmission*, Ph.D. dissertation, Conservatoire National des Arts et Métiers, November 2008.

[42] C. Lélé, R. Legouable, and P. Siohan, "Iterative scattered pilot channel estimation in OFDM/OQAM," in *Proceedings of IEEE Workshop on Signal Processing Advances in Wireless Communications (SPAWC '09)*, pp. 176–180, June 2009.

[43] S. Kay, "Fast and accurate single frequency estimator," *IEEE Transactions on Acoustics, Speech, and Signal Processing*, vol. 37, no. 12, pp. 1987–1990, 1989.

[44] ITU-R, "Guidelines for evaluation of radio transmission technologies for IMT-2000," Recommendation M.1225, 1997.

[45] INFSO-ICT-211887 Project PHYDYAS, "Deliverable 2.2: synchronization and initialization with single antenna. Blind techniques," January 2009, http://www.ict-phydyas.org/userfiles/file/Phydyas-D2-2.pdf.

Publication P4

T. Hidalgo Stitz, T. Ihalainen, and M. Renfors, "Mitigation of narrowband interference in filter bank based multicarrier systems," in *Proc. IEEE Int. Conf. Communications.* 2006, vol.7, pp. 3241-3246, June 2006.

DOI=http://dx.doi.org/10.1109/ICC.2006.255306

Mitigation of Narrowband Interference in Filter Bank Based Multicarrier Systems

Tobias Hidalgo Stitz, Tero Ihalainen, Markku Renfors
Institute of Communications Engineering
Tampere University of Technology
Tampere, Finland
{Tobias.Hidalgo, Tero.j.Ihalainen, Markku.Renfors}@tut.fi

***Abstract*—In this paper we present a method to mitigate the effects of a narrowband interference present in an adjacent subchannel of a filter bank based multicarrier (FBMC) system. For this purpose, we use the spectral shaping capabilities of a low-complexity subchannel equalizer for filter banks. With this method, over 20 dB stronger narrowband interference (NBI) power can be tolerated as compared to a system without interference mitigation. These findings are relevant when improving the throughput / spectral efficiency of an FBMC system in environments with narrowband interference.**

I. INTRODUCTION

Wireless systems that use a wide bandwidth have to face difficult communication environments, e.g., frequency selective channels cause intersymbol interference that has to be equalized [1]. It is also possible that the wideband signal has to coexist with a narrowband signal that distorts part of the desired signal. Narrowband interference (NBI) may be present in a number of scenarios. For example, in ultra-wideband (UWB) systems the reason can be overlaid spectrum, i.e., a narrowband signal using the same frequencies as part of the UWB communication. Other sources may be spurious frequency due to own or nearby transceiver, or even intentional jamming. In this kind of scenario, multicarrier (MC) techniques are increasingly gaining importance because of their advantages. Among them we count robustness in case of frequency selective channels, offering the possibility of simple equalization, simple timing synchronization, as well as insensitivity to limited narrowband interference. These advantages are a good reason for applying MC techniques to more and more existing and emerging communication systems [2] and make them serious candidates for the future "Beyond 3G" mobile communication systems.

Although orthogonal frequency division multiplexing (OFDM) is the most prominent multicarrier technique, in this paper we focus on multirate filter banks (FB) in the transmultiplexer (TMUX) configuration [3]. The main characteristic of FBMC systems is that the subchannels can be designed optimally in the frequency domain, e.g., to have good spectral containment [4]. Basically, the Nyquist pulse shaping principle is used for the subchannel signals, which means that the consecutive symbol waveforms are overlapping in time. Figure 1 compares the subchannel frequency responses of discrete Fourier transform (DFT) -based systems such as OFDM to those of FBMC with frequency-domain optimized characteristics. With sufficient stopband attenuation and assuming a roll-off smaller than 100 %, only the adjacent subchannels may cause crosstalk, or intercarrier interference (ICI), to the subchannel signals in the FBMC system, whereas in the DFT based system the power of a strong narrowband interferer can be present in a much wider range of subchannels.

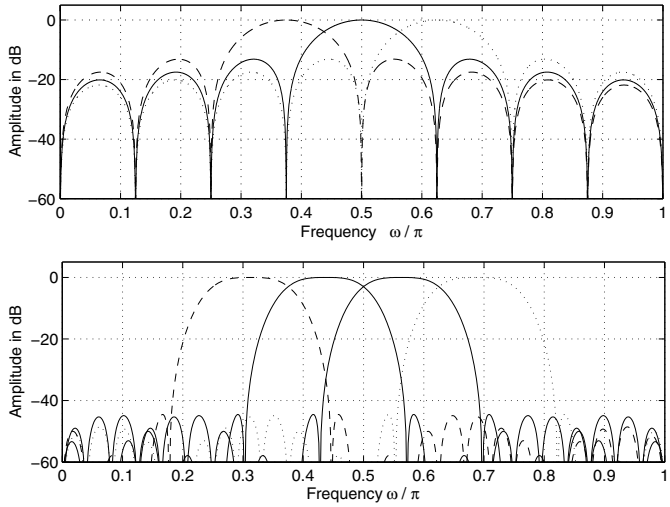

Figure 1. Subchannel frequency responses for DFT and FB-based systems (16 subchannels, overlapping factor of 4, 100 % roll-off).

In this paper we use a 2x oversampled complex modulated FB [5] in a frequency selective transmission channel. The adverse channel conditions are worsened by the presence of a narrowband interferer. We apply the amplitude-phase adaptive sine-modulated/cosine-modulated filter bank equalizer for TMUXs (AP-ASCET) proposed in [6] and extend its use to successfully mitigate the distortion caused on a subchannel by a NBI located at an adjacent subchannel, on the roll-off band of the desired subchannel.

This research was supported by Nokia and the Academy of Finland (project Advanced Multicarrier Techniques for Wireless Communications).

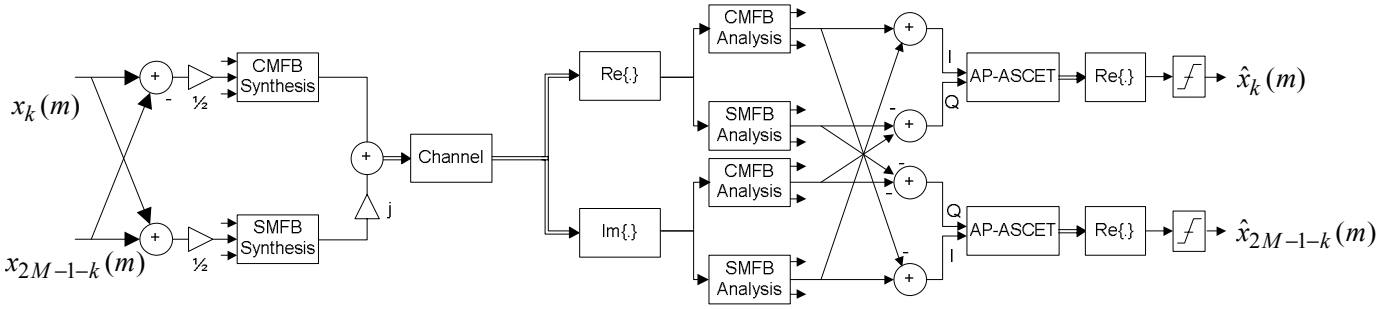

Figure 2. FBMC system with 2x oversampled analysis bank and AP-ASCET equalization.

The AP-ASCET is a low-complexity solution for the still somewhat immature field of equalization in the FBMC context. Because of the overlapping symbols in FBMC systems, guard intervals are not used against intersymbol interference (ISI) and some other form of channel equalization needs to be implemented. Thanks to the good spectral containment of FBs, it is sufficient to equalize each subchannel within the bandwidth of about twice the subchannel spacing using the AP-ASCET.

The paper is structured as follows. First we introduce the AP-ASCET as part of an oversampled FBMC system in TMUX configuration. Then we show how the AP-ASCET can be tuned to provide protection against a narrowband interferer. In Section IV we present our simulation setup and the results. Finally we discuss these results in the conclusions of Section V.

II. AP-ASCET IN FBMC COMMUNICATIONS

A. Filter bank structure for complex transmultiplexers

In FBMC communications, the filter banks are used in the TMUX configuration, with the synthesis bank in the transmitter and the analysis bank in the receiver. Complex filter bank structures can produce a complex baseband I/Q signal for transmission. This is suitable for FBMC systems in spectrally efficient radio communications.

We consider exponentially modulated filter banks (EMFBs), a class of complex filter banks in which the subfilters are formed by modulating a low-pass prototype filter $h_p(n)$ with an exponential sequence [5]. Exponential modulation translates the frequency response of $h_p(n)$ around a new center frequency determined by k. In a general form, the synthesis filters of EMFBs can be written as

$$f_k(n) = \sqrt{\frac{2}{M}} h_p(n) \exp\left(j\left(n + \frac{M+1}{2}\right)\left(k + \frac{1}{2}\right)\frac{\pi}{M}\right), \qquad (1)$$

where $n = 0,1,\ldots,N\text{-}1$ and $k = 0,1,\ldots, 2M\text{-}1$. Furthermore, it is assumed that $N = 2KM$ is an even integer multiple of the number of complex subchannels $2M$. K is the overlapping parameter of the transform and can be used as a design parameter since it affects on how much stopband attenuation we can achieve. The roll-off is another essential design parameter, which determines how much adjacent subchannels overlap. Typically, a roll-off of 100 % can be used, in which case only the neighboring subchannels are overlapping with each other, and the overall subchannel bandwidth is twice the subchannel spacing.

The analysis filters are obtained by time-reversing the conjugate of the synthesis filters as

$$h_k(n) = f_k^*(N-1-n). \qquad (2)$$

To obtain a correct scaling, a factor of ½ has to be included at some point of the synthesis-analysis cascade.

The prototype filter $h_p(n)$ can be optimized in such a manner that the filter bank satisfies the perfect reconstruction (PR) condition, i.e., the analysis transform is invertible by the synthesis transform [4, 5]. In our studies we use a real-valued prototype filter of a cosine modulated filter bank (CMFB). As a matter of fact, our EMFB is implemented by a combination of CMFBs and sine modulated filter banks (SMFBs) [5], as can be seen in Figure 2, which also includes the equalization part. PR CMFBs and SMFBs can be efficiently implemented with extended lapped transforms (ELTs) [4, 5].

The relation between the synthesis filters of the $2M$-channel EMFB and the corresponding M-channel CMFB and SMFB with same $h_p(n)$ is

$$f_k(n) = \begin{cases} f_k^c(n) + j f_k^s(n) & , k \in [0, M-1] \\ -(f_{2M-1-k}^c(n) - j f_{2M-1-k}^s(n)), & k \in [M, 2M-1], \end{cases} \qquad (3)$$

where the superscript defines the trigonometric sequence.

One additional feature of the structure of Figure 2 is that the subchannel output signals of the analysis bank are 2x oversampled. This is achieved by using the symbol rate complex (I/Q) subchannel signals, instead of the real ones that are sufficient for detection after the channel equalizer. In case of 100 % roll-off or lower, non-aliased versions of the subchannel signals are obtained in the receiver. Consequently, there are full possibilities to do the channel equalization in an optimal way. In principle, if there is no aliasing of the subchannel signals in the receiver bank, perfect equalization of the distorting channel within the subchannel passband and transition band regions would completely restore the orthogonality of the subchannel signals [8].

B. Channel Equalization

A challenge in filter bank based systems is that the channel equalization is not as well understood as in the DFT-based

systems. We base our equalization approach on the concept introduced in [9] and then further developed in [10] and [6]: the AP-ASCET. It consists of a cascade of an all-pass phase correction section followed by a phase rotator and a linear-phase amplitude equalizer stage. The complexity of each stage can be defined by the user. In an FBMC system there is a trade-off between the number of subchannels within a given bandwidth and the complexity of the AP-ASCET equalization to obtain required performance.

We choose a low–complexity AP-ASCET with a second-order all-pass section, the phase rotator and a five-tap linear-phase FIR filter, as depicted in Figure 3 for a given subchannel k.

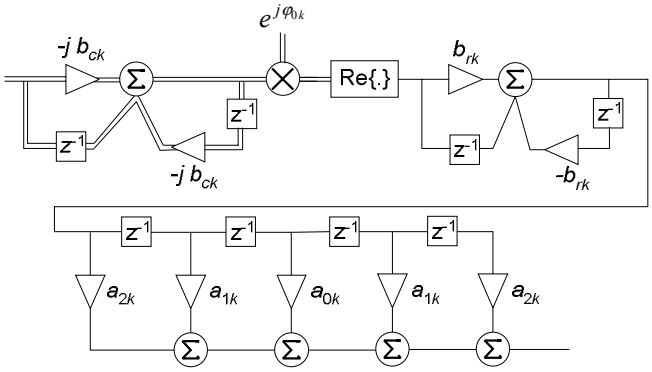

Figure 3. AP-ASCET subchannel equalizer with phase rotator, second order all-pass section and five-tap linear-phase FIR stage.

The transfer functions of the all-pass filters can be written in the non-causal form to facilitate analysis (the realizable causal form needs a multiplication by z^{-1}), as follows:

$$H_{ck}^{(p)}(z)=\frac{1-jb_{ck}z}{1+jb_{ck}z^{-1}},\quad H_{rk}^{(p)}(z)=\frac{1+b_{rk}z}{1+b_{rk}z^{-1}}. \qquad (4)$$

Combining the all-pass filters and the phase rotator, we obtain a phase response for this stage as follows:

$$\arg\left[H_{peq}\left(e^{j\omega}\right)\right]= \\ =\varphi_{ok}+2\arctan\left(\frac{b_{rk}\sin\omega}{1+b_{rk}\cos\omega}\right)+2\arctan\left(\frac{-b_{ck}\cos\omega}{1+b_{ck}\sin\omega}\right). \qquad (5)$$

For the amplitude equalizer the magnitude frequency response is:

$$\left|H_{aeq}\left(e^{j\omega}\right)\right|=a_{0k}+2a_{1k}\cos\omega+2a_{2k}\cos 2\omega. \qquad (6)$$

With this AP-ASCET configuration, we have enough degrees of freedom to exactly define the amplitude and the phase response at three frequency points within each subband by selecting appropriate equalizer parameters. The points where $\omega = 0$, $\omega = \pm\pi/2$ and $\omega = \pm\pi$ are very convenient from the computational point of view. If we want to obtain at these points the target phase responses ζ_0, ζ_1 and ζ_2, respectively, and the target amplitude responses ε_0, ε_1 and ε_2, respectively, then the following values have to be selected:

$$\begin{aligned}
\varphi_{0k}&=\frac{\zeta_{0k}+\zeta_{2k}}{2} & a_{0k}&=\frac{1}{4}\left(\varepsilon_{0k}+2\varepsilon_{1k}+\varepsilon_{2k}\right)\\
b_{ck}&=\pm\tan\left(\frac{\zeta_{2k}-\zeta_{0k}}{4}\right) & a_{1k}&=\pm\frac{1}{4}\left(\varepsilon_{0k}-\varepsilon_{2k}\right)\\
b_{rk}&=\pm\tan\left(\frac{\zeta_{1k}-\varphi_{0k}}{2}\right) & a_{2k}&=\frac{1}{8}\left(\varepsilon_{0k}-2\varepsilon_{1k}+\varepsilon_{2k}\right),
\end{aligned} \qquad (7)$$

where the +/– signs are for even/odd subchannels, respectively.

The target values can be set to fulfill the zero-forcing (ZF) criterion by inverting the estimated channel response values at the given frequency points. Other equalization criteria, such as mean squared error (MSE), can also be applied.

The AP-ASCET described above has been successfully tested in an advanced transceiver simulator including a realistic channel model, practical communication system parameters and channel coding [11], [12].

III. NBI Mitigation

A narrowband interference is a disturbing signal that appears inside the bandwidth of the desired signal and that has a bandwidth that is only a fraction of the bandwidth of the desired signal. There has been extensive research on NBI detection and elimination. Some of them use FBs to detect and remove the subchannels affected by the interferer [7]. In this paper we study the subchannel immediately next to the one in which the NBI is located and take advantage of the spectral shaping capabilities of the AP-ASCET.

In our proposed system, the receiver first calculates the necessary AP-ASCET parameters to compensate the channel at hand. After extensive simulations, we came to the conclusion that MSE equalization performs in a more robust way than the ZF criterion. Therefore, if we estimate within a subchannel k the channel frequency response as h_{ik}, then we want to equalize by setting the target equalizer phase and amplitude responses as

$$\zeta_{ik}=-\arg(h_{ik}) \qquad \varepsilon_{ik}=\frac{|h_{ik}|}{|h_{ik}|^2+\sigma_n^2}. \qquad (8)$$

where i = 0, 1, 2 corresponds to the frequency points $\omega = 0$, $\pm\pi/2$, $\pm\pi$ respectively and σ^2_n is the noise power.

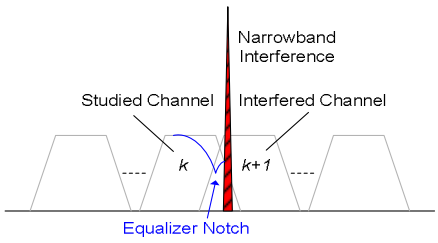

Figure 4. Adjacent subchannel NBI mitigation principle.

Assuming now that a narrowband interferer is present in subchannel k+1 (but still inside of the transition band of

subchannel k) and that ε_{2k} is the target equalizer gain of subchannel k closest to the NBI, we apply a weighting factor w on ε_{2k} in order to reduce the effect of the NBI on subchannel k. Figure 4 sketches the described situation. A straightforward choice is to weight by $w = 0$, obtaining thus a notch at that frequency point. However, depending on the NBI power, there are different weights that yield better performance, as can be seen in the following section.

IV. Simulation Setup and Results

For our simulations we used the aforementioned complex modulated FB in the TMUX configuration with 64 subchannels, a roll-off factor of 100% and an overlapping factor $K = 5$, providing a stopband attenuation of around 50 dB. The FB is the core of a MC system transmitting in a 20 MHz wide channel with a delay spread of 2.5 µs according to the ITU-R Vehicular-A model. The channel is simulated over 10000 realizations and we assume perfect channel knowledge at the equalization points. The E_b/N_0-ratio is 17 dB, yielding an uncoded bit error ratio (BER) of around 10^{-2} for BPSK without NBI.

The NBI is either a continuous wave (CW) signal or a signal generated by a similar filter bank of 256 subchannels, therefore with a bandwidth of 25% of the studied subchannel bandwidth. The interferer is located at $\pi/16$, $\pi/8$ or $\pi/4$ off the passband edge ($\pi/2$ would mean the center of the jammed subchannel). We varied the NBI power to see its effect on the BER performance of the studied subchannel.

Considering the AP-ASCET, we study the effect of applying different weights to the desired equalizer gain at the passband edge, i.e., $\varepsilon'_{ik} = w\varepsilon_{ik}$. The results can be seen in Figure 5, from which can be deduced that the stronger the NBI, the deeper the notch has to be in order to improve performance. However, when the NBI is weak, introducing a notch worsens the received signal. Thus, for each NBI power there is a certain optimal weighting factor.

We also tried to find a simple rule to scale the equalizer gain at the passband edge and obtained very good results if we extended (8) as follows:

$$\varepsilon_{ik} = \frac{|h_{ik}|}{|h_{ik}|^2 + \sigma_n^2 + \sigma_I^2}, \qquad (9)$$

where σ^2_I is the NBI power defined relatively to the power of a subchannel, and it is assumed to be known. Figure 5 also includes this case, showing that it is quite close to the envelope of the BER curves providing optimal BER performance at different NBI powers.

Figure 5 a) shows the CW NBI at $\pi/16$ and b) shows a NBI with relative bandwidth of 25% at the same frequency position. Subfigures c) and d) present the results for a similar setup as in a) and b), but with the interference located at $\pi/4$. In e) we can see a case similar to a), but with $E_b/N_0 = 7$ dB. We see that the presented method works in all of these cases. It also does so in the other mentioned combinations (CW and 25% NBI at $\pi/8$). The performance lies in between the presented cases as expected, therefore it is not presented in separate figures. Evidently, the further away the NBI is from the studied passband, the smaller its effect, but also the less influence our gain weighting method has. This means that the performance improvement possibility becomes smaller in this case.

V. Conclusions

We have presented an effective technique that permits improving the BER performance of an FBMC subchannel partially affected by narrowband interference. In the case a NBI is present, a subchannel originally unsuitable for transmission can be utilized. The BER performance improvement for this subchannel is evident from the results and can in some cases reach 20 dB. The effect on the overall BER may be rather small, but it is still worth saving the subchannel for successful transmission (in our channel setup, one subchannel means 300 kHz bandwidth). It should be noted that the implementation complexity of the proposed scheme is very low: During the channel estimation stage, the parameters of the possible NBI(s) have to be estimated and the equalizer coefficients have to be adjusted correspondingly. However, no additional processing is needed during the data detection.

It is also noticeable that the MSE-like technique from (9) gives the best overall results independent of the tested NBI type and position. Assuming that the channel affected by the interference is known, the only variable that needs to be estimated is the interferer power.

The presented narrowband interference mitigation principle and the AP-ASCET on which it builds is directly applicable to most filter bank based systems, including the novel time-frequency localization (TFL) optimized OQAM/IOTA approaches presented in [13].

Further studies include a reliable form of channel estimation for FBMC systems and also a way to determine the interferer power. We are further interested in the possible combination of FB-based NBI detection and elimination methods as presented in [7] with the method proposed above, since this one concentrates on the *edge effects* of the interference. The technique presented in [7] can be applied to single carrier systems, including CDMA, with frequency domain NBI elimination. The method presented in this paper can also be applied to single carrier systems with frequency domain equalization.

Acknowledgment

The authors would like to acknowledge Mika Rinne from Nokia Research Center for useful discussion during the research that led to these results.

References

[1] J. G. Proakis, *Digital Communications*, 4th. ed., McGraw-Hill International Editions, Electrical Engineering Series 2001.

[2] R. van Nee and R. Prasad, *OFDM for Wireless Multimedia Communications*. Artech House, London, 2000.

[3] S. D. Sandberg and M. A. Tzannes, "Overlapped discrete multitone modulation for high speed copper wire communications," in *IEEE J. on Select. Areas in Commun.*, vol. 13, pp. 1571-1585, Dec. 1995.

[4] H. S. Malvar, *Signal Processing with Lapped Transforms*. Artech House, Boston, MA, 1992.

[5] A. Viholainen, T. Hidalgo Stitz, J. Alhava, T. Ihalainen, and M. Renfors, "Complex modulated critically sampled filter banks based on cosine and sine modulation," in *Proc. IEEE Int. Symp. Circuits and Systems*, Scottsdale, USA, May 2002, pp. 833-836.

[6] T. Ihalainen, T. Hidalgo Stitz, M. Renfors, "Efficient per-carrier channel equalizer for filter bank based multicarrier systems," in *Proc. IEEE Int. Symp. Circuits and Systems* , Kobe, Japan, May 2005, pp. 3175-3178.

[7] T. Hidalgo Stitz, M. Renfors, "Filter bank based narrow band interference detection and suppression in spread spectrum systems," in *EURASIP Journal on Applied Signal Processing*, vol. 2004, no. 8, pp. 1163-1176, July 2004.

[8] S. Nedic, "An unified approach to equalization and echo cancellation in OQAM-based multi-carrier data transmission," in *Proc. Globecom'97*, Nov. 1997, pp. 1519-1523.

[9] J. Alhava and M. Renfors, "Adaptive sine-modulated/cosine-modulated filter bank equalizer for transmultiplexers," in *Proc. European Conf. on Circuit Theory and Design*, Espoo, Finland, Aug. 2001, pp. III/ 337-340.

[10] T. Ihalainen, T. Hidalgo Stitz, M. Renfors, "On the performance of low-complexity ASCET-equalizer for a complex transmultiplexer in wireless mobile channel," in *Proc. 7th Int. OFDM-Workshop 2002*, Harburg, Germany, Sept. 2002.

[11] Tero Ihalainen, Tobias Hidalgo Stitz, Markku Renfors, "Channel Equalization in Filter Bank Based Multicarrier Modulation for Wireless Communications," submitted to EURASIP Journal on Applied Signal Processing.

[12] Tero Ihalainen, Tobias Hidalgo Stitz, Ari Viholainen, Markku Renfors, "Performance Comparison of LDPC-coded FBMC and CP-OFDM in Beyond 3G Context," to appear in *Proc. IEEE Int. Symp. Circuits and Systems*, Kos, Greece, May 2006.

[13] P. Siohan, C. Siclet, and N. Lacaille, "Analysis and design of OFDM/OQAM systems based on filterbank theory," in *IEEE Trans. Signal Processing*, vol., 50, pp. 1170-1183, May. 2002.

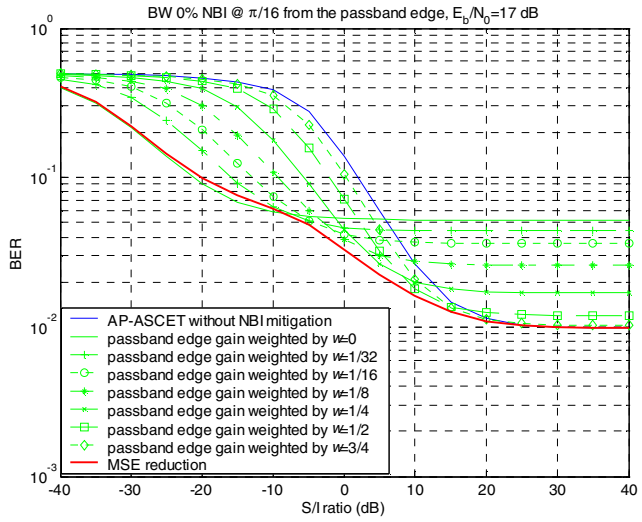

a)

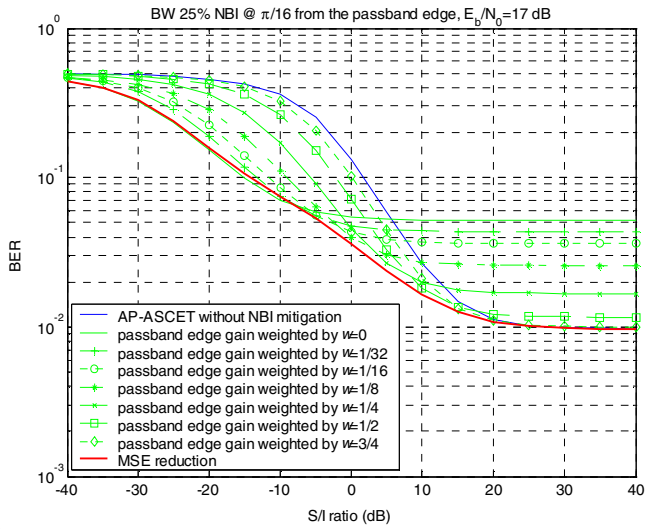

b)

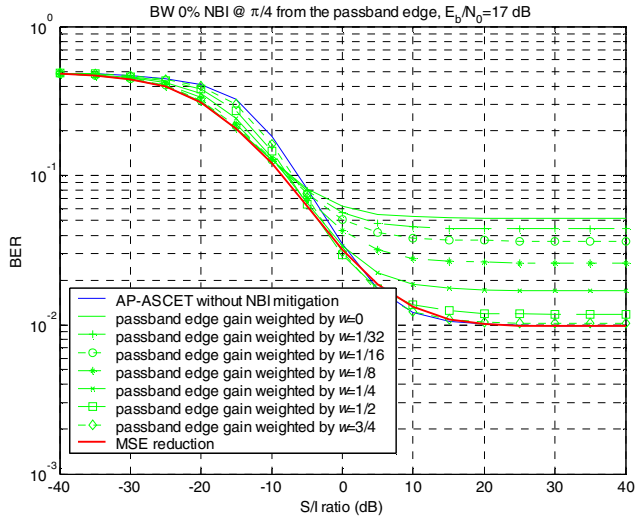

c)

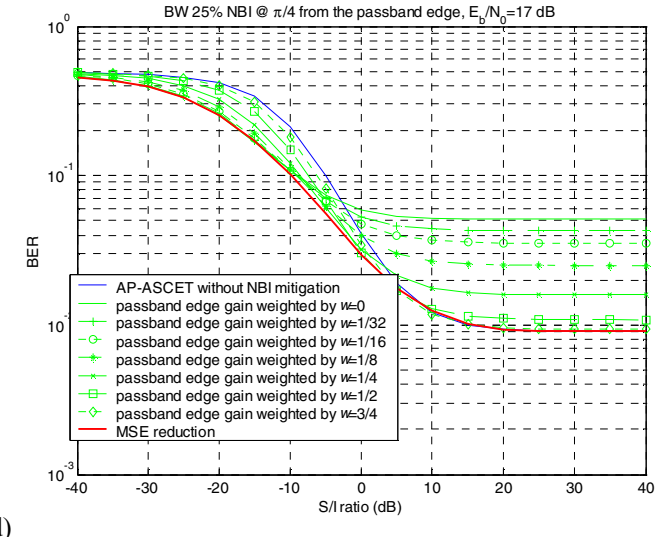

d)

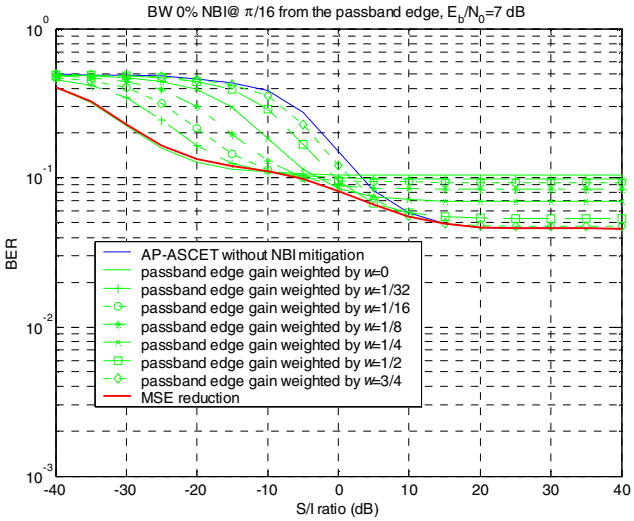

e)

Figure 5. BER performance vs. signal-to-NBI ratio of a FBMC system with 2-PAM subchannel modulation and interference mitigation techniques. The bolder line represents the results for the MSE reduction applying (9). a) CW NBI at π/16, b) 25% NBI at π/16, c) CW NBI at π/4, d) 25% NBI at π/4, e) CW NBI at π/16 and E_b/N_0 = 7 dB.

Publication P5

T. Hidalgo Stitz, T. Ihalainen, and M. Renfors, "Practical issues in frequency domain synchronization for filter bank based multicarrier transmission" in *Proc. IEEE Int. Symp. Communications, Control and Signal Processing.*, pp. 411-416, March 2008.

http://dx.doi.org/10.1109/ISCCSP.2008.4537260

Practical Issues in Frequency Domain Synchronization for Filter Bank Based Multicarrier Transmission

Tobias Hidalgo Stitz, Tero Ihalainen, Markku Renfors
Department of Communications Engineering
Tampere University of Technology. Tampere, Finland
e-mail: {tobias.hidalgo, tero.j.ihalainen, markku.renfors}@tut.fi

Abstract— **In this paper we address the practical problems when dealing with synchronization and channel estimation in a filter bank based multicarrier system. We present an approach for performing timing synchronization, carrier frequency offset estimation and correction, and channel estimation based on the use of the same training sequences for all the three tasks. We show that it is possible to perform them all after the analysis filter bank at the receiver, at low sampling rate, taking advantage of the high selectivity of the subband filters. The possibility to implement all the receiver baseband signal processing functionalities in frequency domain results in a very flexible overall receiver architecture, suitable for dynamic use of the frequency spectrum.**

I. INTRODUCTION

The demand for ever-increasing data rates requires that emerging wireless systems make use of wider transmission bandwidths, therefore facing difficult communication environments. For example, frequency selective channels cause inter-symbol interference that has to be equalized [1]. Another challenge is that the wideband signal may have to coexist with narrowband signals that distort parts of the desired signal, e.g., because of overlaid spectrum in ultra-wideband systems, spurious spectral components due to own or nearby transceivers, or even intentional jamming. Furthermore, for efficient use of the radio spectrum, it may be interesting to use small non-contiguous portions of the frequency band in a dynamic way. Multicarrier (MC) techniques have proven to be effective in such difficult scenarios. Among their advantages in wideband communications we can count robustness in case of frequency selective channels, offering the possibility of simple equalization, simple timing synchronization, as well as insensitivity to limited narrowband interference (NBI). Further, MC systems are scalable and flexible to configure, offering a beneficial use of limited resources. Due to these advantages, MC techniques are always taken into consideration when developing emerging wideband communication systems [2].

Orthogonal frequency division multiplexing (OFDM) with cyclic prefix (CP) [2] has been so far the most prominent multicarrier technique. Because of its inherent robustness to multipath propagation and very simple equalization (one complex coefficient per subcarrier), OFDM is applied, e.g., in wireless local area network (WLAN) and digital broadcasting (DAB, DVB) standards. Multirate filter banks (FB) in the transmultiplexer (TMUX) configuration are a second choice when designing MC transmission systems [3]. There are two fundamental advantages of FBMC over OFDM, at a cost of a somewhat higher implementation complexity. First, the subchannels can be optimally designed in the frequency domain to have desired spectral containment [4]. Second, CP, which is pure redundancy that reduces throughput efficiency, is not used. Basically, the Nyquist pulse shaping principle is used for the subchannel signals, which means that the consecutive symbol waveforms are overlapping in time.

Good spectral containment is crucial for avoiding distortion from non-synchronous signals in adjacent bands. Further, the high spectral definition is desirable when performing spectral sensing, which is a basic element in the cognitive radio concept [5]. The performance of Haykin's method of choice for radio-scene analysis, the multitaper method [6], can be well approximated using FBs with greatly reduced complexity [7].

Our research group has presented an FBMC scheme that uses a 2x oversampled analysis bank at the receiver, as can be seen in Figure 1. In order to exploit the advantages of FBMC and to avoid the higher complexity, we have proposed a solution that only uses a fraction of the subchannels that OFDM would use in a similar environment. The result is a mildly selective channel fading within the subchannels, which is then compensated by the low-complexity amplitude and phase subchannel equalizers (AP-SCE) [8]. In this paper we present how the problems of synchronization and channel estimation for the mentioned approach can be practically solved with the help of training sequences. The discussion focuses here on the downlink case, but the algorithms are equally well applicable to the uplink.

The high stopband attenuation of FB permits channel selection filtering and possible NBI suppression directly at the receiver analysis bank, without prior processing, except for the anti-aliasing filtering determined mostly by the sampling rate at the analysis filter bank input. Since the FB provides good frequency selection for the desired spectral components, it is natural to strive for an overall receiver architecture where all the baseband signal processing functions are implemented in frequency domain, i.e., after the analysis filter bank. Therefore, it is desirable to do all channel parameter estimation processing in the low rate domain, after the analysis FB. We show here how it is possible to synchronize, estimate carrier frequency offset (CFO), and calculate the coefficients needed by the AP-SCEs with subcarrier-wise processing.

978-1-4244-1688-2/08/$25.00 ©2008 IEEE

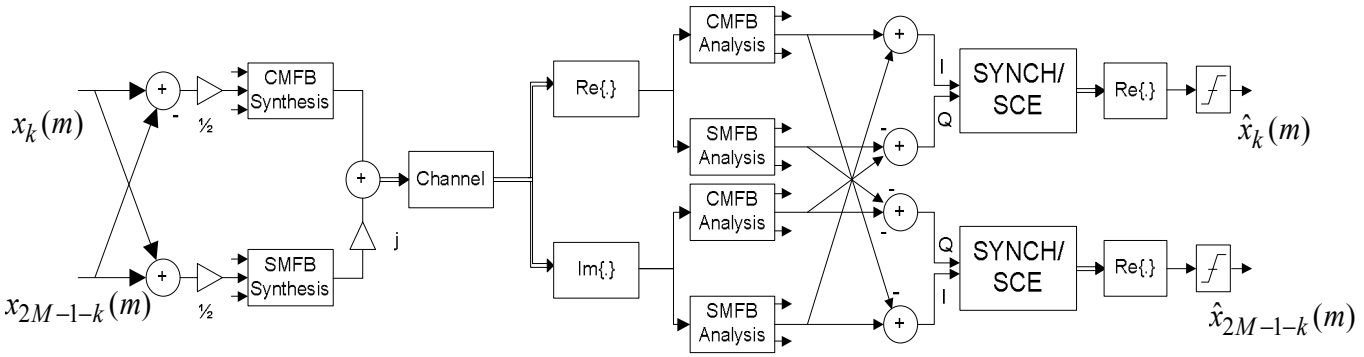

Figure 1. FBMC system with oversampled analysis bank and subcarrier-wise synchronization and equalization.

The paper is structured as follows. First, we introduce the oversampled FBMC system with subcarrier-wise equalization. Then we present the training sequences and show how they are used for synchronization and channel estimation. In Section IV we present our simulation setup and the results. Finally, we discuss these results in the conclusions in Section V.

II. Channel Equalization in FBMC Communications

A. Filter Bank Structure for Complex Transmultiplexers

In FBMC communications, the filter banks are used in the TMUX configuration, with the synthesis bank in the transmitter and the analysis bank in the receiver. Complex filter bank structures can produce a complex baseband I/Q signals for transmission, making them suitable for FBMC systems for spectrally efficient radio communications.

We consider exponentially modulated filter banks (EMFBs), a class of complex filter banks in which subfilters are formed by modulating an exponential sequence with a low-pass prototype impulse response $h_p(n)$ [8]. Exponential modulation translates the frequency response of $h_p(n)$ around a new center frequency determined by k. In a general form, the synthesis filters of EMFBs can be written as

$$f_k(n) = \sqrt{\frac{2}{M}} h_p(n) \exp\left(j\left(n + \frac{M+1}{2}\right)\left(k + \frac{1}{2}\right)\frac{\pi}{M}\right) \quad (1)$$

where $n = 0,1,\ldots,N\text{-}1$ and $k = 0,1,\ldots, 2M\text{-}1$. Furthermore, it is assumed that $N = 2KM$ is an integer multiple of the number of complex subchannels $2M$. K is the overlapping parameter of the transform and can be used as a design parameter as it affects on how much stopband attenuation we can achieve. The roll-off is another essential design parameter, which determines how much adjacent subchannels overlap. Typically, a roll-off of 100 % can be used, in which case only the neighboring subchannels are overlapping with each other, and the overall subchannel bandwidth is twice the subchannel spacing.

The analysis filters are obtained by time-reversing the conjugate of the synthesis filters as

$$h_k(n) = f_k^*(N-1-n) \quad (2)$$

To obtain a correct scaling, a factor of ½ has to be included at some point of the synthesis-analysis cascade.

The prototype filter $h_p(n)$ can be optimized in such a manner that the filter bank satisfies the perfect reconstruction (PR) condition, i.e., the analysis transform is invertible by the synthesis transform [4][8]. In our studies we use a real-valued prototype filter of a cosine modulated filter bank (CMFB). As a matter of fact, our EMFB is implemented by a combination of CMFBs and sine modulated filter banks (SMFBs) [8], as can be seen in Figure 1. PR CMFBs and SMFBs can be efficiently implemented with extended lapped transforms (ELTs) [4][8].

One additional feature of the structure of Figure 1 is that the subchannel output signals of the analysis bank are 2x oversampled. This is achieved by using the symbol rate complex (I/Q) subchannel signals, instead of the real ones that are sufficient for detection after the channel equalizer. In case of 100 % roll-off or lower, essentially non-aliased versions of the subchannel signals are obtained in the receiver. Consequently, there are full possibilities to do the channel equalization in an optimal way. In principle, if there is no aliasing of the subchannel signals in the receiver bank, perfect equalization of the distorting channel within the subchannel passband and transition band regions would restore the orthogonality of the subchannel signals completely [9].

B. Channel Equalization

We base our equalization approach on the concept thoroughly discussed in [8]: the AP-SCE. In that paper, also another low complexity equalizer, the 3-tap complex FIR (CFIR) SCE, was considered. In the basic equalization task, these two structures have very similar performance. However, the AP-SCE equalizer has some advantages, since it is more flexible and performs better in the phase equalization.

AP-SCE consists of a cascade of an all-pass phase correction section followed by a phase rotator and a linear-phase amplitude equalizer stage. In an FBMC system there is a trade-off between the number of subchannels used in the communications and the complexity of the AP-SCE equalization to obtain required performance. Here we choose a low–complexity AP-SCE with a second-order all-pass section, the phase rotator and a five-tap linear-phase FIR filter, as depicted in Figure 3 for a given subchannel k.

The subcarrier equalizers are adjusted using a frequency-sampling approach, based on estimated channel frequency response. With this AP-SCE configuration, we have enough degrees of freedom to exactly define the amplitude and the phase responses at three frequency points with each subband. The points where $\omega = 0$, $\omega = \pm\pi/2$ and $\omega = \pi$ are very convenient from the computational point of view.

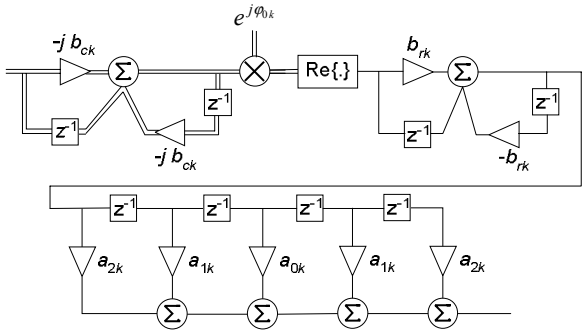

Figure 2. AP-SCE subchannel equalizer with phase rotator, second order all-pass section and five-tap linear phase FIR stage.

If we want to obtain at these points the target phase responses ζ_0, ζ_1 and ζ_2, respectively, and the target amplitude responses ε_0, ε_1 and ε_2, respectively, then the following values have to be selected:

$$\begin{aligned} \varphi_{0k} &= \frac{\zeta_{0k}+\zeta_{2k}}{2} & a_{0k} &= \frac{1}{8}\left(2\varepsilon_{0k}+4\varepsilon_{1k}+2\varepsilon_{2k}\right) \\ b_{ck} &= \pm\tan\left(\frac{\zeta_{2k}-\zeta_{0k}}{4}\right) & a_{1k} &= \pm\frac{1}{8}\left(2\varepsilon_{0k}-2\varepsilon_{2k}\right) \\ b_{rk} &= \pm\tan\left(\frac{\zeta_{1k}-\varphi_{0k}}{2}\right) & a_{2k} &= \frac{1}{8}\left(\varepsilon_{0k}-2\varepsilon_{1k}+\varepsilon_{2k}\right), \end{aligned} \tag{3}$$

where the +/– signs are for even/odd subchannels, respectively.

The target values can be set to fulfill the zero-forcing (ZF) criterion by inverting the estimated channel response values at the given frequency points. Here we use the mean squared error (MSE) equalization criterion, which yields somewhat better performance at low signal-to-noise ratios (SNR):

$$\zeta_{ik} = -\arg(h_{ik}) \qquad \varepsilon_{ik} = \frac{|h_{ik}|}{|h_{ik}|^2+\sigma_n^2}, \tag{4}$$

where h_{ik} is the channel frequency response at subchannel k and the frequency index i = 0, 1, 2, corresponds to frequency positions ω = 0, π/2, π in the even subchannels and ω = -π, -π/2, 0 in the odd subchannels, respectively.. σ^2_n is the noise power, assuming that the signal power is normalized to 1. In this paper we assume σ^2_n to be known at the receiver.

III. Training Sequence Based Channel Estimation and Synchronization

In order to equalize, the AP-SCE has to be fed with channel estimates $\hat{h}_{ik}$ (i.e., estimates of h_{ik}) to obtain the target values in (4) that permit calculating the coefficients in (3). We utilize subchannel-wise training sequences to perform channel estimation and also the other synchronization tasks. We desire that our training sequences have their energy concentrated at the subchannel frequencies used in the frequency-sampled scheme. The simplest sequences that fulfill this criterion are repetitions of the following:

$$\begin{aligned} t^e &= \ldots 1,1,0,0,\ldots \\ t^o &= \ldots 0,0,-1,1\ldots \end{aligned}, \tag{5}$$

where the superscripts stand for the even and odd subchannels, respectively. Figure 3 sketches the frequency power spectrum of the training sequences in FBMC.

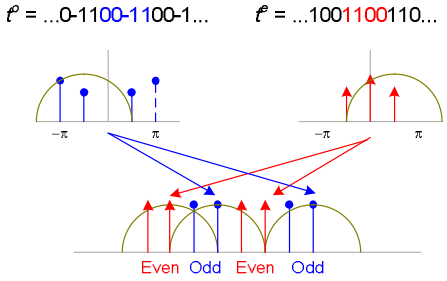

Figure 3. Spectral energy content of the transmitted training sequences with FBMC.

Notice that the frequency bins at the passband edges are shared by adjacent subcarriers, but the training energy for each bin comes from one subcarrier only. The total length of the training sequence, composed of repetitions of the sequences in (5), will have an effect on the performance of the channel parameter estimation because the truncation of the sequences spreads part of the energy outside the used frequency bins.

Figure 4 shows how the transmission data could look like in a FBMC system with transform size $2M$=256, out of which 168 subchannels are used. The training sequence power is boosted by 1 dB with respect to the 2-PAM data.

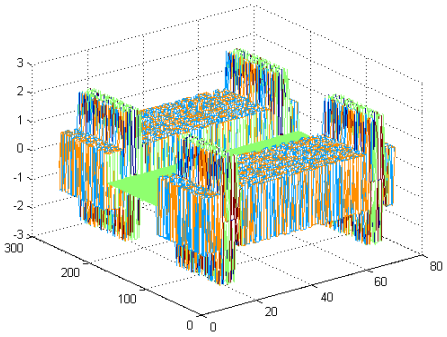

Figure 4. Training sequences and data in FBMC.

The synchronization blocks at the receiver have to perform the following tasks: First the timing synchronization has to find the location of the training sequences within the stream of data. It is enough to estimate the timing with the resolution of ± half a subcarrier symbol interval; the fractional timing offset is compensated by the phase response of the subcarrier equalizers. Then the training sequences are used to calculate possible carrier frequency offsets (CFO). Finally, after the CFO has been corrected, the channel estimation block uses the training sequences to obtain the desired estimates.

A. Timing Synchronization

To find the training sequence, we detect the peak of the correlation of the received subchannel streams with the training sequence at the receiver. It is important to note that here the training sequences are not anymore real valued. In an ideal case without channel, the sequences (5) will be in the real part of the received subchannel signal. The transmission channel

rotates the symbols (apart from introducing ISI) in a way that the real part does not correspond anymore to the subchannel data.

In the likely case of non-zero CFO, consecutive similar symbols will be rotated with respect to each other. For certain CFOs this can lead to situations in which the correlation of the received signal with the receiver training sequence is not having a maximum at the location of the training sequence within the data. In our experiments we have concluded that the correlation of the absolute values is effective and robust against frequency offsets. Performing the operation on the strongest 25% of the subchannels permits localizing the training sequence most of the times by finding the peak of the sum of the correlations.

$$m_0 = \arg\max_m \left(\sum_{\substack{k \in \text{strongest} \\ \text{subchannels}}} \sum_{n=0}^{L-1} \left| t_k^r[n] \right| \left| r_k[n+m] \right| \right), \qquad (6)$$

where L is the length of the correlation, usually the size of the transmission block, r_k is the received data in subchannel k and the superscript r indicates the receiver training sequence.

B. Carrier Frequency Offset Estimation

The effect of a constant CFO is that the subchannel symbols have a linearly time-dependent phase rotation. If the frequency shift is measured in radians with respect to the subchannel bandwidth, a series of consecutive similar symbols will show a relative phase rotation with respect to each other equal to the frequency shift. Therefore, if the relative phases of a received sequence are known in an ideal case, the CFO can be inferred by comparing those phases with the actually received ones. In our synchronization approach we use the 1's of the training sequences as a reference to compare the received phase differences. The estimate of the CFO is obtained after averaging over all the subchannels. Depending on the estimated CFO, the frequency shift can be corrected subchannel-wise or by tuning the local oscillator at the receiver front-end. With CFO's greater than a certain amount, the interference from the neighboring channel grows significant and subchannel-wise frequency correction is not able to satisfactorily compensate for this.

C. Channel Estimation

After finding the training sequences and compensating for possible CFO, the energy of the training sequence signal is located at the frequencies of interest for the AP-SCE. It is very simple and convenient to estimate the channel at these points, within each subband, with the help of a 4-point FFT. Thus, using the notation from the equalization section, we can estimate at the frequency response as follows:

$$\begin{aligned} \hat{h}_{ik} &= \frac{1}{r_i^e} \sum_{n=0}^{3} d_k[n] e^{-j\frac{2\pi in}{4}} \quad , k = \text{even} \\ &= \frac{1}{r_i^e} \sum_{n=0}^{3} d_k[n] j^{-in} \quad , i = 0,1,2. \end{aligned} \qquad (7)$$

$$\begin{aligned} \hat{h}_{ik} &= \frac{1}{r_i^o} \sum_{n=0}^{3} d_k[n] e^{-j\frac{2\pi in}{4}} e^{-j\pi n} \quad , k = \text{odd} \\ &= \frac{1}{r_i^o} \sum_{n=0}^{3} d_k[n] j^{-in} (-1)^n \quad , i = 0,1,2. \end{aligned} \qquad (8)$$

Here r_i^x is a normalization factor due to the filter bank design, the training sequence and the frequency points studied. With the PR design we use, in the even subchannels, $r_i^e = 2$; $-2 + 2j$ and $-2j$; in the odd ones, $r_i^o = -2$; $-2 + 2j$ and $2j$, for $i = 0$, 1 and 2, respectively. d_k is the received signal corresponding to the synchronized and frequency corrected training sequence. Note that the 4-point FFT is extremely simple to realize. The values obtained as described can be directly applied in (5) to obtain the AP-SCE parameters of (4).

Note that for all subchannels k which have a neighboring subchannel k+1, $\hat{h}_{2,k}$ and $\hat{h}_{0,k+1}$ are channel estimates at the same frequency location. This opens the possibility to further exploit this redundancy for enhancing the estimates at these points.

IV. Simulation Setup and Results

For our simulations we used the aforementioned complex modulated FB in the TMUX configuration with $2M = 256$ subchannels. The prototype filter has a roll-off factor of 100% and an overlapping factor $K = 5$, hereby achieving a stopband attenuation of around 50 dB. 168 active subchannels transmit over an almost 18 MHz wide channel modeled according to the extended ITU-R Vehicular A guidelines [10], centered at 5 GHz and with a maximum delay spread of 2.51 μs. With a sampling rate of 26.88 MHz, the subchannel bandwidth is 105 kHz. The channel is assumed to be quasi-stationary, remaining constant over the transmission of two consecutive training sequences and the data in between. The general model for the transceiver setup is shown in Figure 1. At the receiver, the AP-SCE equalizer as described in Section II.B compensates for the channel distortion. A transmission frame consists of 53 MC-symbols, which add up to slightly more than 250 μs of duration. We have studied the cases in which out of the 53 MC-symbols, 6 or 10 are training sequence symbols (TSL = 6 or 10). The average training sequence power is boosted by 1 or 4 dB with respect to the data power (TSB = 1 or 4 dB).

A. Timing Synchronization Results

To assess the performance in localizing the training sequence, we performed simulations in which the CFO varies randomly with uniform distribution between ± 50% of the subchannel bandwidth (± 52.5 kHz). The training sequence is embedded within a data stream on a random location, including a random fractional time delay (FTD), and the synchronization mechanism tries to locate it as described in III.A. Figure 5. shows the number of synchronization errors out of 10000 frame transmissions, with different training sequence location, CFO, and channel realization each time.

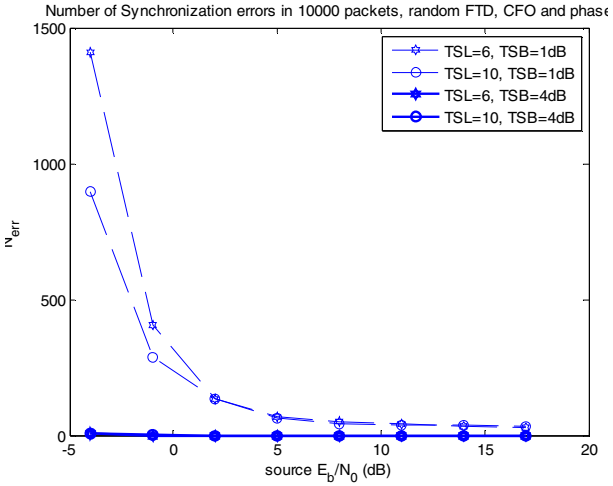

Figure 5. Synchronization errors in 10000 frames with training sequences of different lengths and boosts.

We observe the great effect of the different training sequence boosts on the synchronization performance, whereas the length of the training sequence has a lower impact, comparatively. Further, we can notice that even in the case of the 'weaker' training sequences, synchronization is successful in more than 85% of the cases, even at very high noise levels. As a final remark, the error floor, to which the less boosted training sequences seem to converge represent realizations at which the CFO is very close to 50% of the subchannel BW.

B. CFO Correction

The next two figures present the effect of the subchannel-wise CFO correction on the BER performance of a 2-PAM transmission, assuming perfect timing synchronization. CFO estimation happens as described above, averaging the estimated CFO's over all active subchannels. The performance reference (green, dashed and dotted lines) is the BER of an ideal subchannel-wise CFO compensator that has perfect knowledge of the CFO. From the figures it can be noticed that subchannel-wise CFO correction makes sense for offsets up to 10% of the subchannel bandwidth. With higher carrier offsets, the ICI is so strong that it compromises the following channel estimation and equalization stages. With higher CFOs, the compensation should be done at the local oscillator.

In the course of the simulations, we realized that the CFO is underestimated with the presented method, but by iterating the method a few times, the performance was improved to the results shown. Figure 6. presents the BER performance for the longest and strongest training sequence, while Figure 7. corresponds to the shorter and weaker version. The performance difference is considerable, suggesting that a reliable CFO estimation with the presented method requires a stronger boost for the training sequence.

Lastly, Figure 8. compares the actual CFO and the estimated CFO, at two different SNR's, with randomly generated CFO's at each channel realization The training sequence is 6 MC symbols long and is boosted by 1 dB. The estimation is quite accurate for CFO's up to approximately 25% of the subchannel bandwidth. The range, in which CFO offset is accurate, is reduced with stronger noise presence. Anyway, with the used parameters, the reliable CFO estimation

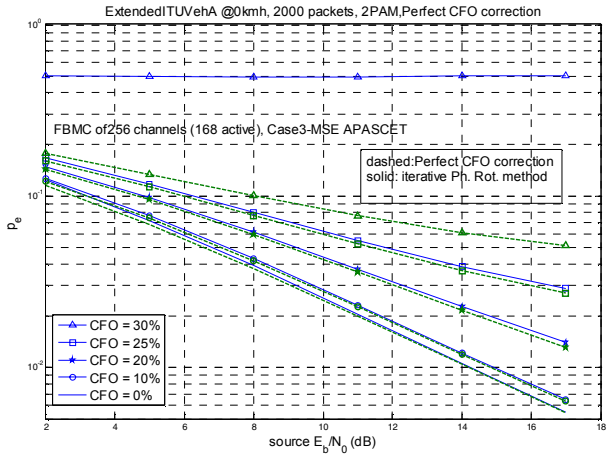

Figure 6. BER performance of the CFO estimation and correction. Training sequence length 10 MC symbols, boost = 4 dB.

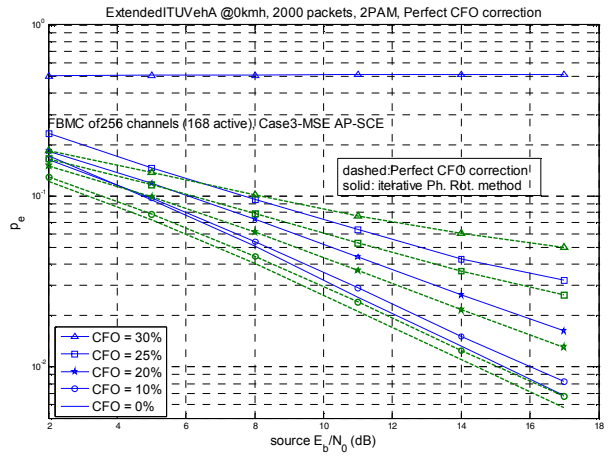

Figure 7. BER performance of the CFO estimation and correction. Training sequence length 6 MC symbols, boost = 1 dB.

range is in the order of ± 20 kHz, which is quite sufficient for practical receivers.

C. Channel Estimation

Finally, we present the performance of the whole synchronization chain, i.e., the timing synchronization, the CFO estimation and correction and the channel estimation. The simulations are performed over 5000 realizations, with 2-PAM data modulation. In these simulations, the actual CFO = 0, but it is still estimated and 'corrected' by the synchronization logic. This represents the steady-state operation after the outer frequency synchronization loop, affecting on the receiver front-end local oscillator, has converged. The results presented here include several small enhancements on the channel estimation: The double estimation at the subchannel edge frequencies is averaged to get a better estimate; the estimates of two consecutive training sequences are also averaged and windowing in frequency over the estimates helps at denoising them, since the neighboring estimates present quite high correlation with the used channel model.

Figure 9. shows the BER results for different training sequence choices. There are also two reference curves: (i) case with perfect channel information and synchronization and (ii) performance of the developed channel estimation method

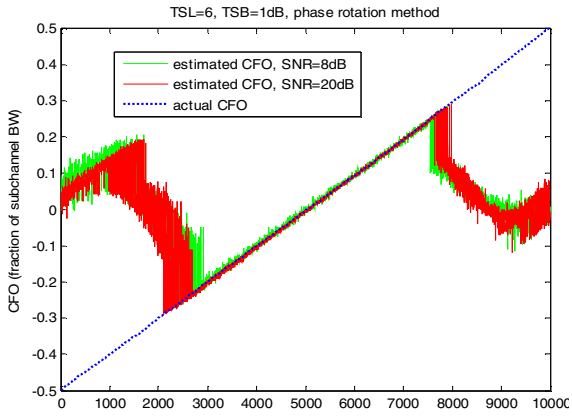

Figure 8. Accuracy of CFO estimation at SNR = 8 dB and 20 dB. Training sequence length 6 MC symbols, boost = 1 dB.

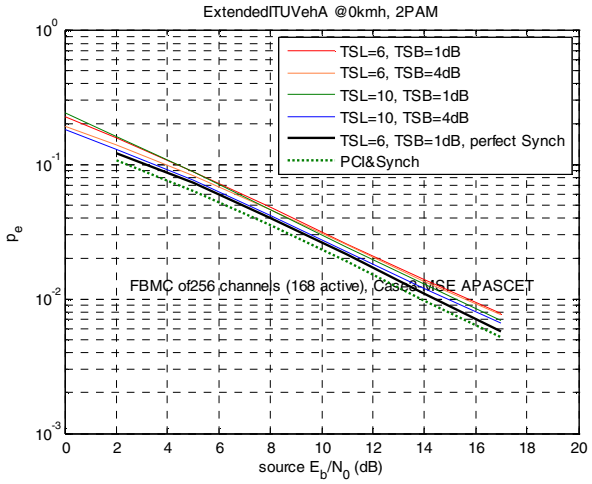

Figure 9. BER performance of whole synchronization and estimation chain for CFO = 0 and different training sequence lengths and boosts.

assuming perfect synchronization, with the weaker and shorter training sequence. The performance degradation between these two is around 0.6 dB, and this gap is reduced using longer and stronger training sequences (which for readability are not included in the figure). When including the synchronization elements, stronger training sequences perform better in the low SNR region and longer sequences perform better when the signal is strong as compared to the noise. From the presented results, the performance degradation in the case of the most 'economical' training sequence seems to be mainly due to the CFO estimation and compensation logic.

V. Conclusions

We have aimed to provide a complete, practical training sequence based solution for signal synchronization and channel estimation in FBMC systems. Due to the high stopband attenuation of the subchannel filters, the analysis FB at the receiver can be used for channel selection filtering, inviting to perform all synchronization processing tasks utilizing the subcarrier signals at the low sampling rate.

Here we designed training sequences that are well suited for localizing them among a stream of user data for timing synchronization. Further, they are applied for estimating the CFO, which can consequently be corrected subchannel-wise. Finally, the same training sequences permit obtaining channel estimates that are used by the low-complexity AP-SCE to perform channel equalization. With the studied training sequences we have concluded that all these operations are realizable effectively after the receiver analysis bank. The training sequence can be separated from the data even at low SNR's and high CFO's. Further, the CFO can be estimated quite accurately for CFO's of up to 25% of a subchannel bandwidth. The degradation of the BER performance at 0% frequency offset with the complete synchronization and estimation logic active varies from 1 to 2 dB, depending on the training sequence parameters selected. The main reason for degradation is the inaccuracy in CFO correction.

The main result is that the considered synchronization procedures can be successfully performed at the low rate, without need of prior processing before the analysis filter bank, apart from coarse CFO compensation.

Future steps in this research include the inclusion of further practical elements in the transmission chain, such as the power amplifier. The effect of its non-linearity on the quality of the synchronization and on the signal spectrum during the boosted training sequence is a matter of crucial importance. The development from a quasi-stationary channel model to one with a mobile receiver is also a high-priority research topic.

Acknowledgment

The authors would like to acknowledge Mika Rinne from Nokia Research Center for useful discussion during the research that led to these results.

References

[1] J. G. Proakis, Digital Communications, 4th. ed., McGraw-Hill International Editions, Electrical Engineering Series 2001.

[2] R. van Nee, and R. Prasad, OFDM for Wireless Multimedia Communications. Artech House, London, 2000.

[3] S. D. Sandberg, and M. A. Tzannes, "Overlapped discrete multitone modulation for high speed copper wire communications," IEEE J. on Select. Areas in Commun., vol. 13, pp. 1571-1585, Dec. 1995.

[4] H. S. Malvar, Signal Processing with Lapped Transforms. Artech House, Boston, MA, 1992.

[5] S. Haykin, "Cognitive radio: brain-empowered wireless communications," IEEE Journal Selected Areas in Communications, vol. 23, no. 3, pp. 201-220, Feb. 2005.

[6] D.J. Thomson, "Spectrum estimation and harmonic analysis," Proceedings of the IEEE, vol. 70, no. 9, pp. 1055-1096, Sept. 1982.

[7] B. Farhang-Boroujeny, and R. Kempter, "Multicarrier communication techniques for spectrum sensing and communication in cognitive radios", *submitted to IEEE J. Select. Areas Commun*.

[8] T. Ihalainen, T. Hidalgo Stitz, M. Rinne, and M. Renfors, "Channel equalization in filter bank based multicarrier modulation for wireless communications," EURASIP Journal on Advances in Signal Processing, vol. 2007, pp. Article ID 49 389, 18 pages, 2007, doi:10.1155/2007/49389.

[9] S. Nedic, "An unified approach to equalization and echo cancellation in OQAM-based multi-carrier data transmission," in Proc. Globecom'97, pp. 1519-1523, Nov. 1997.

[10] T.B. Sorensen, P.E. Mogensen, and F. Frederiksen, "Extension of the ITU channel models for wideband OFDM systemns," in Proc. IEEE Vehicular Technology Conf., Dallas, USA, Sep. 2005